
THE UNIVERSITY OF HULL

**Liquid Crystalline Organic Semiconductors
for Application in Opto-electronic Devices**

being a Thesis submitted for the Degree of
Doctor of Philosophy (PhD)

in the University of Hull

by

Weixiao Bao

September 2014

Acknowledgments

I would like to thank my supervisor Professor Stephen M. Kelly for all the sound advice and guidance he has give the desired product asn to me throughout the course of the research. I am also grateful for his assistance and patience in the preparation of this report.

I would like to express my gratitude to the members inC314, for their support and assistance during my time spent at the bench. Special thanks are reserved for Dr Michael Hird, Dr Stuart Kitney and Dr Fei Cheng, for useful suggestions and guidance during the research. I would also like to thank all the technical staff of the chemistry department for providing the necessary analysis of the compounds synthesised in this work, especially Dr Kevin Welham (MS) and Mrs Carol Kennedy (elemental analysis).

I also wish to thank Professor Mary O'Neill and other members (Brian Lambert, William Harrison and Stephen Mayers) of the Department of Physics for useful discussions and physical evaluation of the compounds synthesised in this thesis. I would like to thank the University of Hull and Polar OLED for funding this physics research.

I am grateful to the China Scholarship Council (CSC) for the funding of my study and University of Hull for a fee waiver and for allowing me to carry out my research in the Department of Chemistry.

Finally, I would like to thank my parents and all of my friends and family for their support and encouragement.

Abstract

This thesis collates and describes the research work carried out during my PhD programme. This work of research is mainly based on the synthesis and evaluations of novel liquid crystalline materials for use in plastic electronic applications, such as Organic Light Emitting Diode (OLED) and Organic Photovoltaic (OPV) devices. It also focuses on the study of the relationship between chemical structures and the mesomorphic behaviour, the liquid crystalline transition temperatures and energy levels of these new compounds.

Optical Polarising Microscopy (OPM) and Differential Scanning Calorimetry (DSC) were used to identify the mesomorphic behaviour and transition temperatures of all the new liquid crystals. A combination of UV-vis absorption and Cyclic Voltammetry (CV) was used to characterize the Highest Occupied Molecular Orbitals (HOMO), Lowest Occupied Molecular Orbitals (LUMO) energy levels and, therefore, the band gap (E_g) of the final compounds.

Another primary focus of this work was the study and application of various aryl-aryl, cross-coupling reaction methods, including the Stille and the Suzuki reactions and a new direct arylation method. The reaction conditions were optimised during the research work for different compounds. The direct arylation method was found to be a successful and efficient way to synthesise new thiophene derivatives using aryl halides *via* C-H bond activation by palladium catalysts, but unfortunately not for all substrates.

A series of fluorene- and carbazole-based materials have been developed for use as hole-transporting materials and electroluminescent materials in plastic electronic applications. Some of these materials exhibit nematic phases, which is beneficial due to the lower viscosity present in the nematic phase compared to that of the smectic phases. Some of them are found to form a glass above room temperature without any observable liquid crystal phases, despite significant supercooling below the melting

point. The transition temperatures and mesomorphic behaviours of these novel materials were determined. The materials are expected to exhibit appropriate ionization potential (IP) and energy levels (HOMO, LUMO and E_g).

A number of compounds incorporating a thiophene-based central core have been synthesized and evaluated as hole-transporting materials in OLEDs or/and as electron-donors in OPVs hopefully with the required appropriate energy levels. A compound with four 2,5-disubstituted thiophene rings in the molecular core shows promising properties for use as an electron-donor material with PCBM as an electron-acceptor in test OPV cells fabricated by members in the Organic Semiconductor Group in the Department of Physics at the University of Hull.

Several liquid crystals based on thiazolo[5,4-d]thiazole central cores were synthesised by various aryl-aryl cross-coupling reaction pathways. The thiazolo-thiazole compounds based on five-membered rings only exhibit a nematic phase, while some thiazolo-thiazole compounds incorporating six-membered rings exhibit both a smectic phase and a nematic phase. However, this class of compounds exhibit relatively high melting points and liquid crystalline transition temperatures, as well as a very poor solubility, which indicates that they were not able to be used as organic semiconductors in plastic electronics applications.

A class of oxadiazole homologues and a small number of isoxazole derivatives were successfully synthesized and purified. They were expected to possess relatively high electron affinity (EA) and strong fluorescence as potential materials for use as electron-transporting layers and/or emissive layers in OLEDs. The mesomorphic behaviour of these compounds is interesting and includes an unidentified SmX phase and a banana phase. The relationships between the chemical structures and mesomorphic behaviours of these materials were established.

Acknowledgments	2
Abstract	3
1 Introduction.....	10
1.1 Liquid Crystals.....	10
1.1.1 A brief history of liquid crystals	11
1.1.2 Morphology of liquid crystals.....	13
1.1.2.1 Calamitic Liquid Crystals.....	14
1.1.2.2 Nematic Phase (N).....	16
1.1.2.3 Smectic Phase	18
1.1.2.4 Smectic A Phase (SmA)	18
1.1.2.5 Smectic C Phase (SmC)	19
1.1.3 Mesophase Identification	19
1.1.3.1 Optical Polarising Microscopy (OPM).....	19
1.1.3.2 Differential Scanning Calorimetry (DSC).....	20
1.1.3.3 X-ray Diffraction	20
1.2 Liquid Crystal Displays	22
1.3 Organic Semiconductors	24
1.3.1 Semiconductors.....	24

1.3.2	Organic Semiconductors and applications	26
1.4	Luminescence	28
1.4.1	Electroluminescence	28
1.4.2	Photoluminescence	30
1.4.3	Fluorescence and phosphorescence	31
1.5	Organic Light-Emitting Diodes (OLEDs).....	32
1.5.1	Single Layer OLEDs.....	33
1.5.2	Bi-Layer OLEDs.....	35
1.5.3	Tri-Layer OLEDs	36
1.5.4	Materials for OLEDs.....	37
1.6	Liquid Crystals as Charge Transport Materials	40
1.6.1	Charge transport in LMMMs	40
1.6.2	Charge transport in polymer materials.....	43
1.7	Organic Photovoltaic Devices (OPVs)	44
1.7.1	Power conversion efficiency of OPVs	44
1.7.2	Construction and Mechanisms of OPVs	45
1.7.3	Materials in OPVs.....	46
1.8	Aryl-aryl, cross-coupling reactions.....	49

1.8.1	The Stille Reaction.....	50
1.8.2	The Suzuki Reaction	51
1.8.3	Direct Arylation of Heteroatom-Containing Aromatic Compounds	53
1.9	References.....	55
2	Research Aims	62
2.1	References.....	66
3	Experimental.....	67
3.1	Evaluation of the Materials.....	67
3.2	Synthetic pathways	72
3.2.1	Scheme 1	72
3.2.2	Scheme 2 and 2.1	72
3.2.3	Scheme 3 and 3.1	73
3.2.4	Scheme 4.....	74
3.2.5	Scheme 5.....	74
3.2.6	Scheme 6-8.....	75
3.2.7	Schemes 9-11	76
3.2.8	Scheme 12.....	77
3.2.9	Scheme 13, 14, 15 and 16	77

3.2.10	Scheme 17-21.....	78
3.2.11	Scheme 22 and 23	78
3.3	Reaction Schemes	80
3.4	Synthesis of the Materials.....	105
3.5	References.....	179
4	Results and Discussion	181
4.1	Synthetic discussion.....	181
4.1.1	Failed schemes	181
4.1.1.1	Scheme 3.1	181
4.1.1.2	Scheme 4	182
4.1.1.3	Scheme 5	182
4.2	Reaction conditions for thiazolo[5,4- <i>d</i>]thiazole	184
4.3	Mesomorphic behaviour and physical properties	189
4.3.1	2,7-Disubstituted-9-Alkylcarbazoles (Scheme 1).....	189
4.3.2	2,7-Disubstituted-9,9-Dialkylfluorenes(Schemes 2, 2.1 and 3).....	191
4.3.3	3-Substituted Carbazoles (Schemes 6-8 and 12)	197
4.3.4	Thiazolo[5,4- <i>d</i>]thiazoles (Schemes 9-11)	207
4.3.5	2,2'-Bithiophenes (Schemes 13-16).....	214

4.3.6	Oxadiazoles (Schemes 17-21).....	221
4.3.7	Isoxazoles (Scheme 22 and 23).....	228
4.3.8	Cyclic Voltammetry (CV) and Ultraviolet–visible spectroscopy(UV-vis)	231
4.4	References.....	236
5	Conclusions.....	240

1 Introduction

1.1 Liquid Crystals

Normally, there are three common states of matters in nature, i.e., solids, liquids and gases. Liquid crystals which exhibit an intermediate state between liquids and solids are often referred to now as a fourth state of matter. This state of matter possesses a higher degree of order than those present in isotropic liquids, but lower than those in crystalline solids. Constituent molecules in liquids can move and rotate freely in all three dimensions, while those in solids are fixed in place, usually on a regular, periodic crystal lattice, and not able to rotate freely. However, in the liquid crystalline state made up of calamitic liquid crystals, i.e., those with a semi-rigid, rod-like or lath-like molecular structure, these molecules are able to move or rotate to some degree, but they also exhibit a specific degree of orientation with the long molecular axes aligned on average in a parallel direction, called the director, n ,^[1] see Fig. 1.1.

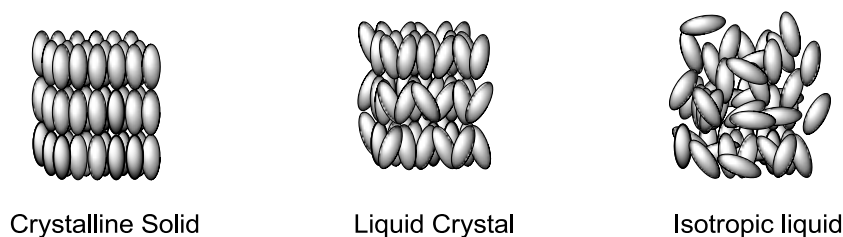


Fig. 1.1 Schematic arrangement of molecules in various phases

The degree of order can be represented by the order parameter S , which is less than unity (crystalline solids), but more than zero (isotropic liquids) and is usually about 0.7 in the liquid crystalline state. Liquid crystalline mesophases formed on heating, such as that observed by Reinitzer, are defined as thermotropic and those formed on the addition of solvents are referred to as lyotropic.

1.1.1 A brief history of liquid crystals

The history of liquid crystals can be dated back to before 1888^[1,2], the year that Friederich Reinitzer^[3,4] discovered this new state of matter. When he was observing the melting behaviour of cholesteryl benzoate, see Fig. 1.2, which he had synthesized himself by esterification of samples of cholesterol isolated from gall stones, he noted a strange “double” melting point for this compound. The crystal sample of cholesteryl benzoate was first transformed into a cloudy, opaque, but coloured fluid, when the sample was heated to a temperature above 146 °C, then into a clear, transparent and colourless liquid at a temperature above 178 °C. He thought that this strange optical behavior could be evidence of a new kind of state of matter and so he sent samples of this material to Otto Lehmann⁵, a professor of physics in Germany and a specialist in optical microscopy. Lehmann also considered that a new class of compounds exhibiting a new state of matter had been found. He named these materials “liquid crystals”^[6] because they appeared to exhibit some of the physical properties of both liquids and solids at the same time.

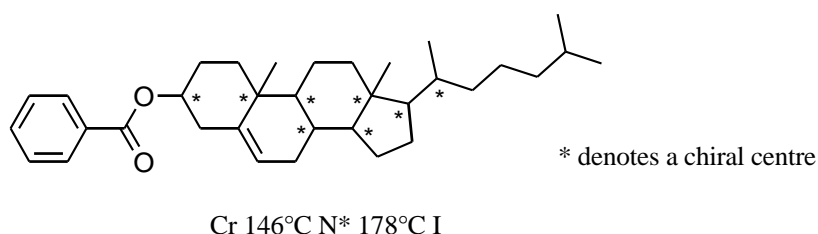


Fig.1.2. Cholesteryl benzoate.

The first totally synthetic liquid crystal was prepared by Gatterman and Ritschke with the synthesis of *p*-azoxyanisole in 1890^[7]. Later in 1922, a French chemist, Georges Freidel, introduced a classification of liquid crystal mesophases, which may be considered as one of the most important developments in the history of liquid crystals^[8]. It was in his research paper ‘Les Etats Mesomorphes de la Matière’ that several different liquid crystal phases were first named as ‘either nematic, smectic or cholesteric phases’. Furthermore, other scientists, for example, Fredericksz^[9], Born^[10], Kast^[11] Lichtennecker^[12], investigated the influences of electric and

magnetic fields on the physical properties of liquid crystalline phases. A systematic programme started by Vörländer^[12] during the early 1900s, was designed to study the relationship between molecular structures and liquid crystalline behaviors and their transition temperatures. As a consequence of this research, he suggested that the liquid crystalline state is usually exhibited by compounds possessing a highly linear molecules with a rigid rod-like or lath-like shape with a high length-to-breadth (aspect) ratio.^[13,14] Later during the war years, there were some experiments on liquid crystals around the world, most of which were carried out in Germany and France, but the work slowed significantly after the Second World War probably due to the fact that no one could imagine a practical application for them.

In 1950s, Onsager^[15] and Flory^[16] contributed to the theory explaining the relationships between the molecular structure of rigid rod polymers and the formation of liquid crystalline phases. The development of these theories generally guided the following research of polymer liquid crystals and further development was promoted by it. Shortly before 1960, interest in liquid crystals re-awakened mostly in the United States, Great Britain and the Soviet Union^[17]. During the 1970s and 1980s, a lot of research on liquid crystals was carried out probably due to the potential development of electro-optical applications using liquid crystals.

In 1973, perhaps the most important landmark in the history of liquid crystals was the synthesis by Gray *et al.*^[16] at the University of Hull of a new class of thermotropic, calamitic liquid crystals, i.e., the 4'-alkyl-1,1'-biphenyl-4-carbonitriles, more commonly known as the 4'-alkyl-4-cyanobiphenyls, see Fig. 1.3, which exhibit either a smectic or nematic phase at or near to room temperature.

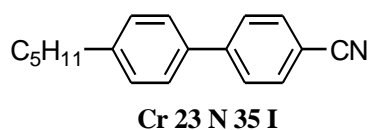


Fig. 1.3. 4'-n-Pentyl-1,1'-biphenyl-4-carbonitrile.

The 4'-alkyl-4-cyanobiphenyls are chemically, photochemically, electrochemically and thermally stable^[18,19,20]. Some homologues of 4-alkyl-4'-cyanobiphenyls and the corresponding terphenyls were used to make nematic mixtures, e.g., E7, for early liquid crystal displays (LCDs) since they exhibit an advantageous combination of the desired physical properties^[18-19].

Nowadays, liquid crystals have become a part of our daily lives, for example, playing an important role in digital wrist watches, pocket calculators, displays in various instrumentation, including devices of computers, televisions, ipads and mobile phones. Liquid crystal displays (LCDs) exhibit the advantages of low power consumption, low-operating voltage, thinness and low weight. Besides, LCDs are competitive with other digital display technologies for attractiveness, ease of viewing, cost, sizes and durability. Currently, research into the development of liquid crystals with new molecular structures is continuing to improve the physical properties of liquid crystals, so that more advanced displays can be realized. Furthermore, liquid crystals also play a key role in interdisciplinary research, involving chemistry, physics, biology, engineering, mathematics, etc, for a wide range of applications, such as pressure sensitive paints, photochromics, and organic semiconductors that are used in plastic electronics²¹.

1.1.2 Morphology of liquid crystals

The liquid crystalline state is usually observed for compounds, which possess either a rod-like or disk-like shape, see Fig. 1.4, since this facilitates a parallel alignment. Fig 1.4 summarises the main types of liquid crystals, i.e., *thermotropic* liquid crystals, which are dependent on temperature, and *lyotropic* liquid crystals, which are formed in the presence of a solvent. This work is mainly focused on thermotropic liquid crystals, so no further discussion of lyotropic liquid crystals will be made. Meanwhile, liquid crystals can also be divided into low-molar-mass materials (LMMs) and

Polymeric ones, according to the molar mass of the liquid crystals, see Fig. 1.4. There are mainly three ways to form polymeric liquid crystals, by side chain, main chain and networks.

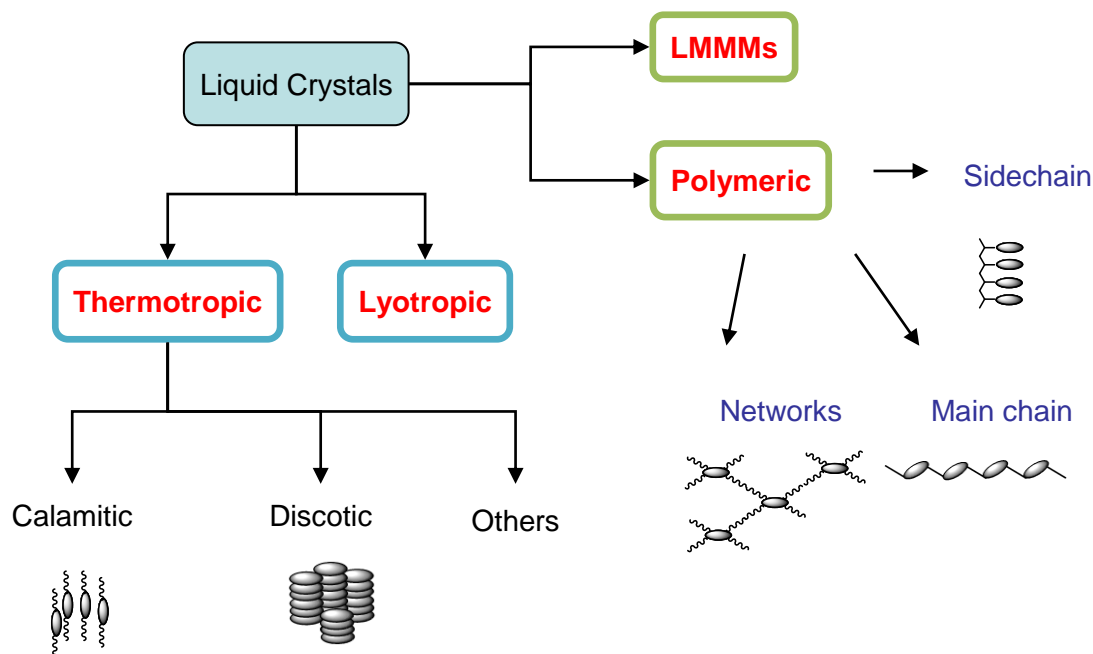


Fig. 1.4. A general classification of liquid crystals.

1.1.2.1 Calamitic Liquid Crystals

Calamitic liquid crystals are rod-like or lath-like in shape and are the most widely studied liquid crystalline sub-group. They usually consist of a relatively rigid, “rod-like” molecular core, often containing co-linear six-membered rings, either aromatic or alicyclic, lateral substituents and flexible or polar end groups. The structure of calamitic liquid crystals can be generally represented as shown in Fig. 1.5.

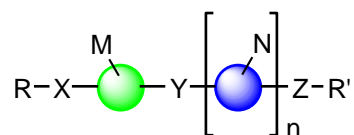


Fig. 1.5. A general model of calamitic liquid crystals.

The R and R' groups are usually aliphatic chains, which can be attached directly to a ring in the molecular core, *e.g.*, alkyl groups, or with a linking group (X, Z) such as an

oxygen atom, *e.g.*, alkoxy groups. The lateral substituents (M, N), each of which can affect the mesomorphic behaviour and physical properties of the compounds, can vary in size, polarity and position. Common lateral substituents include F, Cl, CN, CH₃, CF₃, NO₂, etc. The compounds with lateral substituents usually exhibit lower transition temperatures than analogous materials with a similar structure, but without the lateral substituents.

The mesophases of calamitic liquid crystals can be mainly subdivided into two categories: nematics and smectics, although other mesophases do exist. The usual sequence of liquid crystalline behaviour for a calamitic liquid crystal is summarized in Fig. 1.6^[5]. Not all of the possible calamitic phases are shown in Fig. 1.6. However, a large number of liquid crystals only exhibit one of these two kinds of mesophases. From the diagram, we can see that the melting transition from a crystal state (Cr) to an isotropic liquid (I) or liquid crystalline phase is often irreversible, since a large degree of hysteresis may happen during heating-cooling cycles. However, liquid crystal–liquid crystal transitions involve little hysteresis in temperature and are reversible. The word *enantiotropic* phase is referred to the mesophases that can be observed during the heating cycles, and those which occur below the melting point are called *monotropic* phases.

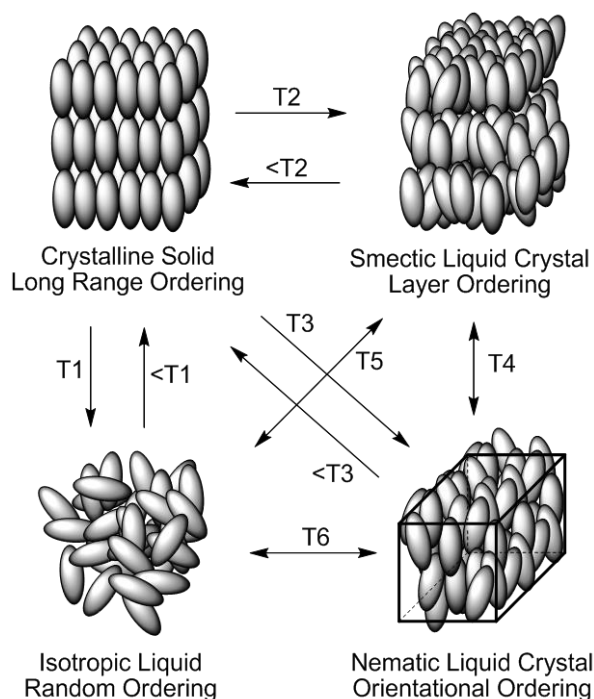


Fig. 1.6. Mesomorphic behaviour of a typical liquid crystal.

1.1.2.2 Nematic Phase (N)

The term “nematic phase” was introduced by Friedel, who derived it from the Greek word *nematos*, meaning thread-like, which is related to the thread-like appearance of the microscopic texture of the nematic phase often observed between crossed polarisers^[22].

The nematic phase is the least ordered of the liquid crystalline phases. In this phase, the compound essentially becomes a one dimensionally-ordered fluid, because there is no long-range positional ordering of the molecules making up the nematic phase. There is only orientation ordering of the molecule in the nematic phase, where the rod-like molecules tend to align with their long molecular axis pointing in the same direction, which is described as the nematic director, n . The structure of the nematic phase is shown schematically in Fig. 1.7.

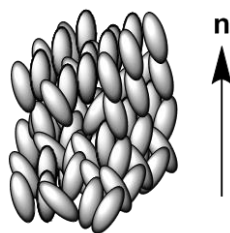


Fig. 1.7. A schematic representation of the nematic phase.

The rod-like molecules in the nematic phase are able to rotate freely about their short molecular axes and, to some degree, about their long molecular axes. An order parameter, S , refers to the degree of alignment of the molecules relative to the director, n , according to the equation shown below:

$$S = \frac{1}{2} \langle 3 \cos^2 \theta - 1 \rangle$$

θ is the angle between the long molecular axis of each individual molecule and the nematic director, n . The equation represents an average of a large number of molecules. If $S=0$, it indicates that all molecules are completely disordered, that means isotropic, while $S=1$ suggests that all the molecules are completely aligned parallel with the director and the phase is ideally ordered, which should actually be a crystalline solid. A higher order parameter always indicates one of the more ordered liquid crystalline phases. Normally, for a nematic phase, the value of order parameter, S , lies between 0.4 and 0.7. The nematic phase can be easily identified by optical polarising microscopy, see Fig 1.8. The nematic phase is the most fluid-like phase with a low viscosity due to its relatively disordered structure. It has been used widely in LCD applications because of its rapid response to an applied weak electric field, partly due to its low viscosity.

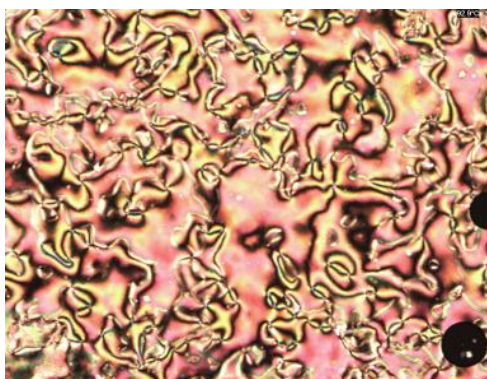


Fig.1.8 schlieren texture of Nematic phase observed from optical polarising microscopy

1.1.2.3 Smectic Phase

The smectic state was also named by Friedel^[21] from the Greek word *smectos*, which means soap-like. Smectic phases are more ordered than nematic phases and always occur at lower temperature than a nematic phase exhibited by the same compound. The different types of smectic phase were recorded using letters and are usually abbreviated to Sm, e.g., SmA. The letters were originally assigned in the chronological order of their discovery^[5]. There are many different types of smectic phases, including five true liquid crystal smectic phases (SmA, SmB, SmC, SmI and SmF), like those shown in Fig. 1.9 and Fig. 1.10. There are six crystal smectic phases (B, J, O, E, K, H)^[23,24,25], which are considered to be soft crystals due to their high degree of order and the fact that they do not exhibit any fluid properties. In smectic phases, the molecules are arranged in layers. The long axis of molecules can be either orthogonal, as in the smectic A (SmA) phase or tilted, as in the smectic C (SmC) phase, with respect to the layer plane.

1.1.2.4 Smectic A Phase (SmA)

The smectic A phase exhibits a layer structure and is the least ordered among all of the smectic phases. Compared with the molecules in the nematic phases, which are free to rotate about their short molecular axis very rapidly also about their long molecular axis with a much lesser degree, the molecules in smectic A phases have an average direction of the long axis, i.e., the director, which is perpendicular to the smectic layer

plane, see Fig. 1.9. The smectic A phase occurs at a higher temperature than other smectic phases exhibited by the same compound. The SmA phase is optically uniaxial as the director is orthogonal to the layer planes.

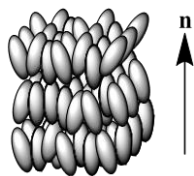


Fig. 1.9. Schematic representation of the smectic A (SmA) phase.

1.1.2.5 Smectic C Phase (SmC)

The molecules in the smectic C phase are arranged in a similar way as those in smectic A mesophase, but with a tilt angle, θ , between the director and the layer plane, Fig. 1.10.^[26,27] As a consequence of the tilt angle, the layer spacing of the smectic C phase is smaller than that of the smectic A phase for the same compound. The layer structure of the smectic A and C phases are not fixed and are more like a density wave, i.e., molecules in these smectic phases can move easily from one layer to another.

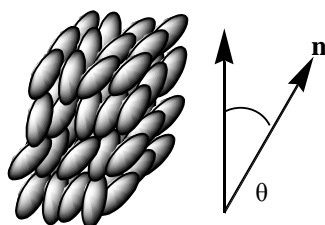


Fig. 1.10. A schematic representation of the smectic C phase.

1.1.3 Mesophase Identification

A combination of some of the following techniques is often used to identify the nature and transition temperatures of the liquid crystalline mesophases exhibited by liquid crystals:

1.1.3.1 Optical Polarising Microscopy (OPM)

This is one of the simplest and widely used technique to identify phase types, often in

combination with Differential Scanning Calorimetry (DSC) and X-Ray Diffraction (XRD) measurements. A thin sample is placed on a glass microscope slide and covered by a glass cover slip. The slide is placed in a temperature-controlled hot-stage, which is then fixed on the microscope, situated between crossed polarisers. If it is isotropic liquid, the light is extinguished, so a black image will be observed in the field of view. When a non-symmetrical crystalline sample or liquid crystals are placed in the microscope in a similar way the transmitted light is not completely extinguished and an optical texture appears because the orientation of the polarised light is altered. This is due to the birefringent nature of these materials. Liquid crystalline phases exhibit various characteristic textures under OPM, which yield important information relating to the structural arrangement of each of the liquid crystalline phases.

1.1.3.2 Differential Scanning Calorimetry (DSC)

This analytical method is used to confirm the number, enthalpy of transition and the transition temperatures of the mesophases exhibited by liquid crystals. This technique involves measuring the enthalpy changes at phase transitions. Two micro-furnaces, each with a separate heater and temperature sensor, are linked together. A reference material, which has a known heat of fusion, is placed in one of the micro-furnaces. The other micro-furnace contains the questioned sample. Then both samples are heated at a constant heating rate. Additional energy, as heat, is supplied to the sample in order to maintain the uniform heating rate at which the desired product undergoes an exothermic transition, such as the melting process, occurs. This measured extra energy input is converted to a value for the enthalpy change (ΔH). DSC is useful for identifying the presence of a phase transition and confirming the transition temperatures determined in many cases using OPM. However, DSC can also be used to identify the presence of glass transitions, which is almost impossible using OPM, and to determine the corresponding glass transition temperature.

1.1.3.3 X-ray Diffraction

X-ray diffraction (XRD) is used to determine the structure of a mesophase and, as a

result, identify the type of the phase. Aligned samples are necessary to distinguish and classify highly ordered smectic or crystal phases. However, this technique is not always required as a combination of DSC and optical microscopy often proves to be sufficient to identify simple mesophases, such as the nematic, smectic A or smectic C phases, while X-ray is very useful in the identification of more ordered phases.

1.2 Liquid Crystal Displays

Liquid crystal displays (LCDs) represent the most important and widespread application of liquid crystal materials to date. LCDs have dominated the market for flat panel displays (FDP) for the past 30 years.^[28,29] The electro-optical characteristics of liquid crystals were widely studied for more than 100 years after their first discovery by Reinitzer^[3] and Lehmann^[5], however, the first operational liquid crystal displays were not fabricated until the late 1960s, e.g., by Heilmeyer et al.^[30] Later in 1969, German researchers^[31] first reported the synthesis of the liquid crystalline compound, 4-methoxybenzylidene-4'-n-butyraniline (MBBA), see Fig. 1.11, which exhibits a nematic phase at and above room temperature. MBBA was suitable for using in dynamic scattering (DS)-LCD applications due to its low or negative dielectric anisotropy ($\Delta\epsilon$), birefringent nature and its mesomorphic behaviour. Unfortunately, the disadvantages of DS-LCD lie in the low clearing point of nematic phase, high operating voltages and low working lifetime, which all limited the commercial success of the DS-LCDs manufactured.

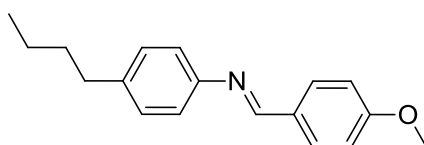


Fig. 1.11 Structure of 4-methoxybenzylidene-4'-n-butyraniline (MBBA)

Thereafter, a wide variety of different types of LCDs were created and studied, which were mostly based on nematic liquid crystal materials^[32], including electrically controlled birefringence (ECB)-LCDs^[33,34,35], twisted nematic (TN)-LCDs^[36], super twisted nematic (STN)-LCDs^[37,38,39], super birefringent effect (SBE)-LCDs^[40] and active matrix (AA), thin film transistor (TFT)-LCDs^[41]. All these displays share the common advantages of a thin planar construction, low weight, low operating voltages and power consumption, as well as acceptable to very good optical contrast and viewing angles. The detailed differences between these LCDs will not be discussed in this work as the research for this thesis was not designed for LCDs. The TN-LCD, as

the most successful type of LCD, normally consists of a nematic liquid crystal mixture of positive dielectric anisotropy contained in a cell with an alignment layer on both substrate surfaces, usually rubbed polyimide, crossed polarisers and a cell gap of 5-10 μm ^[32], see Fig. 1.12.^[42]

Thin film transistor (TFT)-LCDs use active-matrix addressing technology, which is different from passive-matrix LCDs or simple, direct-driven LCDs with a few segments, to improve image quality. The large scale manufacture of TFT-LCDs started a new era of very fast displays with very high information content, full colour and video rate addressing for moving images as well as the manufacture of very large-area LCDs. This active matrix-addressed technology led to TFT-LCDs becoming the dominant LCD type in the commercial market, especially after their price unexpectedly fell in 1995^[43]. Benefiting from the high information content, TFT-LCDs are widely used in lap-top computers, TVs, ipads, mobile phones, etc.

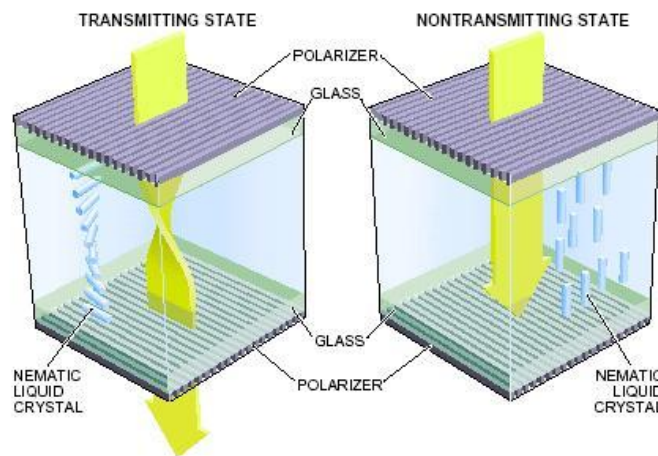


Fig. 1.12 Representation of a twisted nematic liquid crystal display (TN-LCD)^[42]

1.3 Organic Semiconductors

1.3.1 Semiconductors

According to their ability to conduct an electric current, materials can be categorized broadly into conductors, semiconductors and insulators(dielectrics)^[27].The difference can be explained using energy band theory, see Fig. 1.13.According to this theory, materials have energy levels fully filled with electrons (valence band) and empty energy levels (conduction band).

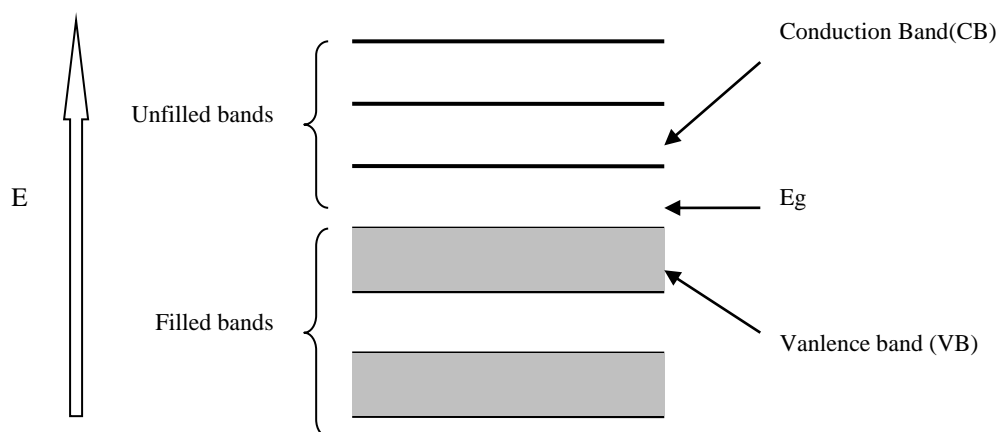


Fig. 1.13 Band structures by energy band theory

In conductors, such as metals, for example, the energy levels between the conduction bands (CB) and valence bands (VB) are closely spaced or sometimes the bands even overlap. Consequently, the band gap (E_g), which is a forbidden energy gap between the highest energy states of the VB and the lowest energy states of the CB, is very low. As a result, the electrons can be easily promoted into new energy levels and move freely in the CB under room temperature as very little energy is required. Therefore, an electrical current is able to flow through the conductor when a potential is applied.

Insulators (dielectrics)do not conduct electricity because the band gap is too wide for

the electrons in the valence band to overcome. Valence electrons, especially in organic compounds, are not able to move freely throughout insulators. If the electrons are free to move within the bulk of the material, they just occupy a position in the valence energy levels. Therefore, no half-filled energy level with free electrons or holes exists and no technically-relevant conductivity is observed.^[44, 45]

Semiconductors exhibit an electrical conductivity between that of conductors and insulators. In semiconductors the magnitude of the band gap lies between that of conductors and insulators, e.g., several eV. At absolute zero (0 K) semiconductors are insulators, as they have both a fully filled valence band and a completely empty conduction band. However, when a quantum of energy with a value greater than E_g is absorbed by semiconductors, an electron can be promoted into one of the empty and available energy states of the conduction band. In semiconductors, at room temperature, the thermal energy is high enough to promote sufficient electrons into the CB, while leaving holes in VB, to generate an electrical current. Electrons and holes are called charge carriers.^[46] A schematic representation of the energy levels and band gaps in conduction, semiconductors and insulators is shown in Fig. 1.14^[28].

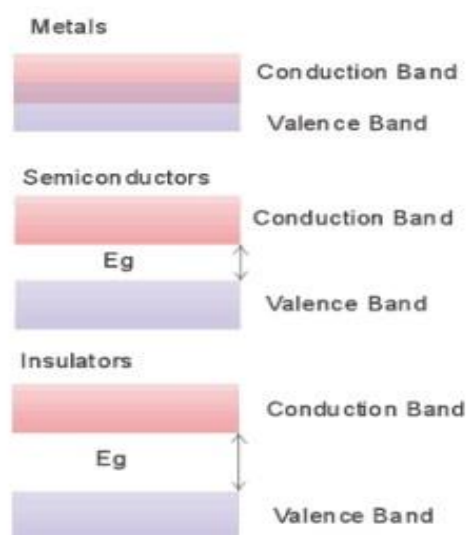


Fig. 1.14. Schematic representation of energy levels and the band gap between the valence and conduction bands^[28].

Semiconductors can be modified to produce higher degrees of conductivity by various techniques, usually doping or gating, into two different types: p-type semiconductors, containing electron-deficient dopants, and n-type semiconductors, incorporating electron-rich dopants.^[47,48,49]

1.3.2 Organic Semiconductors and applications

Organic semiconductors are defined as organic materials, which exhibit semiconductor properties, rather than acting as insulators as many organic compounds do, due to the fact that the valence electrons in most organic compounds are very tightly bound and fixed in place in covalent bonds between individual atoms. However, when a high degree of conjugation is present in the molecular core of large aromatic compounds and these electrons exhibit a high degree of delocalization, then these organic compounds may act as semiconductors^[50]. The π_{pz} orbitals in carbon-carbon double bonds of unsaturated organic compounds overlap to form a pair of π molecular orbitals. The lower energy level π orbital is the bonding molecular orbital and the higher energy π^* orbital is the anti-bonding molecular orbital^[51]. The bonding and anti-bonding orbitals in organic semiconductors, which are usually called highest occupied molecular orbitals (HOMO) and lowest unoccupied molecular orbitals (LUMO), respectively, can be regarded as equivalent to valence band and conduction band of inorganic or metallic semiconductors and conductors, respectively. Consequently, the band gap is the energy difference between the HOMO and the LUMO of an organic semiconductor, see Fig. 1.15.

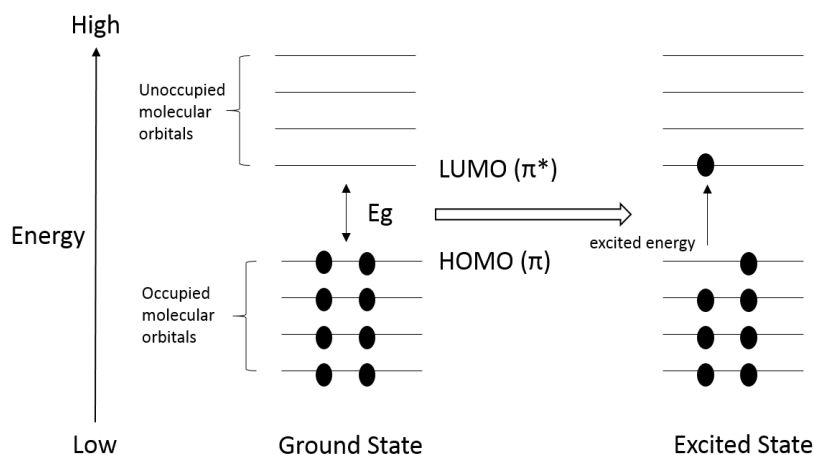


Fig. 1.15 . Schematic representation of HOMO, LUMO, ground state and excited state of organic semiconductors

Organic semiconductors can be single molecules, oligomers, or polymers, see Fig. 1.16. These materials have a wide application in various fields, for instance, organic photoconductors in copy machines and laser printers, organic field-effect transistors (OFETs)^[52], low-cost organic electronics (smart labels), solar cells/organic photovoltaic (OPVs) and organic light-emitting diodes (OLEDs), etc.

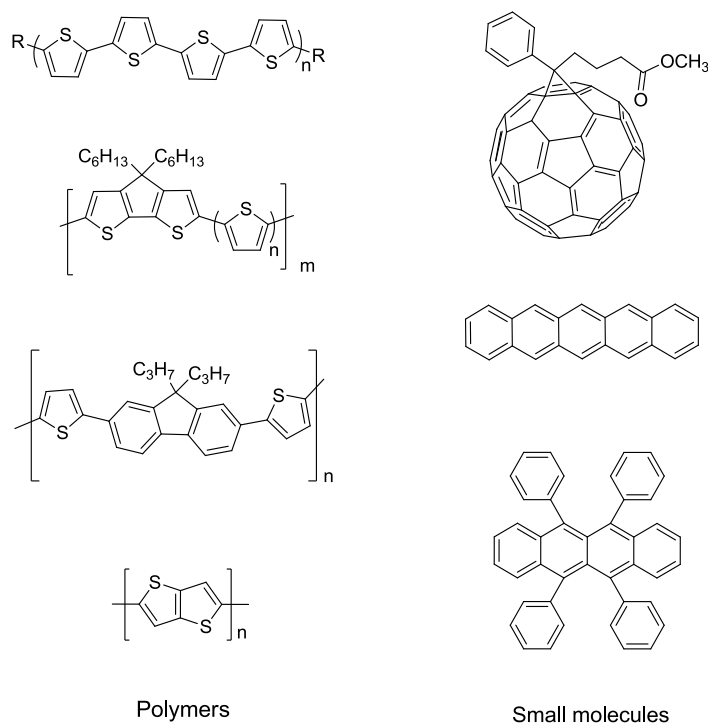


Fig. 1.16. Structures of some common organic semiconductors

1.4 Luminescence

Luminescence means the emission of light from an excited electronic state of a substance. The first record of luminescence in scientific reports dates back to at least the middle of the 18th century. Sir J. F. W Herschel^[53] reported in 1845 that in one of his experiments 20 years earlier, he had observed a blue colour that was emitted from a colourless solution of quinine in water under certain conditions. He concluded that a kind of “specie” in this solution, “exerts its peculiar power on the incident light” and disperses the blue light.^[54] The term 'luminescence' itself was introduced in 1888 by Eilhard Wiedemann.^[556]

Luminescence is divided into various types according to the cause for emitting light, which can be a result of a chemical reaction (chemiluminescence), a biochemical reaction by a living organism (bioluminescence), crystallization (crystalloluminescence), a mechanical action on a solid (mechanoluminescence), etc. In this work, we will limit the discussion to two of the most widely researched forms of luminescence, i.e., electroluminescence, which is results from an electric current passing through a substance, such as a semiconductor, and photoluminescence, which is caused by the absorption of photons.

1.4.1 Electroluminescence

Electroluminescence (EL) is defined as luminescence caused by the passage of an electric current through a light-emitting substance. It can convert electrical energy directly into light. Inspired by this phenomenon, people invented light emitting diodes (LEDs) which emit light under an applied voltage through a thin layer of electroluminescent material, usually a semiconductors. The first commercial LEDs were manufactured in the early 1960s, using inorganic semiconductors such as GaAsP, However, the first LEDs were simple monochromatic, alpha-numeric, digital displays with a very low-information-content.^[57] LEDs based on improved inorganic semiconductors exhibit very high electroluminescence efficiency. However, the high

cost and difficulties in the manufacture of high-information-content, full-colour (RGB) LED have driven the study and development of organic LEDs (OLEDs), which are inherently more promising as large, full-colour flat panel displays.

Electroluminescence from organic materials was first observed using a very thick (~5 mm) single crystal of anthracene (Fig. 1.17) at high voltage ranging from 400-2000 V using liquid electrolytic electrodes for charge injection to generate blue light emission.^[58,59,60] It was found that a much lower threshold voltage can work using thin wafers of cleaved anthracene crystals or thin films with solid electrodes.^[61] However, the efficiency of these devices was still very low.

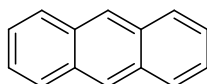


Fig. 1.17: Chemical structure of anthracene.

Much more efficient OLEDs with much lower operating voltages were made thanks to the introduction of vapour-deposited thin films.^[62] In 1987, Tang and van Slyke^[63] reported efficient electroluminescence from *tris*(8-hydroxyquinolate)aluminium (III) (Alq₃), see Fig. 1.18 (a), from a bilayer OLED. In 1989 efficient electroluminescence was also observed by Richard Friend and colleagues from a highly conjugated main chain polymer, i.e., poly(*para*-phenylenevinylene) (PPV), see Fig. 1.18 (b),^[64]

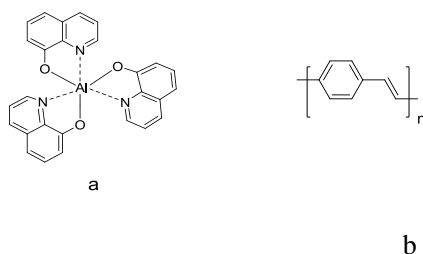


Fig. 1.18: Chemical structure of (a) *tris*(8-hydroxyquinolate)aluminium (III) (Alq₃; and (b). poly(*para*-phenylenevinylene) (PPV).

The advantage of organic EL materials is that their wavelength of emission can be practically controlled by modifying chemical structures, as the emission colour is depending on the value of energy band gap between HOMO-LUMO.

1.4.2 Photoluminescence

Photoluminescence (PL) is another kind of luminescence caused by absorption of photons to excite electrons in the valence band into higher energy state, i.e., the conduction band, which then relax back to the ground state accompanied by the emission of light. The re-emitted light is normally emitted with a red shift due to the Stokes shift.^[65] The time between absorption and emission is extremely short, typically in the order of 10 nanoseconds.^[66] This period can last longer to minutes or hours under some special circumstances. In highly conjugated organic molecules, light absorption can give the desired product as rise to an $n\text{-}\pi^*$ or $\pi\text{-}\pi^*$ transition,^[32] where electrons are promoted from HOMO to LUMO, followed by a thermal relaxation to the bottom of LUMO, before relaxation to the HOMO by the emission of a photon, i.e., ground state, see Fig. 1.19 for a typical Jablonski diagram describing these luminescence phenomena.

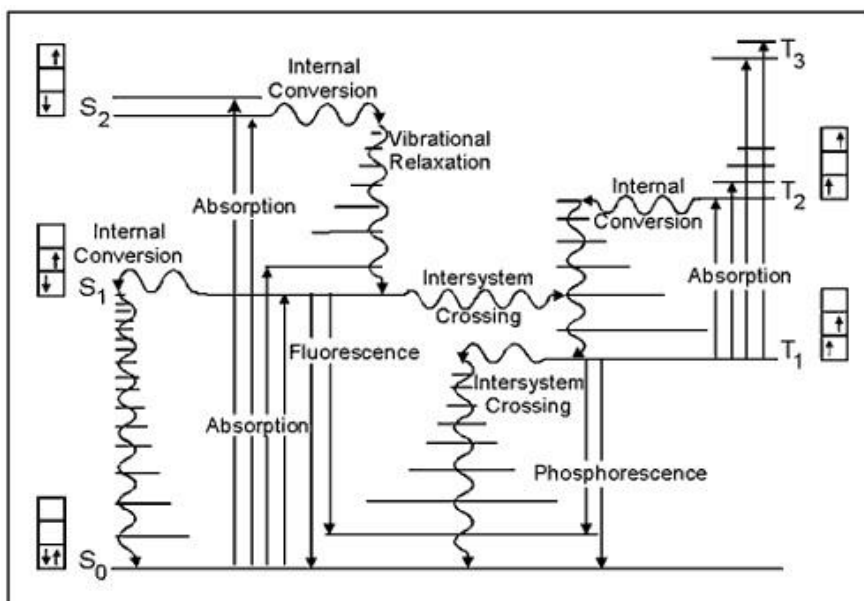


Fig. 1.19 Partial energy diagram for a photoluminescence system (the Jablonski diagram)

1.4.3 Fluorescence and phosphorescence

Luminescent organic materials are often divided into two main types, which are referred as being either fluorescent or phosphorescent. The difference lies in different states from which the excited electrons are relaxed back to the ground state. As shown in Jablonski diagram (Fig. 1.19), the ground, first and second singlet states are marked as S_0 , S_1 and S_2 and the first triplet states are marked as T_1 . Fluorescence occurs when the excited electrons relax from the singlet state (S_1) to the ground state. Phosphorescence is the process whereby relaxation of excited electron to the ground state occurs from the triplet state (T_1).

Besides fluorescence, there are a number of alternative relaxation mechanisms for electrons in excited singlet states. For instance, internal conversion is a kind of radiationless process, whereby molecules in excited states may return to ground state by converting all the excitation energy into heat and emission of a photon does not occur.^[67]

In phosphorescence, the electrons in the triplet state can be achieved both by direct absorption of light and transition from singlet state whereby the latter process is more efficient than the former. In other words, the electrons in the S_1 state can undergo a spin conversion to the first triplet state T_1 ^[67], which is called intersystem crossing, see Fig. 1.19 above.

1.5 Organic Light-Emitting Diodes (OLEDs)

An organic light-emitting diode (OLED) is a flat-panel display device incorporating a series of organic thin films between two electrodes, i.e., an anode for hole injection and a cathode for electron injection. When an electrical current passes through the organic layers and between the electrodes under the application of a bias voltage, light is emitted by one of the organic layers. As an emissive technology, OLEDs do not need a back-light unlike LCDs, which render OLEDs more promising than LCDs in terms of overall efficiency and very wide viewing angles due to the Lambertian emission of light as well as a very thin device configuration. Another advantage is that OLEDs exhibit very high image sharpness and resolution. A combination of these properties results in thin, very compact and highly efficient flat panel displays. OLEDs have a wider viewing angle, up to 160 degrees, than LCDs, as well a slower power consumption, i.e., 2-10 volts, than LCDs, which provides for a maximum efficiency and helps minimize heat and electric interference in electronic devices⁶⁸.

The configuration of current commercial OLEDs often involves a metallic cathode, e.g., LiF-doped calcium with a low work function, an anode, usually Indium Tin Oxide (ITO), with a high work function, an electron-transporting/hole blocking layer (ETL), a highly-efficient fluorescent or phosphorescent emitter or a combined transport and emission layer (EL), a hole-transporting/electron blocking layer (HTL), and a hole-injection layer, which is often poly(3,4-ethylenedioxythiophene)-poly(styrenesulfonate) (PEDOT:PSS), although this has been replaced in the latest OLEDs^[32].

A variety of classes of electroluminescent organic materials have been used in OLEDs, such as low-molar-mass materials (LMMs), oligomers, side-chain polymers, polymer blends, conjugated main-chain polymers and cross-linked polymers networks.

1.5.1 Single Layer OLEDs

Single layer OLEDs possess a simple sandwich structure, consisting of a layer of organic electroluminescent material placed between a cathode and an anode on a solid transparent substrate, such as glass, see Fig. 1.20.

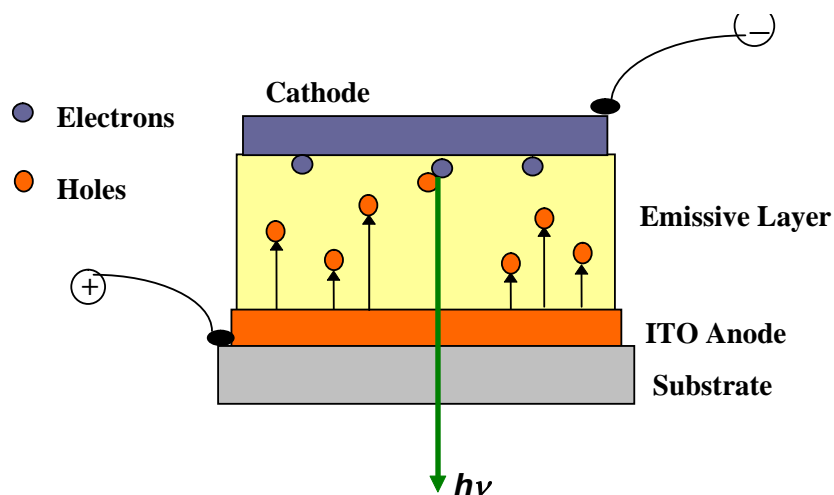


Fig. 1.20. A typical single layer device structure

The most common anode material is Indium/Tin Oxide (ITO), which possesses good electrical conductivity and transparency with a high work function^[69]. A thin layer ($\approx 7\text{-}15$ nm) of metal, such as LiF-doped aluminium, calcium or a magnesium/silver alloy, is used as a cathode with a low work function. In the single layer OLED, the electrons and holes are injected from the cathode and anode, respectively. Recombination of an electron with a hole then promotes an electron into the lowest unoccupied molecular orbital (LUMO) from the highest occupied molecular orbital (HOMO). Then as a result of the applied electric field, the anion charge-carriers (electrons) and cation charge-carriers (holes) move through into the organic emissive layer and recombine there to form either a singlet or triplet excited state, from which they relax to the ground state accompanied by the emission of a photon of visible light. However, relaxation from the triplet excited state often occurs by a non-radiative, thermal pathway.

Some of the major processes operating within an electroluminescent device are summarised in Fig. 1.21^[70].

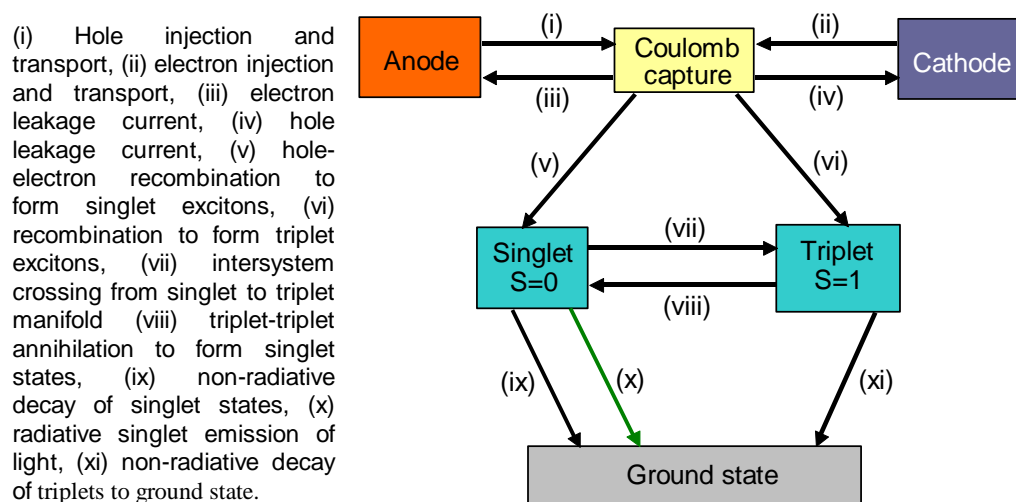


Figure 1.21^[70] A summary of the main processes operating in a simple electroluminescent device.

Some electroluminescent polymers, such as poly(*p*-phenylenevinylene) (PPV), see Fig. 1.18, tend to exhibit a low electron affinity (EA). Impurities in the film are often electronegative and serve to trap electrons. These phenomena, therefore cause imbalances in the holes/electron injection and transport and, consequently, reduce the actual efficiency compared with the theoretical value. Furthermore, when excited states are formed by the recombination of holes and electrons, three times as many triplet states as the fluorescent singlet states are produced. As a result, a low device efficiency is observed due to the unbalanced charge injection and recombination, since in a single-layer device, electron-transport, hole-transport and light-emission all happen within one layer of organic material. Significant leakage currents can also occur, if holes or electrons pass through the organic emissive material without recombination.

From Fig. 1.22, we can clearly see that, another problem for improving the device performance is the matching of the work functions of the electrode materials and the energy levels of the active organic materials. In order to solve these problems, two or

more organic layers are used in multi-layer OLEDs to match the work function of cathode and anode with the HOMO and LUMO energy levels of the electroluminescent layers.

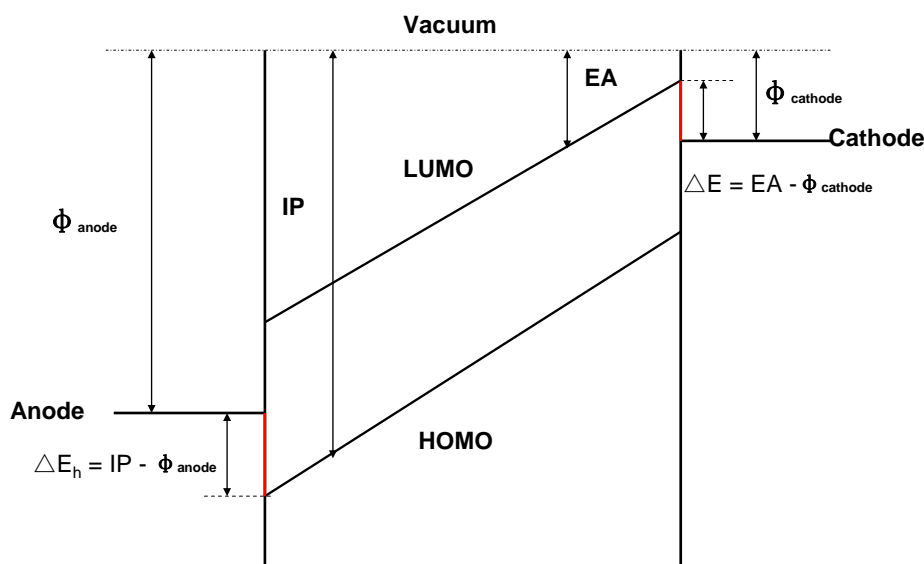


Fig. 1.22. Energy barriers for charge injection for a single layer OLED.⁷¹

1.5.2 Bi-Layer OLEDs

In order to improve the efficiency of the single-layer devices mentioned above, multilayer OLEDs were produced. It was found that multilayer OLEDs could exhibit higher luminous efficiency, lower threshold and operating voltages, leading to a significant reduction in power consumption. Furthermore, the life-time of multilayer devices, such as bi-layer OLEDs, tends to be much longer than those of single layer OLEDs using either electroluminescent low-molar-mass materials (LMMs) or highly conjugated main-chain polymer materials (PMs).^[71]

In order to ensure charge recombination and exciton formation within the emissive layer, an electron-transporting/hole-blocking (ET-HB) layer was added to bi-layer OLEDs. The device structure is similar to that of a single layer device, but with the

addition of an ET-HB layer between the emissive layer and the cathode. A typical bi-layer device is shown in Fig. 1.23^[72].

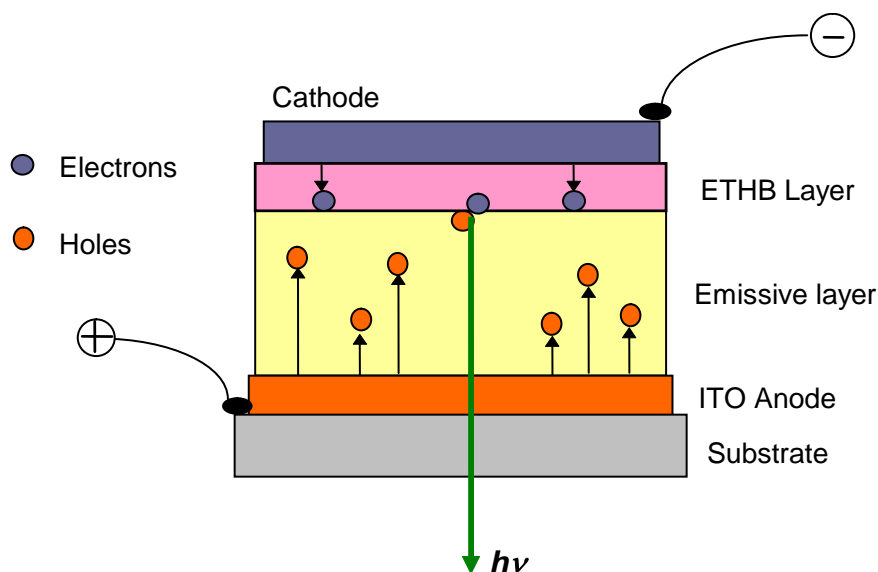


Figure 1.23A typical Bi-layer device structure^[72]

One example of an efficient bi-layer polymer organic light-emitting diode (PLED) was demonstrated by Friend et al (1992)^[73] using poly(*p*-phenylene-vinylene) (PPV) as the hole-transporting/emissive layer and an electron-transporting/hole-blocking layer of 2-(biphenyl-4-yl)-5-(*tert*-butylphenyl)-1,3,4-oxadiazole (PBD). An eight fold increase in efficiency was observed for this bi-layer device compared to a similar single layer OLED using PPV as the emissive layer.

1.5.3 Tri-Layer OLEDs

A typical tri-layer OLED, see Fig. 1.24., consists of glass substrate with an ITO anode deposited on top, then hole-transporting layer (HTL) emissive layer (EL) in the middle, followed by electron-transporting layer (ETL) and a cathode. An advantage of tri-layer OLED is that the electroluminescent layer can be very thin (< 100 angstroms), which means that the electrons and holes can be constrained to a very small area, which ensures a very high degree of charge recombination and, consequently, the light emission is more efficient and the multi-layer OLED is much brighter.

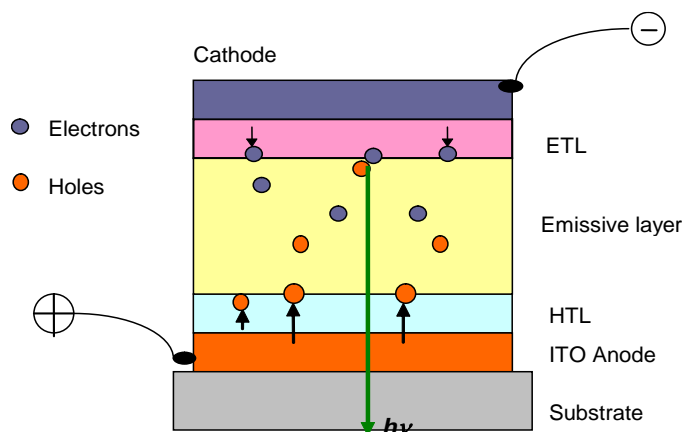


Fig. 1.24. A typical tri-layer device structure.

The tri-layer OLED was first developed by Adachi et al.^[74] One of the major drawbacks of the multilayer architecture of such OLEDs is that inter-layer mixing may occur when depositing the individual layers, e.g., using vapour-deposition or using spin-casting techniques from solution.

1.5.4 Materials for OLEDs

One of the advantages of using organic materials lies in the very large number of compounds that are potentially available. Novel materials can be made to emit light of different wavelengths, achieve brighter electroluminescence and/or transport charge more efficiently by modifying their molecular structures.

Organic materials used in commercial OLEDs are usually either low-molecular-mass materials (LMMs) or highly conjugated main chain polymeric materials (PMs). LMMs benefit from their thermally, chemically, photochemically and electrochemically stable properties also the capability of being deposited as a pure, uniform, thin solid film by vapour deposition under high vacuum. However, one of the disadvantages of LMMs is that they are more likely to form polycrystalline films, which can result in the formation of crystal grain boundaries, which can act in turn as quenching sites for electroluminescence and thereby reduce the OLED efficiency. On the other hand, polymers do not have such problems as they tend to

form glassy films without crystal boundary defects. Another essential requirement for OLEDs is a very high purity of materials, since dramatic reductions in the OLED performance can be caused by the presence of very small amounts of impurities, which may act as dopants or quenching sites. Polymers are, however, often more difficult to purify than small molecules. Sometimes rigid polymers are more difficult to process due to limited solubility in common organic solvents used to deposit organic compounds from solution by spin coating, or doctor blade techniques, for example. Two main approaches were proposed to solve these problems. One is to synthesize a soluble precursor polymer to form the thin film by being processed from solution, followed by further steps, such as heating, to convert these films into the desired polymers effectively *in situ* on the device substrate. This method suffers from a problem of producing conducting by-products in the final chemical conversion step. The other way is to modify the molecular structure of the polymer in order to improve its solubility, e.g., some soluble PPV derivatives were synthesized for use in OLEDs.^[75,76,77]

Organic luminescent compounds often consist of a molecular core consisting of a number of chromophoric functional groups made up of a number of aromatic rings, e.g., some typical functional groups are shown in Fig. 1.25. The design of aromatic compounds for use in OLEDs and the choice of their functional groups depends on the desired role of the target compound in the OLED, e.g., they may be required to transport holes or electrons and/or emit bright visible light. When designing charge-transport materials, the valence and conduction band equivalents, i.e., the HOMO and LUMO energy levels, have to be matched with the work function of the anode and the cathode, respectively. This requirement can be achieved by design of the molecular structures of the organic semiconductors to be used in the OLEDs. The brightness and the colour of a desired product with a given chromophore can also be adjusted by modification of the molecular structure as required.

Many more factors must be considered in order to render OLEDs commercially

successful, e.g., they must be stable over long periods of time, i.e., exhibit a sufficiently long life-time. However, the brightness should not decay over time and the operating voltage should also remain as constant as possible.

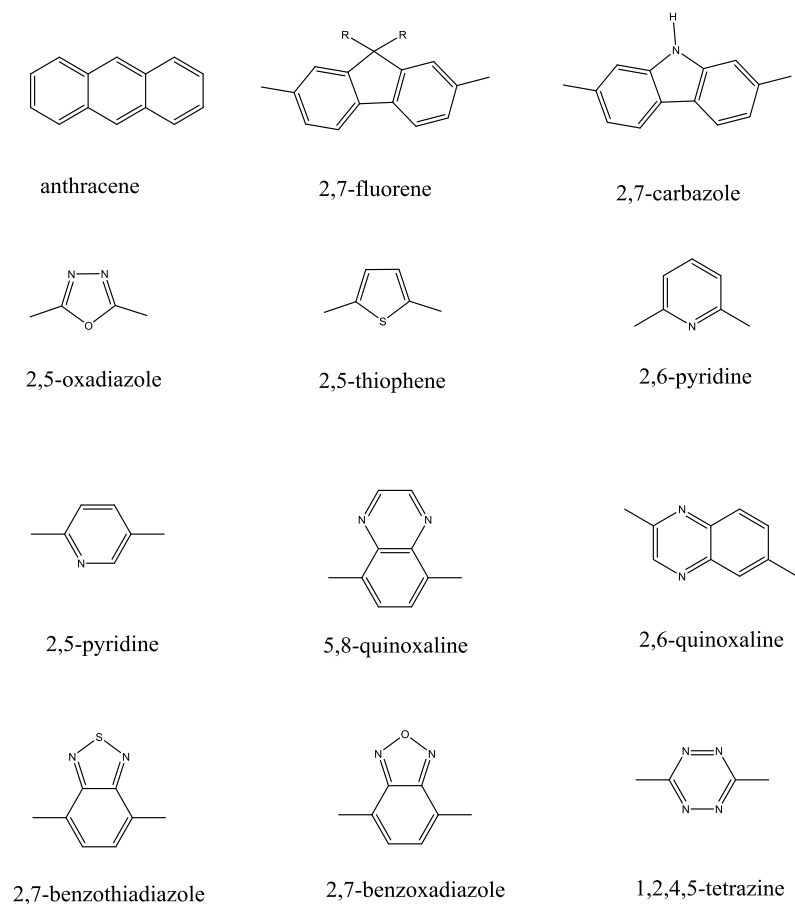


Fig. 1.25. Typical aromatic chromophores useful as emissive materials

1.6 Liquid Crystals as Charge Transport Materials

In order to improve the performance of electroluminescent devices, a very wide range of charge transport materials have been synthesized, evaluated and optimized either as separate charge-transport layers, dopants or used in combined emissive/charge-transport layers. Compounds containing an electron-deficient moiety, such as nitrogen-heterocycles, for example, 2,5-disubstituted-1,3,4-oxadiazole rings, are usually used as electron-transporting layers (ETL) or combined electron-transporting/hole-blocking materials (ET-HB) in OLEDs due to their high electron affinity. Electron-rich aromatic rings with a low ionisation potential, such as 2,5-disubstituted thiophene rings, are often present in hole-transporting layers (HTL), or combined hole-transporting/electron-blocking materials (HT-EB). For example, the electron-transport material 2-(4-biphenyl)-5-(5-*tert*-butylphenyl)-1,3,4-oxadiazole (PBD, Fig. 1.26) has been synthesized and used as a dispersion in poly(methylmethacrylate) as an electron transporting/hole-blocking (ET-HB) layer.^[73]

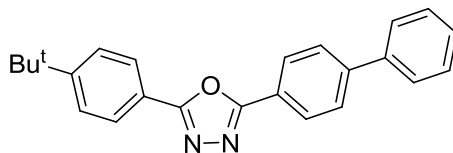


Fig. 1.26 PBD – An electron transport/hole blocking materials for electroluminescent devices

Liquid crystalline materials have also been investigated for use in OLEDs because they were expected to exhibit a higher charge carrier mobility than materials in the crystalline state or in the liquid state, because they possess a high degree of molecular order without grain boundary defects and traps. Studies by Haarer in 1990s have proved that liquid crystals can indeed have high charge carrier motilities.^[78]

1.6.1 Charge transport in LMMMs

In order to act as effective charge-transport materials, low-molar-mass materials

(LMMMs) are expected to be semiconductors with a very specific physical property profile. An essential requirement is the ability to be deposited as thin, uniform solid film by vapour deposition under high vacuum with a very high degree of purity. Secondly, a high glass transition temperature is desired in order to avoid crystallization of the film with the creation of crystal boundaries around crystalline domains that act as traps for charge carriers and also lead to quenching of emission. Finally, LMMMs should exhibit thermal, chemical, photochemical and electrochemical stability over the operational life-time of the OLED. For liquid crystalline LMMMs, charge is usually transported by an intermolecular hopping mechanism. A wide range of inconclusive studies have been carried out in order to establish the nature and transport of charge in the nematic phase of a range of materials, especially of ions during the research of their electro-optic performance in LCDs before they were proposed to be used as charge transporting materials in OLEDs. ^[79]It was initially found that the charge transport through the nematic phase under an applied electric field was mainly ionic in nature and not electronic. ^[80,81]However, in the ordered columnar liquid crystalline phase and smectic phases, it was proved that the photo-generation of electrons and holes and their transport under applied electric field are both electronic that their subsequent mobility through the liquid crystalline material can be quite high ($10^{-1} \text{ cm}^2\text{V}^{-1}\text{s}^{-1} > \mu > 10^{-3} \text{ cm}^2\text{V}^{-1}\text{s}^{-1}$). ^[82,83,84] Therefore, LMMMs as organic semiconductors possessing more ordered liquid crystalline phases were studied as potentially very efficient charge transporting layers. A good example of these studies are the hexakis(*n*-alkoxy)triphenylenes, see Fig. 1.27 (a), which were found to exhibit a similar magnitude of hole mobility in the columnar phase as that determined for some organic single crystals. ^[85,86]The charge, i.e., holes, travels unidirectionally through the highly conjugated and planar aromatic cores, i.e., parallel to the director (along the columns), of the disc-shaped molecules that are aligned with the columns orthogonal to the substrate, because of the insulating nature of the aliphatic chains.

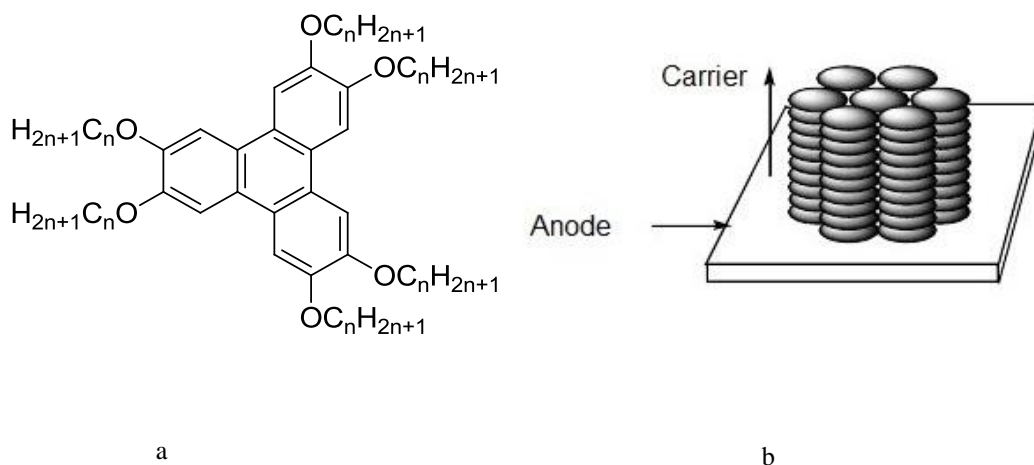


Figure 1.27: Chemical structure of triphenylene(a) and the schematic representation of charge mobility in columnar phase(b).

The benzothiazole, see Fig. 1.28 (a), is a good example of an organic semiconductor in the smectic phase. The charge carrier mobility was found to be two orders of magnitude higher in the (ordered) smectic A phase than that in the (isotropic/disordered) liquid state of the same compound.^[87] This good charge carrier mobility is due to the fact that, the molecules are aligned in layers in the smectic A phase with the director is parallel to the long axis and orthogonal to the layer plane.

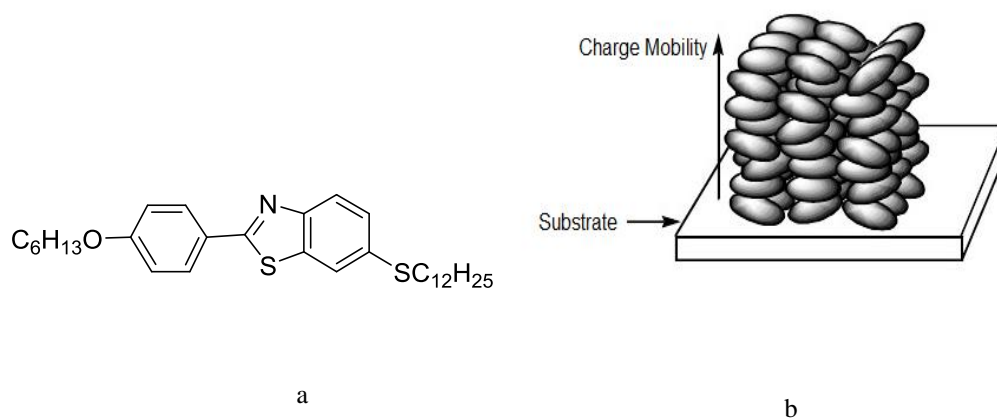


Figure 1.28:(a)Chemical structure of a benzothiazole compound and (b)Schematic representation of charge mobility in a smectic A phase.

1.6.2 Charge transport in polymer materials

One problem with using LMMMs is that they have tendency to crystallize during device operation as a consequence of their low glass transition temperatures, e.g., OLEDs using 2,5-disubstituted-1,3,4-oxdiazoles as an electron-transport layer suffered from crystallisation problems. In order to solve this problem, analogous oxadiazole-based polymers were developed.^[88] In order to be used as an amorphous, non-crystalline electron-transport layer, the polymer materials must exhibit a stable, high glass transition temperature and a high electron affinity.

Unfortunately, most conjugated aromatic polymers tend to transport holes rather than electrons as a result of the high density of delocalized electrons in aromatic rings. The presence of electron deficient atoms, such as nitrogen and oxygen in the aromatic rings making up the aromatic core of the polymer, can help to increase the electron affinity, so the polymers can be suitable to transport electrons, as similarly expected for LMMMs. Besides, polymers are more frequently used in OLEDs as hole-transport and emissive layers rather than electron-transporting layers.

The main practical problems for polymer-based OLEDs (PLEDs) lies in the requirement for a very high degree of purity and good solubility in common organic solvents used to deposit layers of organic semiconductors from solution, e.g., by spin coating, doctor blade techniques, inkjet printing, etc.

1.7 Organic Photovoltaic Devices (OPVs)

Organic photovoltaic devices (OPVs) use organic semiconductors to convert visible light and sometimes infrared (IR) or ultraviolet (UV) radiation into direct current (DC) electricity.

1.7.1 Power conversion efficiency of OPVs

Compared with the commercial inorganic solar cells, devices using organic materials should be cheaper, more robust and simpler to manufacture, especially as large-area devices. However, the power conversion efficiency (PCE) of OPVs for sunlight still remains low (up to 4.2%^[89]), which lags behind the performance of inorganic solar cells (as high as 24%^[90] for single crystal silicon). The reported efficiency for OPVs for monochromatic light is often significantly higher, but this fact is not of wide general commercial relevance.

The PCE can be obtained by calculation through Eq. 1.01, where η_{PCE} stands for power conversion efficiency; P_{in} is the incident optical power density.

$$\eta_{\text{PCE}} = J_{\text{SC}} V_{\text{OC}} \text{FF} P_{\text{in}}^{-1} \quad \text{eq. 1.01}$$

As Eq. 1.01 shows, the performance of OPV is mainly determined by the short-circuit current density J_{SC} , the open-circuit voltage V_{OC} , and the fill factor (FF), which is the ratio of the actual maximum obtainable power to the product of the V_{OC} and J_{SC} , see Eq. 1.02.

$$\text{FF} = V_{\text{mp}} I_{\text{mp}} / V_{\text{oc}} J_{\text{sc}} \quad \text{eq. 1.02}$$

Here, V_{mp} is the maximum point of voltage and I_{mp} is maximum point of current density.

1.7.2 Construction and Mechanisms of OPVs

Fig. 1.29 shows the construction and working mechanism of a typical bulk heterojunction, multilayer organic photovoltaic cell (OPV), which contains two different layers (electron-donating layer and electron-accepting layer) located between the conductive electrodes with different work functions, as in an OLED. The layer of electron acceptor must possess a high electron affinity (EA) and the layer of electron donor should exhibit a low ionization potential (IP). When photons of incident light of sufficient energy is absorbed, electrons will be excited to the LUMO and leave holes in HOMO to form excitons as a bound electron/hole pair. The potential created by the different work functions between two electrodes helps to separate the exciton pairs, pulling electrons to the positive electrode and holes to the negative one. This process is a form of charge photogeneration.

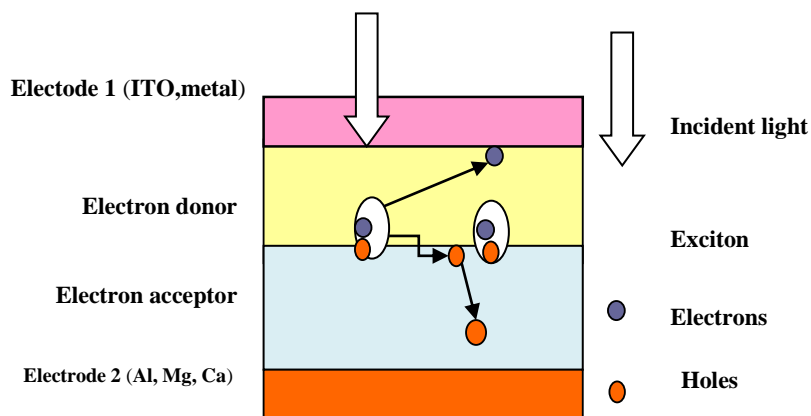


Fig. 1.29. Sketch of multilayer organic photovoltaic cell

One of the primary limitations of this OPV configuration is that charge photogeneration takes place only in a very thin boundary layer at the planar heterojunction between the electron-donating and the electron-accepting layers. Therefore, a range of OPV cells have been designed with a distributed heterojunction, in order to increase the interface between the electron-donating and the

electron-accepting layers. This configuration also shortens the path to the electrodes and so reduces the degree of charge carrier recombination that reduces the current flowing through the OPV cell, which is a second major disadvantage of bulk heterojunction OPVs. The diffusion distance of holes and electrons in organic semiconductors is some tens of nanometers, so the recombination of dissociated holes and electrons to generate heat, rather than electric current, is a real limitation of OPVs in general and of bulk heterojunction OPVs in particular. A polymeric electron donor and polymeric acceptor are often mixed together in this kind of cells to form a micro-phase-separated polymer blend with a large distributed interface between these two materials, see Fig. 1.30.

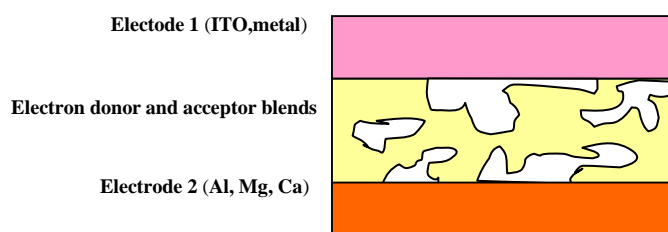


Fig. 1.30. Sketch of bulk heterojunction photovoltaic cells

Two different directions regarding investigation of OPVs' have been explored, according to the types of materials and fabrication methods, one of which is based on small molecular materials and the other is polymer photovoltaics.

1.7.3 Materials in OPVs

The first OPVs exhibiting reasonable power conversion efficiencies were fabricated by Tang and Van Slyke^[91] using the phthalocyanine and perylene derivatives as LMM organic semiconductors. Derivatives of polythiophene and polyfluorene have also been investigated for use in polymer OPVs^[92]. Fig. 1.31 shows the chemical structures of some typical LMM and polymers commonly used as organic semiconductors in OPVs. OPVs using such compounds generally suffer from low

charge mobility, which limits the power generation efficiency. High charge carrier mobility is required as it influence the dissociation efficiency of excitons into electron-hole pairs by reducing charge carrier recombination.

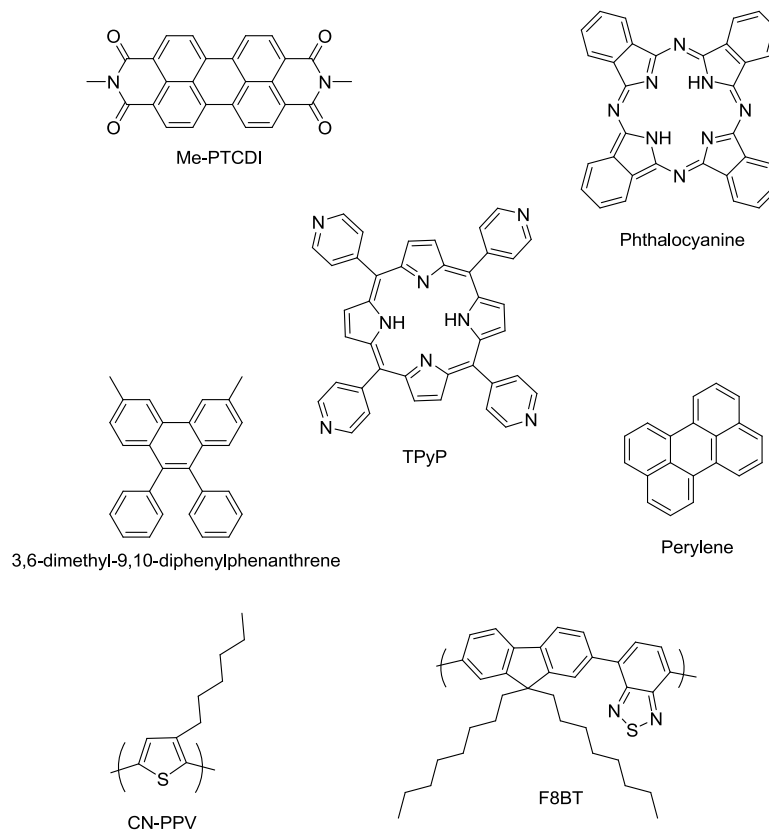


Fig. 1.31 Chemical Structures used in OPVs

Liquid crystalline semiconductors were considered for use in OPVs, since their high degree of order can potentially lead to higher charge carrier mobility in OPVs as well as in OLEDs as demonstrated earlier. A new liquid-crystal photovoltaic concept using a nematic gel template was reported. In this new approach, a hole-transporting reactive mesogen was mixed with a low ionization potential and analogous liquid crystal containing the same aromatic core, and then to form an electron-donating liquid crystalline gel, which is cross-linked to be more thermally stable. This novel approach to the fabrication of OPVs also allows photolithographic patterning.^[89]

Fig 1.32 illustrates an ideal LC composite photovoltaic. It contains three distinct

organic layers, the first of which consists of an insoluble electron-blocking polymer network formed by crosslinking of an electron donating reactive mesogen, next is a sponge-like electron donor layer and followed by a layer of electron-accepting, hole-blocking materials.

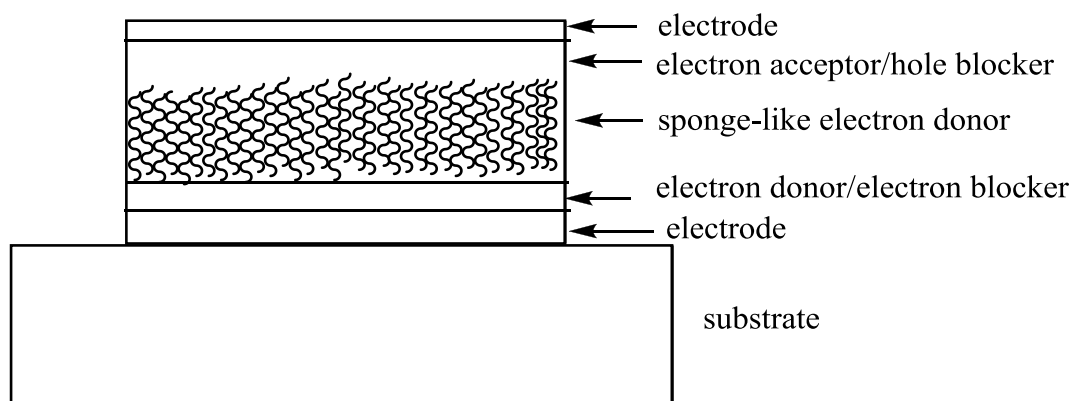
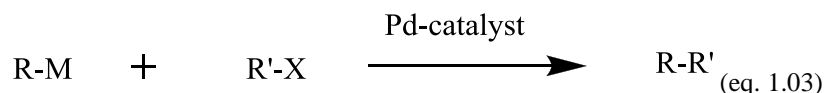


Fig. 1.32 An illustration of an ideal LC composite photovoltaic.

1.8 Aryl-aryl, cross-coupling reactions

In the area of liquid crystal research, one of the most important aspects are the many methods for synthesizing novel liquid crystalline materials in order to facilitate the study of the relationship between molecular structure and the physical properties of various mesophases of relevance to plastic electronics applications, such as OLEDs and OPVs. One of the most valuable synthetic processes in organic chemistry in general and the synthesis of liquid crystals in particular is the formation of a carbon-carbon bond, as large molecules can be produced through such reactions *via* small and more easily-prepared units or building blocks. There are several basic reaction types which would generate a new carbon-carbon bond. In 1972, Kumada and Tamao^[93] and Corriu^[94] reported independently that the cross-coupling of Grignard reagents with aryl and alkenyl halides could be catalyzed by nickel-phosphine complexes. After this discovery, a wide variety of organometallics containing zinc, aluminium, zirconium, tin or boron, were proved to undergo cross-coupling reactions with organic halides using a palladium catalyst (Eq. 1.03).



A general catalytic cycle for the Pd-catalyzed, aryl-aryl, cross-coupling reaction, which involves a series of oxidative-addition, transmetalation and reductive-elimination reaction steps, is shown in Fig. 1.33^[95]. The relative reactivity of aromatic halides in such reactions decreases in the order of $\text{I} > \text{Br} \gg \text{Cl}$. Usually, the oxidative addition is the rate-determining step in the catalytic cycle of a palladium-catalyzed, carbon-carbon bond formation reaction. A very wide range of palladium(0) catalysts or precursors can be used in such reactions, among which $\text{Pd}(\text{PPh}_3)_4$ is the most common catalyst used, although $\text{PdCl}_2(\text{PPh}_3)_2$ or $\text{Pd}(\text{OAc})_2$ plus PPh_3 or other phosphine ligands, are also efficient palladium catalysts in this kind of reaction.

The four most commonly used catalytic methods for direct C-C bond formation are the Kharasch, Negishi, Stille and Suzuki reactions^[96]. With respect to the tolerance of a wide range of substituents on both coupling reagents and extreme versatility, the Stille reactions and Suzuki reactions are mainly used in the synthetic work of this thesis.

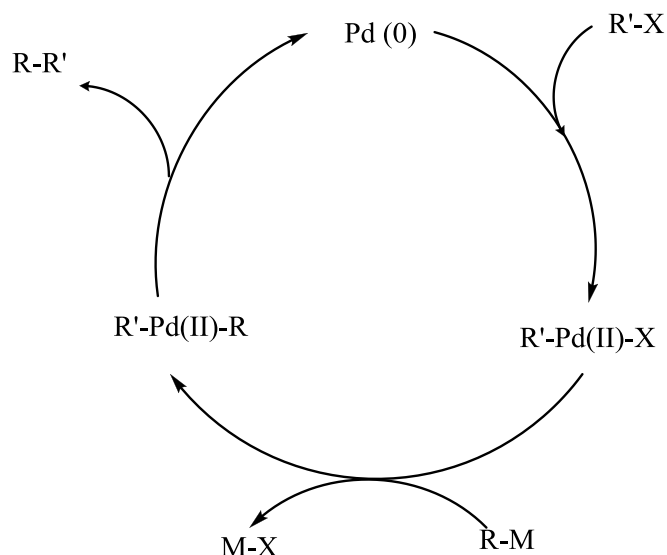
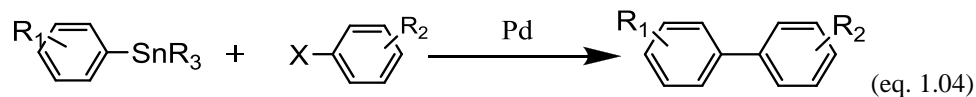


Fig. 1.33. A general catalytic cycle for cross-coupling.

1.8.1 The Stille Reaction

The Stille reaction uses arylstannanes (Ar_1SnR_3 , $\text{R} = \text{Me, Bu}$) and aryl halides (Ar_2X) as the coupling partners in palladium-catalysed biaryl synthetic reactions (Eq. 1.04).



Arylstannanes containing a tributyltin or trimethyltin moiety are the most commonly used biaryl precursors in the Stille reaction. The coupling partner of the arylstannane also can be an aryl triflate, for example, whereby lithium chloride is usually necessary as a co-reagent. This type of Stille reaction is often improved by the addition of copper salts^[97]. One of the explanations for the positive effect of the presence of copper in these reactions is that transmetallation of the arylstannane by the copper salt

may occur to yield a more reactive organo-copper reagent.

A general schematic catalytic cycle for the Stille reaction in biaryl synthesis using aryl-aryl cross-coupling reactions is given as shown in Fig. 1.34. The major disadvantage of the Stille reaction is the toxicity of the organotin and of the by-products formed in the Stille reaction and the difficulty in removing them completely from the organic products prepared using them.

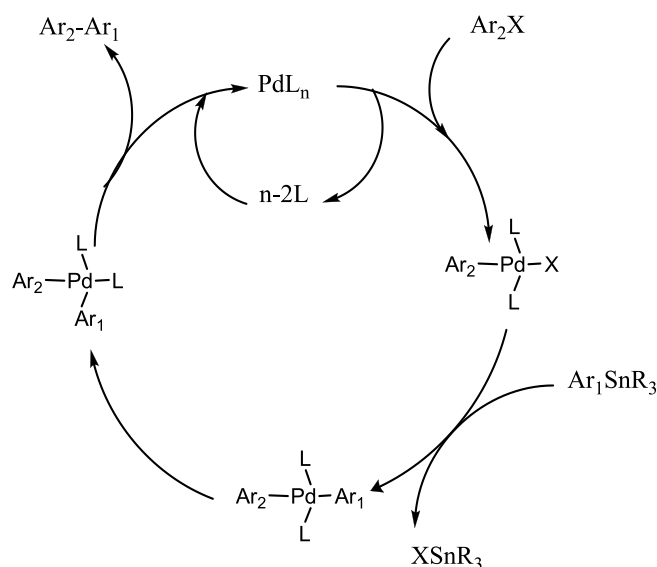


Fig. 1.34. A general catalytic cycle for biaryl Stille reaction.

1.8.2 The Suzuki Reaction

The best overall method for the synthesis of unsymmetrical biaryl or multi-aryl systems is the Suzuki reaction. The procedure (Eq. 1.05) involves the palladium-catalyzed, aryl-aryl, cross-coupling of an arylboronic acid or ester with an aryl bromide, aryl iodide or an activated aryl chloride.



Phosphine-based palladium catalysts are generally used in the Suzuki reaction, since they are stable on prolonged heating and the reaction proceeds more successfully in homogeneous conditions, e.g., aqueous base in dimethoxyethane (DME). A

combination of $\text{Pd}(\text{PPh}_3)_4$ or $\text{PdCl}_2(\text{PPh}_3)_2$ and aqueous Na_2CO_3 in (DME) works satisfactorily in most cases. The boronic acid can be easily prepared in good yield from an aryllithium by treatment with tri-isopropyl borate or trimethyl borate in THF at -78°C under an anhydrous inert atmosphere, e.g., a nitrogen atmosphere, followed by the hydrolysis of the borate ester with weak hydrochloric acid.

A simplified representation of the catalytic cycle of the Suzuki reaction is shown in Fig. 1.35^[97]. As shown in the catalytic cycle, aryl boronic acids do not participate themselves in the trans-metalation processes. They need to be activated by reacting with a nucleophile, or base, to form the corresponding borate complex. As a result, a suitable base/nucleophile is necessary for the reaction, which is largely unaffected by the presence of water. The Suzuki reaction generally tolerates a broad range of functional groups in the reactants, although it does also yield a range of non-toxic by-products. Additionally, it offers the great advantage of being insensitive to the presence of heteroaromatic rings, which is very useful in the synthesis of liquid crystalline materials, especially for use in plastic electronics applications, such as OLEDs and OPVs.

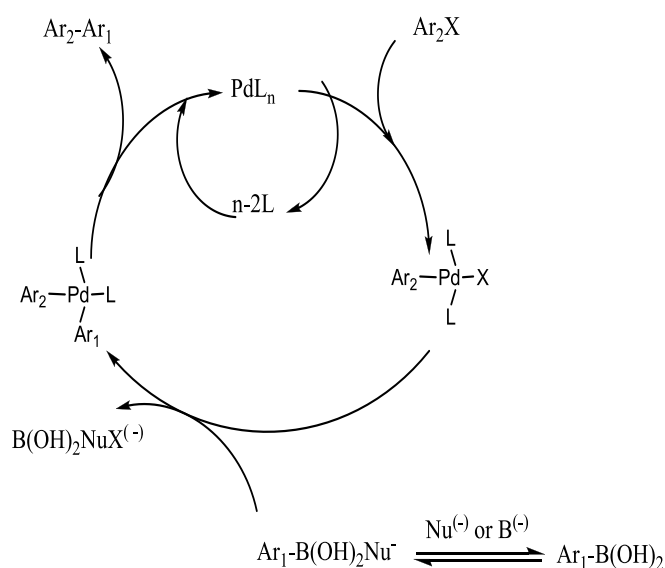
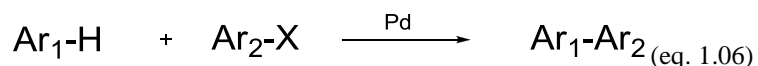


Fig. 1.35. A simplified catalytic cycle for Suzuki reaction.

1.8.3 Direct Arylation of Heteroatom-Containing Aromatic Compounds

Over the past decade, palladium-catalyzed direct arylation reactions are emerging as a valuable and efficient alternative to traditional metal-catalyzed, aryl-aryl cross-coupling reactions in the synthesis of a wide range of poly-aryl aromatic compounds ^[98] (Eq. 1.06). This direct method of arylation is desirable because it avoids pre-functionalization of either aryl substrate prior to the coupling reaction, thus being more time-saving and environmentally friendly, the reaction product is usually easier to purify and the production of toxic or non-environmentally friendly waste is avoided.



Palladium acetate, in conjunction with sterically hindered alkylphosphine ligands, e.g., tricyclohexylphosphine, in its bench-stable phosphonium tetrafluoroborate form ($\text{PCy}_3 \cdot \text{HBF}_4$), was used as the catalyst in these direct arylation reactions. The use of sub-stoichiometric amounts of pivalic acid (usually 30 mol%) with an excess of potassium carbonate base (generating potassium pivalate *in situ*) was shown to increase the reactivity of the biaryl reactions involving aromatic heterocycles, including 2,5-disubstituted thiophenes, 2,5-disubstituted furans, 2,5-disubstituted 1,3,4-benzoxazoles, indoles, pyrroles and so on.^[98]

Among several proposed reaction pathways^[99], two of mechanisms in particular have received the most support: electrophilic aromatic substitution (S_EAr)^[100] with electron-rich, π -nucleophilic heteroarenes and concerted metalation-deprotonation (CMD)^[99] with simple and electron-deficient phenyl derivatives, see Fig. 1.36.

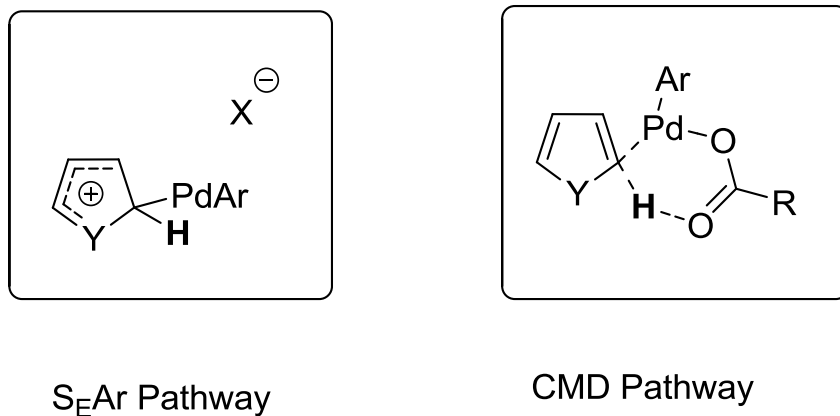


Fig. 1.36^[99] S_EAr and CMD Pathways

1.9 References

-
- 1G. W.Gray,in “*Handbook of Liquid Crystals*” Eds.,D. Demus,J. W. Goodby, G. W. Gray, H.-W.SpiessV. Vill.,Wiley-VCH, Verlagsgesellschaft GmbH, Weinheim, Cambrigde, N. York, 1998, **1**,1.
- 2V. Vill, *Mol. Cryst. Liq. Cryst.*, 1992, **213**, 67.
- 3F. Reinitzer,*Monatsch. Chem.*, 1888, **9**, 421.
- 4F. Reinitzer, *Liq. Cryst.*, 1989, **5**, 7.
- 5O. Lehmann, *Z. Physik. Chem.*, 1889, **4**, 462.
- 6P. J.Collings and M.Hird, “*Introduction to Liquid Crystals Chemistry and Physics*”, Taylor&Francis, 1997.
- 7L. Gattermann and A. Rischke, *Ber. Dtsch. Chem. Ges.*, 1890, **23**, 1738.
- 8G. Friedel, *Ann. Phys.*, 1922, **18**, 273.
- 9V. Freedericksz, V. Zolina, *Trans. Faraday Soc.*, 1933, **29**, 919.
- 10M. Born, *Chem. Zentr.*, 1916, **11**, 366.
- 11W. Kast, *Z. Physik.*, 1932, **76**, 115.
- 12K. Lichtennecker, *Z. Physik.*, 1926, **27**, 116.
- 13D. Vörländer, in “*Chemische Kristallographie der Flüssigkeiten*”, Akadem. Verlagsanstalt, Leipzig, 1924.
- 14D. W. Bruce, K. Heynsand V.Vill, *Liq. Cryst.*, 1997, **23**, 813.
- 15L. Onsager, *ANN. N. Y. Acad. Sci.*, 1949, **51**, 627.
- 16P. J. Flory, *Proc. Roy. Soc., Ser. A.*, London, 1956, **234**, 73.

-
- 17G. W. Gray, K. J. Harrison J. A. Nash, *Electron. Lett.*, 1973, **9**, 130.
- 18G. W. Gray, K. J. Harrison and J. A. Nash, *J. Chem. Soc. Commun.*, 1974, **35**, 431.
- 19G. W. Gray, *J. Phys. (Paris)*, 1975, **36**, 337.
- 20G. W. Gray, A. Mosley, *J. Chem. Soc. Perkin*, 1976, 11, 97.
- 21P. J. Colling, “*Liquid Crystals: Nature’s Delicate Phase of Matter*”, Adam Hilger, England, 1990.
- 22G. Friedel, *Ann. Phys.*, 1922, **18**, 273.
- 23A. Vries and D. L. Fischel, *Mol. Cryst. Liq. Cryst.*, 1972, **16**, 311.
- 24H. Sackmann and D. Demus, *Mol. Cryst. Liq. Cryst.*, 1973, **21**, 239.
- 25E. M. Barrall, J. W. Goodby and G. W. Gray, *Mol. Cryst. Liq. Cryst.*, 1979, **49**, 319.
- 26T. R. Taylor, S. L. Arora and J. L. Fergason, *Phys. Rev. Lett.*, 1970, **25**, 722.
- 27R. A. Wise, D. H. Smith and J. W. Doane, *Phys. Rev.*, 1973, **A7**, 1366.
- 28T. Geelhaar, *Liq. Cryst.*, 1998, **24**, 91.
- 29E. P. Raynes, *Proc. SID Euro Display*, 1996, **96**, 7.
- 30G. H. Heilmelie, L. A. Zanoni and L. Barton, *Proc. IEEE*, 1968, **56**, 1162.
- 31M. Schadt, *Liq. Cryst.*, 1989, **5**, 57.
- 32S. M. Kelly, “*Advanced Organic Materials for Flat Panel Displays*”, RSC Monograph Series, ed. J. A. Connor, 2000.
- 33M. F. Schiekel and K. Fahrenschon, *Appl. Phys. Lett.*, 1971, **15**, 391.
- 34 M. Hareng, G. Assouline and F. Leiba, *Appl. Opt.*, 1972, **11**, 2920.

-
- 35 G. Labrunie and J. Robert, *J. Appl. Phys.*, 1973, **44**, 869.
- 36M. Schadtand W. Helfrich, *Appl. Phys. Lett.*, 1971, **18**, 127.
- 37 D. W. Berreman and W. R. Heffner, *J. Appl. Phys.*, 1985, **122**, 1.
- 38 E. P. Raynes and C. M. Waters, *Displays*, **1987**, 59.
- 39F. Moia, M. Schadt and H. Seiberle, *Proc. SID'93*, **1993**, 1.
- 40T. J. Scheffer and J. Nehring, *Ann. Rev. Sci.*, 1997, **27**, 555.
- 41T. Geelhaar, K. Tarumi and H.Hirschmann, *Trends in LC Materials, SID'96 Digest*, 1996, 167-170.
- 42 S.W Depp and W.E Howard, *Scientific American*, 1993, **3**, 90.
- 43T. Geelhaar, K. Tarumi and H.Hirschmann, *Trends in LC Materials, SID'96 Digest*, 1996, 167.
- 44 W. D. Callister, *"Fundamentals of Material science and Engineering"*, Wiley, New York, 2001.
- 45 B.G.Yacobi, *"Semiconductor Materials: An Introduction of Basic Principles"*, Springer Science & Business Media, 2003.
- 46 Charles Kittel. *"Introduction to Solid State Physics, (Seventh ed.)"*, Wiley, New York, 1996.
- 47A. Tsukazaki, A. Ohtomo, T. Onuma, M. Ohtani, T. Makino, M. Sumiya, K. Ohtani, S. F. Chichibu, S. Fuke, Y. Segawa, H. Ohno, H. Koinuma and M. Kawasaki, *Nature Materials*, 2005, **4**, 42.
- 48P. A. Kohl, S. F. Frank and A. J. Bard, *J. Electrochem. Soc.*, 1977, **2**, 225.
- 49J. W. Allen, *Nature*, 1960, **187**, 403.

50 K. C. Kao and W. Hwang, "*Electrical Transport in Solids. With particular reference to organic semiconductors*", Pergamon, Oxford, 1981.

51 P. Vlachos, "*Heterogenic Liquid Crystal Material for Organic Light Emitting Diodes*", PhD Thesis, University of Hull, 2003.

52 A. Tsumura, H. Koezuka and T. Ando, *Appl. Phys. Lett.* 1986, **49**, 1210.

53 P. F. Lott and R. J. Hurtubise, *J. Chem. Educ.*, 1974, **51**, 315.

54 <http://cdn.intechopen.com/pdfs-wm/37662.pdf>

55 E. Wiedemann, *Annalen der Physik*, 1888, **34**, 446.

56 B. Valeur and M. N. Berberan-Santos, *J. Chem. Educ.*, 2011, **88** (6), 731.

57 N. Holonyak and S. F. Bevacqua, *Appl. Phys. Lett.*, 1962, **1**, 82.

58 M. Pope, H. P. Kallmann and P. Magnante, *J. Chem. Phys.*, 1963, **38**, 2042.

59 W. Helfrich and W. G. Schneider, *Phys. Rev. Lett.*, 1965, **14**, 229.

60 R. E. Kellogg, *J. Chem. Phys.*, 1966, **44**, 411.

61 P. S. Vincent, W. A. Barlow, R. A. Hann and G. G. Roberts, *Thin Solid Films*, 1982, **94**, 171.

62 F. J. Campas and M. Goutermann, *Chem. Phys. Lett.*, 1977, **48**, 233.

63 C. W. Tang and S. A. Van Slyke, *Appl. Phys. Lett.*, 1987, **51**, 913.

64 J. H. Burroughes, D. D. C. Bradley, A. R. Brown, R. N. Marks, R. H. Friend, P. L. Burn and A. B. Holmes, *Nature*, 1990, **347**, 539.

65 D. Pauluth and K. Turami, *J. Mater. Chem.*, 2004, **14**, 1219.

66 <https://www.princeton.edu/~achaney/tmve/wiki100k/docs/Photoluminescence.html>

67 [https://physik.unibas.ch/Praktikum/VPII/Fluoreszenz/Fluorescence and Phosphorescence.pdf](https://physik.unibas.ch/Praktikum/VPII/Fluoreszenz/Fluorescence_and_Phosphorescence.pdf)

68 B. N. Patel and M. M. Prajapati, “*International Journal of Scientific and Research Publications*”, 2014, **6**, 1.

69 S. P. Kitney, “*Liquid Crystalline Semiconductors for Organic Electronics*”, PhD Thesis, University of Hull, 2008.

70 G. J. Richards, “*Novel Organic Materials for Electroluminescent Display Devices*”, PhD Thesis, University of Hull, 2001.

71 C. W. Tang and S. A. Van Slyke, *Appl. Phys. –Semicond.* 1973, **51**, 913.

72 M. P. Aldred, “*Charge-Transporting and Electroluminescent Liquid Crystals for Organic Light-Emitting Diodes*”, PhD Thesis, University of Hull, 2004

73 A. R. Brown, D. D. C. Bradley, P. L. Burn, J. H. Burroughes, R. H. Friend, N. Greenham, A. B. Holmes and A. Kraft, *Appl. Phys. Lett.*, 1992, **61**, 2793.

74 C. Adachi and T. Tsutsui Saito, *Appl. Phys. Lett.*, 1990, **57**, 531.

75 S. H. Askari, S. D. Rughooputh, F. Wudl and A. J. Heeger, *Polym. Preprints*, 1989, **30**, 157.

76 J. Salbeck, Ber. Bunsenges, *Phys. Chem.*, 1996, **100**, 1667.

77 C. Liedenbaum, Y. Croonen, P. Van de Weijer, J. Vleggaar and H. Schoo, *Synth. Met.*, 1997, **91**, 109.

78 S. Sun and N. S. Sariviftci, “*Organic Photovoltaics: Mechanisms, Materials Devices*”, Taylor&Francis, 2005, p. 274.

79 A. Sugimura, N. Matsui, H. Takahashi, H. Sonomure, H. Natio and M. Okuda, *Phys. Rev. B.*, 1991, **43**, 8272.

-
- 80K. Okamoto, S. Nakajima, M. Ueda, A. Itaya and S. Kusabayashi, *Bull. Chem. Soc. Jpn.*, 1983, **56**, 3830
- 81H. Naito, M. Okuda and A. Sugimura, *Phys. Rev. A.*, 1991, **44**, 3434.
- 82 M. Funahashi and J. -I. Hanna, *Appl. Phys. Lett.*, 1997, **71**, 2639.
- 83 S. H. Chen, D. Katsis, A. W. Schmidt, J. C. Mastrangelo, T. Tsutsui and T. N. Blanton, *Nature*, 1999, **397**, 506.
- 84 A. E. A. Contoret, S. Farrar, L. May, J. E. Nicholls, M. O'Neill, S. M. Kelly and A. J. Eastwood, *Appl. Phys. Lett.*, 2000, **12**, 971.
- 85D. Adam, D. Haarer, F. Closs, T. Frey, D. Funhoff, H. Ringsdorf, P. Schuhmacher and K. Siemensmeyer, *Ber. Buns. Phys. Chem.*, 1993, **79**, 276.
- 86D. Adam, P. Schumacher, J. Simmerer, K. Haussling, K. Siemensmeier, K. H. Etzbach, H. Ringsdorf and D. Haarer, *Nature*, 1994, **371**, 141.
- 87 M. Funahashi and J.-I. Hanna, *Appl. Phys. Lett.*, 1997, **78**, 2184.
- 88E.Buchwald, M.Meier, S.Karg, P.Pösch, H.Schmidt, P.Strohriegl, W.Rieß and M.Schwoerer, *Adv. Mater.*, 1995, **7**, 839.
- 89M. Tsoi, W. C.Carrasco-Orozco, M.O'Neill, M. P.Aldred, P.Vlachos and S. M.Kelly, *Adv. Mater.*, 2006, **18**, 1754.
- 90J.Zhao, A.Wang, M. A.Green and F.Ferrazza, *Appl. Phys. Lett.*, 1998, **73**, 1991.
- 91C. W.Tang, *Appl. Phys. Lett.* 1986, **48**, 183.
- 92 A. A. Bakulin¹, A. Rao¹, V. G. Pavelyev, P. H. M. van Loosdrecht, M. S. Pshenichnikov, D. Niedzialek, J. Cornil, D. B. Richard and H. Friend,*Science*,2012, **335**, 1340.
- 93K.Tamao, K.Sumitani and M.Kumada, *Am. Chem. Soc.*, 1972, **94**, 4374.

-
- 94R. J. P. Corriu, J. P.Masse, *J. Chem. Soc., Chem. Commun.*, 1972, 144.
- 95N.Miyaura and A.Suzuki, *Chem. Rev.*, 1995, **95**, 2457.
- 96M.Hird, G. W.Gray and K. J.Toyne, *Mol. Cryst. Liq. Cryst.*, 1991, **206**, 187.
- 97A. N.Cammidge, V. H. M.Goddard and H.Gopee, *Organic Letters*, 2006, **8**, 4071.
- 98B.Liegault, D.Lapointe, C. Laurence,A.Vlassova andK. Fagnou, *J. Org. Chem.*, 2009, **74**, 1826.
- 99S.Gorelsky,D. Lapointe and K.Fagnou, *J. Am. Chem. Soc.*, 2008, **130**, 10848.
- 100C.-H.Park, V.Ryabova, I.V. Seregin, A. W.Sromek and V.Gevorgyan, *Org. Lett.*, 2004, **6**, 1159.

2 Research Aims

The overall aim of this thesis is to synthesize novel liquid crystal materials as light-emitting and/or charge transporting materials in organic semiconductor devices. Liquid crystalline organic semiconductors are widely studied as promising materials due to their optical properties and are contributing significantly to various optoelectronic devices such as organic light emitting diodes (OLEDs)^{[1][2]}, organic photovoltaics (OPVs)^[3] and organic field-effect transistors (OFETs).

A prime general aim of the research for this work is to synthesize new liquid crystalline semiconductors incorporating electron-deficient heterocyclic aromatic rings, such as 2,5-disubstituted-1,3,4-oxadiazoles, or electron-rich heteroaromatic rings, such as 2,5-disubstituted thiophene rings. Fig 2.1 shows the main aromatic rings used as constituent parts of both central cores and end groups, throughout the whole of the research work in this thesis.

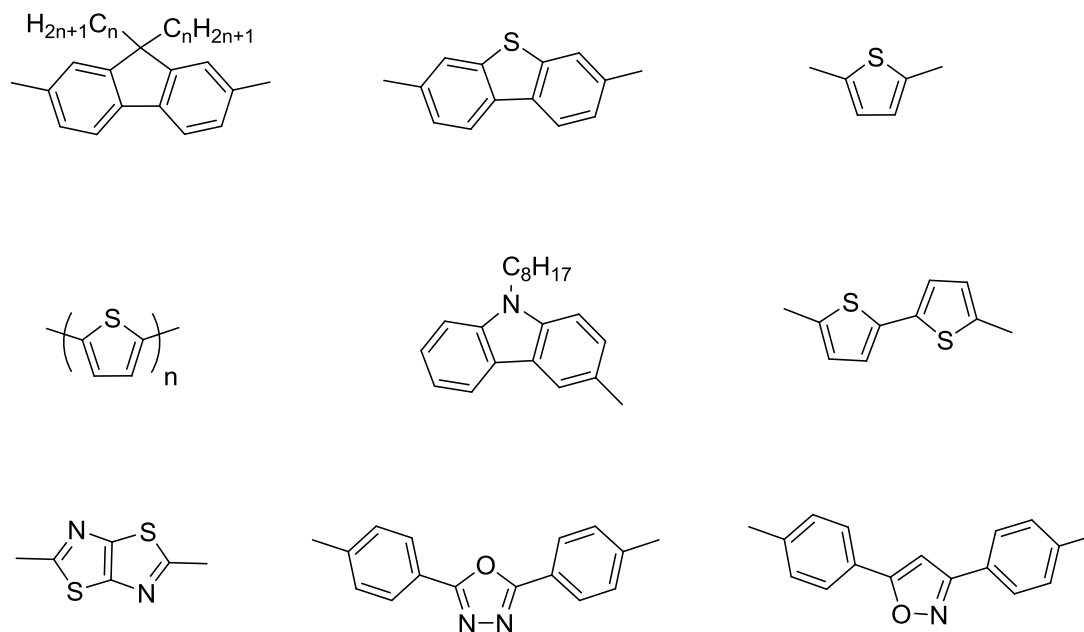


Fig. 2.1 The main aromatic rings used as constituent parts of the molecules throughout this research.

It is hoped to synthesize materials possessing a low melting point (Cr-N), a high clearing point (N-I), high charge-mobility and/or high efficiency of electroluminescence, which can be used as hole-transporting, electron-transporting and/or emissive layers for OLEDs or as electron-donating or electron-accepting materials in OPVs.

The new liquid crystalline organic semiconductors will either form molecular glasses at room temperature or will be polymerized photochemically, if they incorporate polymerisable end-groups at the end of the aliphatic terminal chains, to form insoluble and intractable polymer networks. Such liquid crystalline monomers are referred to as reactive mesogens (RMs). A specific aim of the programme of this work is to synthesize colorless electron-rich RMs with a low ionisation potential for use as insoluble and intractable hole-transporting/electron-blocking layers, once photopolymerised, in OLEDs.

The secondary aim of this research work is to synthesise liquid crystalline materials more efficiently *via* simple synthetic pathways, especially using direct arylation of thiophene with aryl halides *via* C-H bond activation using palladium catalysts.^[4] Compared to the traditional method to synthesize *via* Suzuki-Miyaura, Stille other aryl-aryl cross-coupling reactions, this new kind of pathway saves both time and cost. No prior pre-preparation of organometallic monomers are required, which means fewer synthetic steps are required to produce the desired materials. Furthermore, it is also a more environmentally friendly synthetic process, which is a very important consideration for the large scale manufacture of new organic semiconductors.^{[5][6]}

A further aim is to study the relationship between molecular structures and liquid crystalline behaviour and physical properties of the materials, such as transition temperatures, ionization potential, HOMO energy levels, band gaps and electron affinity, etc. The judicious choice of heteroaromatic rings and other molecular components of the new materials should yield the desired combination of physical properties described above for application of these materials in OLEDs and OPVs.

A series of reactive mesogens (RMs) with either *N*-alkyl-substituted carbazole cores or 2,7-disubstituted-9,9-dialkylfluorene cores are firstly aimed to be synthesized. It is believed that the presence of a 2,7-disubstituted-9,9-dialkylfluorene unit in the structure of materials should be beneficial for good solubility and lead to lower transition temperatures, especially the melting point, due to the steric effects.

Another class of materials incorporating 3-substituted carbazole moieties as end-groups are targeted for synthesis. They are expected to lower the HOMO energy levels and band gaps, so maybe suitable for use as electron-donor materials in OPVs and hole-transporting materials for OLEDs.

The thiazolo-thiazoles based compounds with two fused five-membered rings at the cores are also targets for synthesis as they are believed to exhibit high charge carrier mobilities and promising fluorescence.^[7] This class of materials are all expected to be liquid crystals, and the relationship between chemical structures, especially the length of alkyl chains upon the mesophase behaviour will be studied.

A further aim is to synthesize a series of novel compounds comprising molecular cores incorporating 2,2'-bithiophene cores attached to 1,4-disubstituted-phenyl or 2,5-disubstituted-pyridine rings, as they were reported to exhibit relatively larger charge carrier mobility.^[8,9,10] The relationship between their chemical structures and mesomorphic behaviour as well as their electrochemical properties and energy levels will be studied.

A new class of 1,3,4-disubstituted-oxadiazole homologues will be synthesized as they are expected to possess relatively high values of the electron-affinity and strong fluorescence, which should render them potential materials for use as electron-transporting layers and/or emissive layers. Two isoxazole derivatives will be synthesized as comparison compounds to the oxadiazole compounds. Again, all the materials of this class are expected to be liquid crystals, and the relationship between the chemical structures of these materials and their mesophases will be studied.

Meanwhile, the influence of the flexible end groups upon liquid crystalline behavior will also be studied by synthesizing and evaluating a series of homologues systematically with increasing or decreasing spacer lengths, i.e., number of methylene units (-CH₂-) in the chain.

2.1 References

- 1 T. Yamamoto, *Macromol. Rapid Commun.*, 2002, **23**, 583-606.
- 2 S. M. Kelly, “*Advanced Organic Materials for Flat Panel Displays*”. RSC Monograph Series, ed. J. A. Connor, 2000.
- 3 M. T. Bernius, M. Inbasekaran, J. O’Brien and W. Wu, *Adv. Mater.*, 2000, **12**, 1737-1750.
- 4 D. J. Schipper and K. Fagnou, *Chem. Mater.*, 2011, **23**, 1594.
- 5 Y. Fujinami, J. Kuwabara, W. Lu, H. Hayashi and T. Kanbara, *ACS Macro Lett.*, 2012, **1**, 67–70.
- 6 J. Roger, F. Požgan and H. Doucet, *Green Chem.*, 2009, **11**, 425-432.
- 7 I. Osaka, G. Sauve, R. Zhang, T. Kowalewski, R. D. McCullough, *Adv. Mater.*, 2007, **19**, 4160.
- 8 M. Funahashi and J. Hanna, *Appl. Phys. Lett.*, 2000, **76**, 2574.
- 9 M. Funahashi and J. Hanna, *Mol. Cryst. Liq. Cryst.*, 2005, **436**, 1179.
- 10 K. Oikawa, H. Monobe, J. Takahashi, K. Tsuchiya, B. Heinrich, D. Guillon and Y. Shimizu, *Chem. Commun.*, **2005**, 5337.
- 11 T. Maegawa, Y. Kitamura, S. Sako, T. Udz, A. Sakurai, A. Tanaka, Y. Kobayashi, K. Endo, U. Bora, T. Kurita, A. Kozaki, Y. Monguchi and H. Sajiki, *Chem. Eur. J.*, 2007, **13**, 5937.

3 Experimental

3.1 Evaluation of the Materials

¹H Nuclear Magnetic Resonance (NMR) Spectrometry

The structures of the reaction intermediates and final products prepared in this thesis were confirmed by ¹H NMR spectroscopy using a JEOL Lambda 400 or JEOL JNM-GX270 FT spectrometer. Tetramethylsilane (TMS) was used as an internal standard.

The following abbreviations show examples which used to describe the splitting patterns:

s - Singlet d - doublet t - Triplet

quart - quartet quint - quintet sext - Sextet

dd - double doublet m - Multiplet

Mass spectroscopy (MS)

Mass spectra were recorded using a Gas Chromatography/Mass Spectrometer. Generally, for compounds with a RMM < 800 g mol⁻¹, (GC/MS)-QP5050A Shimadzu with Electron Impact (EI) at a source temperature of 200 °C was used. Compounds with a RMM > 800 g mol⁻¹ were analyzed using a Bruker, reflex IV, Matrix Assisted Laser Desorption/Ionisation (MALDI), Time of Flight (TOF) MS. A384 well microlite plate format was used with a scout target. M⁺ marks the mass ion and M100 indicates the

most stable fragment observed in the mass spectrum.

Chromatography

The progress of the reactions was monitored by thin layer chromatography (TLC). Aluminium backed TLC plates, coated with silica gel (60 F254), from Merck were used.

Most of the reaction intermediates and final products were purified by column chromatography, using silica gel 60 (230 – 400 mesh). Dry flash column vacuum chromatography was also carried out using silica gel (Fluorochem, 6–35 Å) for easily-purified materials. The reaction products were dried under vacuum and then stored in sample tubes.

Structure and purity identification

A Fisons EA 1108 CHN apparatus was utilized for elemental analysis of all the final compounds reported in this thesis in order to confirm the molecular structure of the synthesized compound as well as its purity, which was also determined by gas chromatography using a chromopack CP3800 capillary gas chromatograph fitted with a CP-SIL 5CB capillary column. High-performance liquid chromatography (HPLC) [5 µm, 25 cm × 0.46 cm, ODS Microsorb column, methanol, > 99%] was used as well for the intermediates or those not suitable for GC. The purity of the intermediates was normally found to be above 95%, unless otherwise stated.

Melting points and transition temperatures

An Olympus BH2 polarising microscope with a Mettler FP-5 hot stage or Olympus BX51 polarising microscope in collaboration with Linkam LTS 350

temperature-controlled stage were utilized to measure the melting point and other transition temperatures for each of the compounds synthesized in this thesis. Differential scanning calorimetry (DSC) using a Perkin-Elmer DSC 7 or a Mettler Toledo DSC1 differential scanning calorimeter, which is used conjunction with a TAC 7/3 instrument controller, was used to determine the transition temperatures of liquid crystal phases and also to calculate their enthalpies of transition. The calibration of the calorimeter was carried out using an indium standard reference (melting point onset = 156.6 °C, $\Delta H = 28.45$ J/g).

Reagents and reaction solvents

Reagents were purchased from Alfa Aesar Acros Organics, Sigma Aldrich, Fisher, TCI and Apollo and were used without further purification unless stated. Reaction solvents, such as tetrahydrofuran and diethyl ether, were pre-dried, distilled over sodium wire under nitrogen then stored over molecular sieves (4Å). Triethylamine was distilled over potassium hydroxide pellets then stored over molecular sieves (4Å). Dimethylformamide was distilled over P₂O₅ and dried over molecular sieves (4Å). Other solvents were used directly as purchased. All reactions were carried out under an atmosphere of nitrogen even water was present as solvent or reagent, unless otherwise stated.

Common abbreviations

DCM	-	Dichloromethane
<i>n</i> -BuLi	-	<i>n</i> -butyllithium
DME	-	1,2-Dimethoxyethane
DMSO	-	Dimethyl sulfoxide
NBS	-	<i>N</i> -Bromosuccinimide
THF	-	Tetrahydrofuran
DMF	-	<i>N,N</i> -dimethyl formamide
TBAB	-	Tributylammonium bromide
EtOH	-	Ethanol
MeOH	-	Methanol
IPA	-	Propan-2-ol
NMP	-	<i>N</i> -Methyl-2-pyrrolidone
RT	-	Room temperature
Lit.	-	Literature
TLC	-	Thin layer chromatography
NMR	-	Nuclear magnetic resonance
MS	-	Mass spectrometry
DSC	-	Differential scanning calorimetry
Cr	-	Crystal
N	-	Nematic phase
N*	-	Chiral Nematic phase
Sm	-	Smectic phase
B _x	-	Banana phase
I	-	Isotropic liquid
EL	-	Electroluminescence
PL	-	Photoluminescence
LCD	-	Liquid crystal display
OLED	-	Organic light emitting diode

OPVs - Organic photovoltaics

3.2 Synthetic pathways

The synthetic pathways of all the intermediates and final products are shown in schemes 1-23. A brief discussion of some synthesis problems encountered to give the desired products is shown as below, more synthetic discussion, for example some optimization of reaction conditions, will be given in Results and Discussion chapter.

3.2.1 Scheme 1

A ring closing condensation reaction of 4,4'-dibromo-2-nitrobiphenyl (**1**) was carried out using triethyl phosphite as reagent and solvent to give the desired product as 2,7-dibromo-9-carbazole (**2**) in moderate yield (33%), which was alkylated subsequently with 1-bromooctane to give the desired product as 2,7-dibromo-9-octylcarbazole (**3**). A palladium-catalyzed Suzuki aryl-aryl cross-coupling reaction was utilized for the carbon-carbon bond formation step to produce 2,7-*bis*-[4'-(octyloxy)biphenyl-4-yl]-9-(octyl)carbazole (**5**), unfortunately, the yield was poor (16%). The possible reason for the poor yield may be the choice of solvent. IPA/H₂O was used rather than an aprotic polar solvent, such as DMF and DME, commonly used in traditional homogeneous palladium-catalyzed Suzuki reactions,^[1,2] which may have had detrimental effect on the yield of this reaction.

3.2.2 Scheme 2 and 2.1

A Suzuki aryl-aryl cross-coupling reaction of 4-bromoanisole with thiophene-2-boronic acid was carried out to give the desired product 2-(4-methoxyphenyl)thiophene (**8**) in good yield (67%), which was then reacted with *n*-BuLi in hexanes and followed by the addition of tributylstannyl chloride to make the tin compound (**9**) in high yield (98%), which was used without further purification in the next reaction. A Stille aryl-aryl cross-coupling of

2-bromothiophene and stannane (**9**) in DMF/toluene, using Pd(OAc)₂ plus P(Ph)₃ as the catalyst formed *in situ*, afforded compound (**10**), which was then brominated, using NBS, in position 5 of the 2-substituted thiophene ring, to produce 5-bromo-5'-(4-methoxyphenyl)-2,2'-bithiophene (**11**) in good yield (65 %). Diboronic acid formation of 2,7-dibromo-9,9-dioctylfluorene(**12**) afforded the diboronic acid (**13**) in moderate yield (48 %). A Suzuki aryl-aryl cross-coupling reaction of compound **11** and **13** in a ratio of 2:1, afforded compound **14** with eight rings in the molecular core in moderate yield (43 %). The reaction intermediate **14** is a liquid crystal material. Deprotection using boron tribromide gave the compound **15**, which was used to prepare the desired final product **16** using a Williamson-ether synthesis in high yield (71%).

3.2.3 Scheme 3 and 3.1

2,7-Dibromo-9,9-dipropyl-9*H*-fluorene (**18**) was synthesised in a one-step procedure from commercially available 2,7-dibromofluorene (**17**) using aqueous NaOH (50% solution), 1-bromopropane, a phase transfer catalyst (TBAB) and toluene in high yield (77%). A Stille coupling of 2-(tributylstannyl)thiophene and compound **18** in DMF, using *tetrakis*(triphenylphosphine)palladium(0), afforded the symmetrical *bis*-thiophene intermediate (**19**), in high yield (77%), which was then dibrominated using NBS in position 5 of the thiophene rings, to produce the dibromo-intermediate (**20**). Alkylation of bromophenol with 1-bromooctane and 1-bromododecane and subsequent boronic acid formation produced the 4-*n*-alkoxyphenyl boronic acid (**25-27**) in good yield (86%, 74%, 74%, respectively). An Suzuki aryl-aryl cross-coupling reaction between the dibromide **20** and the phenyl boronic acids **25-27** produced the diethers **28-30** with seven aromatic rings in the molecular core in moderate yields (32-43%). However, the purification of compound **28-30** was difficult because unwanted side reactions produced impurities that have similar retention times to these products and as a result very careful purification by column chromatography was required. The deprotection, using boron tribromide, was carried

out to produce compound **33**. The compound shown in Fig. 2.1 was meant to be synthesized by alkylating the *bis*-phenol **33** on one side, by a Williamson-ether synthesis, using the bromo-THP compound **32**, which was previously prepared from 1-bromononan-9-ol **31** in excellent yield (94%). However, this reaction pathway finally failed and only compound **34**, which had reacted on both sides, was isolated in moderate yield (34%). Consequently, further steps with this intermediate could not be continued.

Fig. 3.1 Structure designed for Scheme 3.1

3.2.4 Scheme 4

3.2.5 Scheme 5

1,6-dibromohexane to give the desired product as compound (**42**) in moderate yield (39%), which subsequently produced the compound (**43**) with pyrocatechol by a Suzuki aryl-aryl cross-coupling reaction in high yield (70%). Compound (**43**) was then dibrominated with NBS to give the desired product as compound (**44**) in excellent yield (92%). The 2-(9-bromononyloxy)tetrahydro-2H-pyran (**32**) was reacted with thiophene in 2-position to produce compound (**45**) using *n*-BuLi reaction in high yield (78%), which led to the tin compound (**46**) with *n*-BuLi in THF followed by the addition of tributylstannyl chloride in excellent yield (98%). The stannane (**46**) was found to be sensitive to acidic conditions, such as dilute hydrochloric acid and even silica gel and undergo de-stannylation in which the product was converted back to the starting material^[3]. Therefore, compound (**46**) was not purified and fortunately, the crude product was pure enough to be used in the next step. A Stille aryl-aryl coupling reaction between compounds **44** and **46** was used to afford the compound **47**, which was, however, not reactive, although several solvents, including DMF, DME, IPA, NMP, toluene, higher temperature and longer reaction time (48-72 h) were tried. As a result, the following steps using this intermediate (**47**) could not be carried out and the reaction scheme could subsequently not be completed.

3.2.6 Scheme 6-8

NBS was used to brominate the commercially available carbazole (**50**) in the 3-position followed by an addition of a saturated Na₂S₂O₃ solution to reduce any free bromine produced in the reaction, to give the desired product as compound **51** in a good yield (76%). Then compound **51** was reacted with commercially available 1-bromooctane at room temperature to afford the carbazole **52** in excellent yield (88%). Compound **49**, **53**, **54** and **58** were synthesised by a new pathway, using a one-step Pd-catalysed direct arylation reaction^[4] with potassium pivalate as base. Tricyclohexylphosphonium tetrafluorobromide (PCy₃.HBF₄) was used to stabilize the palladium catalyst. Using this method avoided pre-functionalization of either substrate prior to the coupling reaction compared with both the Suzuki and Stille reactions^[4].

However, the best reaction conditions for this kind of reaction are still being studied. The yield of compound **49**, **53** and **58** were not high (about 20%), while compound **54** was prepared in a moderate yield (45%). An interesting point is that, compared with a reaction time of 16-20 h, which usually meant that the reaction was carried out overnight, we found that sometimes a reaction time of just 3-4 h, see compound **54** was enough for completion of the direct arylation reaction. It was also noted that when the reaction lasted longer, some side products, such as polymers, were formed, which increased the difficulty of purifying the final product and led to a low yield, see compound **58**. This reaction method can also be used in the preparation of other aromatic compounds, including fluorenes, thiophenes and carbazoles. The low yield obtained in the synthesis of compounds **49** and **53** may also be attributable to some unknown influence of the dibenzothiophene core.

3.2.7 Schemes 9-11

In these three schemes, a number of liquid crystal compounds (**63**, **64**, **68**, **69**, **70**, **72**) incorporating a thiazolo[5,4-*d*]thiazolearomatic core incorporating a total of five aryl rings were synthesized using the Suzuki aryl-aryl, cross-coupling reaction. The wide range of yields achieved (43%-85%) were caused by different reaction conditions, for example, different solvents, different type and amount of base used in the reaction, etc. The detailed optimization of reaction condition will be discussed in Chapter 4. Compound **59** was produced by a ring-closing reaction with commercially available dithiooxamide and thiophene-2-carbaldehyde in moderate yield (39%), which was probably due to the low solubility of compound **59** in DMF. This compound was then di-brominated using NBS to afford compound **60** in an excellent yield (98%). A number of commercially available 2-*n*-alkylthiophenes were reacted with *n*-BuLi under -78°C then quenched by the addition of 2-isopropoxy-4,4,5,5-tetramethyl-1,3,2-dioxaborolane, to afford the boronic acid pinacol esters **61**, **62** in very good yield (91%, 97%). The boronic acids **66**, **67** and **71** were obtained from other research programmes and were used without further

purification. 4-Butylphenylboronic acid (**65**) was purchased and used directly also without further purification. The final liquid crystal products were synthesized using the Suzuki palladium-catalysed aryl-aryl cross-coupling reaction as usual.

3.2.8 Scheme 12

The synthesis of compound **60** was discussed in the above scheme 9-11. The thiazolo[5,4-*d*]thiazole with carbazoles on both ends **74** was synthesized by Stille reaction, using compound **60** and tin compound **73**, which was previously prepared by *n*-BuLi reaction on 3-position of carbazole under -78°C and following addition of tributylstannyl chloride in a good yield (63%). The yield of final product **74** was not very high (65%), probably because the tin compound **73** was used without any further purification.

3.2.9 Scheme 13, 14, 15 and 16

Various liquid crystals **77-83** and **85** incorporating bithiophene cores also incorporating 1,4-disubstituted phenyl rings were synthesized as shown in these schemes. The boronic acids **26**, **75**, **76**, **65**, **66**, **67**, **71** **84** with either *n*-alkyl or *n*-alkoxy chains were produced through *n*-BuLi reactions with good-to-high yield (74-91%) by similar procedures as discussed before in scheme 9-11, or obtained from other research programmes. The final step was carried out using the Suzuki aryl-aryl cross-coupling reactions as usual, using potassium carbonate as base, DMF as solvent and Pd(OAc)₂ as catalyst. Among these reactions the yields of products **77-79** incorporating 1-*n*-alkoxy-4-phenyl rings were low (34%, 22%, 23% respectively). However, the yield achieved in the synthesis of compound **85**, which has a 1,4-disubstituted-3-fluoro-phenyl ring instead of a 1,4-disubstituted-phenyl ring without the fluorine lateral substituent, was quite high (84%). The yield for the other products **77-79** was also high (overall above 80%). This is in spite of the fact that the compounds **77-79** were difficult to purify, as they were not stable enough to be

purified by column chromatography with silica gel. Consequently a yield loss probably took place during the washing of the crude products using a large amount of solvents (EtOH, MeOH, hexane and DCM) and recrystallisation as well. Details will be discussed in next chapter.

3.2.10 Scheme 17-21

The compound 4-bromo-*N'*-(4-bromobenzoyl)benzohydrazide (**86**) was synthesised by reaction with 4-bromobenzoyl chloride, which was obtained from other programmes and was used without any further purification, and commercially available 4-bromobenzohydrazide, in high yield (84%). A cyclisation reaction using thionyl chloride (SOCl₂) gave the dibromo-oxadiazole compound **87** in excellent yield (95%). The synthesis of the boronic acids **26**, **65**, **67**, **84**, **71** and **75** with 1,4-disubstituted phenyl rings or 2,5-disubstituted pyridine rings were discussed in schemes 3, 10, 11 and 16. The synthesis of 5-hexylthiophene-2-boronic acid pinacol ester (**61**) was discussed in scheme 9. The Suzuki palladium-catalysed, aryl-aryl cross-coupling reactions were carried out using Pd(OAc)₂ as the catalyst, sodium carbonate as the base and DMF as the solvent to produce the 2,5-disubstituted-1,3,4-oxadiazole compounds **88-93** and **95** in a good-to-high overall yield (70-87%). Meanwhile, a palladium-catalysed direct arylation of compound **87** and commercially available 2-butylthiophene using potassium pivalate as base with PCy₃.HBF₄ to stabilise catalyst Pd(OAc)₂, was carried out to give the desired product as product **94** in very good yield (86%).

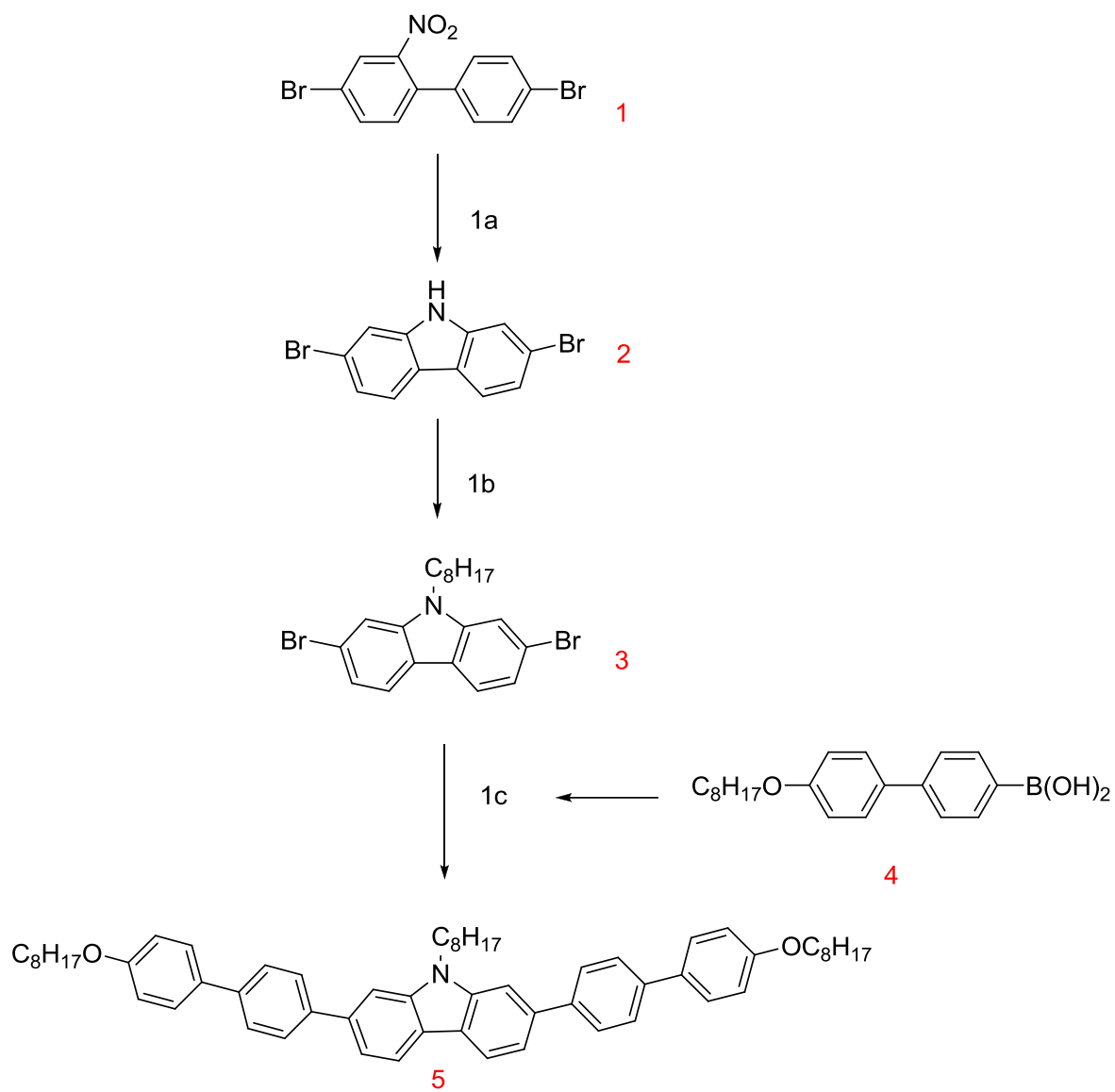
3.2.11 Scheme 22 and 23

The compound 3,5-*bis*-(4-bromophenyl)isoxazole (**96**) was cyclized from 1,3-*bis*-(4-bromophenyl)propane-1,3-dione, which was obtained from other programme intermediates and was used without further purification, with hydroxylamine using NaOH as the base and dioxane as solvent in very good yield

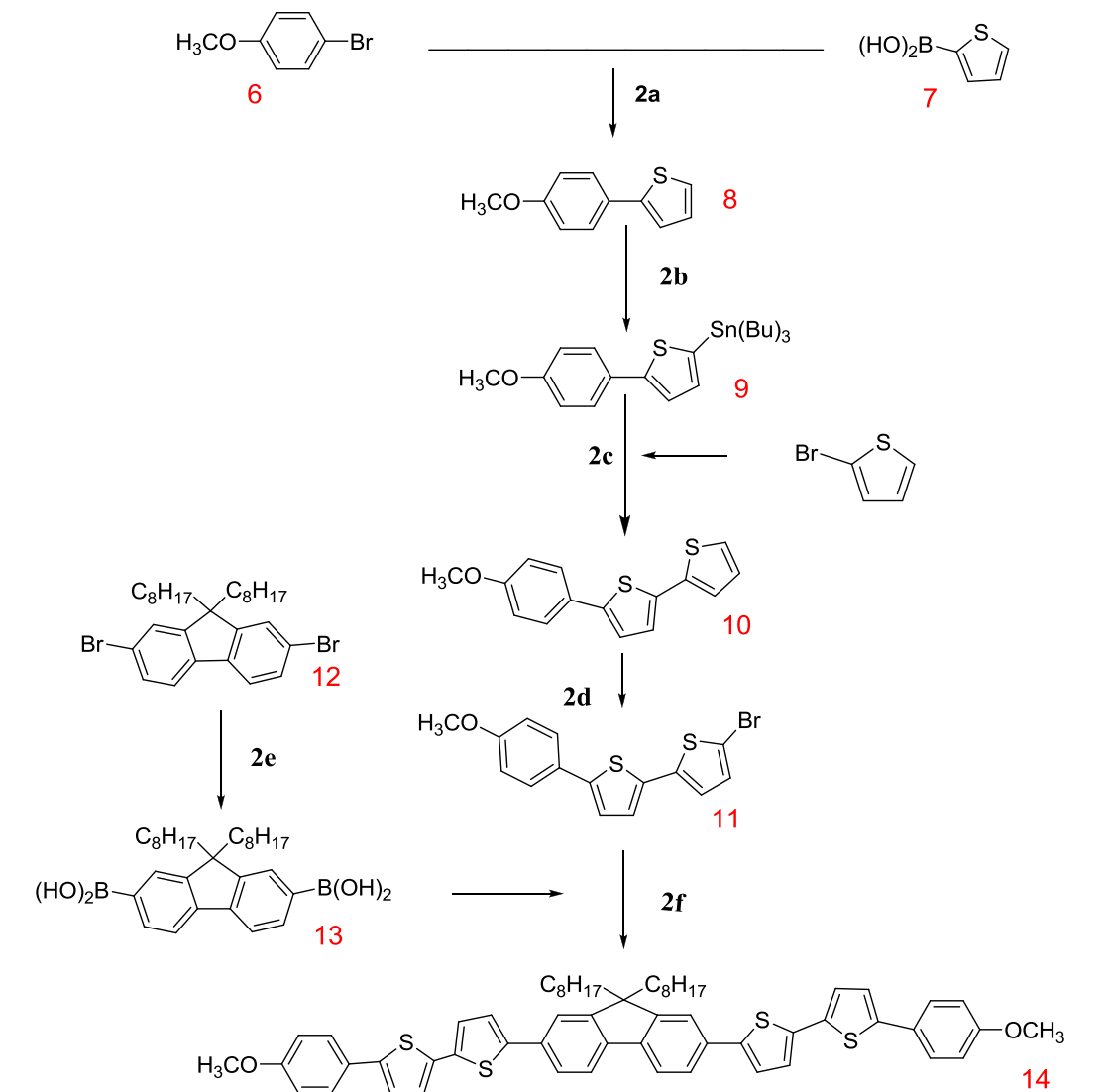
(85%). The synthesis of 4-butylphenylboronic acid (**65**) and 2-(5-butylthiophen-2-yl)-4,4,5,5-tetramethyl-1,3,2-dioxaborolane (**62**) have been discussed already in schemes 9 and 10. Then a Suzuki Pd-catalysed, aryl-aryl, cross-coupling reaction using potassium carbonate as base and DMF as solvent was carried out to afford the final compounds **97** and **98** in high-to-excellent yield (79% and 92%, respectively).

3.3 Reaction Schemes

Scheme 1

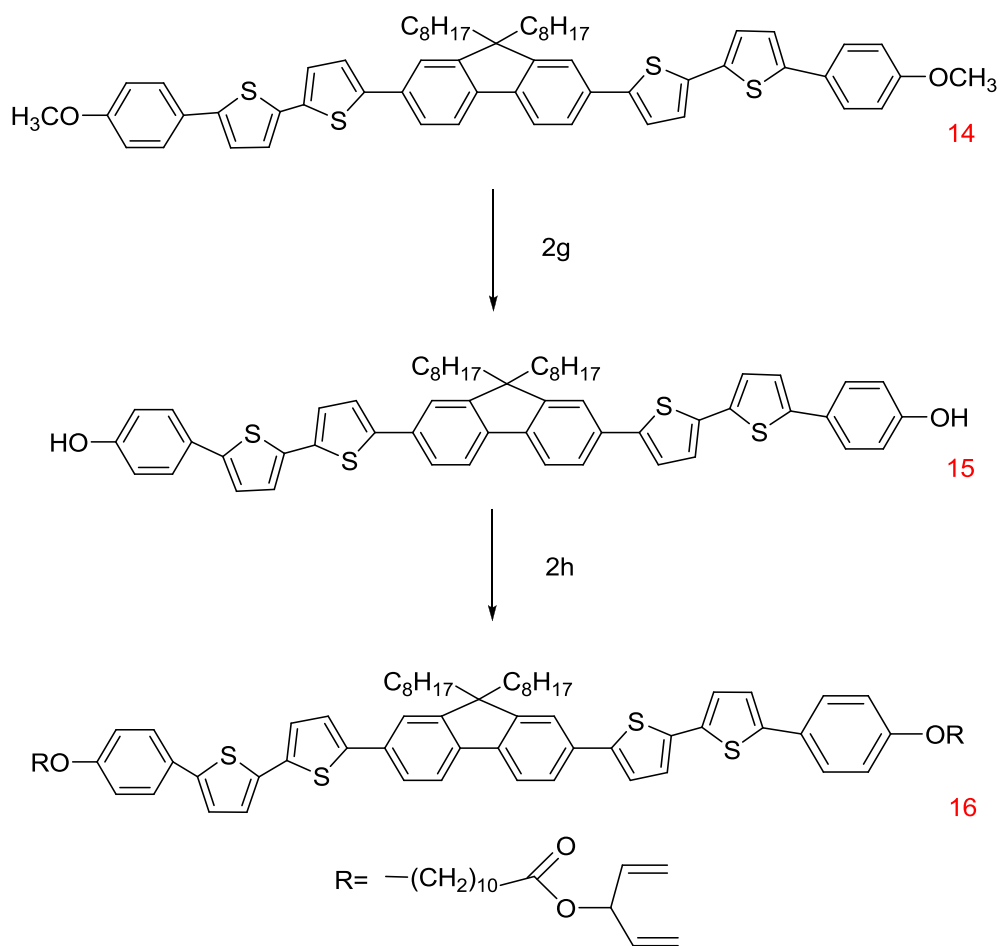


a: $\text{P}(\text{OEt})_3$.
b: NaH , $\text{BrC}_8\text{H}_{17}$, DMF .
c: $\text{Pd}(\text{OAc})_2$, $\text{IPA}/\text{H}_2\text{O}$, K_3PO_4



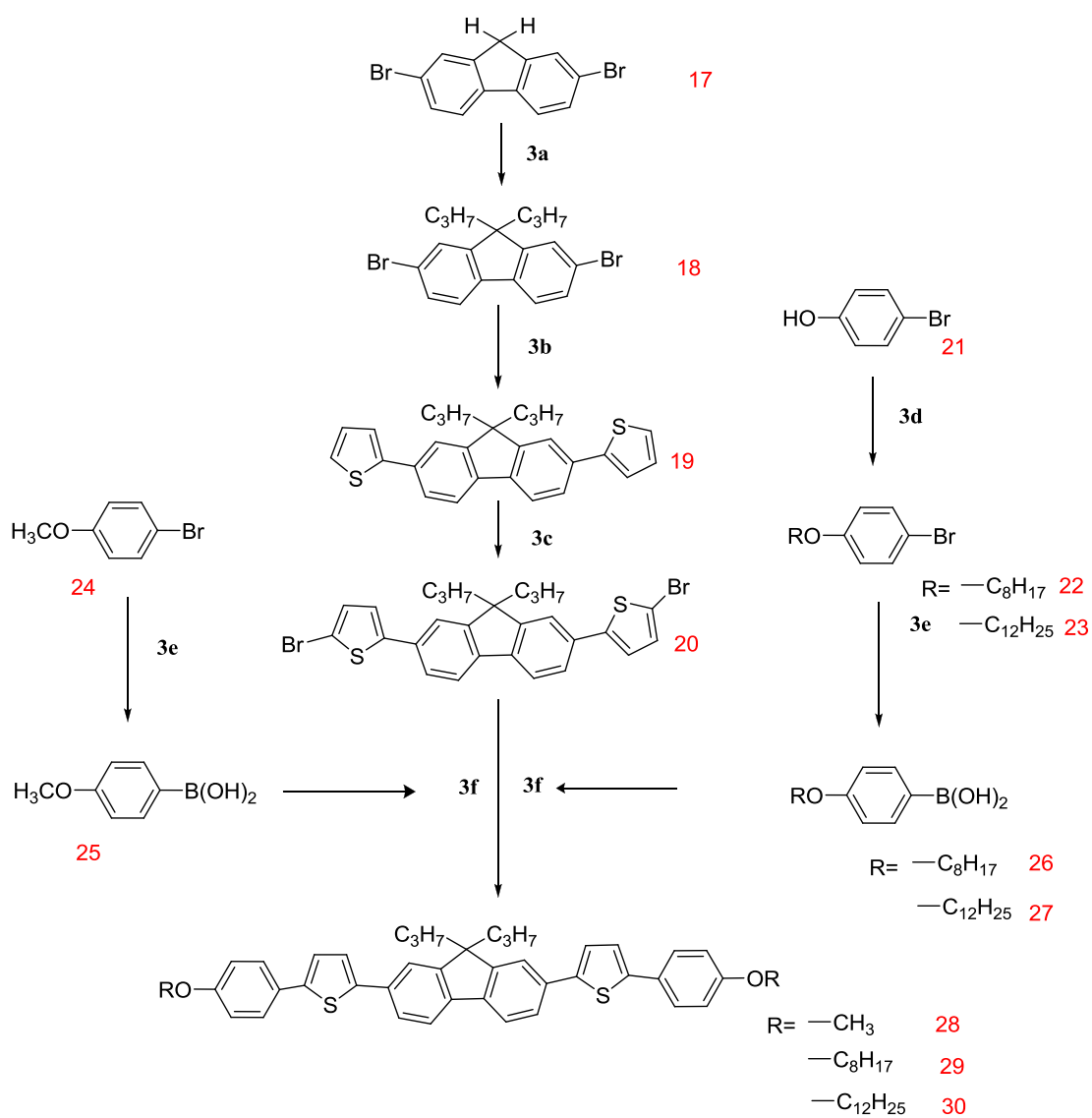
a: Pd(OAc)₂, P(Ph)₃, Na₂CO₃, THF/H₂O.
b: (i) *n*-BuLi, THF, (ii) Tributylstannyl chloride
c: Pd(OAc)₂, P(Ph)₃, DMF/toluene.
d: NBS, silica gel, chloroform.
e: *n*-BuLi, trimethyl borate, THF, HCl.
f: Pd(OAc)₂, P(Ph)₃, THF/H₂O, K₂CO₃.

Scheme 2.1



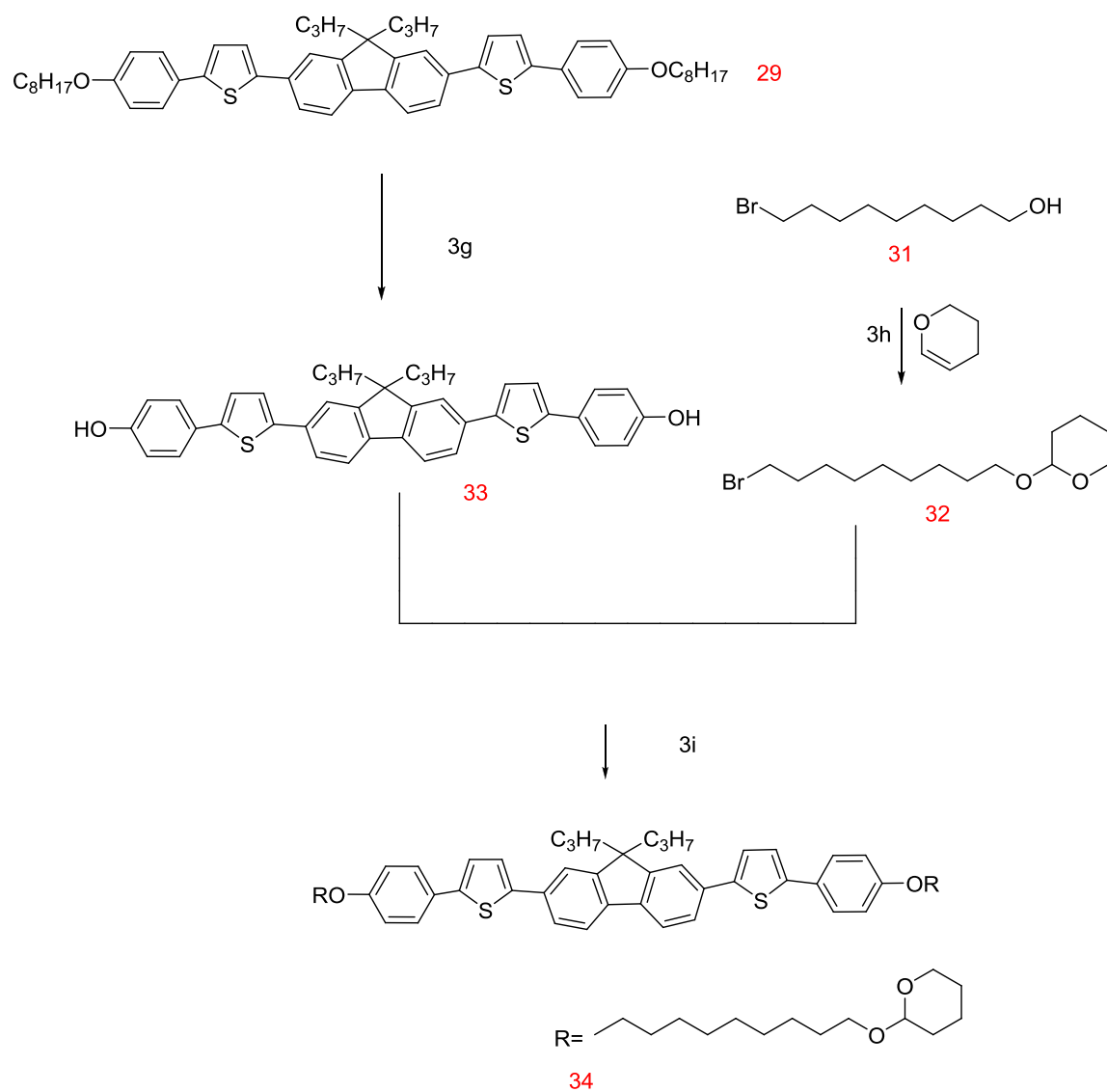
g: (i) BBr₃, DCM, chloroform, (ii) ice/H₂O.

h: 1,4-pentadien-3-yl-11-bromoundecanoate, K₂CO₃, DMF



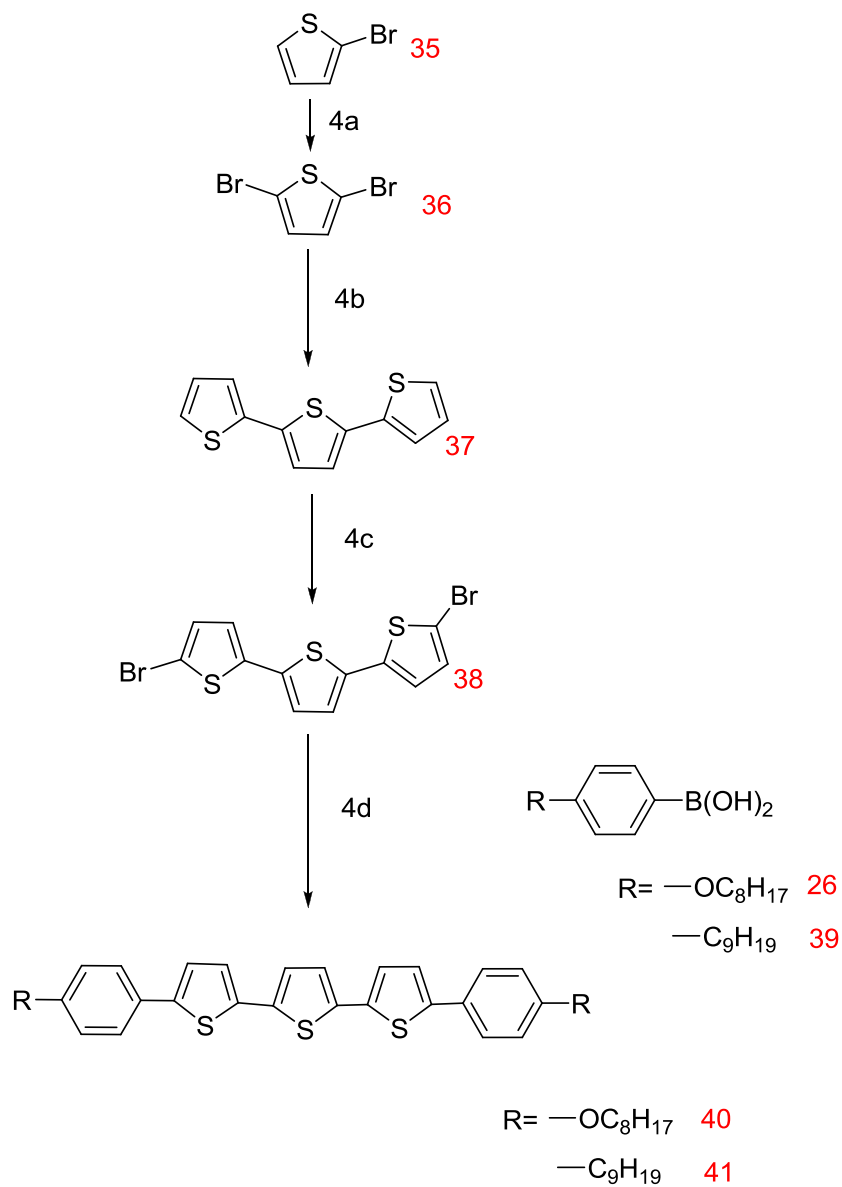
- a: NaOH (50% aqueous), TBAB, toluene, 1-bromopropane.
b: 2-(Tributylstannyl)thiophene, Pd(PPh₃)₄, DMF .
c: NBS, silica gel, DCM.
d: K₂CO₃, acetone.
e: i) n-BuLi, THF, ii) Triisopropyl borate, iii) H₃O⁺.
f: DMF, Pd(PPh₃)₄, K₂CO₃.

Scheme 3.1



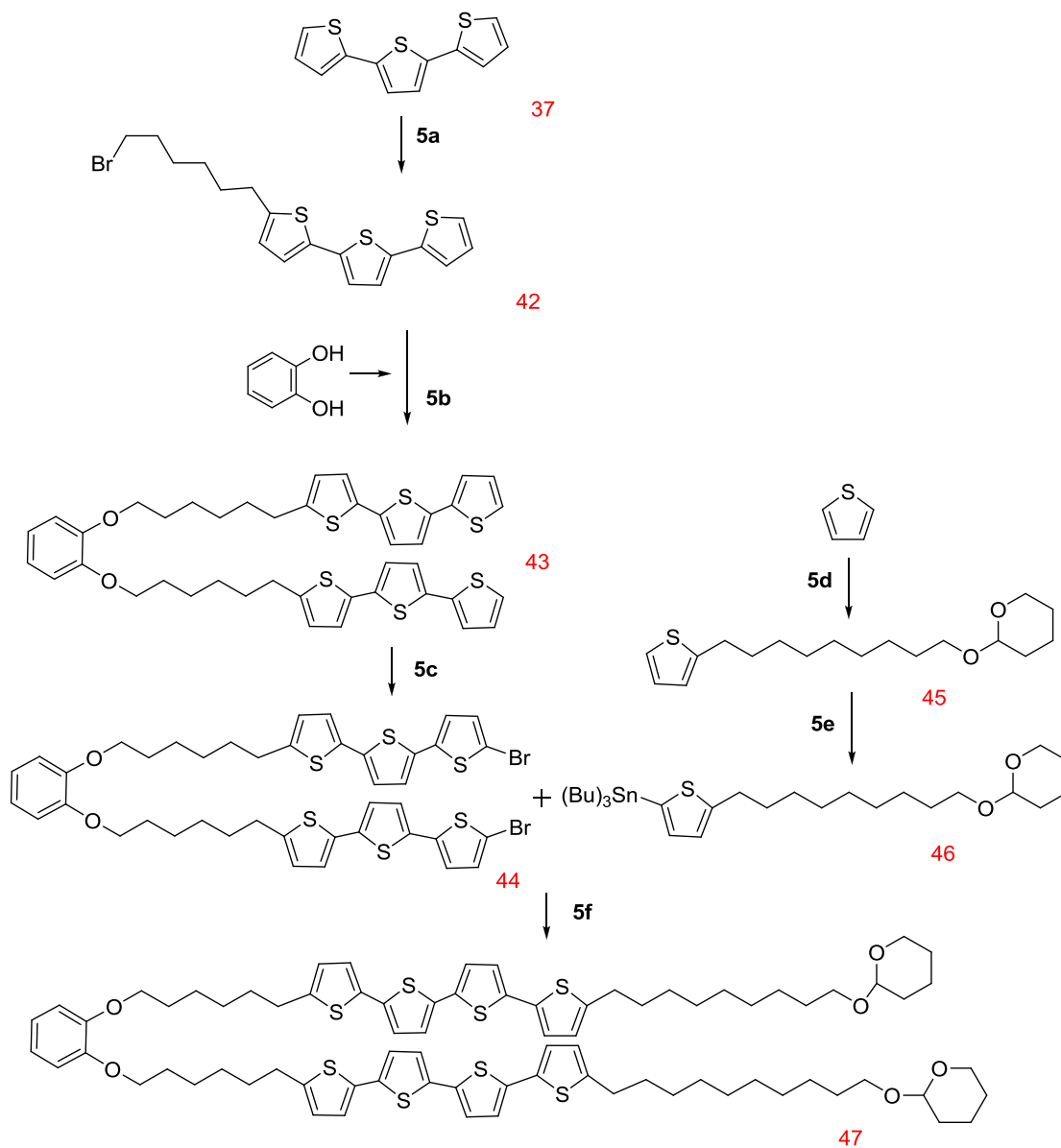
g: (i) BBr_3 , DCM, (ii) ice, H_2O .
 h: H_2SO_4 , DCM
 i: K_2CO_3 , DMF

Scheme 4



- a: NBS, silica gel, DCM.
 b: 2-(Tributylstannyl)thiophene, $\text{Pd}(\text{PPh}_3)_4$, DMF, K_2CO_3 .
 c: NBS, silica gel, DCM.
 d: $\text{Pd}(\text{PPh}_3)_4$, DMF, K_2CO_3 .

Scheme 5



a: (i) n-BuLi, THF, (ii) 1,6-Dibromohexane.

b: Pd(PPh₃)₄, DMF, K₂CO₃.

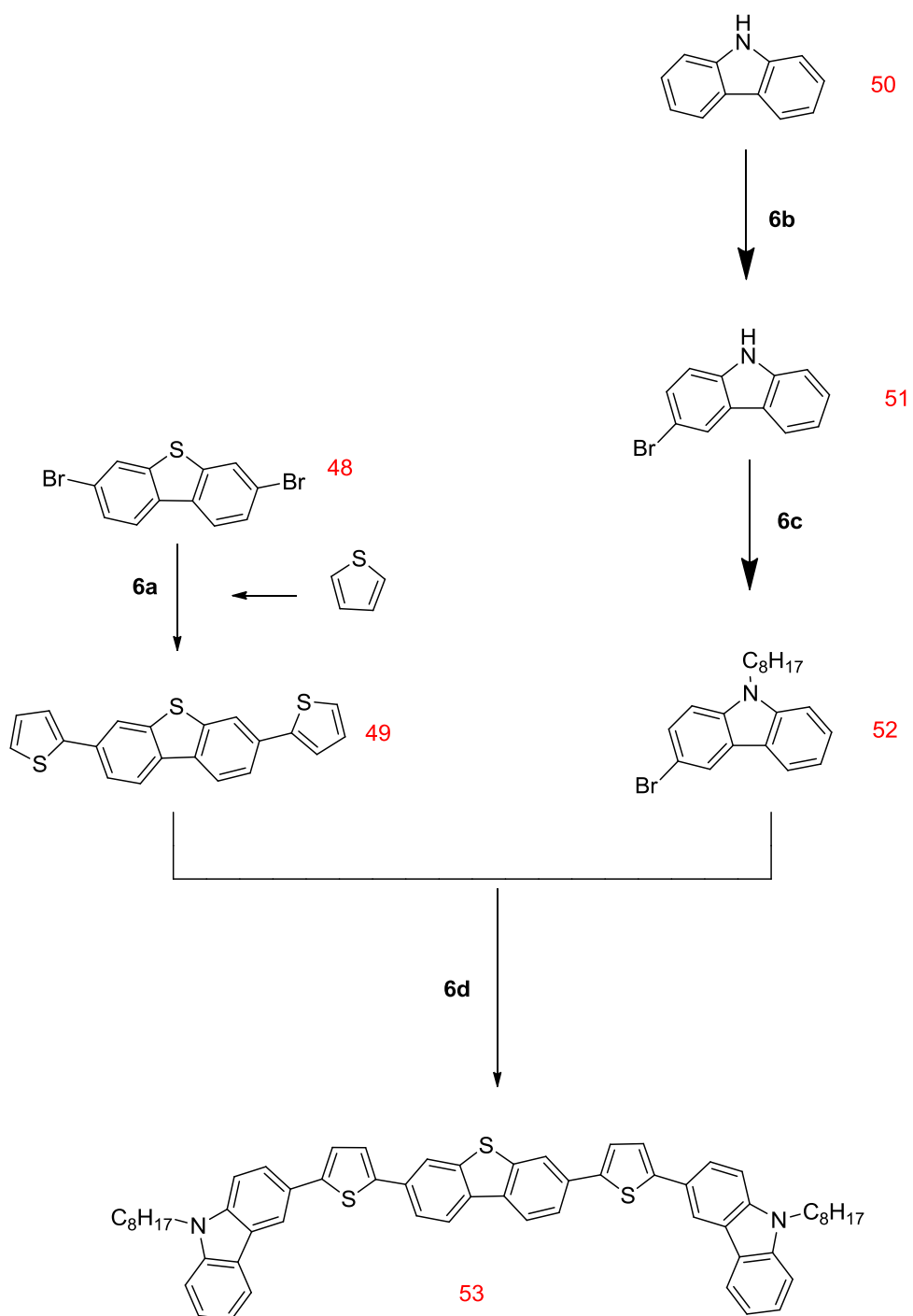
c: NBS, DCM, silica gel

d: (i) n-BuLi, THF, (ii) 2-((9-bromononyl)oxy)tetrahydro-2H-pyran.

e: (i) n-BuLi, THF, (ii) Tributylstannyl chloride.

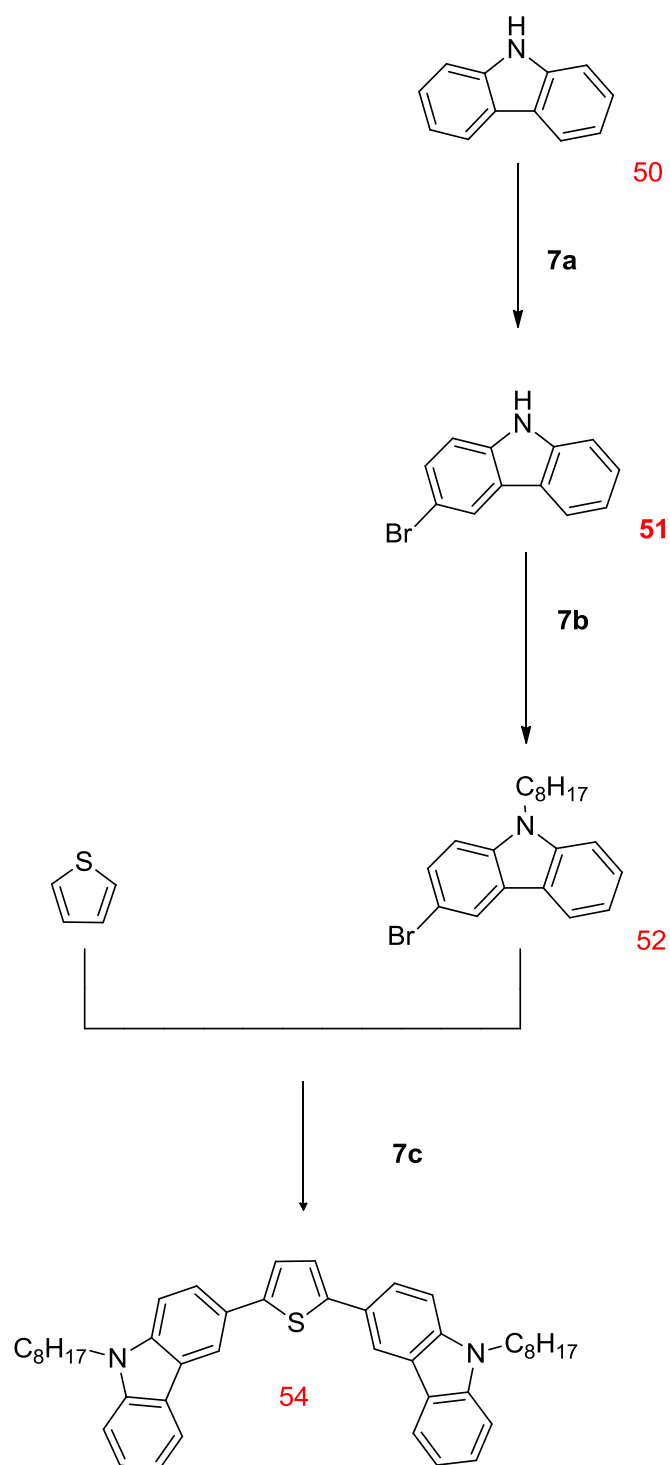
f: Pd(PPh₃)₄, DMF, K₂CO₃.

Scheme 6



- a: K_2CO_3 , Pivalic acid, $Pd(OAc)_2$, PCy_3HBF_4 , DMF.
 b: N-bromosuccinimide (NBS), DMF, 0 °C.
 c: 1-Bromooctane, DMSO, NaOH.
 d: K_2CO_3 , Pivalic acid, $Pd(OAc)_2$, PCy_3HBF_4 , DMF.

Scheme 7

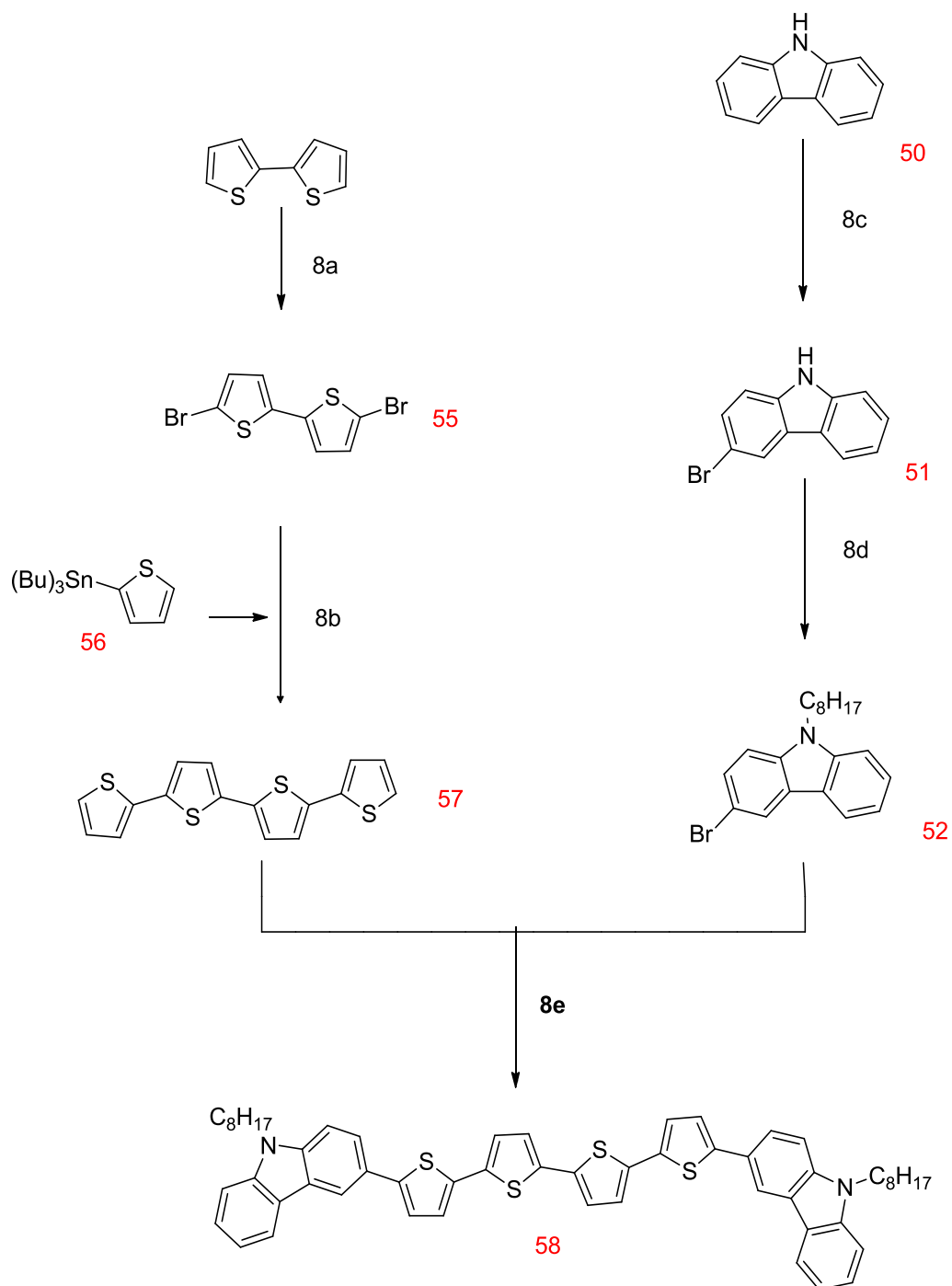


a: N-bromosuccinimide (NBS), DMF, 0 °C.

b: 1-Bromooctane, DMSO, NaOH.

c: K_2CO_3 , Pivalic acid, $Pd(OAc)_2$, PCy_3HBF_4 , DMF.

Scheme 8



a: N-bromosuccinimide (NBS), DCM, silica gel.

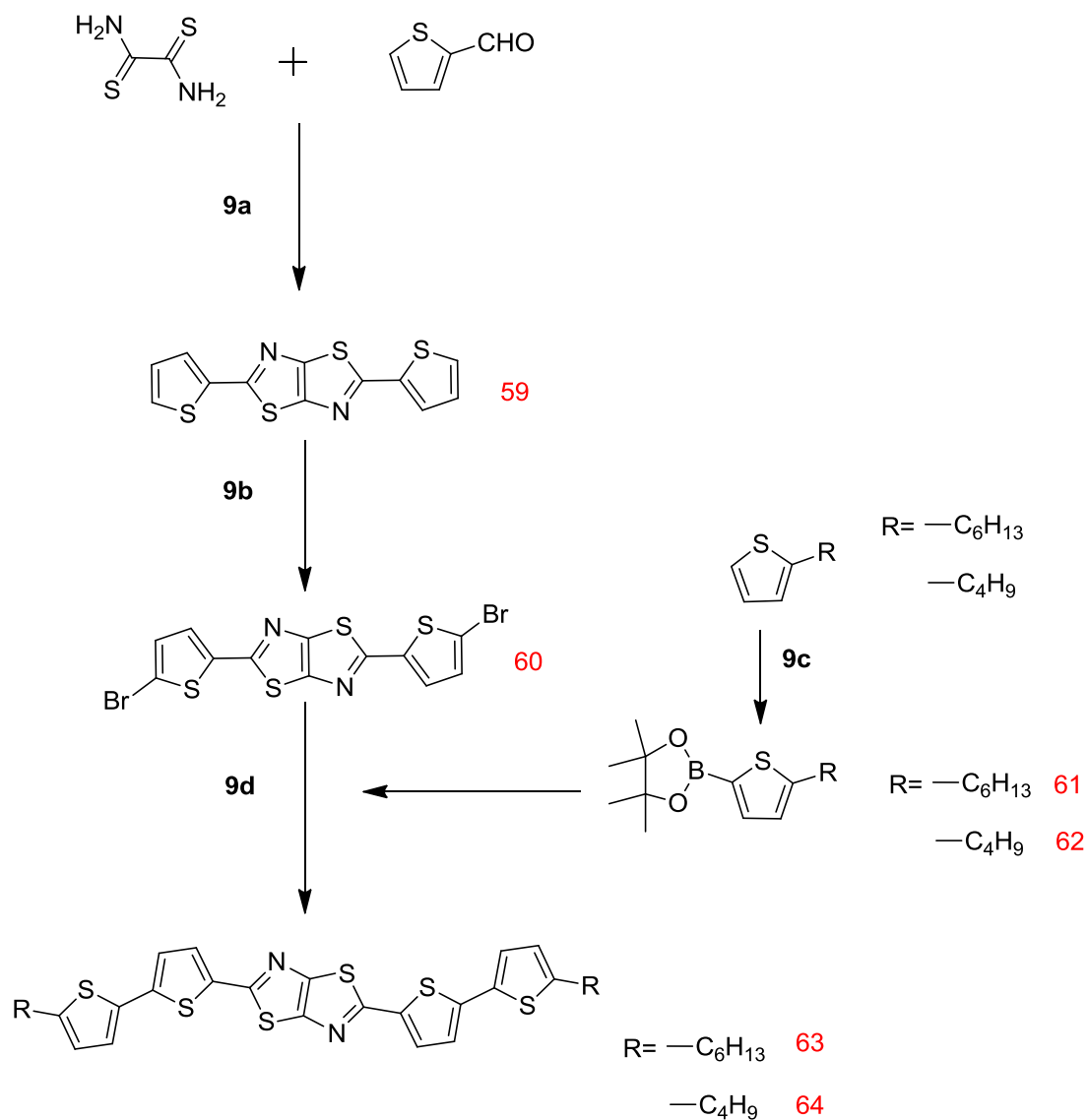
a: $\text{Pd}(\text{PPh}_3)_4$, DMF, K_2CO_3 .

b: N-bromosuccinimide (NBS), DMF, 0 °C.

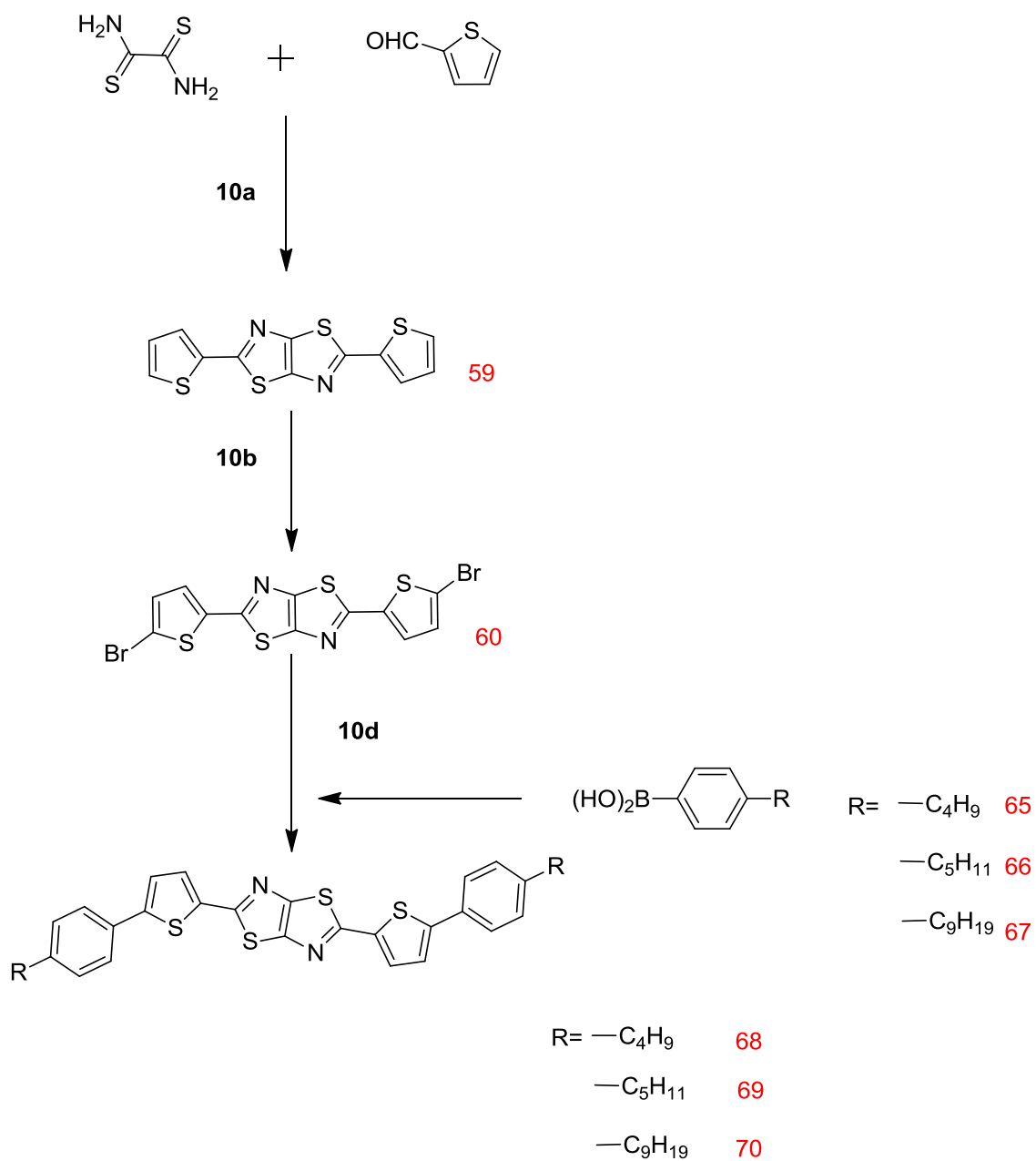
c: 1-Bromooctane, DMSO, NaOH.

d: K_2CO_3 , Pivalic acid, $\text{Pd}(\text{OAc})_2$, PCy_3HBF_4 , DMF.

Scheme 9

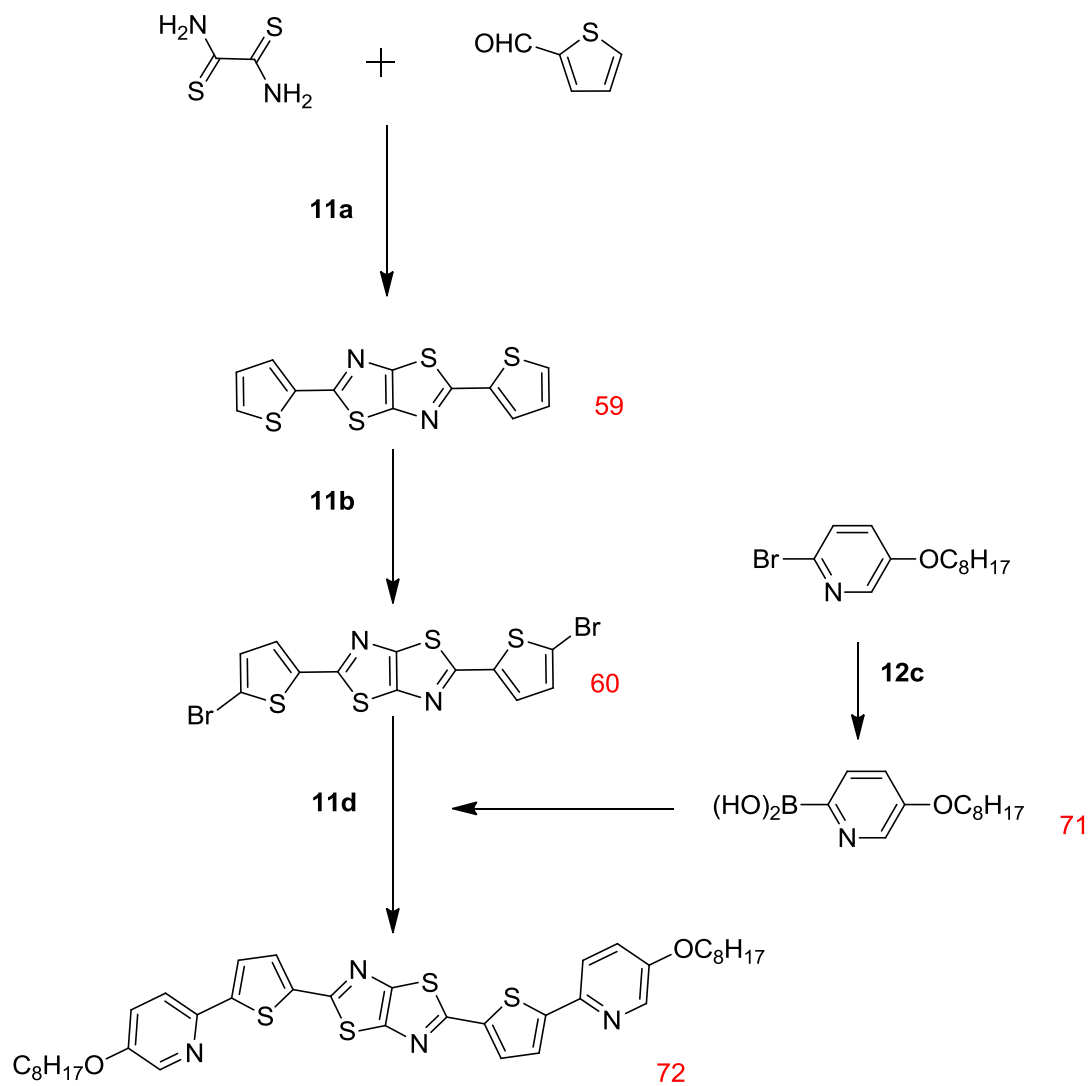


Scheme 10



a: DMF, reflux overnight
 b: NBS, DMF
 c: $\text{Pd}(\text{OAc})_2$, PPh_3 , Na_2CO_3 , THF

Scheme 11



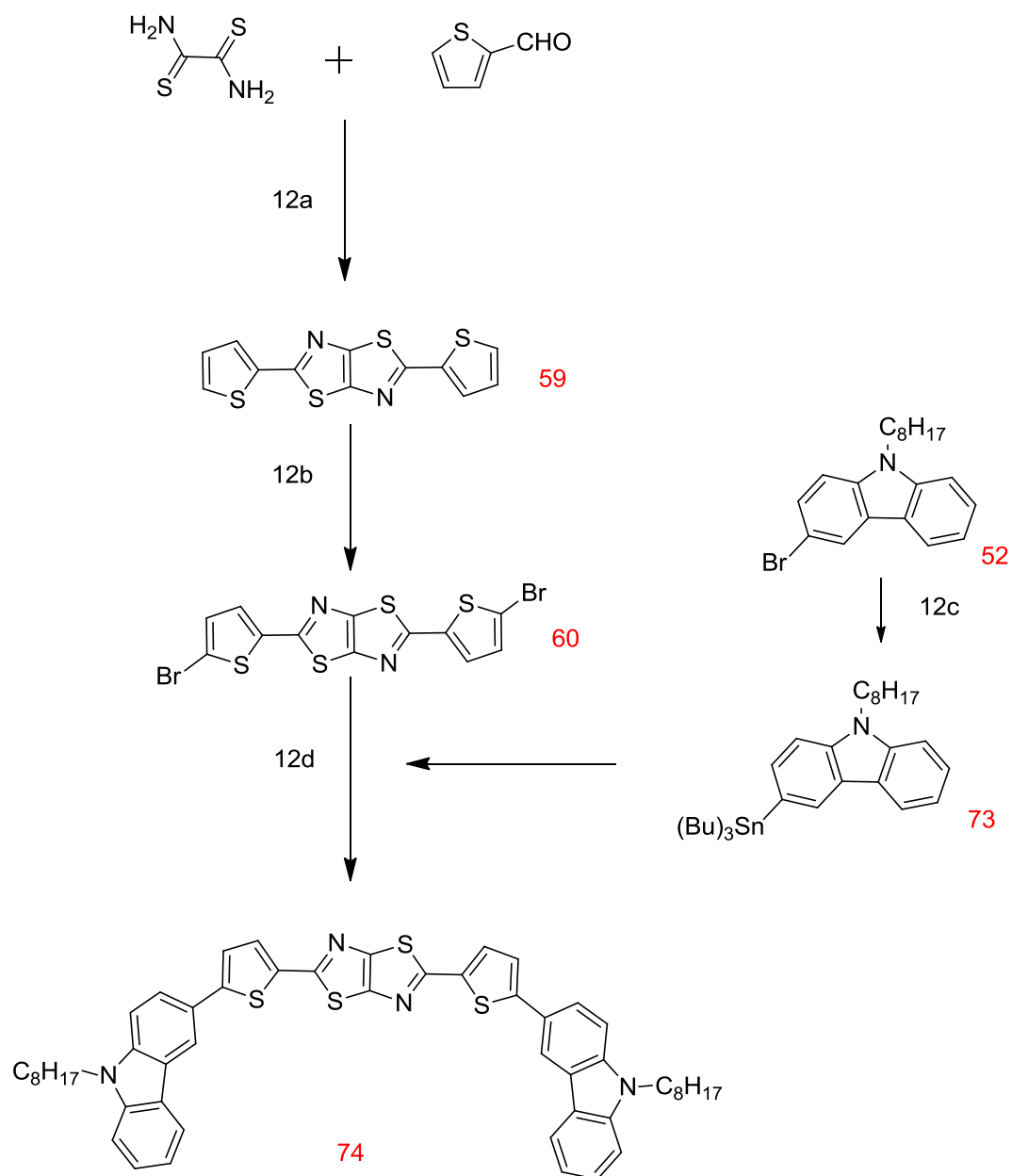
a: DMF, reflux overnight

b: NBS, DMF

c: (i) n-BuLi, THF; (ii) Triisopropyl borate; (iii) H₂O

d: Pd(OAc)₂, PPh₃, Na₂CO₃, THF

Scheme 12



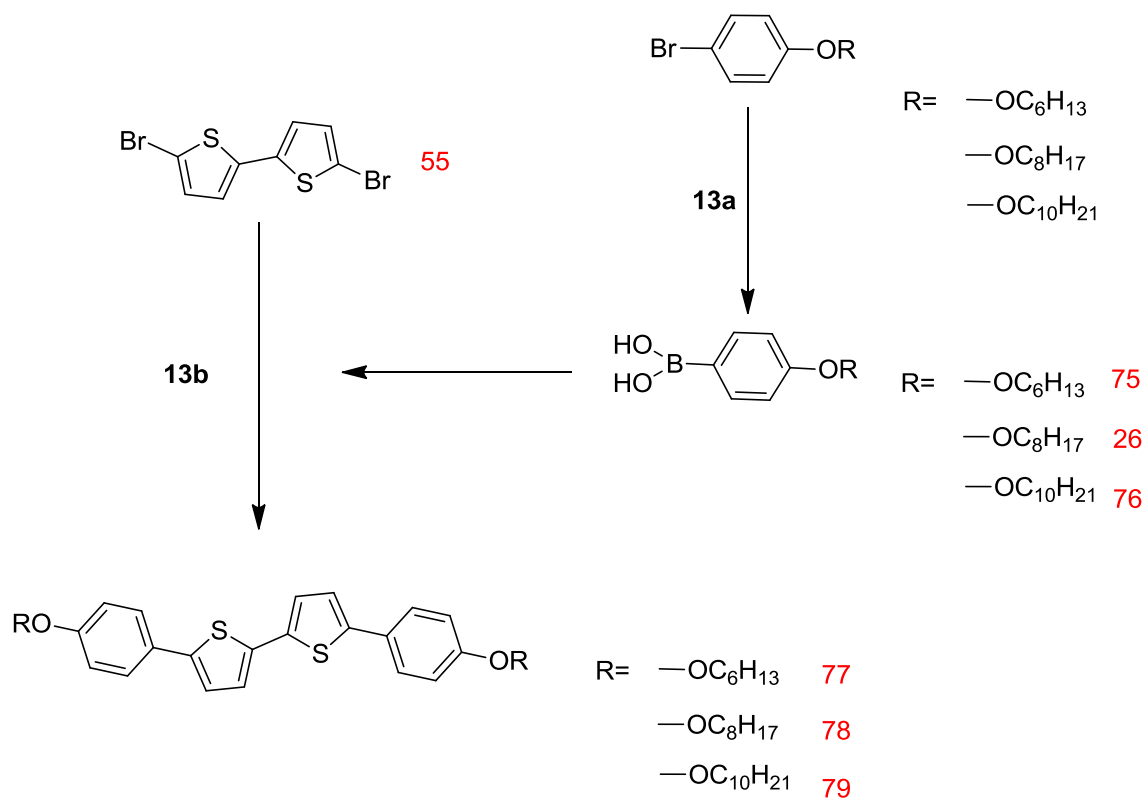
a: DMF, reflux overnight

b: NBS, DMF

c: (i) *n*-BuLi, THF; (ii) Tributylstannyl chloride

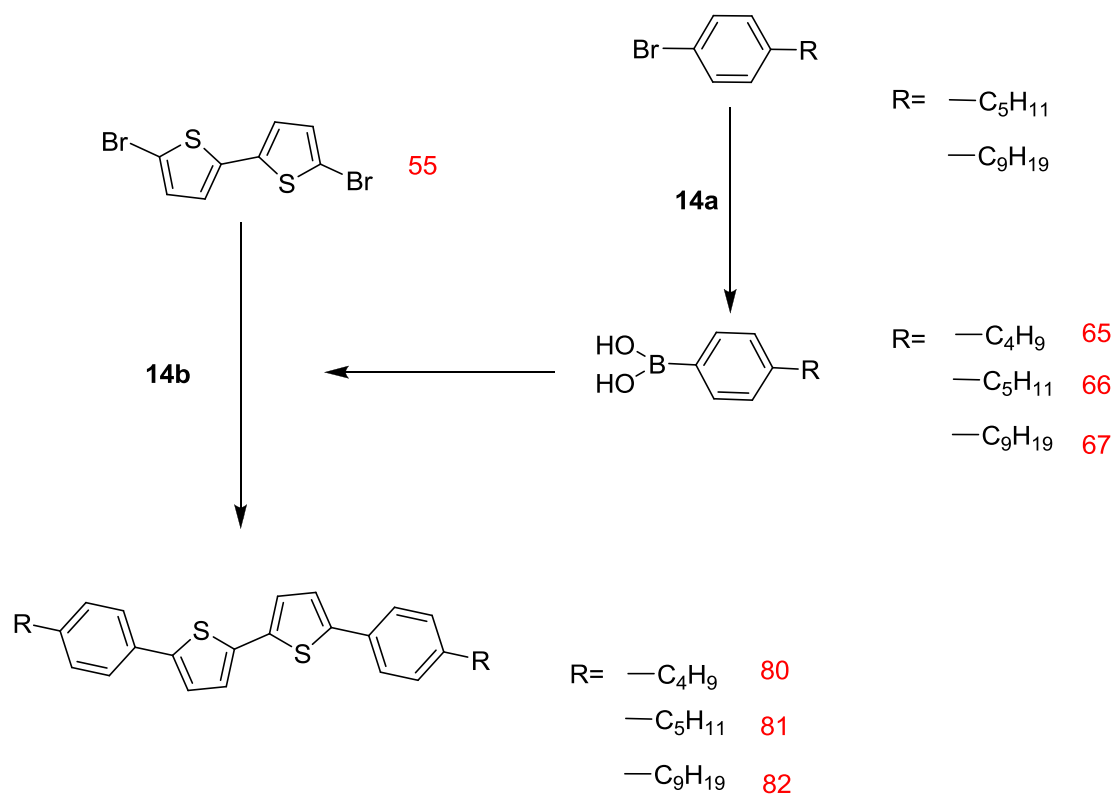
d: Pd(Ph₃)₄, K₂CO₃, DMF

Scheme 13



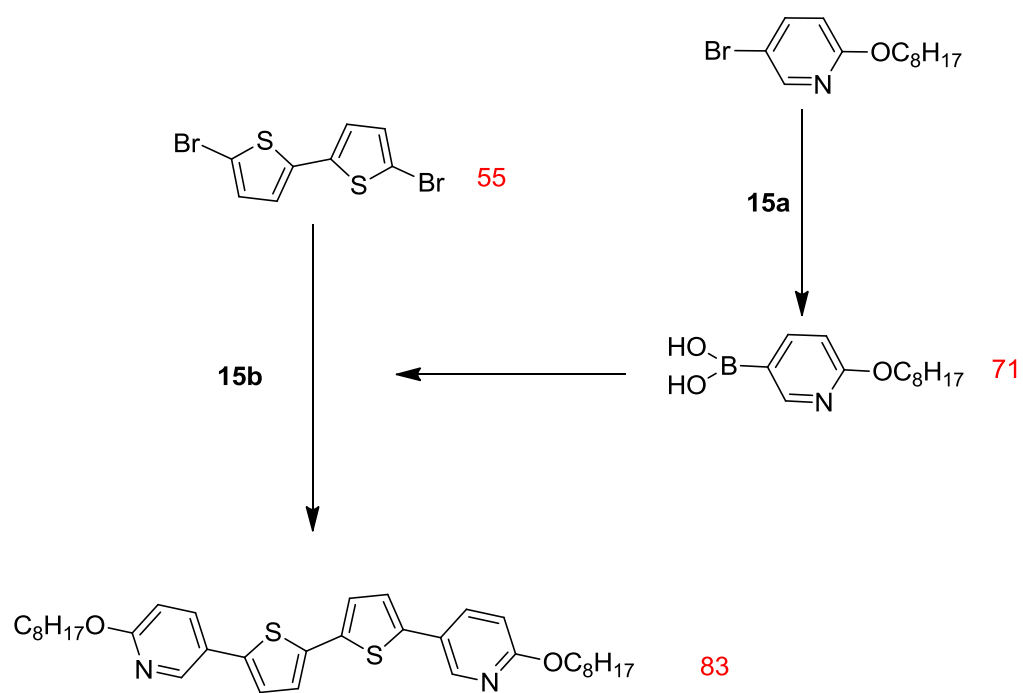
a: (i) n-BuLi, THF; (ii) Triisopropyl borate; (iii) H₂O
 b: K₂CO₃, DMF, Pd(OAc)₂

Scheme 14



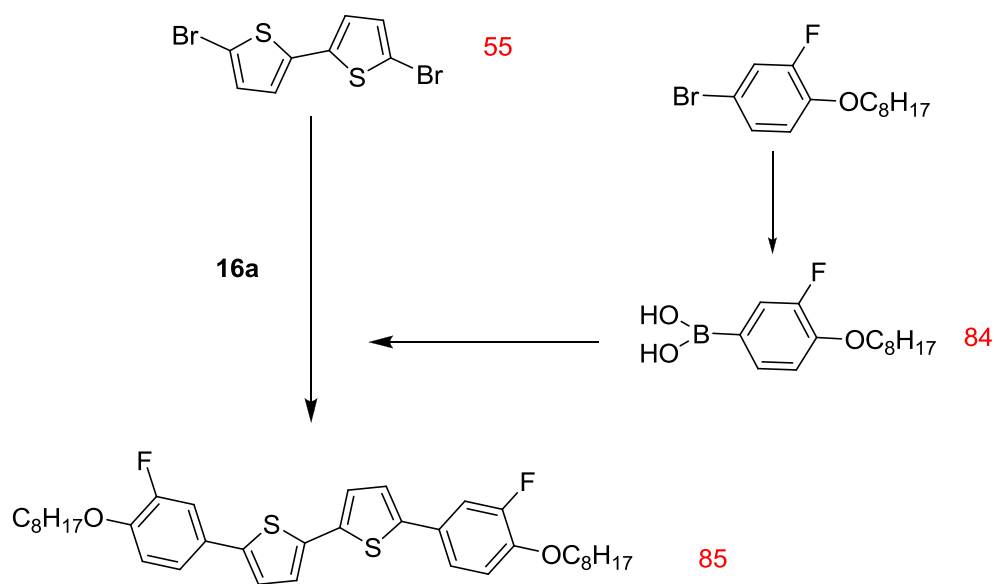
a: (i) n-BuLi, THF; (ii) Triisopropyl borate; (iii) H₂O
 b: K₂CO₃, DMF, Pd(OAc)₂

Scheme 15



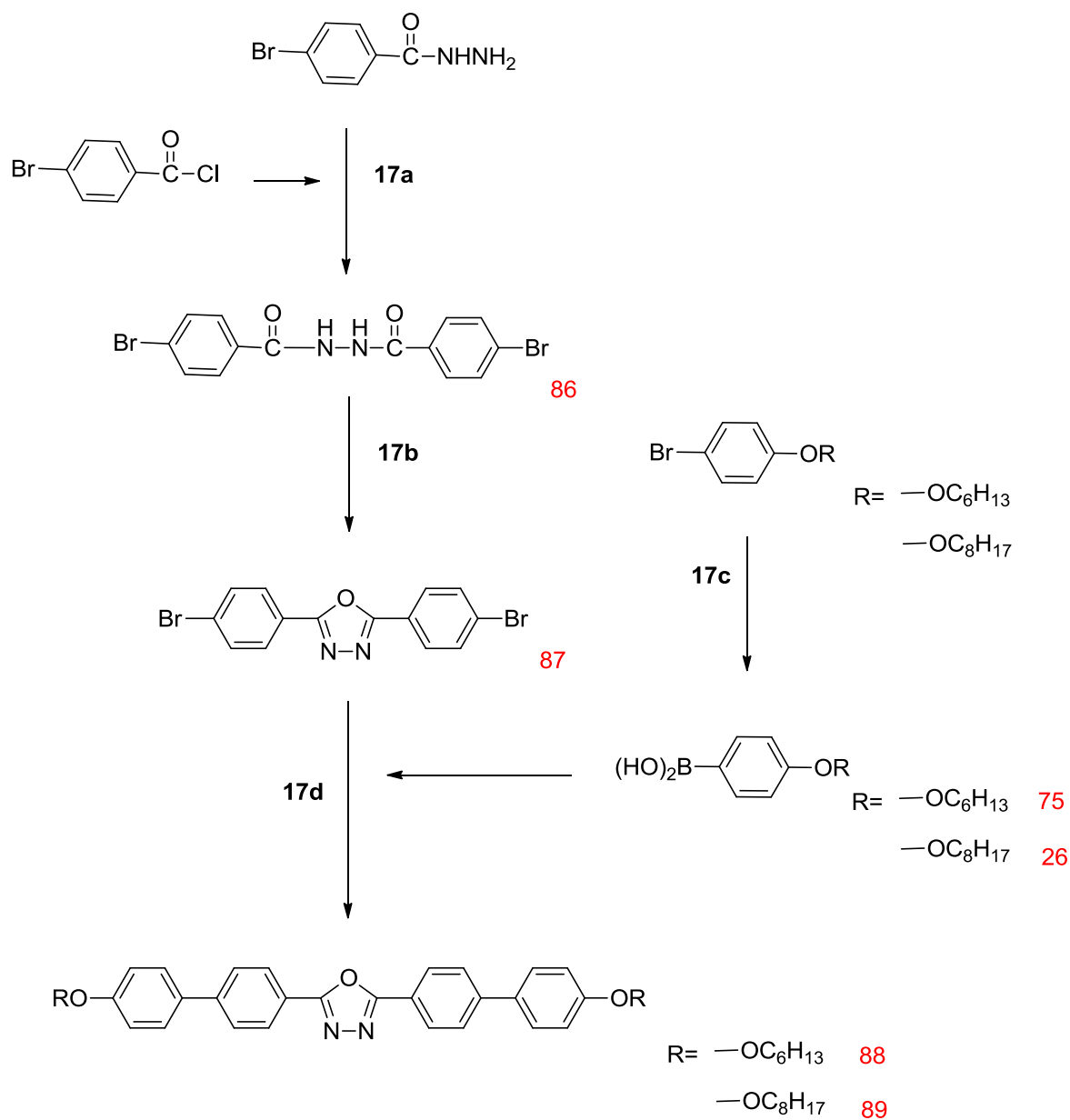
a: (i) n-BuLi, THF; (ii) Triisopropyl borate; (iii) H₂O
b: K₂CO₃, DMF, Pd(OAc)₂

Scheme 16



a: K_2CO_3 , DMF, $\text{Pd}(\text{OAc})_2$

Scheme 17

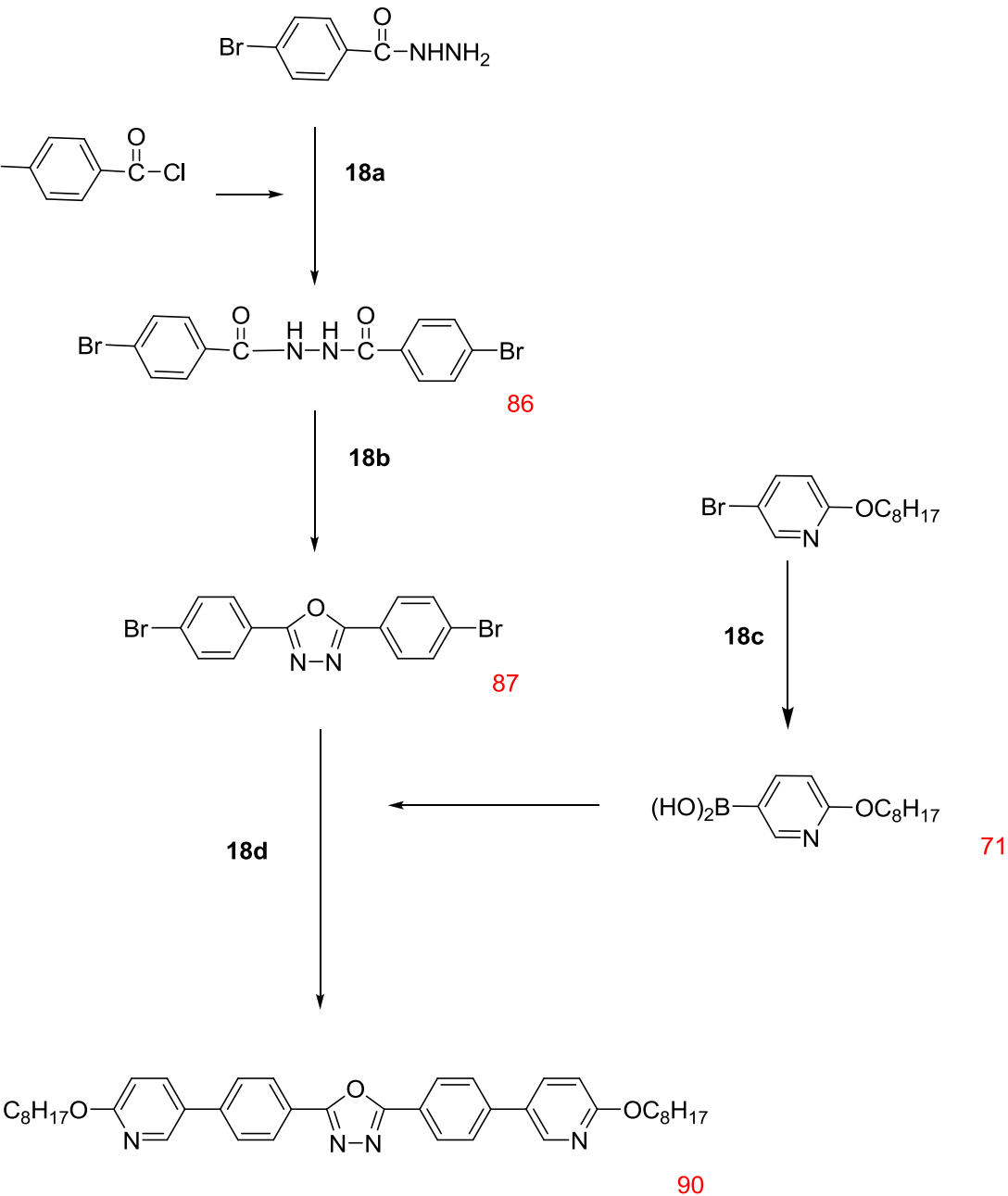


a: Pyridine, 120 °C

b: SOCl_2 , 90 °C

c: (i) n-BuLi, THF; (ii) Triisopropyl borate; (iii) H_2O

d: $\text{Pd}(\text{OAc})_2$, DMF, K_2CO_3

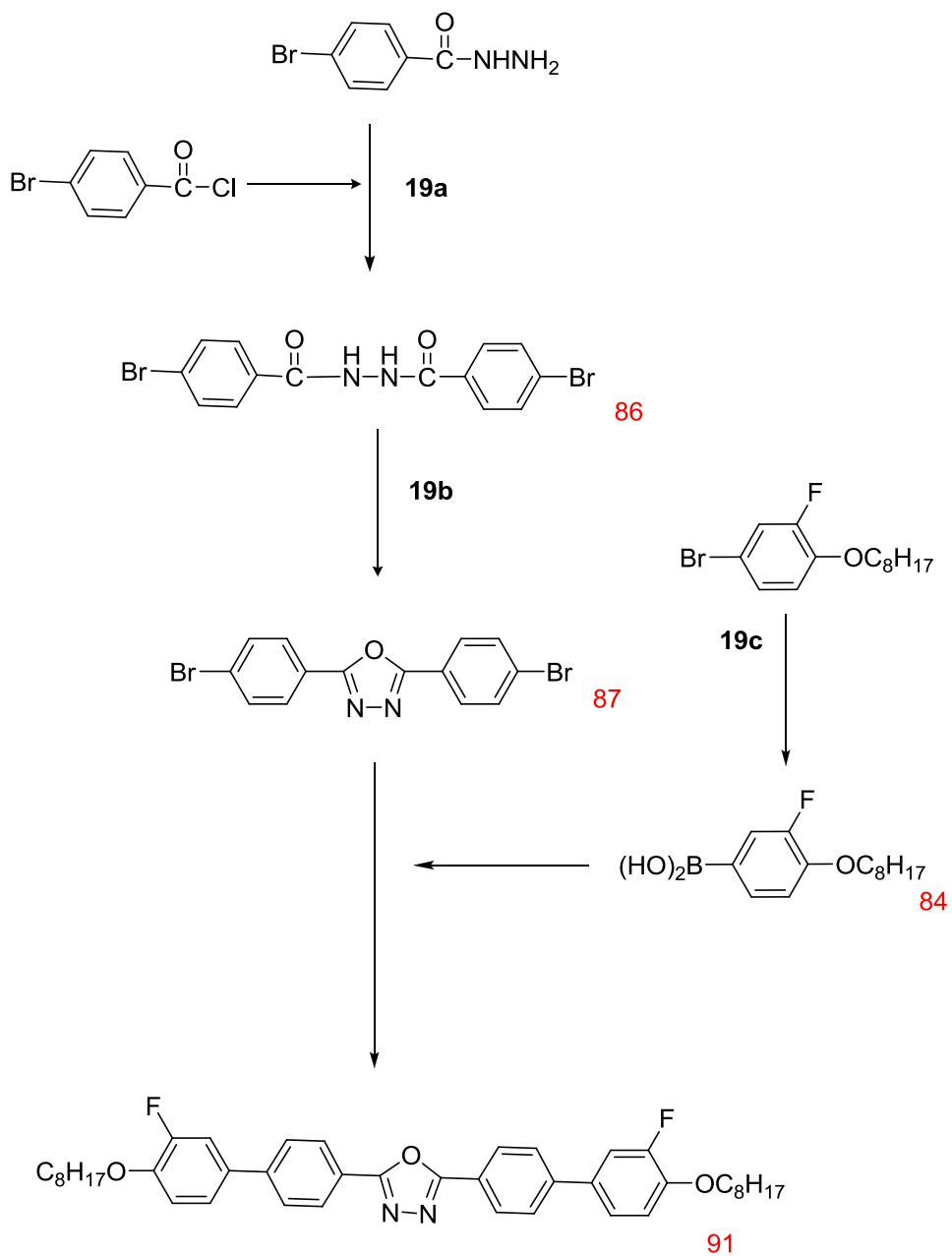


a: Pyridine, 120 °C

b: SOCl_2 , 90 °C

c: (i) n-BuLi, THF; (ii) Triisopropyl borate; (iii) H₂O

d: Pd(OAc)₂, DMF, K₂CO₃



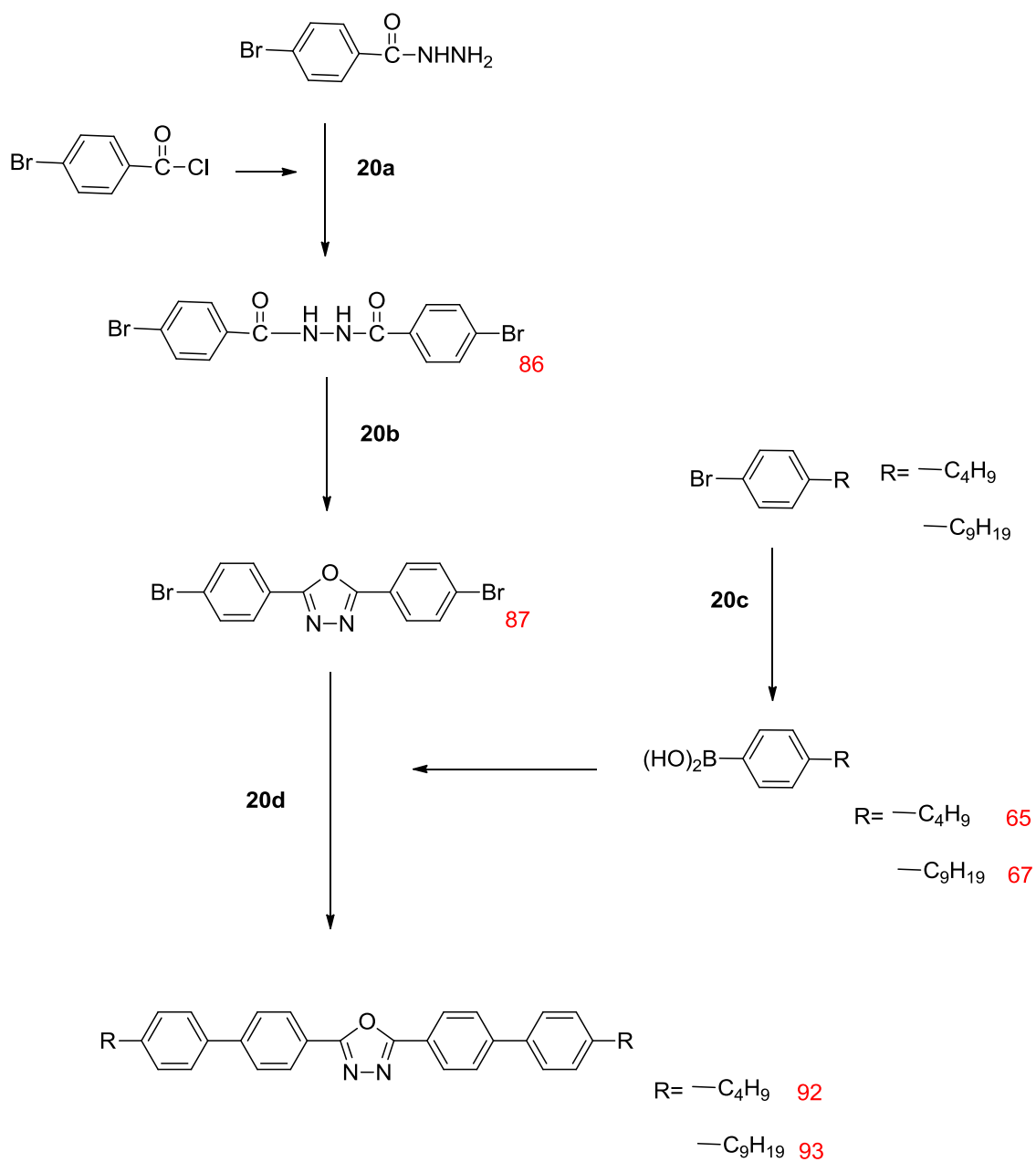
a: Pyridine, 120 °C

b: SOCl_2 , 90°C

c: (i) n-BuLi, THF; (ii) Triisopropyl borate; (iii) H₂O

d: Pd(OAc)₂, DMF, K₂CO₃

Scheme 20



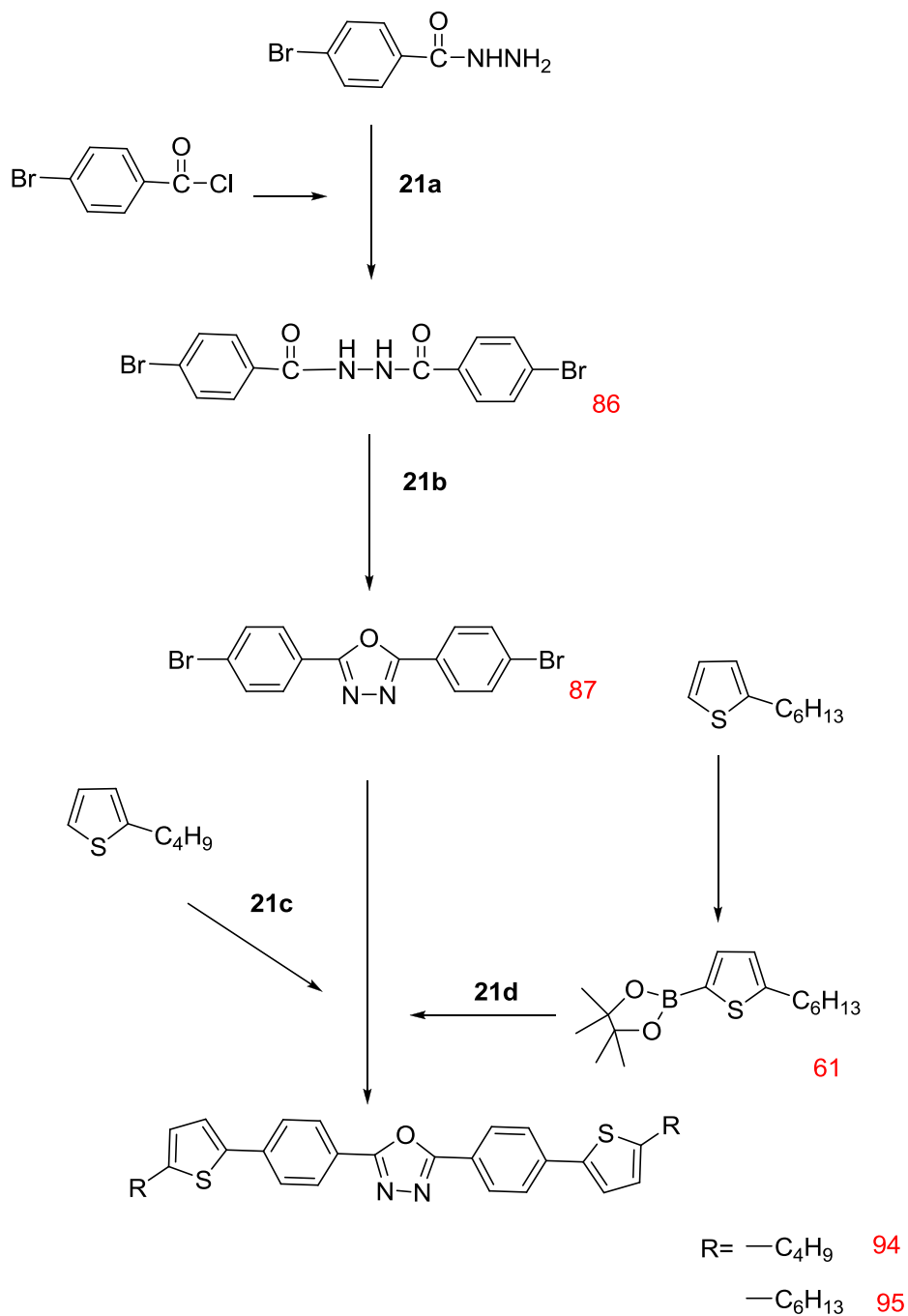
a: Pyridine, 120 °C

b: SOCl_2 , 90 °C

c: (i) $n\text{-BuLi}$, THF; (ii) Triisopropyl borate; (iii) H_2O

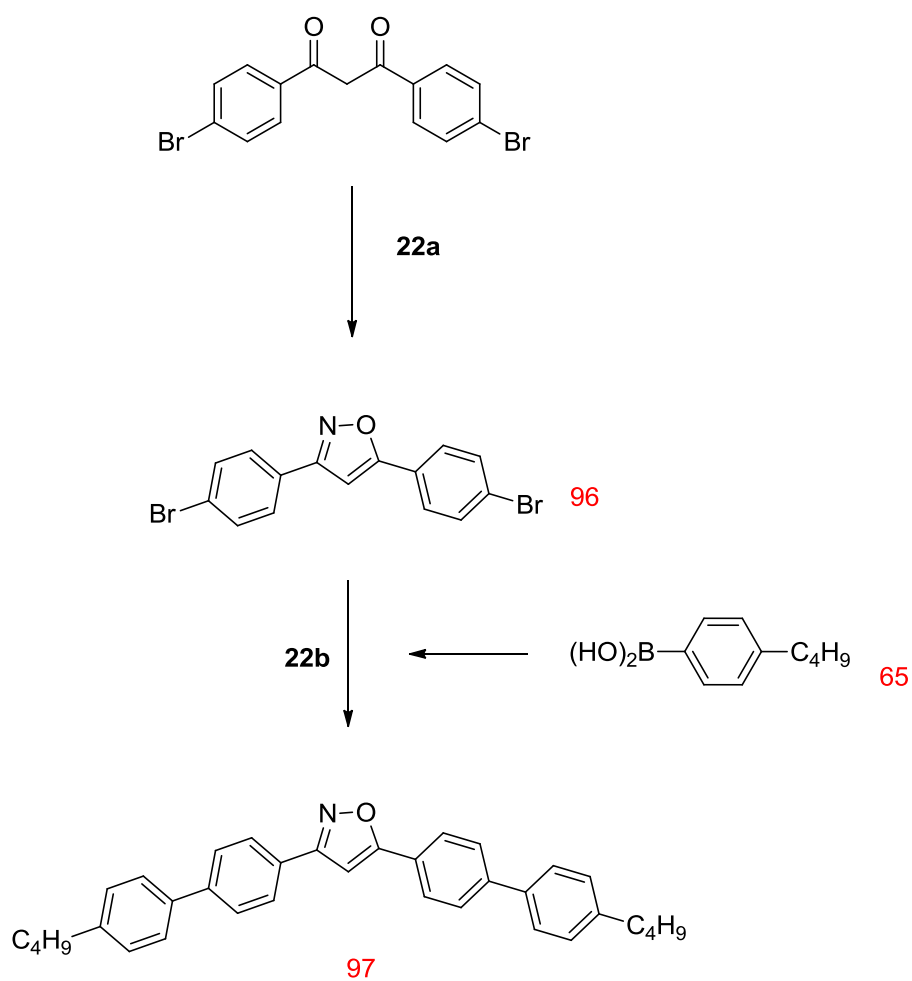
d: $\text{Pd}(\text{OAc})_2$, DMF, K_2CO_3

Scheme 21



a: Pyridine, 120 °C
 b: SOCl_2 , 90 °C
 c: $\text{Pd}(\text{OAc})_2$, PCy_3BF_4 , DMF, K_2CO_3 , PivOH
 d: $\text{Pd}(\text{OAc})_2$, DMF, K_2CO_3

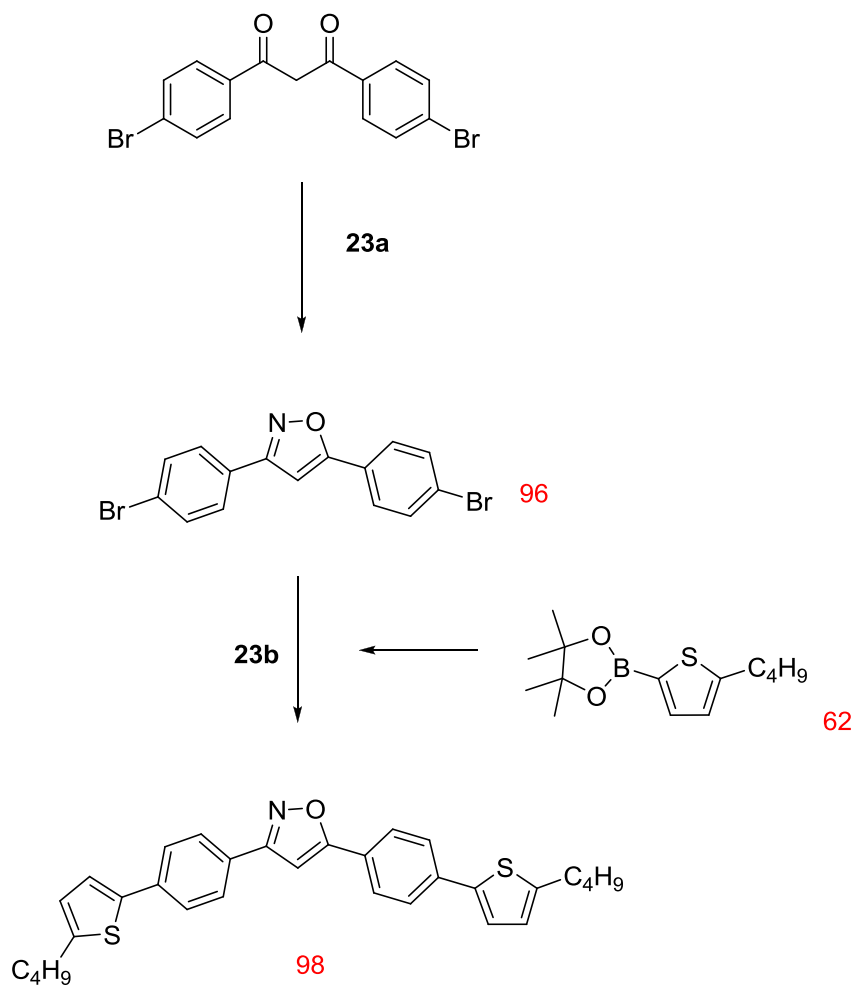
Scheme 22



a: aq. $\text{NH}_2\text{OH}\cdot\text{HCl}$, NaOH , Dioxane

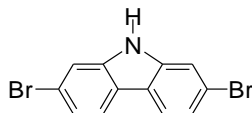
b: $\text{Pd}(\text{OAc})_2$, K_2CO_3 , DMF

Scheme 23



a: aq. $\text{NH}_2\text{OH}\cdot\text{HCl}$, NaOH , Dioxane
b: $\text{Pd}(\text{OAc})_2$, K_2CO_3 , DMF

3.4 Synthesis of the Materials



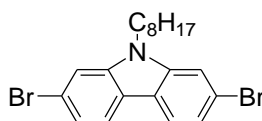
2,7-Dibromo-9-carbazole (2).

A mixture of 4,4'-dibromo-2-nitrobiphenyl (**1**) (10.54 g, 28 mmol) and triethyl phosphite (28 cm³, 0.1 M) was stirred and heated under reflux for 20 h. Then the excess triethyl phosphite was distilled off and the crude product purified via column chromatography [silica gel, ethyl acetate:hexane, 2:3] to yield a white crystalline solid (2.97 g, 33%).

Melting Point/°C: 238-239. (Lit. 236-238, 233-234^[5])

¹H NMR (CDCl₃) δ H: 1.59 (1H, s), 7.35 (2H, dd, J = 1.6, 8.3 Hz), 7.57 (2H, dd, J = 1.6, 8.3Hz), 7.87 (2H, d, J = 8.4 Hz).

MS m/z (EI): 327, 325 (M⁺), 323.



2,7-Dibromo-9-octylcarbazole (3).

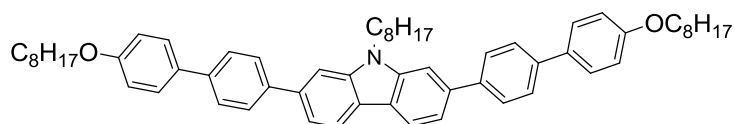
NaH (0.20 g, 60% dispersion in mineral oil, 8.40 mmol) was added in small portions to a solution of 2,7-dibromo-9-H-carbazole (**2**) (2.21 g, 6.85 mmol) in DMF (27.2 cm³) the mixture was stirred for 30 min. 1-Bromooctane (1.45 g, 7.53 mmol) was then added to the mixture and stirred overnight. The reaction was quenched with water (100 cm³) and the crude product extracted into DCM (3 x 50 cm³). The combined extracts were washed with brine (100 cm³), dried over MgSO₄, filtered off and then

evaporated down by rotavapor under reduced pressure. Purification was carried out via column chromatography [silica gel, 5% DCM in hexane] to yield a white crystalline solid (1.05 g, 35%).

Melting Point/ $^{\circ}\text{C}$: 67-68. (Lit. 66-67 ^[6])

^1H NMR (CDCl_3) δ_{H} : 0.90 (3H, t, $J = 6.8$ Hz), 1.29-1.36 (10H, m), 1.80 (2H, quint), 4.01 (2H, t, $J = 6.6$ Hz), 6.98 (2H, dd, $J = 1.54\text{ Hz}, 8.2$ Hz), 7.59 (2H, d, $J = 1.56$ Hz), 7.72 (2H, d, $J = 8.1$ Hz).

MS m/z (EI): 439, 437 (M^+), 435.



2,7-bis-[4'-(Octyloxy)biphenyl-4-yl]-9-(octyl)carbazole (5)

$\text{Pd}(\text{OAc})_2$ (0.005 g, 0.022 mmol) was added to a degassed solution of 2,7-dibromo-9-octylcarbazole (**3**) (1.00 g, 2.3 mmol) and 4-octyloxybiphenyl-4'-yl boronic acid (**4**) (1.64 g, 5.03 mmol) in propan-2-ol/ H_2O (1:1, 18.3 cm^3) the reaction mixture stirred for 10 min at room temperature. Anhydrous potassium phosphate (1.95 g, 9.1 mmol) was then added to the reaction mixture and the temperature increased to 150 $^{\circ}\text{C}$. The mixture was stirred overnight then allowed to cool to room temperature and water (100 cm^3) added. The organic layer was extracted into DCM (3 x 50 cm^3) and the combined extracts washed with brine (50 cm^3), dried over MgSO_4 , filtered off and then evaporated down by rotavapor under reduced pressure. Purification was carried out via column chromatography [silica gel, DCM:hexane, 1:1] and recrystallisation from toluene/EtOH to yield a white crystalline solid (0.32 g, 16 %).

Transition Temp./ $^{\circ}\text{C}$: Cr 229 N 310 I

^1H NMR (CDCl_3) δ_{H} : 0.85-0.92 (9H, m), 1.25-1.37 (26H, m), 1.49 (4H, quint), 1.83 (4H, quint), 1.96 (2H, quint), 4.02 (4H, t, $J = 6.6$ Hz), 4.42 (2H, t, $J = 7.7$ Hz), 7.02 (4H, d, $J = 9.0$ Hz), 7.54 (2H, dd, $J = 1.5$ Hz, 8.0 Hz), 7.59-7.63 (6H, m), 7.68 (4H, d, $J = 8.4$ Hz), 7.79 (4H, d, $J = 8.4$ Hz), 8.16 (2H, d, $J = 8.0$ Hz).

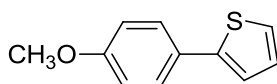
^{13}C NMR (CDCl_3): 159, 142, 139, 132, 131, 129, 126, 117, 114, 112, 110, 69, 58, 32, 30, 26, 23, 14.

MS m/z (MALDI): 839 (M^+).

Combustion analysis:

Expected: C, 85.77%; H, 8.76%; N, 1.67%

Obtained: C 85.74%, H, 8.73%, N, 1.69%.



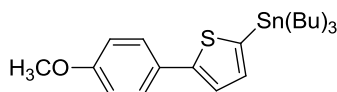
2-(4-Methoxyphenyl)thiophene (8)

A mixture of thiophene-2-boronic acid (**7**) (5.75 g, 0.045 mol), 4-bromoanisole (**6**) (6.72 g, 0.036 mol), sodium carbonate (3.37 g, 0.22 mol), palladium (II) acetate (0.2 g, 2.5 mol%) and triphenylphosphine (0.47 g, 5 mol%) in THF (250 cm^3) and water (25 cm^3) was stirred and heated under reflux for 24 h. The mixture was stirred overnight then allowed to cool to room temperature and water (100 cm^3) added. The organic layer was extracted into DCM (3 x 50 cm^3) and the combined extracts washed with brine (50 cm^3), dried over MgSO_4 , filtered off and then evaporated down by rotavapor under reduced pressure. Purification was carried out via column chromatography [silica gel, DCM:hexane, 1:1] and recrystallisation from DCM/EtOH to yield a white solid (4.58 g, 67%).

Melting Point/°C: 105-107. (Lit. 106-107^[7])

¹H NMR (CDCl₃) δ _H: 3.84 (3H, s), 6.92 (2H, d, *J* = 6.7 Hz), 7.02 (1H, t), 7.17 (1H, d, *J* = 3.8 Hz), 7.21 (1H, d, *J* = 3.8 Hz), 7.52 (2H, d, *J* = 6.8 Hz).

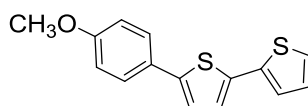
MS *m/z* (EI): 190, 191 (*M*⁺), 192.



5-[(4-Methoxyphenyl)-2-tributylstannyl]thiophene (**9**)

The solution of 2-(4-methoxyphenyl)thiophene (**8**) (4.36 g, 22.9 mmol), which was available from another research programme, in THF (230 cm³) was cooled to -78°C and stirred for 30 min. A 2.5 M solution of *n*-butyllithium (11.0 cm³, 27.5 mmol) was then added to the nitrogen-purged solution using a syringe and the resultant reaction solution stirred for 1 h at this temperature. Tributylstannyl chloride (8.96 g, 27.5 mmol) was then added with a syringe. The reaction mixture was allowed to warm gradually to room temperature overnight. Then water was added to the reaction mixture and stirred for another 1 h. The organic layers were separated and the water layer was extracted with DCM (3 x 50 cm³) and the combined extracts washed with brine (50 cm³), dried over MgSO₄, filtered off and then evaporated down by rotavapor under reduced pressure to afford the desired product (10.74 g, 98%). The material was used directly without further purification.

¹H NMR (CDCl₃) δ _H: 0.97 (9H, t), 1.41 (6H, quint), 1.58-1.68 (12H, m), 3.84 (3H, s), 6.92 (2H, d, *J* = 6.8 Hz), 7.17 (1H, d, *J* = 3.8 Hz), 7.21 (1H, d, *J* = 3.8 Hz), 7.52 (2H, d, *J* = 6.8 Hz).



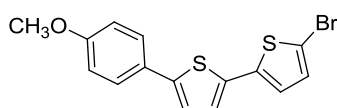
5-(4-Methoxyphenyl)-2,2'-bithiophene (10)

The solution of 5-[(4-methoxyphenyl)-2-tributylstannyl]thiophene (**9**) (10.74 g, 22.4 mmol), which was available from another research programme 2-bromothiophene (3.02 g, 18.7 mmol) in DMF/toluene (0.15 M, 1:4) was degassed with nitrogen and stirred for 10 min. Palladium(II) acetate (0.08 g, 2.0 mol%) and triphenylphosphine (0.25 g, 5 mol%) were added to the reaction mixture, which was heated at 80 °C under reflux overnight. The reaction mixture was then allowed to cool to room temperature, treated with a 1M solution of sodium hydroxide (60 cm³) and filtered through a layer of silica gel with hexane/ethyl acetate/DCM (7:1:2) to remove the tin side product. The crude product was extracted into ethyl acetate/hexane (1:4, 3 x 50 cm³) the combined organic layer washed with water (100 cm³), dried over MgSO₄ and then concentrated under reduced pressure. Purification was carried out via column chromatography [silica gel, DCM:hexane, 1:1] and recrystallisation from EtOH/DCM to yield the desired product as a white crystalline solid (1.00 g, 16.0%).

Melting Point/°C: 150-153

¹H NMR (CDCl₃) δ_{H} : 3.84 (3H, s), 6.92 (2H, d, J = 6.7 Hz), 7.02 (1H, t), 7.12 (2H, m), 7.17 (1H, d, J = 3.8 Hz), 7.21 (1H, d, J = 3.8 Hz), 7.52 (2H, d, J = 6.8 Hz).

MS m/z (EI): 274, 272 (M^+ , M100), 257.



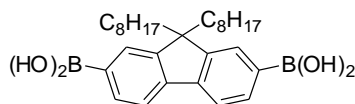
5-Bromo-5'-(4-methoxyphenyl)-2,2'-bithiophene (11)

N-Bromosuccinimide (0.65 g, 3.7 mmol) was added in small portions to the a stirred mixture of 5-(4-methoxyphenyl)-2,2'-bithiophene (**10**) (0.91 g, 3.3 mmol) and silica gel (0.09 g, 10%) in chloroform (13.4 cm³). The reaction mixture was heated and stirred overnight and then allowed to cool to room temperature. The reaction precipitate was filtered off to yield the crude product, which was recrystallized from EtOH/DCM to give the desired product as a yellow crystalline solid (0.75 g, 65%).

Melting Point/°C: 164-166

¹H NMR (CDCl₃) δ_{H} : 3.84 (3H, s), 6.92 (2H, d, $J = 6.5$ Hz), 6.93 (1H, d, $J=3.8$ Hz), 6.97 (1H, d, $J = 3.8$ Hz), 7.05 (1H, d, $J = 3.8$ Hz), 7.09 (1H, d, $J = 3.8$ Hz), 7.51 (2H, d, $J = 6.8$ Hz).

MS m/z (EI): 353, 352 (M^+), 350.



9,9-Dioctyl-9H-fluorene-2,7-diboronic acid (**13**)

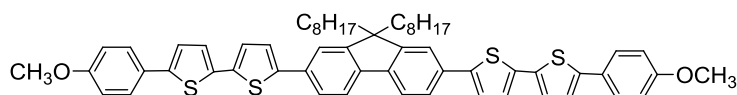
A solution of 2,7-dibromo-9,9-dioctylfluorene (**12**) (11.1 g, 20mmol) in THF (200 cm³) was cooled to -78°C and stirred for 30 min. A 2.5 M solution of *n*-butyllithium (17.6 cm³, 44 mmol in hexane) was then added to the nitrogen-purged solution using a syringe and the resultant reaction solution stirred for 1 h at this temperature. Trimethyl borate (9.35 g, 90 mmol) was then added with a syringe. The resultant reaction mixture was allowed to warm gradually to room temperature overnight. Then 2N hydrochloric acid (100 cm³) was added to the reaction mixture the resultant mixture stirred at room temperature for 1 h. The organic layers were separated and the water layer was extracted with diethyl ether (3 x 50 cm³). The combined organic layers were washed with water (3 x 50 cm³), brine (2 x 50 cm³), dried over MgSO₄,

filtered off and then evaporated down by rotavapor under reduced pressure. The crude product was purified by recrystallisation from hexane to give the desired product as a white power (5.26 g, 48%).

Melting Point/ $^{\circ}\text{C}$: 129 (Lit. 129-130^[8])

^1H NMR (DMSO- d_6) δ_{H} : 0.62-0.99 (30H, m), 1.79-1.81 (4H, m), 7.11-7.13 (2H, m), 7.49 (2H, d, $J = 7.5$ Hz), 7.64 (2H, d, $J = 7.6$ Hz).

MS m/z (EI): 479, 478 (M^+ , M100), 445, 378.



2,7-bis-{5-[5-(4-Methoxy)phenyl]thiophen-2-yl}thiophen-2-yl-9,9-dioctyl-9H-fluorene (14)

$\text{Pd}(\text{OAc})_2$ (0.0045 g, 0.020 mmol) and triphenylphosphine (0.01 g, 0.39 mmol) were added to a degassed solution of 9,9-dioctylfluorene-2,7-diboronic acid (**13**) (0.38 g, 0.78 mmol) and 5-bromo-5'-(4-methoxyphenyl)-2,2'-bithiophene (**11**) (0.75 g, 1.97 mmol) in THF/ H_2O (1:2, 10 cm^3) the resultant reaction mixture stirred for 10 min at room temperature. Anhydrous potassium phosphate (0.44 g, 3.2 mmol) was then added to the reaction mixture and the temperature increased to 60 $^{\circ}\text{C}$. The reaction mixture was stirred overnight then allowed to cool to room temperature and water (100 cm^3) was then added. The aqueous layer was extracted into DCM (3 x 50 cm^3) and the combined organic extracts were washed with brine (100 cm^3), dried over MgSO_4 , filtered off and then evaporated down by rotavapor under reduced pressure. Purification was carried out via column chromatography [silica gel, DCM:hexane, 1:1] and recrystallisation from EtOH/DCM to yield the desired product as a yellow green crystalline solid (0.31 g, 43%).

Melting Point/°C: Cr 69 N 155 I

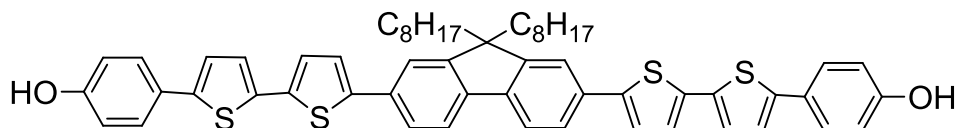
^1H NMR (CDCl_3) δ_{H} : 0.72 (6H, t, $J = 7.5$ Hz), 1.00-1.12 (24H, m), 1.96 (4H, quint), 3.77 (6H, s), 6.86 (4H, d, $J = 9.3$ Hz), 7.05 (2H, d, $J = 3.8$ Hz), 7.11 (4H, t, $J = 3.8$ Hz), 7.23 (2H, d, $J = 3.8$ Hz), 7.48-7.53 (8H, m), 7.61 (2H, d, $J = 7.8$ Hz).

^{13}C NMR(CDCl_3): 161, 148, 141, 138, 136, 133, 131, 129, 126, 125, 124, 115, 56, 48, 44, 32, 30, 24, 22, 14.

Combustion analysis:

Expected: C, 76.08%; H, 6.71%, S, 13.77%

Obtained: C, 76.04%; H, 6.75%; S, 13.74%



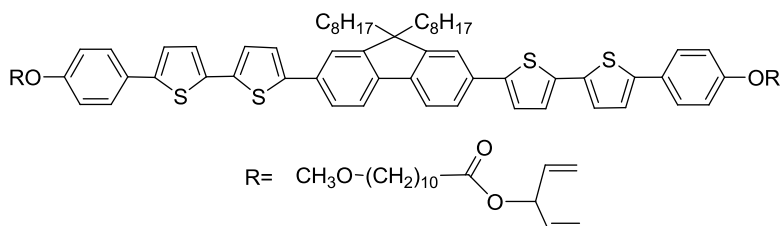
2,7-bis-{5-[5-(4-Hydroxyphenyl)thiophen-2-yl]thiophen-2-yl}-9,9-dioctyl-9H-fluorene (15).

Boron tribromide (0.096 cm³, 0.99 mmol) in DCM (1 cm³) was added dropwise to a cooled (0 °C) stirred solution of 2,7-bis-{5-[5-(4-methoxy)phenyl]thiophen-2-yl}thiophen-2-yl}-9,9-dioctylfluorene (**14**) (0.31 g, 0.33 mmol) in chloroform (9 cm³). The reaction mixture was stirred at room temperature overnight, then poured onto an ice/water mixture (40 g) and stirred for 30 min. Chloroform (150 cm³) was added and the resultant organic layer separated off, washed with water (3×100 cm³), dried over MgSO₄, filtered off and then evaporated down by rotavapor under reduced pressure. The crude product was purified by recrystallisation from hexane to yield the desired product as a green powder (0.20 g, 67%).

Melting Point/°C: 88-90.

¹H NMR (CDCl₃) δ _H: 0.79 (6H, t, *J* = 6.8 Hz), 1.07-1.21 (24H, m), 2.04 (4H, quint), 4.89 (2H, s), 6.87 (4H, d, *J* = 8.6 Hz), 7.13 (2H, d, *J* = 3.6 Hz), 7.18 (4H, t, *J* = 4.2 Hz), 7.30 (2H, d, *J* = 3.8 Hz), 7.50 (4H, d, *J* = 8.6 Hz), 7.55 (2H, d, *J* = 1.3 Hz), 7.60 (2H, dd, *J* = 1.4, 7.7 Hz), 7.68 (2H, d, *J* = 7.7 Hz).

MS *m/z* (MALDI): 903 (M⁺).



2,7-bis-[5-(5-{4-[10-(1-Vinylallyloxycarbonyl)decyloxy]phenyl}thiophen-2-yl)thiophen-2-yl]-9,9-dioctyl-9H-fluorene (16).

A mixture of 2,7-bis-{5-[5-(4-hydroxyphenyl)thiophen-2-yl]thiophen-2-yl}-9,9-dioctylfluorene (**15**) (0.20 g, 0.22 mmol) and potassium carbonate (0.13 g, 0.89 mmol) in DMF (15 cm³) was stirred for 2 h. 1,4-Pentadien-3-yl-11-bromoundecanoate (0.15 g, 0.55 mmol) was added to the reaction mixture, which was then heated to 90 °C under reflux for 48 h. The reaction mixture was cooled to room temperature, water (100 cm³) was added and the product extracted into DCM (5×50 cm³). The combined organic layers were washed with brine (100 cm³), dried over MgSO₄, filtered off and then evaporated down by rotavapor under reduced pressure. The crude product was purified via recrystallisation from EtOH/DCM to yield the desired product as a orange solid (0.22 g, 71 %).

Transition temperature/°C: Cr 52 N 143 I.

¹H NMR (CDCl₃) δ_H: 0.70 (4H, quint), 0.78 (6H, t), 1.02-1.20 (20H, m), 1.28-1.40 (20H, m), 1.46 (4H, quint), 1.64 (4H, quint), 1.79 (4H, quint), 2.00-2.04 (4H, m), 2.34 (4H, t), 3.98 (4H, t), 5.23 (4H, dt), 5.30 (4H, dt), 5.72 (2H, tt), 5.80-5.88 (4H, m), 6.91 (4H, d, *J* = 8.7 Hz), 7.12 (4H, m), 7.20 (2H, d, *J* = 3.9 Hz), 7.34 (2H, d, *J* = 3.9 Hz), 7.56 (4H, d, *J* = 8.7 Hz), 7.58 (2H, d, *J* = 1.5 Hz), 7.62 (2H, dd, *J* = 1.5, 7.8 Hz), 7.67 (2H, d, *J* = 7.9 Hz).

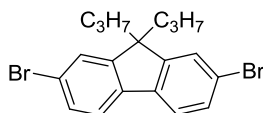
¹³C NMR (CDCl₃): 173, 160, 148, 142, 139, 138, 136, 133, 130, 129, 127, 125, 122, 116, 115, 83, 67, 54, 44, 33, 32, 31, 30, 26, 25, 24, 22, 14

MS *m/z* (MALDI): 1404, 1403 (M⁺, M100).

Combustion analysis:

Expected: C, 76.13%; H, 7.90%; S, 9.13%

Obtained: C 76.20%, H, 7.86%, S, 9.15%



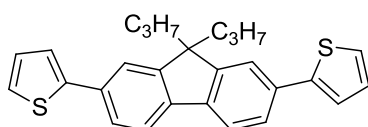
2,7-Dibromo-9,9-dipropyl-9H-fluorene (18)

A 50% aqueous solution of NaOH (70 cm³) was added to a mixture of 2,7-dibromofluorene (**17**) (10.0 g, 0.0309 mol) and TBAB (0.50g, 0.0015 mol) in toluene (70 cm³). 1-Bromopropane (8.73g, 0.0710 mol) in toluene (10 cm³) was then added dropwise at room temperature and the reaction mixture was stirred vigorously overnight at 60 °C under reflux. The reaction mixture was cooled to room temperature, water (100 cm³) was added and the product extracted into DCM (3 x 50 cm³). The combined organic layers were washed with brine (2 x 100 cm³), dried over MgSO₄, filtered off and then evaporated down by rotavapor under reduced pressure. The crude product was purified via recrystallisation from EtOH/DCM to yield the desired product as a white crystalline solid (9.70 g, 77 %).

Melting Point/°C: 136-138 (Lit. 137-137.5^[8])

¹H NMR (CDCl₃) δ_H: 0.61-0.70 (10H, m), 1.89 (4H, m), 7.44 (4H, m), 7.51 (2H, d, *J* = 1.4 Hz).

MS *m/z* (EI): 409, 407 (M⁺, M100), 405.



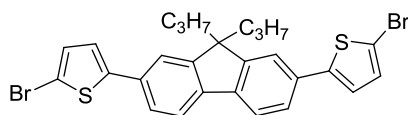
2,7-bis(Thien-2-yl)-9,9-dipropyl-9H-fluorene (19)

A mixture of 2,7-dibromo-9,9-dipropyl-9H-fluorene (**18**) (5.00 g, 12.2 mmol) and 2-(tributylstannyl)thiophene (10.50 g, 28.2mmol) in DMF (81.7 cm³) was stirred and heated to 70 °C. The mixture was degassed with N₂ for 20 min, then Pd(PPh₃)₄ (0.28 g, 2 mol%) was added. The resultant mixture was heated at 90 °C overnight and then cooled to room temperature, water (100 cm³) was added and the product extracted into DCM (3 x 50 cm³). The combined organic layers were washed with brine (100 cm³), dried over MgSO₄, filtered off and then evaporated down by rotavapor under reduced pressure. The crude product was purified by passing through a column (10% K₂CO₃ and 90% silica gel) to remove the tin side products then recrystallized from EtOH/DCM to yield the desired product as a light yellow powder (3.90 g, 77%).

Melting Point/°C: 166-168 (Lit. 165-170^[9])

¹H NMR (CDCl₃) δ _H: 0.68-0.72 (10H, m), 2.01 (4H, m), 7.11 (2H, dd, *J* = 1.4Hz, 7.9Hz), 7.30 (2H, d, *J* = 3.8 Hz), 7.39 (2H, d, *J* = 3.7 Hz), 7.57 (4H, m), 7.67 (2H, d, *J* = 7.9 Hz).

MS m/z (EI): 416, 415 (M⁺, M100), 414.



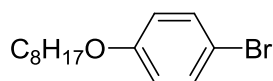
2,7-Bis(5-bromothiophen-2-yl)-9,9-dipropyl-9H-fluorene (**20**)

N-Bromosuccinimide (2.84 g, 15.9 mmol) was added in small portions to the a stirred mixture of 2,7-di(thiophen-2-yl)-9,9-dipropyl-9H-fluorene (**19**) (3.0 g, 7.24 mmol) and silica gel (0.03 g, 10%) in chloroform (60 cm³). The reaction mixture was heated and stirred overnight and then allowed to cool to room temperature. The reaction precipitate was filtered off to yield crude product, which was recrystallized from EtOH/DCM to give the desired product as a light yellow crystalline solid (2.98 g, 72%).

Melting Point/°C: 164-166 (Lit. 160-165^[9])

¹H NMR (CDCl₃) δ_H: 0.68-0.70 (10H, m), 2.01 (4H, m), 7.05 (2H, d, *J* = 3.8 Hz), 7.11 (2H, d, *J* = 3.8 Hz), 7.46 (2H, d, *J* = 7.7 Hz), 7.48 (1H, d, *J* = 1.6 Hz), 7.50 (1H, d, *J* = 1.6 Hz), 7.66 (2H, d, *J* = 7.8 Hz)

MS *m/z* (EI): 574, 572 (M⁺, M100), 570, 529, 500, 487, 450, 420, 377.

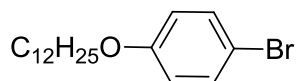


1-Bromo-4-(octyloxy)benzene (**22**)

A mixture of 1-bromooctane (10.70 g, 0.055 mol), 4-bromophenol (**21**) (8.0 g, 0.046 mol) and potassium carbonate (9.50 g, 0.069) in acetone (150 cm³) was heated under reflux for 24 h. After allowing to cool to room temperature, the potassium salts were filtered off. The solvent was removed and the crude product was purified by distillation under vacuum to give the desired product as a colourless oil (5.60 g, 43%)

^1H NMR (CDCl_3) δ_{H} : 0.88 (3H, t), 1.40 (10H, m), 1.76 (2H, quint), 3.93 (2H, t), 6.76 (2H, d, $J = 8.4$ Hz), 7.35 (2H, d, $J = 8.4$ Hz),.

MS m/z (EI): 286, 284 (M^+), 187, 175, 174 ($\text{M}100$), 172, 155, 153, 93.

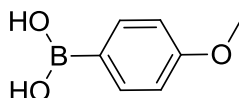


1-Bromo-4-(dodecyloxy)benzene (23).

A mixture of 1-bromododecane (16.75 g, 0.087 mol), 4-bromophenol (**21**) (12.50 g, 0.072 mol) and potassium carbonate (19.98, 0.11 mol) in acetone (200cm^3) was heated under reflux for 24 h. After allowing cooling to room temperature, the potassium salts were filtered off. The excess 1-bromododecane was removed by distillation and the residual oil was crystallized in methanol to give the desired product as colourless oil (23.27 g, 94.7%).

^1H NMR (CDCl_3) δ_{H} : 0.88 (3H, t), 1.40 (18H, m), 1.76 (2H, quint), 3.90 (2H, t), 6.77 (2H, d, $J = 8.4$ Hz), 7.34 (2H, d, $J = 8.4$ Hz).

MS m/z (EI): 342, 341, 340 ($\text{M}100$)



(4-Methoxyphenyl)boronic acid (25)

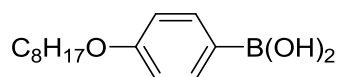
A solution of 4-bromoanisole (**24**) (5.00 g, 0.027 mol) in THF (250cm^3) was cooled to -78°C and stirred for 30 min. A 2.5 M solution of *n*-butyllithium in hexane (14.1cm^3 ,

0.035mol) was then added to the nitrogen-purged solution using a syringe and the resultant reaction solution stirred for 1 h at this temperature. Triisopropyl borate (12.00 g, 0.064mol) was then added with a syringe. The resultant reaction mixture was allowed to warm gradually to room temperature overnight. Then 2N hydrochloric acid (100 cm³) was added to the reaction mixture the resultant mixture stirred at room temperature for 1 h. The organic layers were separated and the water layer was extracted with diethyl ether (3 x 50 cm³). The combined organic layers were washed with water (3 x 50 cm³), brine (50 cm³), dried over MgSO₄, filtered off and then evaporated down by rotavapor under reduced pressure. The crude product was purified by washing with hexane to give the desired product as a white power (3.50 g, 86%).

Melting Point/°C: 80-83(Lit. 79-81 ^[9])

¹H NMR (CDCl₃) δ _H: 2.40 (2H, s), 3.83 (3H, s), 6.76 (2H, d, *J* = 8.4 Hz), 7.35 (2H, d, *J* = 8.4 Hz).

MS *m/z* (EI): 153, 152 (M⁺, M100), 151



4-(Octyloxy)phenylboronic acid (26)

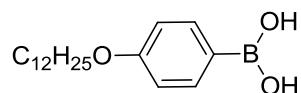
A solution of 1-bromo-4-(octyloxy)benzene (**22**) (5.00 g, 0.018mol) in THF (180 cm³) was cooled to -78°C and stirred for 30 min. A 2.5 M solution of *n*-butyllithium in hexane (8.4cm³, 0.021mol) was then added to the nitrogen-purged solution using a syringe and the resultant reaction solution stirred for 1 h at this temperature. Triisopropyl borate (9.14 cm³, 0.040 mol) was then added with a syringe. The resultant reaction mixture was allowed to warm gradually to room temperature overnight. Then 2N hydrochloric acid (100 cm³) was added to the reaction mixture the

resultant mixture stirred at room temperature for 1 h. The organic layers were separated and the water layer was extracted with diethyl ether (3×50 cm³). The combined organic layers were washed with water (3×50 cm³), brine (50 cm³), dried over MgSO₄, filtered off and then evaporated down by rotavapor under reduced pressure. The crude product was purified by washing with hexane to give the desired product as a white power (3.35 g, 74%).

Melting Point/°C: 71-73 (Lit. 71-75^[10])

¹H NMP (ΨΔΨλ₃) δ_H: 0.88 (3H, t), 1.40 (10H, m), 1.76 (2H, quint), 2.40 (2H, s), 3.93 (2H, t), 6.76 (2H, d, *J* = 8.4 Hz), 7.35 (2H, d, *J* = 8.4 Hz).

MS m/z (EI): 251, 250 (M⁺, M100), 249.



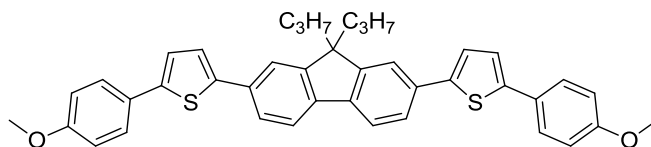
4-(Dodecyloxy)phenylboronic acid (**27**)

A solution of 1-bromo-4-(dodecyloxy)benzene (**23**) (5.17 g, 0.015mol) in THF (180cm³) was cooled to -78 °C and stirred for 30 min. A 2.5 M solution of *n*-butyllithium in hexane (7.3cm³, 0.018mol) was then added to the nitrogen-purged solution using a syringe and the resultant reaction solution stirred for 1 h at this temperature. Triisopropyl borate (6.20 g, 0.033mol) was then added with a syringe. The resultant reaction mixture was allowed to warm gradually to room temperature overnight. Then 2N hydrochloric acid (100 cm³) was added to the reaction mixture the resultant mixture stirred at room temperature for 1 h. The organic layers were separated and the water layer was extracted with diethyl ether (3 x 50 cm³). The combined organic layers were washed with water (3 x 50 cm³), brine (50 cm³), dried over MgSO₄, filtered off and then evaporated down by rotavapor under reduced pressure. The crude product was purified by washing with hexane to give the desired product as a white power (3.35 g, 74%).

Melting Point/°C: 64

¹H NMR (CDCl₃) δ _H: 0.90 (3H, t), 1.38 (18H, m), 1.73 (2H,quint), 2.41 (2H, s), 3.86 (2H, t), 6.75 (2H, d, *J* = 8.4 Hz), 7.32 (2H, d, *J* = 8.4 Hz).

MS *m/z* (EI): 307, 306 (M⁺, M100), 305.



2,7-Bis(5-(4-methoxyphenyl)thiophen-2-yl)-9,9-dipropyl-9H-fluorene (28)

A mixture of 2,7-bis(5-bromothiophene-2-yl)-9,9-dipropyl-9H-fluorene (**20**) (0.50 g, 0.87 mmol), (4-methoxyphenyl)boronic acid (**25**) (0.31 g, 2.06 mmol) and potassium carbonate (0.60 g, 4.3 mmol) in dioxane (20 cm³) was stirred and degassed with N₂ for 30 min. Pd(PPh₃)₄ (0.02 g, 2 mol%) was added to the reaction mixture, which was then heated to 90 °C under reflux for 48 h. The reaction mixture was cooled to room temperature, water (100 cm³) was added and the product extracted into DCM (5×50 cm³). The combined organic layers were washed with brine (100 cm³), dried over MgSO₄, filtered off and then evaporated down by rotavapor under reduced pressure. The crude product was purified via column chromatography [silica gel, DCM:hexane, 2:8] and then recrystallisation from EtOH/DCM to yield the desired product as a yellow powder product (0.27 g, 43 %).

Transition Temperature/°C: Tg 78 Cr 231 N 268 I (Lit. Tg 78 Cr 235 N 265 I^[9])

¹H NMR (CDCl₃) δ _H: 0.89 (6H, t), 1.45 (4H, t), 2.02 (4H, m), 3.99 (6H, s), 6.93 (4H, d, *J* = 6.8 Hz), 7.20 (2H, d, *J* = 3.7 Hz), 7.33 (2H, d, *J* = 3.6 Hz), 7.57 (6H, m), 7.59 (1H, d, *J* = 1.6 Hz), 7.61 (1H, d, *J* = 1.6 Hz), 7.67 (2H, d, *J* = 7.9 Hz)

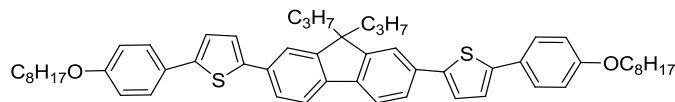
¹³C NMR (CDCl₃): 161, 148, 141, 137, 133, 130, 129, 128, 126, 125, 115, 56, 53, 46, 18, 15.

MS *m/z* (EI): 628, 627 (M⁺), 626.

Combustion analysis:

Expected: C, 78.56%; H, 6.11%; S, 10.23%

Obtained: C, 78.53%; H, 6.12%; S, 10.25%



2,7-Bis(5-(4-octyloxyphenyl)thiophen-2-yl)-9,9-dipropyl-9H-fluorene (29)

A mixture of 2,7-bis(5-bromothiophene-2-yl)-9,9-dipropyl-9H-fluorene (**20**) (2.19 g, 3.8 mmol), 4-(octyloxy)phenylboronic acid (**26**) (2.00 g, 8.0 mmol) and potassium carbonate (2.10 g, 15.0 mmol) in dioxane (38 cm³) was stirred and degassed with N₂ for 30 min. Pd(PPh₃)₄ (0.04 g, 2 mol%) was added to the reaction mixture, which was then heated to 90 °C under reflux for 48 h. The reaction mixture was cooled to room temperature, water (100 cm³) was added and the product extracted into DCM (5×50 cm³). The combined organic layers were washed with brine (100 cm³), dried over MgSO₄, filtered off and then evaporated down by rotavapor under reduced pressure. The crude product was purified via column chromatography [silica gel, DCM:hexane, 2:8] and then recrystallisation from EtOH/DCM to yield the desired product as a yellow powder (1.00 g, 32 %).

Transition Temperature/°C: Cr 162 (N 166) I (Lit. Cr 166 N 173 I^[6])

¹H NMR (CDCl₃) δ_H: 0.67-0.73 (10H, m), 0.89 (6H, t), 1.29-1.35 (20H, m), 1.45 (4H, m), 2.02 (4H, t), 3.99 (4H, t), 6.93 (4H, d, *J* = 6.8 Hz), 7.20 (2H, d, *J* = 3.7 Hz), 7.33 (2H, d, *J* = 3.6 Hz), 7.57 (6H, m), 7.59 (1H, d, *J* = 1.6 Hz), 7.61 (1H, d, *J* = 1.6 Hz), 7.67 (2H, d, *J* = 7.9 Hz)

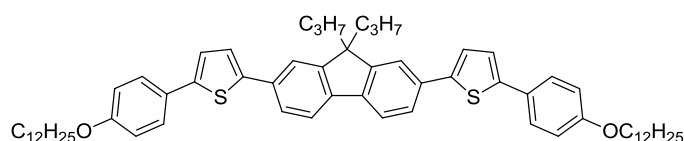
¹³C NMR (CDCl₃): 161, 148, 141, 137, 133, 130, 129, 128, 126, 125, 115, 56, 53, 46, 32, 30, 29, 26, 23, 18, 15, 14.

MS *m/z* (EI): 824, 823 (M⁺), 822.

Combustion analysis:

Expected: C, 80.24%; H, 8.08%; S, 7.79%

Obtained: C, 80.27%; H, 8.06%; S, 7.76%



2,7-Bis(5-(4-dodecyloxyphenyl)thiophen-2-yl)-9,9-dipropyl-9H-fluorene (30)

A mixture of 2,7-bis(5-bromothiophene-2-yl)-9,9-dipropyl-9H-fluorene (**20**) (0.89 g, 1.6 mmol), 4-(dodecyloxy)phenylboronic acid (**27**) (1.00 g, 3.3 mmol) and potassium carbonate (1.10 g, 7.8 mmol) in dioxane (20 cm³) was stirred and degassed with N₂ for 30 min. Pd(PPh₃)₄ (0.018 g, 2 mol%) was added to the reaction mixture, which was then heated to 90 °C under reflux for 48 h. The reaction mixture was cooled to room temperature, water (100 cm³) was added and the product extracted into DCM (5×50 cm³). The combined organic layers were washed with brine (2 x 100 cm³), dried over MgSO₄, filtered off and then evaporated down by rotavapor under reduced pressure. The crude product was purified *via* column chromatography [silica gel, DCM:hexane, 2:8] and then recrystallisation from EtOH/DCM to afford the desired product as a yellow solid (0.52 g, 35 %).

Melting Point/°C: 148

¹H NMR (CDCl₃) δ_H: 0.67-0.73 (10H, m), 0.89 (6H, t), 1.29-1.37 (28H, m), 1.45 (4H, m), 1.80 (4H, m), 2.02 (4H, t), 3.99 (4H, t), 6.93 (4H, d, *J* = 6.8 Hz), 7.20 (2H, d, *J* = 3.7 Hz), 7.33 (2H, d, *J* = 3.6 Hz), 7.57 (6H, m), 7.59 (1H, d, *J* = 1.6 Hz), 7.61 (1H, d, *J* = 1.6 Hz), 7.67 (2H, d, *J* = 7.9 Hz)

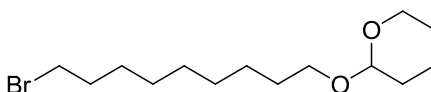
^{13}C NMR(CDCl_3): 160, 147, 141, 137, 133, 130, 129, 128, 126, 125, 115, 69, 53, 46, 32, 29, 25, 23, 18, 15, 14.

MS m/z (EI): 936, 935 (M^+), 934 ($\text{M}100$).

Combustion analysis:

Expected: C, 80.89%; H, 8.84%; S, 6.86%

Obtained: C, 80.85%; H, 8.82%; S, 6.89%

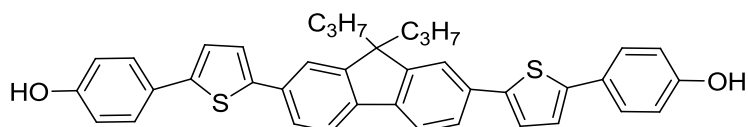


2-(9-Bromononyloxy)tetrahydro-2H-pyran (**32**)

A drop of sulfuric acid was added to the mixture of 9-bromo-1-nonanol (**31**) (5.00 g, 22.4 mmol) and 3,4-dihydro-2H-pyran (3.96 g, 47.0mmol) in DCM (225 cm^3) stirred at 0 °C for 2 h. The reaction mixture was concentrated under reduced pressure and purified by column chromatography [silica gel, hexane:DCM, 2:8] to give the desired product as a light green oil (5.60 g, 94 %).

^1H NMR (CDCl_3) δ_{H} : 1.25-1.42 (10H, m), 1.47-1.61 (6H, m), 1.69-1.73 (2H, m), 1.85 (2H, m), 3.36-3.42 (3H, m), 3.51 (1H, p), 3.72 (1H, q), 3.86 (1H, t), 4.57 (1H, t).

MS m/z (EI): 308 (M^+), 307, 306 ($\text{M}100$).



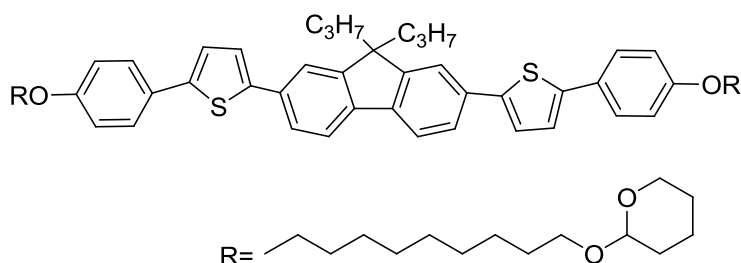
2,7-(5,5'-(Biphenyl-4,4'-diyl)bis(thiophene-5,2-diyl))-9,9-dipropyl-9H-fluorene (33)

Boron tribromide (1.0 cm³, 6.0 mmol) in DCM (1 cm³) was added dropwise to a cooled (0 °C) stirred solution of 2,7-bis(5-(4-octyloxyphenyl)thiophen-2-yl)-9,9-dipropyl-9H-fluorene (**29**) (0.50 g, 0.6 mmol) in DCM (20 cm³). The reaction mixture was stirred overnight and allowed to warm to room temperature gradually, then poured onto an ice/water mixture (40 g) and stirred for 1 h. DCM (150 cm³) was added and the resultant organic layer separated off, washed with water (3×100 cm³), dried over MgSO₄, filtered off and then evaporated down by rotavapor under reduced pressure. The crude product was purified via column chromatography [silica gel, hexane:ethyl acetate, 3:2] to yield the desired product as a light yellow powder (0.23 g, 64%).

Melting Point/°C: 278-279 (Lit. 279 [6])

¹H NMR (CDCl₃) δ _H: 0.67-0.73 (10H, m), 2.04 (4H, t), 5.32 (2H, s), 6.87 (4H, d, *J* = 8.6 Hz), 7.20 (2H, d, *J* = 3.6 Hz), 7.33 (2H, d, *J* = 3.7 Hz), 7.57 (6H, m), 7.59 (1H, d, *J* = 1.6 Hz), 7.61 (1H, d, *J* = 1.6 Hz), 7.67 (2H, d, *J* = 7.9 Hz)

MS *m/z* (EI): 599, 598 (M⁺, M100).



2,7-(Bis(5-(4-(9-(tetrahydro-2H-pyran-2-yloxy)nonyloxy)phenyl)thiophen-2-yl))-9,9-dipropyl-9H-fluorene (34)

A mixture of 2,7-(5,5'-(biphenyl-4,4'-diyl)bis(thiophene-5,2-diyl))-9,9-dipropyl-9*H*-fluorene (**33**) (0.20 g, 0.33 mmol) and K₂CO₃ (0.14 g, 1.0 mmol) in DMF (5 cm³) was stirred for 2 h. Then 2-(6-bromohexyloxy)tetrahydro-2*H*-pyran (**32**) (0.11 g, 0.37 mmol) was added in and the resulted mixture was stirred at 100 °C overnight. The reaction mixture was cooled to room temperature and water (100 cm³) added in. The product was extracted into DCM (3 x 50 cm³) the combined organic layers were washed with brine (100 cm³), dried over MgSO₄, filtered off and then evaporated down by rotavapor under reduced pressure. The crude product was purified via column chromatography [silica gel, DCM:hexane, 2:8] and then recrystallisation from EtOH/DCM to yield a yellow powder product (0.09 g, 32%). This product was very difficult to purify as unwanted side products with similar retention times cannot be removed by column or recrystallization.

Purity: 82%

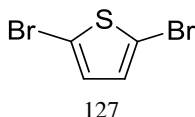
¹H NMR (CDCl₃) δ_H: 0.89 (6H, t), 1.25-1.47 (24H, m), 1.56-1.60 (4H, m), 1.62-1.78 (8H, m), 2.04 (4H, m), 3.37 (4H, t), 3.72-3.87 (4H, m), 4.01 (4H, t), 4.58 (2H, t), 6.91 (4H, d, *J* = 8.8 Hz), 7.63-7.68 (6H, m), 7.71 (4H, d, *J* = 7.5 Hz), 7.75 (2H, s), 7.98 (4H, d, *J* = 7.8 Hz).

MS *m/z* (MALDI): 1053, 1052, 1051 (M⁺, M100).

Combustion analysis:

Expected: C, 76.53%; H, 8.24%; S, 6.10%

Obtained: C, 76.14%; H, 8.86%; S, 5.85%

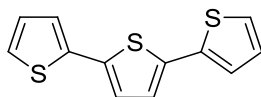


2,5-Dibromothiophene (**36**)

N-Bromosuccinimide (5.87 g, 0.033 mol) was added in small portions to the a stirred mixture of 2-bromothiophene (**35**) (4.90 g, 0.03 mol) and silica gel (0.6 g, 10%) in chloroform (120 cm³). The reaction mixture was heated and stirred overnight and then allowed to cool to room temperature. The reaction mixture was filtered to remove the silica gel and the organic filtrate was concentrated under reduced pressure to yield crude product, which was purified by distillation under vacuum to give the desired product as a dark red oil (6.03 g, 76%).

¹H NMR (CDCl₃) δ_{H} : 6.83 (2H, d, $J = 5.3$ Hz)

MS m/z (EI): 244, 242, (M^+ , M100), 240.



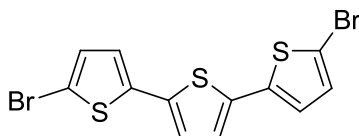
2,2':5',2''-Terthiophene (37)

A mixture of 2,5-dibromothiophene (**36**) (6.00 g, 0.025 mol) and 2-(tributylstannyl)thiophene (21.3 g, 0.057 mol) in DMF (165 cm³) was stirred and degassed with N₂ for 20 min. Then Pd(PPh₃)₄ (0.56 g, 2 mol%) was added into the flask and stirred at 100 °C overnight. The reaction mixture was cooled to room temperature water (100 cm³) was added. The product extracted into DCM (3 x 50 cm³) and combined organic layers were washed with brine (100 cm³), dried over MgSO₄, filtered off and then evaporated down by rotavapor under reduced pressure. The crude product was purified by passing through a column [10% K₂CO₃ and 90% silica gel, hexane:DCM, 3:7] to remove the tin side products then recrystallized from EtOH/DCM to yield the desired products as a yellow powder (4.46 g, 72%).

Melting point/°C: 94-96.

¹H NMR (CDCl₃) δ _H: 7.02 (2H, dd, *J* = 1.1 Hz, 3.6 Hz), 7.08 (2H, s), 7.18 (2H, dd, *J* = 1.1 Hz, 3.8 Hz), 7.22 (2H, dd, *J* = 1.2 Hz, 3.7 Hz)

MS *m/z* (EI): 250, 249, 248 (M⁺, M100), 203, 171, 127.



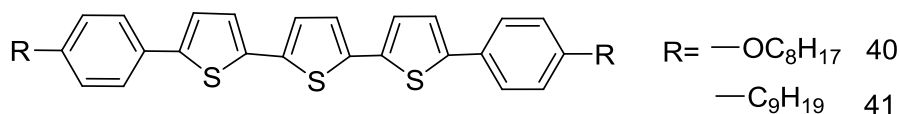
5,5''-Dibromo-2,2':5',2''-terthiophene (38)

N-Bromosuccinimide (2.37 g, 13.31mmol) was added in small portions to the a stirred mixture of 2,2':5',2''-terthiophene (**37**) (1.50 g, 6.04mmol) and silica gel (0.20 g, 10%) in DCM (25 cm³). The reaction mixture was heated and stirred overnight and then allowed to cool to room temperature. The reaction mixture was filtered to remove the silica gel and the organic filtrate was concentrated under reduced pressure to yield crude product, which was recrystallized from EtOH/DCM to give the desired product as a dark yellow powder (1.88 g, 78%).

Melting point/°C: 150-153.

¹H NMR (CDCl₃) δ _H: 6.91 (2H, d, *J* = 3.9 Hz), 6.97 (2H, d, *J* = 3.9 Hz), 6.99 (2H, s).

MS *m/z* (EI): 408, 406, (*M*⁺, *M*100), 404, 327, 283, 246, 201, 145.



5,5''-bis-[4-(Octyloxy)phenyl]-2,2':5',2''-terthiophene (40)

A mixture of 5,5''-dibromo-2,2':5',2''-terthiophene (**38**) (0.90 g, 2.2 mmol), 4-(octyloxy)phenylboronic acid (**26**) (1.50 g, 4.9 mmol) and potassium carbonate (1.25 g, 12.0 mmol) in DMF (15 cm³) was stirred and degassed with N₂ for 30 min. Pd(PPh₃)₄ (0.07 g, 2 mol%) was added to the reaction mixture, which was then heated to 90 °C under reflux for 24 h. The reaction precipitate was filtered off to yield orange yellow product (1.04 g, 76%), which has very poor solubility in organic

solvents (DCM, chloroform, DMSO, etc) so not soluble enough for NMR measurements.

Combustion analysis:

Expected: C, 73.12%; H, 7.36%; S, 14.64%

Obtained: C, 73.20%; H, 7.31%, S, 14.59%

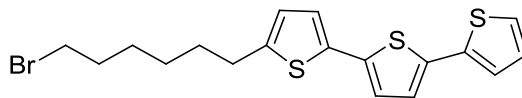
5,5''-bis-(4-Nonylphenyl)-2,2':5',2''-terthiophene (41)

The same procedure was carried out as described for compound **40**, again the product (1.02 g, 71%) was not soluble in common organic solvents, so no NMR or other spectrum data were obtained.

Combustion analysis:

Expected: C, 77.24%; H, 8.03%; S, 14.73%

Obtained: C, 76.98%; H, 8.24%, S, 14.50%



5-(6-Bromohexyl)-2,2':5',2''-terthiophene (42)

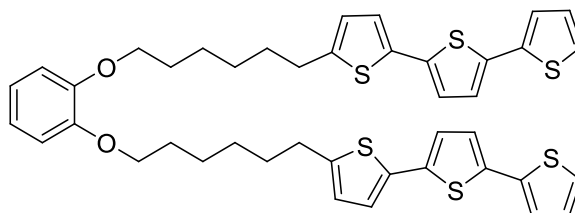
n-BuLi (2.5 M in hexanes, 3.2 cm³) was added dropwise to a solution of terthiophene (**41**) (2.0 g, 8.06 mmol) in THF (80 cm³) at -78 °C. After keeping at this temperature for another 30 min, the reaction mixture was transferred to another flask containing 1,6-dibromohexane (4.00 g, 16.4 mmol) in THF. After complete addition, the mixture

was stirred overnight and warmed to room temperature gradually. The solution was poured into water, extracted with ether (3 x 50 cm³), washed with brine (100 cm³), dried over MgSO₄ concentrated under reduced pressure. The crude product was purified by column chromatography [silica gel, DCM:hexane, 3:7] and then recrystallisation from EtOH to yield the desired product as a light yellow crystalline solid (1.25 g, 39 %).

Melting point/°C: 71-73

¹H NMR (CDCl₃) δ _H: 1.41-1.48 (4H, m), 1.70 (2H, p), 1.87 (2H, p), 2.81 (2H, t), 3.41 (2H, t), 6.69 (1H, d, *J* = 3.6 Hz), 6.97-7.01 (3H, m), 7.06 (1H, d, *J* = 3.8 Hz), 7.15 (1H, dd, *J* = 1.3 Hz, 7.6 Hz), 7.21 (1H, dd, *J* = 1.2 Hz, 7.6 Hz).

MS *m/z* (EI): 413, 412 (M⁺, M100), 410, 281, 261, 207.



1,2-bis-[6-(2,2':5',2''-Terthiophene-5-yl)hexyloxy]benzene (43)

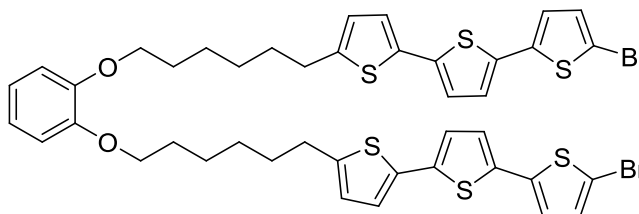
A mixture of 5-(6-bromohexyl)-2,2':5',2''-terthiophene (**42**) (0.50 g, 1.22 mmol), pyrocatechol (0.06 g, 0.545 mmol) and potassium carbonate (0.16 g, 1.16 mmol) in DMF (6 cm³) was stirred and degassed with N₂ for 30 min. Pd(PPh₃)₄ (0.012 g, 2 mol%) was added to the reaction mixture, which was then stirred and heated at 90 °C under reflux for 24 h. After cooling to room temperature, the solution was poured into water, extracted with DCM (3 x 50 cm³), washed with brine (100 cm³), dried over MgSO₄ and then concentrated under reduced pressure. The crude product was purified by column chromatography [silica gel, DCM:hexane, 3:7] and then recrystallised

from EtOH/DCM to give the desired product as a yellow green powder (0.28 g, 70 %).

Melting point/ $^{\circ}\text{C}$: 121

^1H NMR (CDCl_3) δ_{H} : 1.45-1.50 (8H, m), 1.70 (4H, p), 1.82 (4H, p), 2.79 (4H, t), 3.99 (4H, t), 6.65 (2H, d, $J = 3.5$ Hz), 6.88 (4H, s), 6.96 (4H, dd, $J = 3.8\text{Hz}, 4.3\text{Hz}$), 7.00 (2H, dd, $J = 3.7\text{Hz}, 4.3$ Hz), 7.03 (2H, d, $J = 3.6$ Hz), 7.14 (2H, dd, $J = 1.1\text{Hz}, 6.8$ Hz), 7.20 (2H, dd, $J = 1.1\text{Hz}, 6.8$ Hz)

MS m/z (EI): 772 (M^+), 771, 770 ($\text{M}100$).



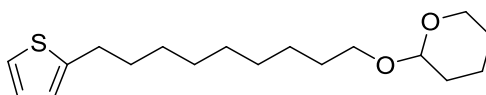
1,2-bis-(6-[5''-Bromo-2,2':5',2''-terthiophene-5-yl]hexyloxy)benzene (44).

N-Bromosuccinimide (0.055 g, 0.311mmol) was added in small portions to the a stirred mixture of 1,2-bis-(6-[2,2':5',2''-terthiophene-5-yl]hexyloxy)benzene (**43**) (0.1 g, 0.14mmol) and silica gel (0.01 g, 10%) in DCM (2.0 cm^3). The reaction mixture was stirred overnight and then filtered to remove the silica gel. The organic filtrate was concentrated under reduced pressure to yield crude product, which was recrystallized from EtOH/DCM to give the desired product as a dark yellow powder (0.12 g, 92%).

Melting point/ $^{\circ}\text{C}$: 127

^1H NMR (CDCl_3) δ_{H} : 1.45-1.53 (8H, m), 1.70 (4H, p), 1.82 (4H, p), 2.78 (4H, t), 3.99 (4H, t), 6.65 (2H, d, $J = 3.6$ Hz), 6.87 (2H, d, $J = 3.8$ Hz), 6.89 (4H, s), 6.93-6.95 (8H, m).

MS m/z (MALDI): 930 (M^+), 929, 928 ($\text{M}100$).

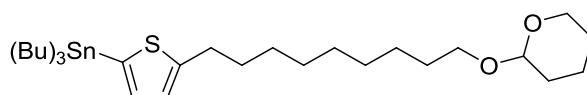


2-[9-(thiophen-2-yl)nonyloxy]tetrahydro-2H-pyran (45)

6.5 cm^3 of $n\text{-BuLi}$ (2.5 M in hexane) was added dropwise to a solution of thiophene (1.14 g, 0.014 mol) in THF (135 cm^3) at -78°C . After keeping at this temperature for another 45 min, the reaction mixture was transferred to another flask containing 2-(9-bromononyloxy)tetrahydro-2H-pyran (**27**) (5.00 g, 0.016 mmol) in THF. After complete addition, the mixture was stirred overnight and warmed to room temperature gradually. The solution was poured into water, extracted with ether (3 x 50 cm^3), washed with brine (100 cm^3), dried over MgSO_4 concentrated by rotovap. The crude product was purified by column chromatography [silica gel, DCM:hexane, 3:7] and then vacuum distilled to give the desired product as a yellow liquid (3.40 g, 78%).

^1H NMR (CDCl_3) δ_{H} : 1.30-1.48 (10H, m), 1.61-1.76 (3H, m), 1.81-1.87 (4H, m), 2.81 (2H, t), 3.52 (2H, p), 3.71 (2H, m), 3.86 (2H, m), 4.57 (2H, t), 6.77 (1H, d, $J = 3.3$ Hz), 6.91 (1H, dd, $J = 1.1\text{Hz}, 3.3$ Hz), 7.09 (1H, dd, $J = 1.1\text{Hz}, 3.4$ Hz).

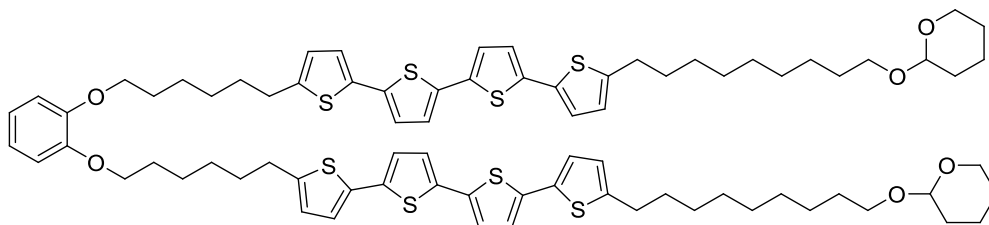
MS m/z (EI): 312, 311, 310 ($\text{M}100$).



Tributyl-{5-[9-(tetrahydro-2H-pyran-2-yloxy)nonyl]thiophen-2-yl}stannane (46).

5.2 cm³ of *n*-BuLi (2.5 M in hexanes) was added dropwise to a solution of 2-[9-(thiophen-2-yl)nonyloxy]tetrahydro-2H-pyran (**45**) (3.40 g, 0.011 mol) in THF (100 cm³) at -78 °C. After keeping at this temperature for another 45 min, tributylstannyl chloride (4.25 g, 0.013 mol) was added into the flask. The mixture was stirred overnight and warmed to room temperature gradually. The solution was poured into water, extracted with ether (3 x 50 cm³), washed with brine (100 cm³), dried over MgSO₄ concentrated by evaporation under reduced pressure to give the desired product as a yellow liquid (6.45 g, 98 %), which was used directly without further purification.

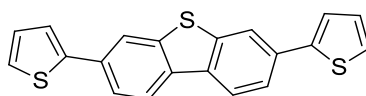
¹H NMR (CDCl₃) δ_H: 0.89 (9H, m), 1.30-1.48 (16H, m), 1.61-1.76 (9H, m), 1.81-1.87 (4H, m), 2.81 (2H, t), 3.52 (2H, p), 3.71 (2H, m), 3.86 (2H, m), 4.57 (2H, t), 6.77 (1H, d, *J* = 3.3 Hz), 6.91 (1H, dd, *J* = 1.1 Hz, 3.3 Hz), 7.09 (1H, dd, *J* = 1.0 Hz, 3.3 Hz).



1,2-bis-(6-{5'''-[9-(Tetrahydro-2H-pyran-2-yloxy)nonyl]-2,2':5',2'':5'',2'''-quaterthiophen-5-yl}hexyloxy)benzene (47)

A mixture of 1,2-bis-(6-[5''-bromo-2,2':5',2''-terthiophene-5-yl]hexyloxy)benzene (**44**) (0.10 g, 0.11 mmol) and tributyl-{5-[9-(tetrahydro-2H-pyran-2-yloxy)nonyl]thiophen-2-yl}stannane (**46**) (0.14 g, 0.24 mol) in DMF (1.5 cm³) was stirred and degassed with N₂ for 20 min. Then Pd(PPh₃)₄ (0.001 g, 2 mol%) was added into the flask and stirred at 100 °C overnight. The reaction mixture was cooled to room temperature and water was added. The

product extracted into DCM (3 x 50 cm³) and the combined organic layers were washed with brine (100 cm³), dried over MgSO₄, filtered off and then evaporated down by rotavapor under reduced pressure. The ¹H NMR of the crude product showed that the reaction did not work, so no further data was obtained and further reaction schemes could not be completed without this intermediate.



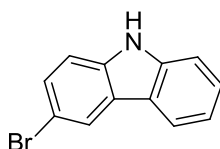
3,7-Di(thiophen-2-yl)dibenzo[*b,d*]thiophene (49)

K₂CO₃ (0.61 g, 4.34 mmol), Pd(OAc)₂ (0.016 g, 0.073 mmol), PCy₃ • HBF₄ (0.054 g, 0.146 mmol), pivalic acid (0.090 g, 0.877 mmol) and 3,7-dibromodibenzo[*b,d*]thiophene (**48**) (1.00- g, 2.92 mmol) were weighed in air and degassed with N₂ for 20 min. Then DMF (12 cm³) and thiophene (0.62 g, 7.37 mmol) were added. The reaction mixture was then vigorously stirred at 100 °C for 4 h. The solution was then cooled to room temperature then poured directly into methanol (250 cm³), stirred for 30min and the crude product was precipitated from methanol. The crude product was filtered off and purified by column chromatography [silica gel, DCM:hexane, 1:4] and recrystallisation to give the desired product as a pale yellow solid (0.62 g, 61%).

Melting point/°C: 202-204

¹H NMR (CDCl₃) δ _H: 7.13 (2H, d, *J* = 3.5Hz), 7.34 (2H, dd, *J* = 0.9Hz, 3.3 Hz), 7.43 (2H, dd, *J* = 0.9Hz, 3.3 Hz), 7.73 (2H, dd, *J* = 1.6Hz, 8.3 Hz), 8.08 (2H, d, *J* = 1.4 Hz), 8.11 (2H, d, *J* = 8.4 Hz).

MS *m/z* (EI): 350, 349, 348 (M100).



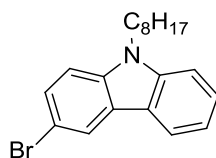
3- Bromocarbazole (**51**).

A solution of *N*-bromosuccinimide (10.64 g, 59.80 mmol) in DMF (150 cm³) was added dropwise to a solution of carbazole (**50**) (10.00 g, 59.80 mmol) in DMF (100 cm³) at 0 °C. The reaction mixture was gradually warmed to room temperature and stirred for an additional 2 h. Then the mixture was poured into a saturated sodium metabisulphite (Na₂S₂O₅) solution (1,000 cm³), and the resultant precipitate was filtered off, dried and dissolved in DCM. The organic solution was washed with water (2 x 100 cm³), dried over MgSO₄, filtered off and then evaporated down by rotavapor under reduced pressure. The crude product was purified by recrystallisation from ethanol to give the desired product as a white crystalline solid (11.25 g, 76%).

Melting point/°C: 195 (Lit. 193-195¹¹)

¹H NMR (CDCl₃) δ_H: 7.31 (2H, d, *J* = 8.4 Hz), 7.5 (1H, d, *J* = 2.0 Hz), 8.01 (2H, dd, *J* = 2.0 Hz, 8.4 Hz), 8.09 (1H, s), 8.18 (2H, d, *J* = 2.0 Hz).

MS *m/z* (EI): 247, 245 (M⁺).

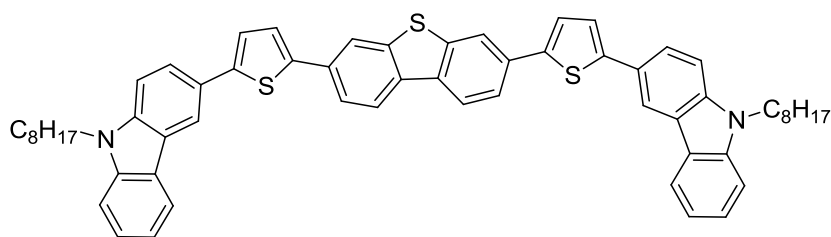


3-Bromo-*N*-octyl-carbazole (**52**).

A mixture of 3-bromocarbazole (**51**) (10.00 g, 0.040 mol), 1-bromooctane (9.41 g, 0.048 mol), DMSO (50 cm³) and a 50% NaOH aqueous solution (40 cm³) was stirred at room temperature overnight. Water (20 cm³) was added into the mixture, and then it was extracted with diethyl ether (3 x 50 cm³). The combined organic layers were washed with brine (2 x 100 cm³), dried over MgSO₄, filtered off and then evaporated down by rotavapor under reduced pressure. The crude product was purified by flash chromatography (silica gel, hexane) to give the desired product as colourless oil (12.58 g, 88%).

¹H NMR (CDCl₃) δ _H: 0.91 (3H, t, *J* = 6.7 Hz), 1.44–1.22 (10H, m), 1.87 (2H, quint), 4.28 (2H, t, *J* = 7.3 Hz), 7.34–7.24 (2H, m), 7.59–7.40 (3H, m), 8.08 (1H, d, *J* = 7.6 Hz), 8.24 (1H, d, *J* = 7.6 Hz).

MS *m/z* (EI): 357 (*M*⁺).



3,7-bis-[5-(9-Octyl-9H-carbazol-3-yl)thiophen-2-yl]dibenzo[b,d]thiophene (**53**)

K₂CO₃ (0.07 g, 0.516 mmol), Pd(OAc)₂ (0.006 g, 0.009 mmol), PCy₃ • HBF₄ (0.006 g, 0.017 mmol), pivalic acid (0.01 g, 0.098 mmol), 3-bromo-*N*-octyl-carbazole (**52**) (0.28 g, 0.792 mmol) and 3,7-di(thiophen-2-yl)dibenzo[b,d]thiophene (**49**) (0.12 g,

0.344 mmol) were weighed in air and placed in a flask, which was degassed with N₂ for 20 min. Then DMF (1.5 cm³) was added and the reaction mixture was then vigorously stirred at 100 °C for 4 h. The solution was cooled to room temperature, diluted with DCM and water. The aqueous phase was extracted with DCM (3 x 50 cm³) and combined organic layers were washed with brine (2 x 100 cm³), dried over MgSO₄, filtered off and then evaporated down by rotavapor under reduced pressure. The crude product was purified by column chromatography [silica gel, DCM:hexane, 3:7] to give the desired product as a light yellow solid (0.12 g, 31%).

Melting point/°C: 189 (Tg 39).

¹H NMR (CDCl₃) δ_H: 0.87 (6H, t), 1.24-1.41 (20H, m), 1.89 (4H, p), 4.31 (4H, t), 7.13 (2H, dd, *J* = 1.8, 3.4 Hz), 7.34-7.36 (4H, m), 7.42 (4H, dd, *J* = 1.8 Hz, 3.5 Hz), 7.48 (2H, dd, *J* = 1.1 Hz, 1.6 Hz), 7.73 (2H, dd, *J* = 1.2 Hz, 1.7 Hz), 8.08-8.11 (6H, m), 8.16 (2H, d, *J* = 7.68 Hz), 8.37 (2H, d, *J* = 1.6 Hz).

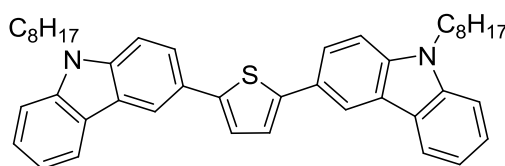
¹³C NMR (CDCl₃): 138, 134, 133, 132, 130, 128, 127, 123, 122, 121, 120, 119, 116, 112, 111, 109, 58, 32, 30, 27, 23, 14.

MS *m/z* (MALDI): 904 (M⁺), 903, 902 (M100).

Combustion analysis:

Expected: C, 79.78%; H, 6.47%; N, 3.10%; S, 10.65%

Obtained: C, 79.75%; H, 6.49%; N, 3.12%; S, 10.63%



2,5-bis-(9-Octyl-9H-carbazol-3-yl)thiophene (54)

K₂CO₃ (0.49 g, 3.56 mmol), Pd(OAc)₂ (0.006 g, 0.029 mmol), PCy₃ • HBF₄ (0.022 g, 0.059 mmol), pivalic acid (0.036 g, 0.342 mmol) and 3-bromo-9-octyl-9H-carbazole (**52**) (2.0 g, 5.58 mmol) were weighed to air and placed in a flask, which was degassed with N₂ for 20 min. Then DMF (10 cm³) and thiophene (0.20 g, 2.37 mmol) were added. The reaction mixture was then vigorously stirred at 100 °C for 3 h. The solution was then cooled to room temperature, diluted with DCM and water. The aqueous phase was extracted with DCM (3 x 50 cm³) and combined organic layers were washed with brine (100 cm³), dried over MgSO₄, filtered off and then evaporated down by rotavapor under reduced pressure. The crude product was purified by column chromatography [silica gel, DCM:hexane, 3:7] to give the desired product as a yellow liquid (0.68 g, 45 %).

Melting point/°C: 62

¹H NMR (CDCl₃) δ_H: 0.87 (6H, t), 1.24-1.41 (20H, m), 1.89 (4H, p), 4.31 (4H, t), 7.35 (2H, s), 7.42 (4H, dd, *J* = 1.8Hz, 3.5Hz), 7.48 (2H, dd, *J* = 1.1Hz, 1.6 Hz), 7.78 (2H, dd, *J* = 1.2Hz, 1.6 Hz), 8.16 (2H, d, *J* = 7.7 Hz), 8.37 (2H, d, *J* = 1.6 Hz).

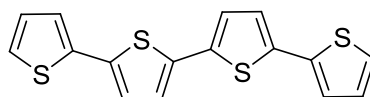
¹³C NMR (CDCl₃): 138, 134, 130, 128, 121, 120, 119, 116, 112, 111, 109, 58, 32, 30, 27, 23, 14.

MS *m/z* (MALDI): 640, 639, 638 (M⁺, M100)

Combustion analysis:

Expected: C, 82.71%; H, 7.89%; N, 4.38%; S, 5.02%

Obtained: C, 82.74%; H, 7.88%; N, 4.36%; S, 5.04%



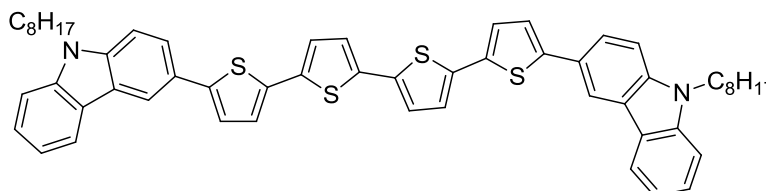
2,2':5',2'':5'',2'''-Quaterthiophene (57)

A mixture of 5,5'-dibromo-2,2'-bithiophene (**55**) (2.00 g, 6.17 mmol) and tributyl(thiophen-2-yl)stannane (**56**) (5.1 g, 13.6 mmol) in DMF (60 cm³) was stirred and degassed with N₂ for 20 min. Then Pd(PPh₃)₄ (0.07 g, 2 mol%) was added into the flask and stirred at 100 °C overnight. The reaction mixture was cooled to room temperature water was added. The product was extracted into DCM (3 x 50 cm³) and combined organic layers were washed with brine (100 cm³), dried over MgSO₄, filtered off and then evaporated down by rotavapor under reduced pressure. The crude product was purified by passing through a column [10% K₂CO₃ and 90% silica gel, hexane:DCM, 1:1] to remove the tin side products then recrystallized from EtOH/DCM to yield the desired product as an orange crystalline solid (1.34 g, 66%).

Melting point/°C: 211-214. (Lit. 216¹²)

¹H NMR (CDCl₃) δ_H: 7.03 (2H, dd, *J* = 3.6 Hz, 8.7 Hz), 7.08 (4H, m), 7.18 (2H, dd, *J* = 1.1 Hz, 3.8 Hz), 7.23 (2H, dd, *J* = 1.1 Hz, 3.7 Hz).

MS (m/z) (EI): 332, 331, 330 (M⁺) (M100).



5,5'''-bis-(9-Octyl-9H-carbazol-3-yl)-2,2':5',2'':5'',2'''-quaterthiophene (58)

K₂CO₃ (0.13 g, 0.907 mmol), Pd(OAc)₂ (0.010 g, 0.015 mmol), PCy₃ • HBF₄ (0.011 g, 0.030 mmol), pivalic acid (0.02 g, 0.181 mmol), 3-bromo-9-octyl-9H-carbazole (52) (0.47 g, 1.31 mmol) and 2,2':5',2'':5'',2''':5'''-quaterthiophene (**57**) (0.20 g, 0.605 mmol) were weighed in air and placed in a flask, which was degassed with N₂ for 20 min. Then DMF (2.5 cm³) was added. The reaction mixture was then vigorously stirred at 100 °C overnight. The solution was then cooled to room temperature, diluted with DCM and water. The aqueous phase was extracted with DCM (3 x 50 cm³) and combined organic layers were washed with brine (100 cm³), dried over MgSO₄, filtered off and then evaporated down by rotavapor under reduced pressure. The crude product was purified by column chromatography [silica gel, DCM:hexane, 1:4] and then recrystallisation from EtOH/DCM to give the desired product as a dark orange powder (0.29 g, 56%).

Melting point/°C: 162 (Tg 4)

¹H NMR (CDCl₃) δ_H: 0.87 (6H, t), 1.24-1.41 (20H, m), 1.89 (4H, p), 4.31 (4H, t), 7.03 (2H, dd, *J* = 3.6Hz, 8.7 Hz), 7.08 (4H, q), 7.18 (2H, dd, *J* = 1.4Hz, 3.8 Hz), 7.42 (4H, dd, *J* = 1.8Hz, 3.7Hz), 7.48 (2H, dd, *J* = 1.6Hz, 3.7 Hz), 7.78 (2H, dd, *J* = 1.6Hz, 7.7Hz), 8.16 (2H, d, *J* = 7.68 Hz), 8.37 (2H, d, *J* = 1.64 Hz).

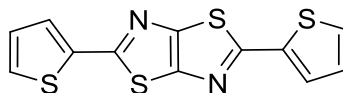
¹³C NMR (CDCl₃): 138, 136, 134, 130, 128, 124, 121, 120, 119, 116, 112, 111, 109, 58, 32, 30, 27, 23, 14.

MS *m/z* (MALDI): 886, 885, 884 (M⁺, M100)

Combustion analysis:

Expected: C, 75.97%; H, 6.38%; N, 3.16%; S, 14.49%

Obtained: C, 75.95%; H, 6.40%; N, 3.13%; S, 14.51%



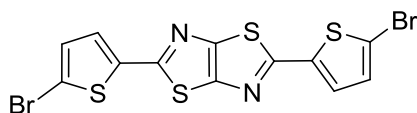
2,5-Di-(thiophen-2-yl)thiazolo[5,4-*d*]thiazole (59)

A mixture of dithiooxamide (2.5 g, 20.8mmol) and thiophene-2-carbaldehyde (4.75 g, 42.4mmol) in DMF (100 cm³) was heated and stirred under reflux overnight. The reaction mixture was cooled to room temperature and then poured into methanol (250cm³), stirred for 1 h. and cooled to 0 °C. The precipitate was then filtered, washed with hexane and minor amount of DCM to yield the crude product then recrystallisation from DCM and dried to give the desired product as a yellow brown solid (2.47 g, 39%).

Melting point/°C: 235 (Lit, 237¹³)

¹H NMR (CDCl₃) δ _H: 7.12 (2H, dd, *J* = 3.7Hz, 5.1 Hz), 7.46 (2H, d, *J* = 5.1 Hz), 7.59 (2H, d, *J* = 5.0 Hz)

MS *m/z* (EI): 308, 307, 306 (*M*⁺, *M*100).



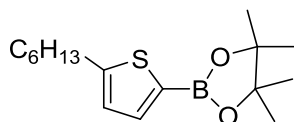
2,5-bis-(5-Bromothiophen-2-yl)thiazolo[5,4-d]thiazole (60)

N-Bromosuccinimide (2.60 g, 14.3 mmol) was added in small portions to the a stirred mixture of 2,5-di(thiophen-2-yl)thiazolo[5,4-*d*]thiazole (**59**) (2.00 g, 6.53mmol) and silica gel (0.20 g, 10%) in DMF (50 cm³). The reaction mixture was stirred overnight and then filtered to yield a crude product, which was recrystallized from NMP to give the desired product as an orange solid (2.90 g, 95%).

Melting point/°C: 280

¹H NMR (CDCl₃)_δH: 7.01 (2H, d, *J* = 3.2 Hz), 7.24 (2H, d, *J* = 3.9 Hz).

MS *m/z* (EI):466, 464 (M100), 462.

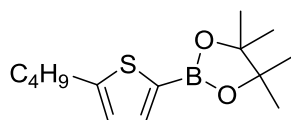


2-(5-Hexylthiophen-2-yl)-4,4,5,5-tetramethyl-1,3,2-dioxaborolane (61)

A solution of 2-hexylthiophene (2.00 g, 11.9 mmol) in THF (120 cm³) was cooled to -78°C and stirred for 30 min with degassed nitrogen. A 2.5 M solution of *n*-butyllithium in hexanes (5.7 cm³, 14.2 mmol) was then added to the solution using a syringe and the resultant reaction solution stirred for 1 h at this temperature. 2-isopropoxy-4,4,5,5-tetramethyl-1,3,2-dioxaborolane (4.86 g, 26.1 mmol) was then added with a syringe into the reaction mixture, which was allowed to warm gradually to room temperature overnight. Then water was added to the reaction mixture the resultant mixture stirred at room temperature for 30min. The organic layers were

separated and the water layer was extracted with DCM (3 x 50 cm³). The combined organic layers were washed with water (3 x 50 cm³), brine (50 cm³), dried over MgSO₄, filtered off and then evaporated down by rotavapor under reduced pressure to give the desired product as a dark orange liquid (3.18 g, 91%). The crude product was used directly without any further purification.

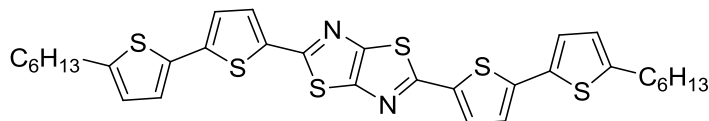
¹H NMR (CDCl₃) δ_{H} : 0.89 (3H, t), 1.24 (12H, s), 1.28-1.32 (6H, m), 1.61 (2H, quint), 2.82 (2H, t), 6.85 (1H, d, $J = 6.5$ Hz), 7.02 (1H, d, $J = 6.4$ Hz).



2-(5-Butylthiophen-2-yl)-4,4,5,5-tetramethyl-1,3,2-dioxaborolane (62)

A solution of 2-butylthiophene (5.0 g, 35.6 mmol) in THF (120 cm³) was cooled to -78°C and stirred for 30 min with degassed nitrogen. A 2.5 M solution of *n*-butyllithium in hexanes (21.4 cm³, 53.5 mmol) was then added to the solution using a syringe and the resultant reaction solution stirred for 1 h at this temperature. 2-Isopropoxy-4,4,5,5-tetramethyl-1,3,2-dioxaborolane (10.15 g, 53.5 mmol) was then added with a syringe into the reaction mixture, which was allowed to warm gradually to room temperature overnight. Then water was added to the reaction mixture the resultant mixture stirred at room temperature for 30 min. The organic layers were separated and the water layer was extracted with DCM (3 x 50 cm³). The combined organic layers were washed with water (3 x 50 cm³), brine (50 cm³), dried over MgSO₄, filtered off and then evaporated down by rotavapor under reduced pressure to give the desired product as an orange oil (9.20 g, 97%). The crude product was used directly without any further purification.

¹H NMR (CDCl₃) δ_{H} : 0.89 (3H, t), 1.24 (12H, s), 1.31 (2H, m), 1.61 (2H, quint), 2.82 (2H, t), 6.85 (1H, d, $J = 6.5$ Hz), 7.02 (1H, d, $J = 6.4$ Hz).



2,5-bis-(5'-Hexyl-2,2'-bithiophen-5-yl)thiazolo[5,4-*d*]thiazole (63)

A mixture of 2,5-bis-(5-bromothiophen-2-yl)thiazolo[5,4-*d*]thiazole (**60**) (0.14 g, 0.31 mmol) and 2-(5-hexylthiophen-2-yl)-4,4,5,5-tetramethyl-1,3,2-dioxaborolane (**61**) (0.23 g, 0.79 mmol) in THF (25 cm³) was stirred and degassed with N₂ for 30 min. Then sodium carbonate (0.10 g, 0.93 mmol) in water (1 cm³) was added into the mixture, followed by the addition of catalyst Pd(PPh₃)₄ (0.007 g, 2 mol%). The resultant reaction mixture was then heated to 90 °C under reflux overnight and cooled to room temperature. The reaction mixture was poured into methanol (250 cm³), stirred for 30 min and cooled to 0 °C, the precipitate was then filtered off and dried to yield the crude product, which was purified by column chromatography [silica gel, DCM:hexane, 3:7] and then recrystallisation from DCM to give the desired product as an orange red powder (0.08 g, 47%).

Melting point/°C: Cr 191 N 269 I

¹H NMR (CDCl₃) δ_H: 0.89 (6H, t), 1.25-1.37 (12H, m), 1.67 (4H, t), 2.81 (4H, t), 6.72 (2H, d, *J* = 4.1 Hz), 7.08 (4H, t), 7.44 (2H, d, *J* = 3.4 Hz).

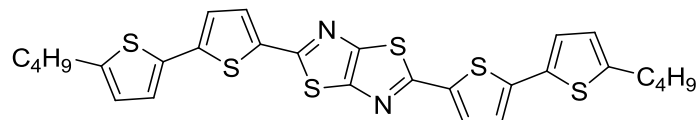
¹³C NMR (CDCl₃): 147, 141, 134, 127, 125, 124, 123, 32, 30, 29, 28, 23, 14

MS *m/z* (MALDI): 640, 639, 638 (M⁺, M100),

Combustion analysis:

Expected: C, 60.15%; H, 5.36%; N, 4.38%; S, 30.11%

Obtained: C, 60.19%; H, 5.32%; N, 4.39%; S, 30.08%



2,5-bis-(5'-Butyl-2,2'-bithiophen-5-yl)thiazolo[5,4-d]thiazole (64)

A mixture of 2,5-bis-(5-bromothiophen-2-yl)thiazolo[5,4-d]thiazole (**60**) (0.20 g, 0.43 mmol) and 2-(5-octylthiophen-2-yl)-4,4,5,5-tetramethyl-1,3,2-dioxaborolane (**62**) (0.46 g, 1.72 mmol) in THF (30 cm³) was stirred and degassed with N₂ for 30 min. Then sodium carbonate (0.14 g, 1.29 mmol) added into the mixture, followed by the addition of catalyst Pd(OAc)₂ (0.0024 g, 2.5 mol%) and PPh₃ (0.0056 g, 5 mol%). The resultant reaction mixture was then heated to 90 °C under reflux overnight and cooled to room temperature. The reaction mixture was poured into methanol (250 cm³), stirred for 30 min and cooled to 0°C, the precipitate was then filtered off and dried to yield the crude product, which was purified by column chromatography [silica gel, DCM:hexane, 3:7] and then recrystallisation from DCM/NMP to give the desired product as an orange powder (0.18 g, 72%).

Melting point/°C: Cr 207 N >350 I

¹H NMR (CDCl₃) δ _H: 0.92 (6H, t), 1.44 (4H, m), 1.69 (4H, quint), 2.83 (4H, t), 6.73 (2H, d, *J* = 3.7 Hz), 7.09 (4H, t), 7.45 (2H, d, *J* = 3.9 Hz)

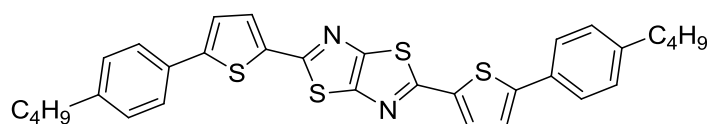
¹³C NMR (CDCl₃): 147, 141, 134, 127, 125, 124, 123, 33, 29, 22, 14

MS *m/z* (MALDI): 584, 583, 582 (M⁺, M100),

Combustion analysis:

Expected: C, 57.69%; H, 4.50%; N, 4.81%; S, 33.01%

Obtained: C, 57.72%; H, 4.48%; N, 4.78%; S, 33.04%



2,5-bis-[5-(4-Butylphenyl)thiophen-2-yl]thiazolo[5,4-*d*]thiazole (68)

A mixture of 2,5-bis-(5-bromothiophen-2-yl)thiazolo[5,4-*d*]thiazole (**60**) (0.24 g, 0.51 mmol) and 4-butylphenylboronic acid (**65**) (0.20 g, 1.12 mmol) in THF (50 cm³) was stirred and degassed with N₂ for 30 min. Then sodium carbonate (0.43 g, 4.1 mmol) in water (2 cm³) added into the mixture, followed by the addition of catalyst Pd(OAc)₂ (0.0028 g, 2.5 mol%) and PPh₃ (0.0066 g, 5 mol%). The resultant reaction mixture was then heated to 90 °C under reflux overnight and cooled to room temperature. The reaction mixture was poured into methanol (250 cm³), stirred for 30 min and cooled to 0 °C, the precipitate was then filtered off and dried to yield the crude product, which was purified by column chromatography [silica gel, DCM:hexane, 3:7] and then recrystallisation from DCM/NMP to give the desired product as an orange red powder (0.19 g, 78%).

Melting point/°C: Cr 264 N>350 I

¹H NMR (CDCl₃) δ _H: 0.94 (6H, t), 1.39 (4H, quint), 1.62 (4H, quint), 2.64 (4H, t), 7.23 (4H, d, *J* = 8.4 Hz), 7.29 (2H, d, *J* = 3.9 Hz), 7.54 (2H, d, *J* = 3.9 Hz), 7.57 (2H, d, *J* = 8.4 Hz).

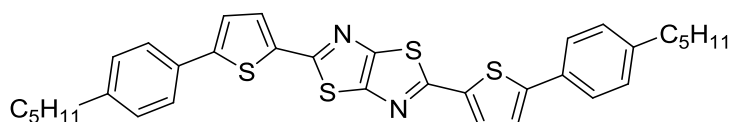
¹³C NMR (CDCl₃): 162, 148, 144, 136, 129, 128, 126, 123, 35, 33, 22, 14

MS *m/z* (MALDI): 572, 571, 570 (M⁺, M100)

Combustion analysis:

Expected: C, 67.33%; H, 5.30%; N, 4.91%; S, 22.47%

Obtained: C, 67.32%; H, 5.33%; N, 4.88%; S, 22.49%



2,5-bis-[5-(4-Pentylphenyl)thiophen-2-yl]thiazolo[5,4-d]thiazole (69)

A mixture of 2,5-bis-(5-bromothiophen-2-yl)thiazolo[5,4-d]thiazole (**60**) (0.20 g, 0.43 mmol) and 4-pentylphenylboronic acid (cm^3) (0.28 g, 1.50 mmol) in NMP (30 cm^3) was stirred and degassed with N_2 for 30 min. Then sodium carbonate (0.18 g, 1.72 mmol) in water (2 cm^3) was added into the mixture, followed by the addition of catalyst $\text{Pd}(\text{OAc})_2$ (0.0028 g, 2.5 mol%) and PPh_3 (0.0066 g, 5 mol%). The resultant reaction mixture was then heated to 90°C under reflux overnight and cooled to room temperature. The reaction mixture was then poured into methanol and stirred for 30 min, and then filtered off to yield the crude product. The crude product was purified by column chromatography [silica gel, chloroform:hexane, 1:1] and then recrystallisation from DCM/NMP to give the desired product as a yellow crystal solid (0.21 g, 85%).

Melting point/ $^\circ\text{C}$: Tg 158 Cr 246 SmC 249 N >350 I

^1H NMR (CDCl_3) δ_{H} : 0.94 (6H, t), 1.33-1.36 (8H, m), 1.62 (4H, quint), 2.64 (4H, t), 7.23 (4H, d, $J = 8.4 \text{ Hz}$), 7.29 (2H, d, $J = 3.9 \text{ Hz}$), 7.54 (2H, d, $J = 3.9 \text{ Hz}$), 7.57 (2H, d, $J = 8.4 \text{ Hz}$).

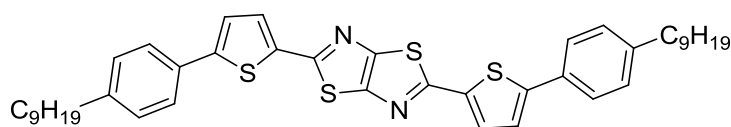
^{13}C NMR (CDCl_3): 162, 148, 144, 136, 129, 128, 126, 123, 35, 33, 31, 22, 14

MS m/z (MALDI): 600, 599, 598 (M^+ , M100)

Combustion analysis:

Expected: C, 68.18%; H, 5.72%; N, 4.68%; S, 21.42%

Obtained: C, 68.19%; H, 5.72%; N, 4.66%; S, 21.43%



2,5-bis-[5-(4-Nonylphenyl)thiophen-2-yl]thiazolo[5,4-d]thiazole (70)

A mixture of 2,5-bis-(5-bromothiophen-2-yl)thiazolo[5,4-d]thiazole (**60**) (0.20 g, 0.43 mmol) and 4-pentylphenylboronic acid (**66**) (0.36 g, 1.50 mmol) in DME (30 cm³) was stirred and degassed with N₂ for 30 min. Then sodium carbonate (0.16 g, 1.50 mmol) added into the mixture, followed by the addition of catalyst Pd(OAc)₂ (0.0028 g, 2.5 mol%) and PPh₃ (0.0066 g, 5 mol%). The resultant reaction mixture was then heated to 90 °C under reflux overnight and cooled to room temperature. The reaction mixture was then poured into methanol (250 cm³), stirred for 30 min and then cooled to 0 °C. The precipitate was filtered off and dried to yield the crude product, which was purified by column chromatography [silica gel, chloroform:hexane, 1:1] and then recrystallisation from DCM/NMP to give the desired product as a yellow crystalline solid (0.13 g, 43%).

Melting point/°C: Tg 201 Cr 227 SmC 286 N 303 I

¹H NMR (CDCl₃) δ _H: 0.94 (6H, t), 1.26-1.32 (24H, m), 1.62 (4H, quint), 2.64 (4H, t), 7.23 (4H, d, *J* = 8.4 Hz), 7.29 (2H, d, *J* = 3.8 Hz), 7.54 (2H, d, *J* = 3.9 Hz), 7.57 (2H, d, *J* = 8.4 Hz).

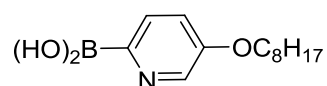
^{13}C NMR (CDCl_3): 162, 148, 144, 136, 129, 128, 126, 123, 35, 33, 32, 30, 29, 23, 22, 18, 14

MS m/z (MALDI): 712, 711, 710 (M^+ , $\text{M}100$).

Combustion analysis:

Expected: C, 70.94%; H, 7.09%; N, 3.94%; S, 18.04%

Obtained: C, 70.95%; H, 7.08%; N, 3.97%; S, 18.01%



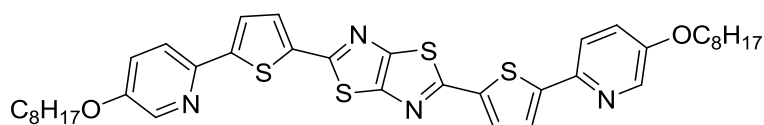
5-(Octyloxy)pyridin-2-ylboronic acid (71)

A solution of 2-bromo-5-octyloxy pyridine (5.0 g, 17mmol) in THF (150 cm^3) was cooled to -78°C and stirred for 30 min. A 2.5 M solution of *n*-butyllithium in hexane (8.8 cm^3 , 22mmol) was then added to the nitrogen-purged solution using a syringe and the resultant reaction solution stirred for 1 h at this temperature. Triisopropyl borate (8.91 cm^3 , 0.039 mol) was then added with a syringe. The resultant reaction mixture was allowed to warm gradually to room temperature overnight. Then 2N hydrochloric acid (100 cm^3) was added to the reaction mixture the resultant mixture stirred at room temperature for 1 h. The organic layers were separated and the water layer was extracted with diethyl ether (3 x 50 cm^3). The combined organic layers were washed with water (3 x 50 cm^3), brine (50 cm^3), dried over MgSO_4 , filtered off and then evaporated down by rotavapor under reduced pressure. The crude product was purified by washing with hexane to give the desired product as a white power (3.87 g, 91%).

Melting point/ $^\circ\text{C}$: 118 (Lit. 118-119^[10])

^1H NMR (CDCl_3) δ_{H} : 0.88 (3H, t), 1.26-1.30 (6H, m), 1.32 (2H, quint), 1.43 (2H, quint), 1.76 (2H, quint), 4.02 (2H, t), 6.76 (1H, d, $J = 8.4$ Hz), 7.71 (1H, dd, $J = 3.3$ Hz, 8.3 Hz), 8.24 (1H, d, $J = 8.4$ Hz).

MS m/z (EI): 249, 248 (M^+ , M100), 247.



2,5-bis-[5-(5-(Octyloxy)pyridin-2-yl)thiophen-2-yl]thiazolo[5,4-d]thiazole (72)

A mixture of 2,5-bis-(5-bromothiophen-2-yl)thiazolo[5,4-d]thiazole (**60**) (0.25 g, 0.54 mmol) and 5-(octyloxy)pyridin-2-ylboronic acid (**71**) (0.41 g, 1.61 mmol) in THF (30 cm^3) was stirred and degassed with N_2 for 30 min. Then a solution of potassium carbonate (0.22 g, 1.61 mmol) in water (2 cm^3) was added into the mixture, followed by the addition of catalyst $\text{Pd}(\text{OAc})_2$ (0.002 g, 2 mol%) and PPh_3 (0.007 g, 5 mol%). The resultant reaction mixture was then heated to 90 $^\circ\text{C}$ under reflux overnight and cooled to room temperature. The reaction mixture was then poured into methanol and stirred for 30 min filtered off to yield the crude product. The resultant crude product was purified by column chromatography [silica gel, Chloroform:hexane, 1:1] and then recrystallisation from DCM to give the desired product as a orange powder (0.19 g, 51 %).

Melting point/ $^\circ\text{C}$: Tg 170 Cr 212 SmC 316 I

^1H NMR (CDCl_3) δ_{H} : 0.88 (6H, t), 1.26-1.32 (16H, m), 1.43 (4H, m), 1.79 (4H, quint), 4.33 (4H, t), 6.79 (2H, d, $J = 8.6$ Hz), 7.23 (2H, d, $J = 3.9$ Hz), 7.54 (2H, d, $J = 3.9$ Hz), 7.80 (2H, d, $J = 8.8$ Hz), 8.46 (2H, d, $J = 3.5$ Hz)

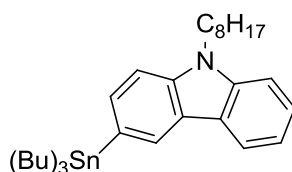
^{13}C NMR (CDCl_3): 162, 148, 144, 140, 136, 129, 128, 126, 123, 69, 32, 29, 26, 23, 14

MS m/z (MALDI): 718, 717, 716 (M^+ , M100)

Combustion analysis:

Expected: C, 63.65%; H, 6.19%; N, 7.81%; S, 17.89%

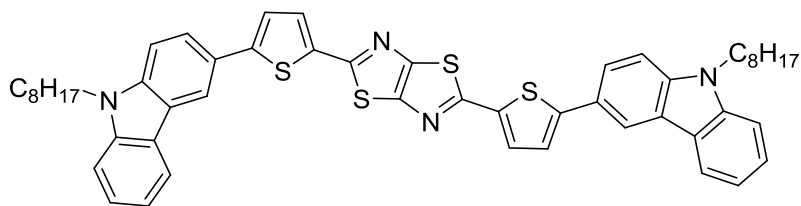
Obtained: C, 63.64%; H, 6.18%; N, 7.83%; S, 17.88%



9-Octyl-3-(tributylstannyl)-9H-carbazole (73)

A solution of *n*-BuLi in hexanes (1.5 cm³, 2.5 M, 3.7 mmol) and hexane (50 cm³) was added dropwise to a cooled (-78 °C) solution of 3-bromo-*N*-octyl-carbazole (**52**) (0.75 g, 2.0 mmol) in THF (30 cm³) over a period of 10 min. The resultant reaction mixture was stirred for 1 h at -78 °C. Tributylstannyl chloride (1.22 g, 3.7mmol) was added dropwise to the reaction mixture, which was then allowed to warm to RT and stirred for an additional 40 min before being quenched with water (20 cm³) and then stirred vigorously for 1 h. The organic layers were separated and the water layer was extracted with DCM (3 x 50 cm³) and the combined extracts washed with brine (50 cm³), dried over MgSO₄, filtered off and then evaporated down by rotavapor under reduced pressure to afford the desired product a white solid (10.74 g, 98%), which was used directly without further purification. (0.64 g, 63%).

¹H NMR (CDCl₃) δ_H : 0.83 (3H, t), 0.91 (9H, t), 1.20-1.30 (16H, m), 1.58-1.63 (12H, m), 1.78 (2H, t, $J = 7.3$ Hz), 4.40, (2H, t), 7.23 (1H, t), 7.46 (1H, t), 7.57 (1H, d, $J = 8.4$ Hz) 7.62 (1H, d, $J = 8.4$ Hz), 7.93 (1H, d, $J = 8.6$ Hz), 8.13 (1H, d, $J = 8.8$ Hz), 8.16 (1H, d, $J = 8.4$ Hz).



2,5-bis-[5-(9-Octyl-9H-carbazol-3-yl)thiophen-2-yl]thiazolo[5,4-d]thiazole (74)

A mixture of 2,5-bis-(5-bromothiophen-2-yl)thiazolo[5,4-d]thiazole (**60**) (0.2 g, 0.43 mmol) and 9-octyl-3-(tributylstannyl)-9H-carbazole (**73**) (0.54 g, 0.95 mmol) in DMF (30 cm³) was stirred and degassed with N₂ for 30 min. Then potassium carbonate (0.24 g, 1.72mmol) was added into the mixture, followed by the addition of catalyst Pd(OAc)₂ (0.007 g, 2.5 mol%) and PPh₃ (0.0056 g, 5.0 mol%). The resultant reaction mixture was then heated to 90 °C under reflux overnight and cooled to room temperature. The reaction mixture was then poured into methanol and stirred for 30 min filtered off to yield the crude product. The resultant crude product was purified by flash column chromatography [silica gel with 10% K₂CO₃, Chloroform and hexane] and then recrystallisation from DCM to give the desired product as a orange red powder (0.24 g, 65%).

Melting point/°C: 173

¹H NMR (CDCl₃) δ_H: 0.88 (6H, t), 1.25-1.28 (12H, m), 1.33-1.39 (8H, m), 1.88 (4H, quint), 4.29 (4H, t), 7.24 (2H, d, *J* = 7.6 Hz), 7.34 (2H, m), 7.40 (4H, dd, *J* = 3.5 Hz, 7.6 Hz), 7.47 (2H, t), 7.58 (2H, m), 7.75 (2H, d, *J* = 8.4 Hz), 8.11 (2H, d, *J* = 7.6 Hz), 8.36 (2H, d, *J* = 6.0 Hz)

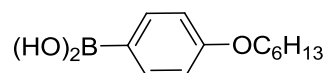
¹³C NMR (CDCl₃):162, 139, 138, 134, 130, 129, 128, 122, 120, 119, 116, 112, 111, 109, 58, 32, 29, 27, 23, 14.

MS m/z (MALDI): 862, 861, 860 (M⁺, M100)

Combustion analysis:

Expected: C, 72.52%; H, 6.09%; N, 6.51%; S, 14.89%

Obtained: C, 72.50%; H, 6.12%; N, 6.52%; S, 14.87%



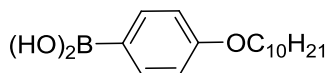
4-(Hexyloxy)phenylboronic acid (75)

A solution of 1-bromo-4-(hexyloxy)benzene (4.00 g, 0.015mol) in THF (180 cm³) was cooled to -78°C and stirred for 30 min. A 2.5 M solution of *n*-butyllithium in hexane (7.3cm³, 0.018 mol) was then added to the nitrogen-purged solution using a syringe and the resultant reaction solution stirred for 1 h at this temperature. Triisopropyl borate (6.27 g, 0.033 mol) was then added with a syringe. The resultant reaction mixture was allowed to warm gradually to room temperature overnight. Then 2N hydrochloric acid (100 cm³) was added to the reaction mixture the resultant mixture stirred at room temperature for 1 h. The organic layers were separated and the water layer was extracted with diethyl ether (3 x 50 cm³). The combined organic layers were washed with water (3 x 50 cm³), brine (50 cm³), dried over MgSO₄, filtered off and then evaporated down by rotavapor under reduced pressure. The crude product was purified by washing with hexane to give the desired product as a white powder (2.56 g, 77%).

Melting Point/°C: 74-77

¹H NMR (CDCl₃) δ_H: 0.90 (3H, t), 1.38 (8H, m), 1.73 (2H, quint), 2.41 (2H, s), 3.86 (2H, t), 6.75 (2H, d, *J* = 7.8 Hz), 7.32 (2H, d, *J* = 7.6 Hz).

MS *m/z* (EI): 223, 222 (M¹⁰⁰), 221 (M⁺)



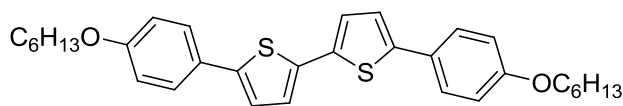
4-(Decyloxy)phenylboronic acid (76)

A solution of 1-bromo-4-(decyloxy)benzene (**23**) (5.50 g, 0.017mol) in THF (180 cm³) was cooled to -78°C and stirred for 30 min. A 2.5 M solution of n-butyllithium in hexane (8.96 cm³, 0.022mol) was then added to the nitrogen-purged solution using a syringe and the resultant reaction solution stirred for 1 h at this temperature. Triisopropyl borate (7.03 g, 0.037 mol) was then added with a syringe. The resultant reaction mixture was allowed to warm gradually to room temperature overnight. Then 2N hydrochloric acid (100 cm³) was added to the reaction mixture the resultant mixture stirred at room temperature for 1 h. The organic layers were separated off and the water layer was extracted with diethyl ether (3 x 50 cm³). The combined organic layers were washed with water (3 x 50 cm³), brine (50 cm³), dried over MgSO₄, filtered off and then evaporated down by rotavapor under reduced pressure. The crude product was purified by washing with hexane to give the desired product as a white power (3.12 g, 80%).

Melting Point/°C: 67-69

¹H NMR (CDCl₃) δ_H: 0.90 (3H, t), 1.38 (16H, m), 1.73 (2H, quint), 2.41 (2H, s), 3.86 (2H, t), 6.75 (2H, d, *J* = 7.8 Hz), 7.32 (2H, d, *J* = 7.6 Hz).

MS *m/z* (EI): 229, 228 (M¹⁰⁰), 227 (M⁺).



5,5'-bis-[4-(Hexyloxy)phenyl]-2,2'-bithiophene (**77**)

A mixture of 5,5'-dibromo-2,2'-bithiophene (**55**) (0.30 g, 0.93 mmol) and 4-(hexyloxy)phenylboronic acid (**75**) (0.47 g, 2.13 mmol) in DME (40 cm³) was stirred and degassed with N₂ for 30 min. Then sodium carbonate (0.39 g, 3.70 mmol) added into the mixture, followed by the addition of catalyst Pd(OAc)₂ (0.02 g, 2.5 mol%) and PPh₃ (0.01 g, 5.0 mol%). The resultant reaction mixture was then heated to 90 °C under reflux overnight and cooled to room temperature. The reaction mixture was then poured into methanol (250 cm³), stirred for 30 min and cooled to 0 °C. The precipitate was filtered off, washed by hexane and ethanol and dried to yield the crude product, which was then purified by recrystallisation from EtOH to give the desired product as a yellow powder (0.16 g, 34%).

Melting point/°C: Tg 54 Cr 242 N256 I (Bx 176)

¹H NMR (CDCl₃) δ _H: 0.89 (6H, t), 1.34-1.37 (8H, m), 1.46-1.49 (4H, m), 1.79 (4H, quint), 3.99 (4H, t), 6.91 (4H, d, *J* = 8.8 Hz), 7.12 (4H, t), 7.53 (4H, d, *J* = 8.8 Hz)

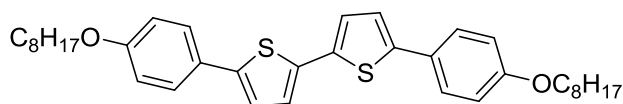
¹³C NMR (CDCl₃): 127, 124, 123, 115, 68, 32, 29, 26, 23, 14

MS *m/z* (MALDI): 520, 519, 518 (M⁺, M100), 434, 433, 351, 350, 349, 322, 321, 292.

Combustion analysis:

Expected: C, 74.09%; H, 7.38%; S, 12.36%

Obtained: C, 74.06%; H, 7.39%; S, 12.34%



5,5'-bis-[4-(Octyloxy)phenyl]-2,2'-bithiophene (78)

A mixture of 5,5'-dibromo-2,2'-bithiophene (**55**) (0.20 g, 0.62mmol) and 4-(octyloxy)phenylboronic acid (**26**) (0.46 g, 1.85mmol) in DMF (30 cm³) was stirred and degassed with N₂ for 30 min. Then potassium carbonate (0.26 g, 1.85mmol) added into the mixture, followed by the addition of catalyst Pd(OAc)₂ (0.01 g, 2 mol%). The resultant reaction mixture was then heated to 90 °C under reflux overnight and cooled to room temperature. The reaction mixture was then poured into methanol (250 cm³), stirred for 30 min and cooled to 0 °C. The precipitate was then filtered off, washed by hexane and ethanol and dried to yield the crude product. The resultant crude product was purified by recrystallisation from EtOH to give the desired product as a yellow powder (0.08 g, 22%).

Melting point/°C: 203

¹H NMR (CDCl₃) δ _H: 0.89 (6H, t), 1.34-1.37 (12H, m), 1.46-1.49 (4H, m), 1.79 (4H, quint), 3.99 (4H, t), 6.91 (4H, d, *J* = 8.8 Hz), 7.12 (4H, t), 7.53 (4H, d, *J* = 8.8 Hz)

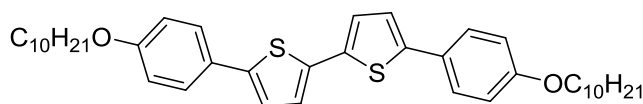
¹³C NMR (CDCl₃):127, 124, 123, 115, 68, 32, 31,29, 26, 23, 14

MS *m/z* (MALDI): 576, 575, 574 (M⁺, M100), 462, 461, 361, 348, 207, 73, 57, 44, 43.

Combustion analysis:

Expected: C, 75.21%; H, 8.07%; S, 11.16%

Obtained: C, 75.20%; H, 8.09%; S, 11.15%



5,5'-bis-[4-(Decyloxy)phenyl]-2,2'-bithiophene (79)

A mixture of 5,5'-dibromo-2,2'-bithiophene (**55**) (0.20 g, 0.62mmol) and 4-(decyloxy)phenylboronic acid (**77**) (0.51 g, 1.85mmol) in DMF was stirred and degassed with N₂ for 30 min. Then potassium carbonate (0.26 g, 1.85mmol) added into the mixture, followed by the addition of catalyst Pd(OAc)₂ (0.01 g, 2 mol%). The resultant reaction mixture was then heated to 90 °C under reflux overnight and cooled to room temperature. The reaction mixture was then poured into methanol and stirred for 30 min filtered off to yield the crude product. The resultant crude product was purified by recrystallisation from EtOH/DCM to give the desired product as a yellow powder (0.09 g, 23%).

Melting point/°C: 169

¹H NMR (CDCl₃) δ _H: 0.89 (6H, t), 1.34-1.37 (16H, m), 1.46-1.49 (4H, m), 1.79 (4H, quint), 3.99 (4H, t), 6.91 (4H, d, *J* = 8.8 Hz), 7.12 (4H, t), 7.53 (4H, d, *J* = 8.7 Hz)

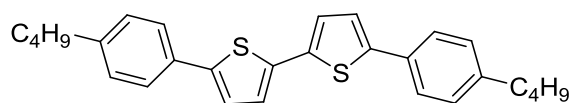
¹³C NMR (CDCl₃): 127, 124, 123, 115, 68, 32, 31, 29, 26, 23, 14

MS *m/z* (MALDI): 632, 631, 630 (*M*⁺, *M*100), 490, 489, 349, 348, 316, 284, 207, 73, 57, 44, 43.

Combustion analysis:

Expected: C, 76.14%; H, 8.63%; S, 10.16%

Obtained: C, 76.17%; H, 8.65%; S, 10.13%



5,5'-bis-(4-Butylphenyl)-2,2'-bithiophene (80)

A mixture of 5,5'-dibromo-2,2'-bithiophene (**55**) (0.20 g, 0.62mmol) and 4-butylphenylboronic acid (**65**) (0.33 g, 1.85 mmol) in DMF (30 cm³) was stirred and degassed with N₂ for 30 min. Then potassium carbonate (0.26 g, 1.85mmol) in water (2 cm³) was added into the mixture, followed by the addition of catalyst Pd(OAc)₂ (0.01 g, 2 mol%). The resultant reaction mixture was then heated to 90 °C under reflux overnight and cooled to room temperature. The reaction mixture was then poured into methanol (250 cm³), stirred for 30 min and cooled to 0 °C. The precipitate was then filtered off and dried to yield the crude product, which was purified by flash column chromatography [silica gel, hexane and DCM] and recrystallisation from EtOH to give the desired product as a yellow powder (0.23 g, 88%).

Melting point/°C: Tg 143 Cr 237 N 246 I

¹H NMR (CDCl₃) δ _H: 0.94 (6H, t), 1.39 (4H, quint), 1.62 (4H, quint), 2.62 (4H, t), 7.15 (2H, d, *J* = 3.9 Hz), 7.19 (2H, d, *J* = 4.1 Hz), 7.21 (4H, d, *J* = 7.1 Hz), 7.51 (4H, d, *J* = 7.0 Hz)

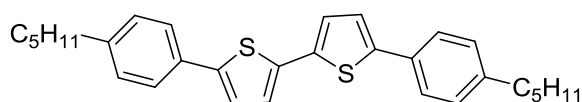
¹³C NMR (CDCl₃):129, 125, 124, 123, 35, 33, 22, 14

MS m/z (MALDI): 432, 431, 430 (M⁺, M100), 387, 344, 172, 43, 32.

Combustion analysis:

Expected: C, 78.09%; H, 7.02%; S, 14.89%

Obtained: C, 78.08%; H, 7.04%; S, 14.88%



5,5'-bis-(4-Pentylphenyl)-2,2'-bithiophene (**81**)

A mixture of 5,5'-dibromo-2,2'-bithiophene (**55**) (0.20 g, 0.62mmol) and 4-pentylphenylboronic acid (**66**) (0.59 g, 3.09 mmol) in DMF (30 cm³) was stirred and degassed with N₂ for 30 min. Then potassium carbonate (0.26 g, 1.85mmol) added into the mixture, followed by the addition of catalyst Pd(OAc)₂ (0.01 g, 2 mol%). The resultant reaction mixture was then heated to 90 °C under reflux overnight and cooled to room temperature. The reaction mixture was then poured into methanol (250 cm³), stirred for 30 min and cooled to 0 °C. The precipitate was then filtered off and dried to yield the crude product, which was purified by flash column chromatography [silica gel, hexane and DCM] and recrystallisation from EtOH to give the desired product as a light orange powder (0.24 g, 86%).

Melting point/°C: Tg 152 Cr 233 SmA 239 N 245 I

¹H NMR (CDCl₃) δ _H: 0.90 (6H, t), 1.32-1.35 (8H, m), 1.62 (4H, quint), 2.62 (4H, t), 7.15 (2H, d, *J* = 3.9 Hz), 7.19 (2H, d, *J* = 4.0 Hz), 7.21 (4H, d, *J* = 6.9 Hz), 7.51 (4H, d, *J* = 7.0 Hz)

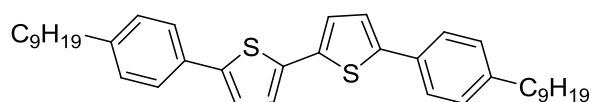
¹³C NMR (CDCl₃):129, 125, 124, 123, 35, 33, 31, 23, 14

MS *m/z* (MALDI): 460, 459, 458 (M⁺, M100), 401, 344, 172, 41.

Combustion analysis:

Expected: C, 78.55%; H, 7.47%; S, 13.98%

Obtained: C, 78.54%; H, 7.49%; S, 13.96%



5,5'-bis-(4-Nonylphenyl)-2,2'-bithiophene (**82**)

A mixture of 5,5'-dibromo-2,2'-bithiophene (**55**) (0.20 g, 0.62mmol) and 4-nonylphenylboronic acid (**66**) (0.46 g, 1.85 mmol) in DMF (30 cm³) was stirred and degassed with N₂ for 30 min. Then potassium carbonate (0.26 g, 1.85mmol) added into the mixture, followed by the addition of catalyst Pd(OAc)₂ (0.01 g, 2 mol%). The resultant reaction mixture was then heated to 90 °C under reflux overnight and cooled to room temperature. The reaction mixture was then poured into methanol (250 cm³), stirred for 30 min and cooled to 0 °C. The precipitate was then filtered off and dried to yield the crude product, which was purified by flash column chromatography [silica gel, hexane and DCM] and recrystallisation from EtOH to give the desired product as an orange powder (0.28 g, 80%).

Melting point/°C: Tg 92 Cr 213 SmA 218 I

¹H NMR (CDCl₃) δ _H: 0.90 (6H, t), 1.27-1.32 (24H, m), 1.62 (4H, quint), 2.62 (4H, t), 7.15 (2H, d, *J* = 3.9 Hz), 7.19 (2H, d, *J* = 4.0 Hz), 7.21 (4H, d, *J* = 6.9 Hz), 7.51 (4H, d, *J* = 7.0 Hz)

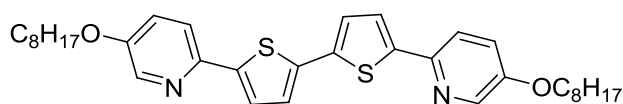
¹³C NMR (CDCl₃):129, 125, 124, 123, 35, 33, 31,30, 29, 28, 23, 14

MS *m/z* (MALDI): 572, 571, 570 (M⁺, M100), 457, 344, 316, 259, 71, 57, 43.

Combustion analysis:

Expected: C, 79.94%; H, 8.83%; S, 11.23%

Obtained: C, 79.95%; H, 8.82%; S, 11.23%



5,5'-bis-[5-(Octyloxy)pyridin-2-yl]-2,2'-bithiophene (83)

A mixture of 5,5'-dibromo-2,2'-bithiophene (**55**) (0.20 g, 0.62mmol) and 5-(octyloxy)pyridin-2-ylboronic acid (**66**) (0.62 g, 2.47 mmol) in DMF (30 cm³) was stirred and degassed with N₂ for 30 min. Then potassium carbonate (0.26 g, 1.85mmol) in water (2 cm³) was added into the mixture, followed by the addition of catalyst Pd(OAc)₂ (0.01 g, 2 mol%). The resultant reaction mixture was then heated to 90 °C under reflux overnight and cooled to room temperature. The reaction mixture was then poured into methanol (250 cm³), stirred for 30 min and cooled to 0 °C. The precipitate was then filtered off and dried to yield the crude product, which was purified by flash column chromatography [silica gel, hexane and DCM] and recrystallisation from EtOH to give the desired product as an orange powder (0.30 g, 84%).

Melting point/°C: Tg 66 Cr 123 (Bx 134) SmX 140 SmA 211 I

¹H NMR (CDCl₃) δ_H: 0.90 (6H, t), 1.30-1.34 (18H, m), 1.41-1.43 (4H, m), 1.79 (4H, quint), 4.32 (4H, t), 6.77 (2H, d, *J* = 8.6 Hz), 7.16 (4H, q), 7.77 (2H, dd, *J* = 2.7, 8.5 Hz), 8.41 (2H, d, *J* = 2.7 Hz)

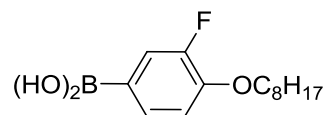
¹³C NMR (CDCl₃):152, 143, 140, 137, 130, 128, 125, 121, 68, 32, 29, 28, 26, 23, 14.

MS m/z (MALDI): 578, 577, 576 (M⁺, M100), 463, 350, 286, 173, 73, 57, 43.

Combustion analysis:

Expected: C, 70.79%; H, 7.69%; N, 4.86%; S, 11.12%

Obtained: C, 70.78%; H, 7.68%; N, 4.89%; S, 11.11%

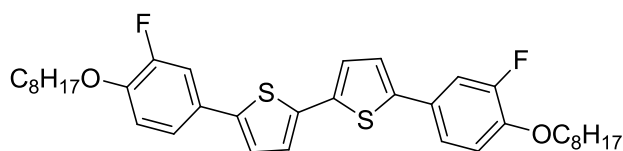


3-Fluoro-4-(octyloxy)phenylboronic acid (84)

A solution of 4-bromo-2-fluoro-1-(octyloxy)benzene (3.00 g, 9.89 mmol) in THF (150 cm³) was cooled to -78°C and stirred for 30 min. A 2.5 M solution of *n*-butyllithium in hexane (5.24cm³, 0.012mol) was then added to the nitrogen-purged solution using a syringe and the resultant reaction solution stirred for 1 h at this temperature. Triisopropyl borate (3.95 g, 0.021 mol) was then added with a syringe. The resultant reaction mixture was allowed to warm gradually to room temperature overnight. Then 2N hydrochloric acid (100 cm³) was added to the reaction mixture the resultant mixture stirred at room temperature for 1 h. The organic layers were separated and the water layer was extracted with diethyl ether (3 x 50 cm³). The combined organic layers were washed with water (3 x 50 cm³), brine (50 cm³), dried over MgSO₄, filtered off and then evaporated down by rotavapor under reduced pressure. The crude product was purified by washing with hexane to give the desired product as a white power (2.01 g, 76%).

¹H NMR (CDCl₃) δ_{H} : 0.90 (3H, t), 1.38 (16H, m), 1.73 (2H, quint), 2.41 (2H, s), 3.86 (2H, t), 6.75 (2H, d, $J = 2.2$ Hz), 7.04 (2H, m), 7.32 (2H, d, $J = 2.3$ Hz).

MS m/z (EI): 229, 228 (M100), 227 (M⁺).



5,5'-bis-[3-Fluoro-4-(octyloxy)phenyl]-2,2'-bithiophene (85)

A mixture of 5,5'-dibromo-2,2'-bithiophene (**55**) (0.2 g, 0.62mmol) and 3-fluoro-4-(octyloxy)phenylboronic acid (**84**) (0.84 g, 2.47 mmol) in DMF (30 cm³) was stirred and degassed with N₂ for 30 min. Then potassium carbonate (0.26 g, 1.85mmol) added into the mixture, followed by the addition of catalyst Pd(OAc)₂(0.01 g, 2 mol%). The resultant reaction mixture was then heated to 90°C under reflux overnight and cooled to room temperature. The reaction mixture was then poured into methanol (250 cm³), stirred for 30 min and cooled to 0 °C. The precipitate was then filtered off and dried to yield the crude product, which was purified by flash column chromatography [silica gel, hexane and DCM] and recrystallisation from EtOH to give the desired product as an orange powder (0.30 g, 84%).

Melting point/°C:Tg 94 Cr 116 SmX 170 N 219 I

¹H NMR (CDCl₃) δ_H: 0.89 (6H, t), 1.30-1.34 (12H, m), 1.46-1.49 (4H, m), 1.85 (4H, quint), 4.06 (4H, t), 6.99 (2H, t), 7.12 (4H,d, *J* = 1.4Hz), 7.27-7.30 (4H, m)

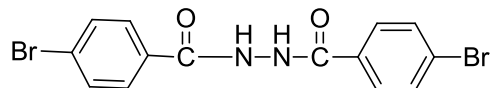
¹³C NMR (CDCl₃):152, 148, 138, 136, 128, 127, 124, 123, 116, 115, 68, 32, 31,29, 26, 23, 14

MS m/z (MALDI): 612, 611, 610 (M⁺, M100), 572, 571, 570, 457, 344, 207, 73, 57, 44.

Combustion analysis:

Expected: C, 70.78%; H, 7.26%; S, 10.50%

Obtained: C, 70.77%; H, 7.29%; S, 10.48%

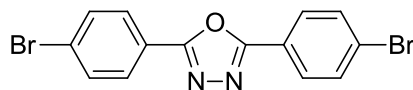


4-Bromo-*N'*-(4-bromobenzoyl)benzohydrazide (86).

A solution of 4-bromobenzohydrazide (2.00 g, 9.25mmol), 4-bromobenzoyl chloride (2.04 g, 9.25 mmol) and pyridine (50 cm³) was heated under reflux for 6 h. After cooling to room temperature, the reaction mixture was poured into methanol (200 cm³). The mixture was cooled to 0 °C and the resultant precipitate filtered off and dried to afford white crystals (3.09 g, 84%) of the desired product.

Melting point/°C: >300^[14].

¹H NMR (CDCl₃) δ_H: 7.66 (2H, d, *J* = 8.6 Hz), 7.78 (2H, d, *J* = 8.6 Hz), 10.56 (2H, s).



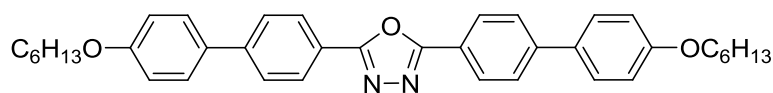
2,5-*bis*-(4-Bromophenyl)-1,3,4-oxadiazole (87)

A solution of 4-bromo-*N'*-(4-bromobenzoyl)benzohydrazide (**86**) (3.00 g, 7.54 mmol) in SOCl₂ (10 cm³) was heated under reflux for 7 h. The excess SOCl₂ was distilled off and then the residue was slowly poured into water (50 cm³). The resultant precipitate was filtered off and then purified via stirring in hexane, the crude product was filtered off and dried to yield the desired product as a white crystalline solid (2.73 g, 95%).

Melting point/°C: 256-258 (Lit.258^[11])

^1H NMR (CDCl_3) δ_{H} : 7.69 (4H, d, $J = 8.8$ Hz), 8.01 (4H, d, $J = 8.8$ Hz).

MS m/z (EI): 379.9 (M^+), 381.9 (M^{+1}).



2,5-bis-[4'-(Hexyloxy)biphenyl-4-yl]-1,3,4-oxadiazole (88)

A mixture of 2,5-bis-(4-bromophenyl)-1,3,4-oxadiazole (**87**) (0.20 g, 0.53 mmol) and 4-(hexyloxy)phenylboronic acid (**75**) (0.35 g, 1.58 mmol) in DMF (30 cm^3) was stirred and degassed with N_2 for 30 min. Then potassium carbonate (0.22 g, 1.59 mmol) added into the mixture, followed by the addition of catalyst $\text{Pd}(\text{OAc})_2$ (0.007 g, 2 mol%). The resultant reaction mixture was then heated to 90 $^\circ\text{C}$ under reflux overnight. After cooling to room temperature, the reaction mixture was then poured into methanol (250 cm^3) and stirred for 30 min, cooled to 0 $^\circ\text{C}$ and filtered off to yield the crude product. The resultant crude product was washed with hexane and ethanol then purified by recrystallisation from EtOH to give the desired product as a white powder (0.21 g, 70%).

Melting point/ $^\circ\text{C}$: Cr 233 N 253 I

^1H NMR (CDCl_3) δ_{H} : 0.93 (6H, t), 1.35-1.39 (8H, m), 1.49 (4H, m), 1.83 (4H, quint), 4.03 (4H, t), 7.02 (4H, d, $J = 9.0$ Hz), 7.60 (4H, d, $J = 8.8$ Hz), 7.73 (4H, d, $J = 8.6$ Hz), 8.21 (4H, d, $J = 8.6$ Hz)

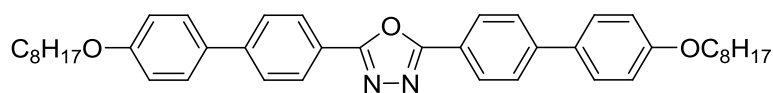
^{13}C NMR (CDCl_3): 165, 159, 144, 132, 128, 127, 126, 121, 115, 68, 32, 29, 26, 23, 14.

MS m/z (MALDI): 576, 575, 574 (M^+ , $\text{M}100$), 536, 477, 435, 391, 331, 284.

Combustion analysis:

Expected: C, 79.41%; H, 7.37%; N, 4.87%

Obtained: C, 79.43%; H, 7.38%; N, 4.85%;



2,5-bis-[4'-(Octyloxy)biphenyl-4-yl]-1,3,4-oxadiazole (89)

A mixture of 2,5-bis-(4-bromophenyl)-1,3,4-oxadiazole (**87**) (0.11 g, 0.28 mmol) and 4-(hexyloxy)phenylboronic acid (**75**) (0.20 g, 0.85 mmol) in DMF was stirred and degassed with N₂ for 30 min. Then potassium carbonate (0.12 g, 0.86 mmol) in water (2 cm³) was added into the mixture, followed by the addition of catalyst Pd(OAc)₂ (0.004 g, 2 mol%). The resultant reaction mixture was then heated to 90 °C under reflux overnight. After cooling to room temperature, the reaction mixture was then poured into methanol (250 cm³) and stirred for 30 min, cooled to 0 °C and filtered off to yield the crude product. The resultant crude product was washed by DCM, hexane and ethanol then purified by recrystallisation from EtOH to give the desired product as a white powder (0.21 g, 70%).

Melting point/°C: Cr 228 N 243 I

¹H NMR (CDCl₃) δ_H: 0.93 (6H, t), 1.35-1.39 (16H, m), 1.49 (4H, m), 1.83 (4H, quint), 4.03 (4H, t), 7.02 (4H, d, *J* = 9.0 Hz), 7.60 (4H, d, *J* = 8.8 Hz), 7.73 (4H, d, *J* = 8.6 Hz), 8.21 (4H, d, *J* = 8.5 Hz)

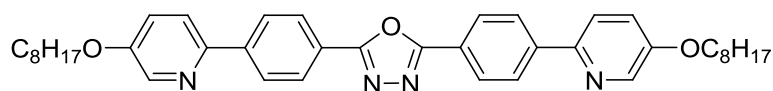
¹³C NMR (CDCl₃): 165, 159, 144, 132, 128, 127, 126, 121, 115, 68, 32, 29, 26, 23, 14.

MS *m/z* (MALDI): 632, 631, 630 (M⁺, M100), 523, 517, 435, 404, 331, 217.

Combustion analysis:

Expected: C, 79.96%; H, 7.99%; N, 4.44%

Obtained: C, 79.98%; H, 7.97%; N, 4.45%



2,5-bis-{4-[5-(Octyloxy)pyridin-2-yl]phenyl}-1,3,4-oxadiazole (90)

A mixture of 2,5-bis-(4-bromophenyl)-1,3,4-oxadiazole (**87**) (0.50 g, 1.31 mmol) and 5-(octyloxy)pyridin-2-ylboronic acid (**71**) (0.83 g, 3.29 mmol) in DMF (40 cm³) was stirred and degassed with N₂ for 30 min. Then potassium carbonate (0.55 g, 3.94 mmol) in water (4 cm³) was added into the mixture, followed by the addition of catalyst Pd(OAc)₂ (0.02 g, 2 mol%). The resultant reaction mixture was then heated to 90 °C under reflux overnight. After cooling to room temperature, the reaction mixture was then poured into methanol and stirred for 30 min, cooled to 0 °C and filtered off to yield the crude product. The resultant crude product was purified via flash column chromatography [silica gel, DCM and ethyl acetate] and then recrystallisation from EtOH to give the desired product as a white solid (0.65 g, 78%).

Melting point/°C: Cr 219 (Bx 232) SmC 256 I

¹H NMR (CDCl₃) δ_H: 0.93 (6H, t), 1.35-1.39 (16H, m), 1.49 (4H, m), 1.83 (4H, quint), 4.03 (4H, t), 6.86 (2H, d, *J* = 8.6 Hz), 7.72 (4H, d, *J* = 8.2 Hz), 7.88 (2H, dd, *J* = 2.7Hz, 8.3 Hz), 8.24 (4H, d, *J* = 8.8 Hz), 8.47 (2H, d, *J* = 2.4 Hz).

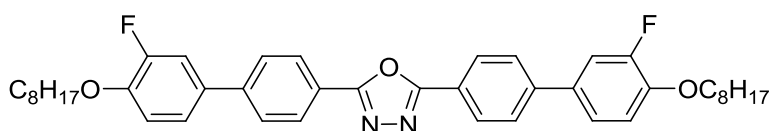
¹³C NMR (CDCl₃):165, 152, 146, 140, 129. 128, 125, 124, 121, 68, 32, 29, 26, 23, 14.

MS m/z (MALDI): 634, 633, 632 (M⁺, M100), 521, 435, 317, 261, 204.

Combustion analysis:

Expected: C, 75.92%; H, 7.65%; N, 8.85%

Obtained: C, 75.93%; H, 7.67%; N, 8.84%



2,5-bis-[3'-Fluoro-4'-(octyloxy)biphenyl-4-yl]-1,3,4-oxadiazole (91)

A mixture of 2,5-bis-(4-bromophenyl)-1,3,4-oxadiazole (**87**) (0.20 g, 0.53 mmol) and 3-fluoro-4-(octyloxy)phenylboronic acid (**84**) (0.42 g, 1.58 mmol) in DMF (40 cm³) was stirred and degassed with N₂ for 30 min. Then potassium carbonate (0.22 g, 1.58 mmol) added into the mixture, followed by the addition of catalyst Pd(OAc)₂ (0.01 g, 2 mol%). The resultant reaction mixture was then heated to 90 °C under reflux overnight. After cooling to room temperature, the reaction mixture was then poured into methanol and stirred for 30 min, cooled to 0 °C and filtered off to yield the crude product. The resultant crude product was purified *via* flash column chromatography [silica gel, hexane and ethyl acetate] and then recrystallisation from EtOH/DCM to give the desired product as a white solid (0.27 g, 76%).

Melting point/°C: Cr 159 SmC 202 N 221 I

¹H NMR (CDCl₃) δ_H: 0.89 (6H, t), 1.29-1.32 (16H, m), 1.49 (4H, m), 1.85 (4H, quint), 4.08 (4H, t), 7.06 (2H, d, *J* = 8.6 Hz), 7.37 (2H, d, *J* = 8.4 Hz), 7.42 (2H, d, *J* = 2.0 Hz), 7.70 (4H, d, *J* = 8.8 Hz), 8.29 (4H, d, *J* = 8.6 Hz)

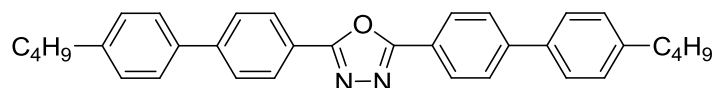
¹³C NMR (CDCl₃): 165, 153, 147, 141, 133, 128, 127, 125, 123, 115, 68, 32, 30, 29, 26, 23, 14.

MS *m/z* (MALDI): 668, 667 (M100), 666 (M⁺), 617, 556, 515, 473, 435, 331, 162.

Combustion analysis:

Expected: C, 75.65%; H, 7.26%; N, 4.20%

Obtained: C, 75.63%; H, 7.29%; N, 4.22%



2,5-bis-(4'-Butylbiphenyl-4-yl)-1,3,4-oxadiazole (92)

A mixture of 2,5-bis-(4-bromophenyl)-1,3,4-oxadiazole (**87**) (0.20 g, 0.53mmol) and 4-butylphenylboronic acid (**65**) (0.28 g, 1.58 mmol) in DMF (40 cm³) was stirred and degassed with N₂ for 30 min. Then potassium carbonate (0.22 g, 1.58 mmol) in water (2 cm³) was added into the mixture, followed by the addition of catalyst Pd(OAc)₂ (0.01 g, 2 mol%). The resultant reaction mixture was then heated to 90 °C under reflux overnight. After cooling to room temperature, the reaction mixture was then poured into methanol and stirred for 30 min, cooled to 0 °C and filtered off to yield the crude product. The resultant crude product was purified via flash column chromatography [silica gel, hexane and ethyl acetate] and then recrystallisation from EtOH/DCM to give the desired product as a white solid (0.21 g, 80%).

Melting point/°C: Cr 238 SmA 248 N 256 I

¹H NMR (CDCl₃) δ _H: 0.97 (6H, t), 1.38-1.44 (4H, quint), 1.67 (4H, quint), 2.70 (4H, t), 7.31 (4H, d, *J* = 8.4 Hz), 7.59 (4H, d, *J* = 8.4 Hz), 7.78 (4H, d, *J* = 8.6 Hz), 8.23 (4H, d, *J* = 8.6 Hz)

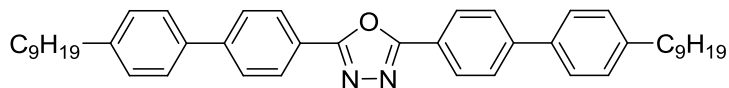
¹³C NMR (CDCl₃):164, 142, 140, 138, 129, 127, 126, 35, 33, 22, 14.

MS m/z (MALDI): 488, 487, 486 (M^+ , M100), 443, 387, 237, 208, 207, 200, 192, 167, 153, 152, 88, 73, 41.

Combustion analysis:

Expected: C, 83.91%; H, 7.04%; N, 5.76%

Obtained: C, 83.93%; H, 7.03%; N, 5.74%



2,5-bis-(4'-Nonylbiphenyl-4-yl)-1,3,4-oxadiazole (93)

A mixture of 2,5-bis-(4-bromophenyl)-1,3,4-oxadiazole (**87**) (0.20 g, 0.53 mmol) and 4-nonylphenylboronic acid (**67**) (0.39 g, 1.58 mmol) in DMF (40 cm³) was stirred and degassed with N₂ for 30 min. Then potassium carbonate (0.22 g, 1.58 mmol) added into the mixture, followed by the addition of catalyst Pd(OAc)₂ (0.01 g, 2 mol%). The resultant reaction mixture was then heated to 90 °C under reflux overnight. After cooling to room temperature, the reaction mixture was then poured into methanol (200 cm³) and stirred for 30 min, cooled to 0 °C and filtered off to yield the crude product. The resultant crude product was purified via flash column chromatography [silica gel, hexane and ethyl acetate] and then recrystallisation from EtOH/DCM to give the desired product as a white solid (0.27 g, 81 %).

Melting point/°C: Cr 168 SmX 203 SmC 218 I

¹H NMR (CDCl₃) δ _H: 0.97 (6H, t), 1.28-1.35 (24H, m), 1.67 (4H, m), 2.67 (4H, t), 7.31 (4H, d, J = 8.0 Hz), 7.59 (4H, d, J = 8.1 Hz), 7.77 (4H, d, J = 8.4 Hz), 8.22 (4H, d, J = 8.6 Hz)

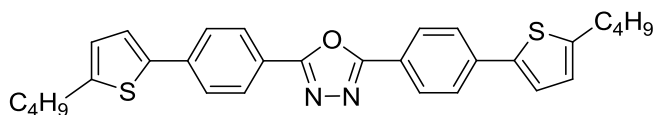
^{13}C NMR (CDCl_3): 164, 142, 140, 138, 129, 127, 126, 36, 32, 31, 29, 23, 14.

MS m/z (MALDI): 628, 627 (M_{100}), 626 (M^+), 523, 435, 331, 284, 189.

Combustion analysis:

Expected: C, 84.30%; H, 8.68%; N, 4.47%

Obtained: C, 84.27%; H, 8.69%; N, 4.48%



2,5-bis-[4-(5-Butylthiophen-2-yl)phenyl]-1,3,4-oxadiazole (94)

K_2CO_3 (0.18 g, 1.32mmol), pivalic acid (0.016 g, 0.16mmol) and 2,5-bis-(4-bromophenyl)-1,3,4-oxadiazole (**87**) (0.2 g, 0.53mmol) were weighed in air and placed in a flask, which was degassed with N_2 for 20 min. Then DMF (30 cm^3) and 2-butylthiophene (0.18 g, 1.32 mmol) were added, followed by the addition of catalyst $Pd(OAc)_2$ (0.007 g, 2%mol) and $PCy_3 \cdot HBF_4$ (0.008 g, 4mol%),. The reaction mixture was then vigorously stirred at 100 $^{\circ}C$ for 4 h. The solution was then cooled to room temperature poured directly into methanol (250 cm^3), stirred for 30min, cooled to 0 $^{\circ}C$ and the crude product was precipitated from methanol. The crude product was filtered off, purified by flash column chromatography [silica gel, DCM/hexane/ethyl acetate] and recrystallisation from EtOH to give the desired product as a white crystalline solid (0.23 g, 86%).

Melting point/ $^{\circ}C$: Cr189 N 194 I

1H NMR ($CDCl_3$) δ_H : 0.94 (6H, t), 1.46 (4H, m), 1.62 (4H, quint), 2.83 (4H, t), 6.89 (2H, d, $J = 3.5$ Hz), 7.26 (2H, d, $J = 3.5$ Hz), 7.69 (2H, d, $J = 8.4$ Hz), 8.10 (4H, d, $J = 8.6$ Hz)

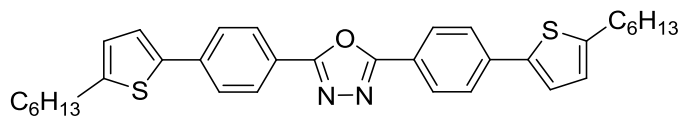
^{13}C NMR ($CDCl_3$):165, 147, 140, 138, 127, 126, 125, 124, 121, 34, 30, 22, 14

MS m/z (MALDI): 500, 499, 498 (M^+ , M100), 455, 345, 301, 243, 214, 207, 172, 171, 115, 71, 61, 45.

Combustion analysis:

Expected: C, 72.25%; H, 6.06%; N, 5.62%; S, 12.86%

Obtained: C, 72.26%; H, 6.04%; N, 5.62%; S, 12.85%



2,5-bis-[4-(5-hexylthiophen-2-yl)phenyl]-1,3,4-oxadiazole (95)

A mixture of 2,5-bis-(4-bromophenyl)-1,3,4-oxadiazole (**87**) (0.20 g, 0.53 mmol) and 2-(5-hexylthiophen-2-yl)-4,4,5,5-tetramethyl-1,3,2-dioxaborolane (**61**) (0.46 g, 1.58 mmol) in DMF (30cm³) was stirred and degassed with N₂ for 30 min. Then potassium carbonate (0.22 g, 1.58 mmol) added into the mixture, followed by the addition of catalyst Pd(OAc)₂ (0.01 g, 2 mol%). The resultant reaction mixture was then heated to 90 °C under reflux overnight. After cooling to room temperature, the reaction mixture was then poured into methanol and stirred for 30 min, cooled to 0 °C and filtered off to yield the crude product. The resultant crude product was purified via flash column chromatography [silica gel, DCM/hexane/ethyl acetate] and then recrystallisation from EtOH to give the desired product as a white powder (0.26 g, 87%).

Melting point/°C: Cr 183 N 188 I

¹H NMR (CDCl₃) δ_H: 0.94 (6H, t), 1.32-1.34 (8H, m), 1.40 (4H, m), 1.72 (4H, quint), 2.84 (4H, t), 6.80 (2H, d, *J* = 3.5 Hz), 7.27 (2H, d, *J* = 3.7 Hz), 7.71 (2H, d, *J* = 8.6 Hz), 8.12 (4H, d, *J* = 8.8 Hz)

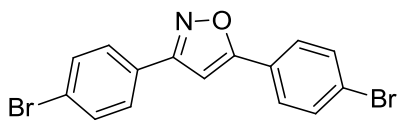
¹³C NMR (CDCl₃): 165, 147, 140, 138, 127, 126, 125, 124, 121, 34, 30, 22, 14

MS m/z (MALDI): 556, 555 (M100), 554 (M⁺), 511, 466, 326, 298, 254, 225.

Combustion analysis:

Expected: C, 73.60%; H, 6.90%; N, 5.05%; S, 11.56%

Obtained: C, 73.64%; H, 6.92%; N, 5.07%; S, 11.55%



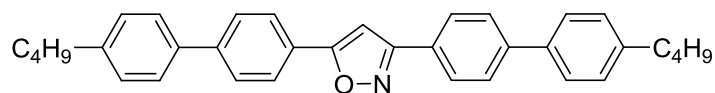
3,5-bis-(4-Bromophenyl)isoxazole (96)

1,3-bis-(4-Bromophenyl)propane-1,3-dione (4.00 g 10.4 mmol) was dissolved in 100 mL dioxane and heated under reflux, then hydroxylamine hydrogen chloride (3.00 g 43.2 mmol) in 10 ml water and 5 N NaOH (5 cm³, 25 mmol) was then dropped into the refluxing mixture. After heating for 12 hours, the reaction mixture was cooled to room temperature, and the solvent was removed by rotavapor under reduced pressure. The crude product was purified by recrystallisation from ethanol to yield the desired product as a white crystalline solid (3.41 g, 85%).

Melting point/°C: 218-219 (Lit. 218.5 - 219.5¹⁵)

¹H NMR (CDCl₃) δ H: 6.82 (1H, s), 7.62 (2H, d, J = 8.4 Hz), 7.66 (2H, d, J = 8.4 Hz), 7.74 (2H, d, J = 8.4 Hz), 7.78 (2H, d, J = 8.3 Hz)

MS m/z (EI): 379 (M⁺), 224, 183, 155



3,5-bis-(4'-Butylbiphenyl-4-yl)isoxazole (**97**)

A mixture of 3,5-bis-(4-bromophenyl)isoxazole (**96**) (0.1 g, 0.26 mmol) and 4-butylphenylboronic acid (**65**) (0.14 g, 0.79 mmol) in DMF (20 cm³) was stirred and degassed with N₂ for 30 min. Then potassium carbonate (0.11 g, 0.79 mmol) in water (1 cm³) was added into the mixture, followed by the addition of catalyst Pd(OAc)₂ (0.006 g, 2 mol%). The resultant reaction mixture was then heated to 90 °C under reflux overnight. After cooling to room temperature, the reaction mixture was then poured into methanol and stirred for 30 min, cooled to 0 °C and filtered off to yield the crude product. The resultant crude product was purified via flash column chromatography [silica gel, hexane and DCM] and then recrystallisation from EtOH/DCM to give the desired product as a white crystalline solid (0.10 g, 79%).

Melting point/°C: 264

¹H NMR (CDCl₃) δ_H: 0.89 (6H, t), 1.30-1.34 (4H, sext), 1.59 (4H, quint), 2.60 (4H, t), 6.82 (1H, s), 7.22 (4H, dd, *J* = 1.6Hz, 8.6 Hz), 7.50 (4H, dd, *J* = 2.6Hz, 8.5 Hz), 7.65 (4H, dd, *J* = 2.4Hz, 8.6 Hz), 7.86 (4H, dd, *J* = 1.7Hz, 8.6 Hz)

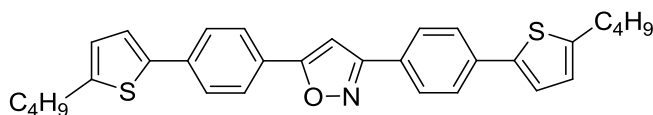
¹³C NMR (CDCl₃): 170, 162, 141, 140, 138, 130, 128, 127, 126, 98, 35, 33, 22, 14.

MS *m/z* (MALDI): 487, 486 (M100), 485 (M⁺), 435, 391, 326, 312, 310, 284, 282..

Combustion analysis:

Expected: C, 86.56%; H, 7.26%; N, 2.88%

Obtained: C, 86.57%; H, 7.23%; N, 2.88%



3,5-bis-[4-(5-Butylthiophen-2-yl)phenyl]isoxazole (**98**)

A mixture of 3,5-bis-(4-bromophenyl)isoxazole (**96**) (0.10 g, 0.26 mmol) and 4-hexylphenylboronic acid (**62**) (0.28 g, 1.06 mmol) in DMF (20 cm³) was stirred and degassed with N₂ for 30 min. Then potassium carbonate (0.11 g, 0.79 mmol) added into the mixture, followed by the addition of catalyst Pd(OAc)₂ (0.01 g, 2 mol%). The resultant reaction mixture was then heated to 90 °C under reflux overnight. After cooling to room temperature, the reaction mixture was then poured into methanol and stirred for 30 min, cooled to 0 °C and filtered off to yield the crude product. The resultant crude product was purified via flash column chromatography [silica gel, hexane and DCM] and then recrystallisation from EtOH/DCM to give the desired product as a white solid (0.12 g, 92%).

Melting point/°C: Tg 99 Cr 219 SmC 236 I

¹H NMR (CDCl₃) δ_H: 0.97 (6H, t), 1.41-1.45 (4H, sext), 1.71 (4H, quint), 2.85 (4H, t), 6.79 (4H, d, *J* = 4.40 Hz), 6.84 (1H, s), 7.23 (2H, d, *J* = 7.8 Hz), 7.70 (4H, dd, *J* = 3.2Hz, 8.4 Hz), 7.84 (4H, dd, *J* = 3.3Hz, 8.5 Hz)

¹³C NMR (CDCl₃): 170, 162, 143, 135, 128, 127, 126, 98, 39, 34, 22, 14.

MS m/z (MALDI): 499, 498, 497 (M⁺, M100), 454, 440, 411, 383, 301, 251, 235, 233.

Combustion analysis:

Expected: C, 74.81%; H, 6.28%; N, 2.81%; S, 12.88%

Obtained: C, 74.82%; H, 6.27%; N, 2.83%; S, 12.84%

3.5 References

- 1 N. Miyauro and A. Suzuki, *Chem. Rev.*, 1995, **95**, 2457.
- 2 W. Bao, M. R. Billa, K. Kassireddy, M. Haro, M. J. Kelly, S. P. Kitney, M. S. A. Kalifah, P. Wei, D. Dong, M. O'Neill and S. M. Kelly, *Liq. Cryst.*, 2010, **37**, 1289.
- 3 L. L. Miller and Y. Yu, *J. Org. Chem.*, 1995, **60**, 6813.
- 4 B. Liegault, D. Lapointe, C. Laurence, A. Vlassova and K. Fagnou, *J. Org. Chem.*, 2009, **74**, 1826.
- 5 F. Diershke, A. C. Grimsdale, K. Mullen, *Synthesis* 2003, **16**, 2470.
- 6 J. Bouchard, S. Wakim, M. Leclerc, *Org. Chem.*, 2004, **69**, 5705.
- 7 A. Yokooji, T. Satoh, M. Miura, M. Nomura, *Tetrahedron*, 2004, **60**, 6757.
- 8 C. J. Kelly, A. Ghiorghis, J. M. Kauffman, *J. Chem. Res.*, 1997, **12**, 2701.
- 9 PhD Thesis of G. J. Richards, "Novel Organic Materials for Electroluminescent Display Devices", University of Hull, 2001.
- 10 PhD Thesis by Kitney, S. P., "Liquid Crystalline Semiconductors for Organic Electronics", University of Hull, 2008.
- 11 Z. Li, X. Sun, L. Wang, Y. Li, Y. Ma, *Journal of the Brazilian Chemical Society*, 2010, **21**, 496 - 501
- 12 A. Facchetti, M. Yoon, C. L. Stern, G. R. Hutchison, M. A. Ratner, T. J. Marks, *J. Am. Chem. Soc.*, 2004, **126**, 13480 - 13501
- 13 S. Ando, J. Nishida, Y. Inoue, S. Tokito, Y. Yamashita, *J. Mater. Chem.*, 2004, **14**, 1787-1790.

-
- 14 X. Zhan, Y. Liu, X. Wu, S. Wang and D. Zhu, *Macromolecules.*, 2002, **35**, 2529-2537.
- 15 L. D. Sychkova, Y. S. Shabarov, *J. Org. Chem. USSR (English Translation)*, 1985, **21**, 261 – 264.
- 16 M. R. Billa, K. Kassireddy, M. Haro, M. J. Kelly, S. P. Kitney, M. S. A. Kalifah, P. Wei, D. Dong, M. O'Neill and S. M. Kelly, *Liq. Cryst.*, 2011, **38**, 813-829.
- 17 K. L. Woon, M. P. Aldred, P. Vlachos, G. H. Mehl, T. Stirner, S. M. Kelly, M. O'Neill, *Chem. Mater.*, 2006, **18**, 2311.
- 18 M. Tavasli, S. Bettington, M. R. Bryce, H. A. A. Attar, F. B. Dias, S. King and A. P. Monkman, *J. Mater. Chem.*, 2005, **15**, 4963.
- 19 M. P. Aldred, A. J. Eastwood, S. M. Kelly, P. Vlachos, A. E. A. Contoret, S. R. Farrar, B. Mansoor, M. O'Neill and W. C. Tsoi, *Chem. Mater.*, 2004, **16**, 4928.
- 20 S. P. Dudek, M. Pouderoijen, R. Abbel, A. P. H. J. Schenning and E. W. Meijer, *J. Am. Chem. Soc.*, 2005, **127**, 11763.
- 21 G. Manolikakes and P. Knochel, *Angew. Chem. Int. Ed. Eng.*, 2009, **48**, 205.
- 22 T. Maegawa, Y. Kitamura, S. Sako, T. Uozu, A. Sakurai, A. Tanaka, Y. Kobayashi, K. Endo, U. Bora, T. Kurita, A. Kozaki, Y. Monguchi and H. Sajiki, *Chem. Eur. J.*, 2007, **13**, 5937.
- 23 PhD Thesis by M. P. Aldred, “*Charge-Transporting and Electroluminescent Liquid Crystals for Organic Light-Emitting Diodes*”, University of Hull, 2004.
- 24 I. Jung, J. Yu, E., Jeong, J. Kim, S. Kwon, H. Kong, K. Lee, H. Woo and H. Shim, *Chem. Eur. J.*, 2010, **16**, 3743 – 3752
- 25 Y. Fujinami, J. Kuwabara, W. Lu, H. Hayashi and T. Kanbara, *ACS Macromol. Lett.*, 2012, **1**, 67–70.
- 26 M. P. Aldred, P. Vlachos, A. E. A. Contoret, S. R. Farrar, W. C. Tsoi, B. Mansoor, K. L. Woon, R. Hudson, S. M. Kelly and M. O'Neill, *J. Mater. Chem.*, 2005, **31**, 3208.

4 Results and Discussion

4.1 Synthetic discussion

4.1.1 Failed schemes

There were two unsuccessful reaction schemes and one scheme that gave the final product, but without any further data due to the insolubility of the final product.

4.1.1.1 Scheme 3.1

In scheme 3.1, the desired unsymmetrical final product could not be synthesized, probably because of the tendency to form the symmetrical product with side-chains on both sides, in spite of very careful dropwise addition of the bromo-substituted THP derivative (**32**). The purification by column chromatography of this reaction mixture was very difficult and, although the desired product was present in the reaction mixture, it could not be isolated in a pure state. Fig. 4.1 shows the proposed final product made from expected intermediate **34**.

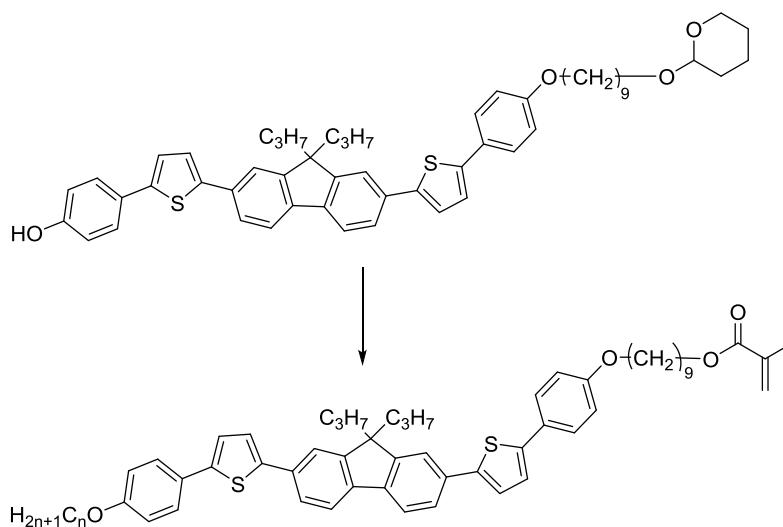


Fig. 4.1 Proposed chemical structure of final product for Scheme 3.1

4.1.1.2 Scheme 4

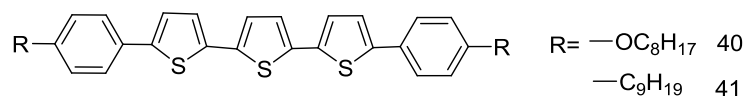


Fig. 4.2. Structures of final products for scheme 4

In scheme 4, both final products, see Fig. 4.2, could not be dissolved in common organic solvents, though both should be liquid crystals, as explained in section 3.4. Therefore no further data were obtained nor finding out the way to purify them. The elemental analysis illustrated that the products were not pure, so DSC was not suitable to determine the transition temperatures. It was also very difficult to identify the liquid crystal phases by microscope because of the impurities.

4.1.1.3 Scheme 5

The asymmetrical reactive mesogen, shown in Fig. 4.3, should have been synthesized as a photopolymerisable hole charge transport material in OLEDs and/or an electron-donor in OPVs, according to the method shown in scheme 5. It was expected to exhibit a nematic phase with lower transition temperatures, especially the melting point.

The procedure to make the intermediates with OTHP-protected end-chains by an *n*-BuLi-mediated reaction was similar to the procedure used successfully to prepare compound **42**, shown in Fig 4.4. However, this reaction failed, probably due to the influence of the long chains and the large molecular structure of compound **43**, reducing the activity of the hydrogen atom in the 5-position of 2-substituted thiophene ring. To achieve the aimed structure, the reaction pathway using the Stille aryl-aryl, cross-coupling reaction, shown in Scheme 5, was carried out instead -unfortunately without success.

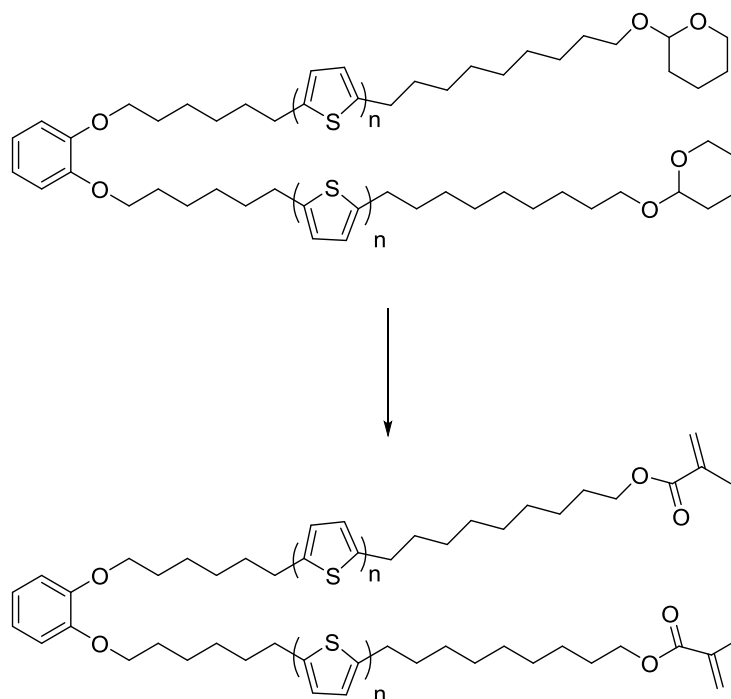


Fig. 4.3 Proposed chemical structure of final product in Scheme 5

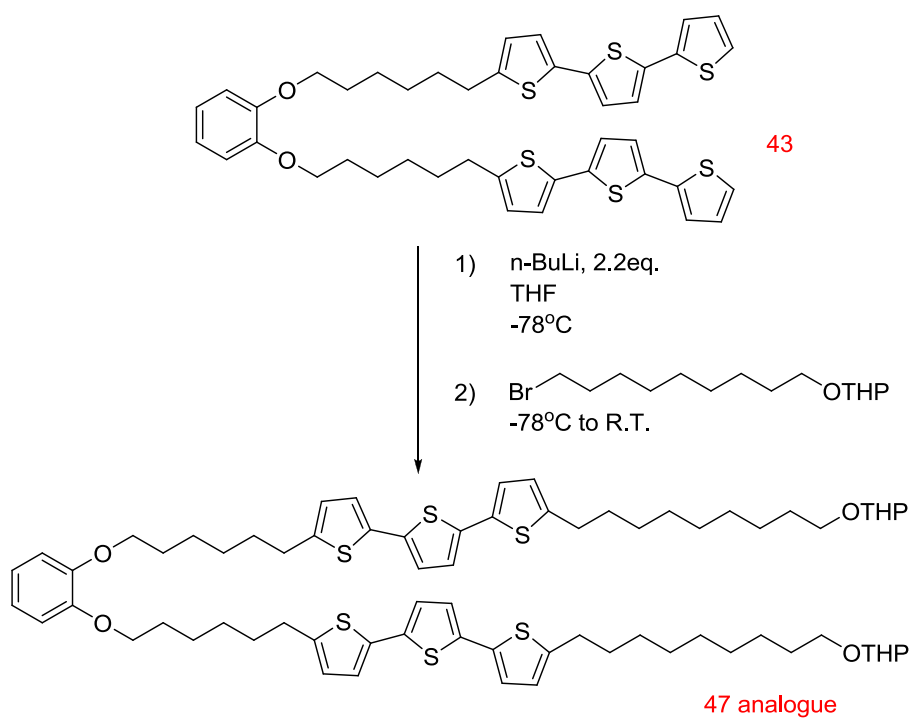


Fig. 4.4 Synthetic pathway by $n\text{-BuLi}$ -mediated reaction

4.2 Reaction conditions for thiazolo[5,4-*d*]thiazole

Different reaction pathways and conditions for the synthesis of a wide range of thiazolo[5,4-*d*]thiazole compounds are shown in Table 4.1. Overall, this series of compounds were very difficult to synthesize and purify mainly due to the low solubility of both the starting materials and the desired products.

From Fig. 4.5, we can see that direct arylation reactions, designed to synthesise compounds **63** and **wb99**, did not work for this kind of compounds. One reason may be that the thiazole core effect on the hydrogen in 5-position may not be active enough (**wb99**), see Fig. 4.5. Another reason may be due to the low solubility of the starting material A (compound **63**).

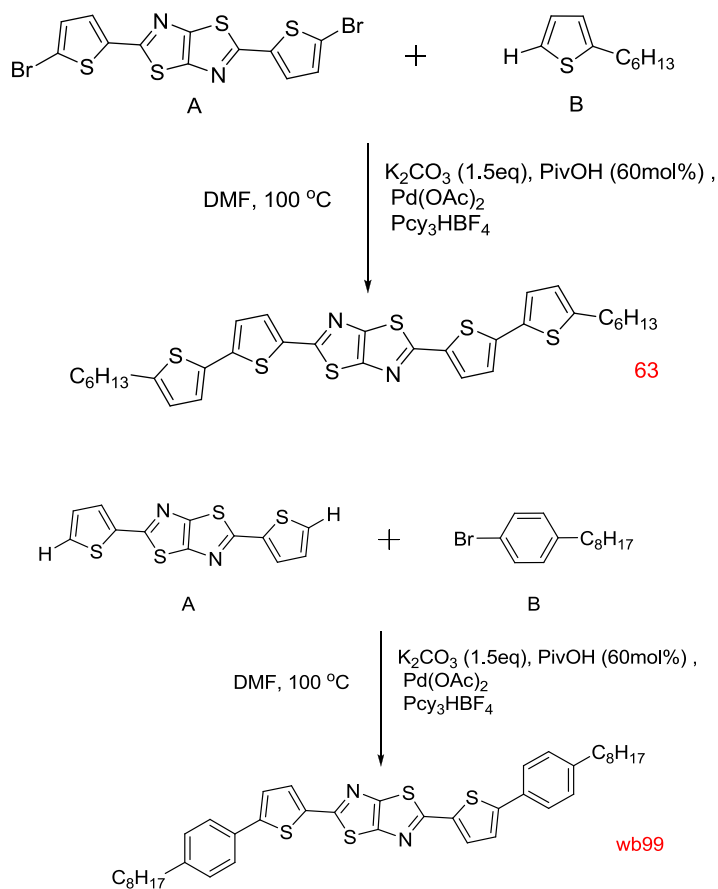


Fig. 4.5 Direct arylation pathway for compound **63** and **wb99**, both with 2.5 equivalent of starting material B

It was found that the Suzuki aryl-aryl, cross-coupling reaction did not work using DMF as the solvent, see compound **63** and **WB96**, while using DME as the solvent at least led to the desired compound if only in low yield, see compound **70**. THF worked better in the synthesis of compounds **63**, **64** and **68** and NMP were best in the synthesis of compounds **69** and **72**. This probably caused by the higher degree of solubility of the reaction intermediates in the latter, rather than the former, solvents. However, NMP was very difficult to remove during the after-reaction work up due to its high boiling point. So THF was chosen as the best compromise solvent for the Suzuki aryl-aryl, cross-coupling reactions of this kind.

Using Na_2CO_3 as base rather than K_2CO_3 resulted into a higher yield (>70% compared to 34-51%, see compounds **63** and **72**). The equivalent of base was varied from 3.0 eq. to 8.0 eq., but this change did not seem make much difference, see compounds **64** and **68**. This finding for these compounds is a little bit unusual, as normally it was found that K_2CO_3 worked better as a base than Na_2CO_3 .

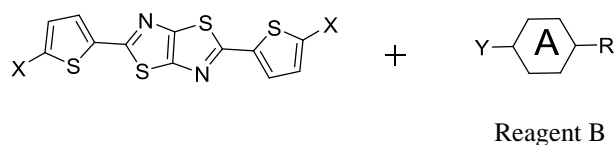
Two different catalysts were used in the Suzuki reactions. Commercial $\text{Pd}(\text{PPh}_3)_4$ was used, but sometimes led to a poor yield, possibly due to part decomposition of this air-sensitive catalyst. $\text{Pd}(\text{OAc})_2$ and PPh_3 as ligand were used to make the $\text{Pd}(0)$ complex *in-situ* during the reaction. Furthermore, $\text{Pd}(\text{PPh}_3)_4$ made in this way and then isolated from the reaction solution appeared to be more stable under laboratory storage conditions.

The number of equivalents of starting material B acted as an influential factor as well, comparing the synthesis of compounds **63** and **64**, since most boronic acids or esters synthesized were used directly without any further purification.

No final products with 4-n-alkoxyphenyl terminal groups attached to the molecular core could be synthesised successfully, see compounds **wb87**, **wb93** and **wb96** (Table 4.2). This lack of success may be attributable to the poor solubility of both reaction intermediate A and expected products, even when NMP was used as solvent, which

led to a significant tendency to form the corresponding mono-substituted products whereby the reaction had only taken place on one end of the bifunctional intermediate A. Several spots on TLC plates attributable to different reaction products were observed. Unfortunately, the desired final product was a minor component of the crude product and it was too difficult to separate the desired disubstitution product from the mono-product using column chromatography on silica gel because of the very close R_f values of both the mono- and di- products and the poor solubility of both products in most common solvents used as eluents, such as chloroform, hexane, DCM, ethyl acetate, acetone, etc. The attempts to synthesize with two-ring boronic acids also failed, again, probably due to the poor solubility of starting material A. As a result, the boronic acids tended to afford self- (homo-) products, e.g., see compounds **wb94**, **wb95**, and **wb97** (Table 4.2).

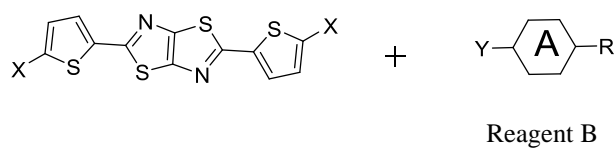
Table 4.1 Reaction method and conditions for thiazolo[5,4-*d*]thiazole compounds



No.	X	Reagent B				Solvent	Base (equiv.)	Catalyst	Yield (%)
			Y	R	Equiv.				
63	Br			C ₆ H ₁₃	3.5	DMF	K ₂ CO ₃ (4 eq)	Pd(PPh ₃) ₄	— ^(a)
63	Br			C ₆ H ₁₃	3.0	THF	K ₂ CO ₃ (4 eq)	Pd(PPh ₃) ₄	34
63	Br			C ₆ H ₁₃	2.5	THF	Na ₂ CO ₃ (3 eq)	Pd(PPh ₃) ₄	47
64	Br			C ₄ H ₉	4.0	THF	Na ₂ CO ₃ (3eq)	Pd(OAc) ₂ PPh ₃	72
68	Br			C ₄ H ₉	4.0	THF	Na ₂ CO ₃ (8 eq)	Pd(OAc) ₂ PPh ₃	78
69	Br			C ₅ H ₁₁	3.5	NMP	Na ₂ CO ₃ (4 eq)	Pd(OAc) ₂ PPh ₃	85
70	Br			C ₉ H ₁₉	3.5	DME	Na ₂ CO ₃ (3.5 eq)	Pd(OAc) ₂ PPh ₃	43
72	Br			OC ₈ H ₁₇	3.0	THF	K ₂ CO ₃ (3 eq)	Pd(OAc) ₂ PPh ₃	51
72	Br			OC ₈ H ₁₇	3.0	NMP	Na ₂ CO ₃ (3.5 eq)	Pd(OAc) ₂	75

All the reactions were carried out under N₂ protecting conditions, heated to 90 °C stirred overnight. (a)The reactions did not work, leaving starting materials left in the reaction mixture after overnight time.

Table 4.2 Reaction method and conditions for the failed reactions to produce the thiazolo[5,4-*d*]thiazoles **wb87** and **wb93-wb97**.



No.	X	Reagent B				Solvent	Base (equiv.)	Catalyst	Yield (%)
			Y	R	Equiv.				
wb87	Br			OC ₁₂ H ₂₅	3.0	THF	Na ₂ CO ₃ (8 eq)	Pd(OAc) ₂ PPh ₃	— ^(b)
wb93	Br			OC ₄ H ₉	3.5	THF	K ₂ CO ₃ (8 eq)	Pd(PPh ₃) ₄	— ^(b)
wb93	Br			OC ₄ H ₉	3.5	NMP	Na ₂ CO ₃ (3.5 eq)	Pd(OAc) ₂ PPh ₃	— ^(b)
wb94	Br			OC ₁₀ H ₂₁	3.0	THF	K ₂ CO ₃ (3 eq)	Pd(OAc) ₂ PPh ₃	— ^(c)
wb95	Br			C ₅ H ₁₁	2.2	THF	Na ₂ CO ₃ (8 eq)	Pd(OAc) ₂ PPh ₃	— ^(c)
wb96	Br			OC ₆ H ₁₃	3.0	DMF	Na ₂ CO ₃ (4 eq)	Pd(OAc) ₂ P Ph ₃	— ^(a)
wb96	Br			OC ₆ H ₁₃	4.0	THF	Na ₂ CO ₃ (8 eq)	Pd(OAc) ₂ PPh ₃	— ^(b)
wb97	Br			C ₃ H ₇	4.0	NMP	Na ₂ CO ₃ (8 eq)	Pd(OAc) ₂ P Ph ₃	— ^(c)

All the reactions were carried out under N₂ protecting conditions, heated to 90 °C stirred overnight. (a) The reactions did not work, leaving starting materials left in the reaction mixture after overnight time. (b) One-side reacted products were afforded as main product. (c) Self-coupling product of boronic acid was afforded as main products.

4.3 Mesomorphic behaviour and physical properties

4.3.1 2,7-Disubstituted-9-Alkylcarbazoles (Scheme 1)

N-Alkyl-substituted carbazoles with an aliphatic chain attached to the bridging nitrogen atom of the carbazole moiety were reported to exhibit a nematic phase, blue photoluminescence in solution and as thin solid films a relatively-low melting point (Cr-N) as well as significantly broader nematic temperature range for the analogues with branching aliphatic chain^[1]. The transition temperatures of compound **5** are compared with those of other materials made previously by other members of our research group, see Table 4.3.^[1] A nematic phase was observed for compound **5** whereas no smectic phases were identified, despite substantial cooling below the melting point, see Figure 4.6. Compound **5** has much higher transition temperatures (Cr-N = 229 °C; N-I = 310 °C) than those of compounds **SPK1** and **SPK2** (Cr-N = 115 °C; N-I = 168 °C and Cr-N = 163 °C; N-I = 228 °C, respectively^[1]). This fact can be explained by the presence of chain branching and the non-linear and non-coaxial 2,5-disubstituted thiophene ring, both of which can lead to low melting point and clearing point due to the steric effects, in compounds **SPK1** and **SPK2**.

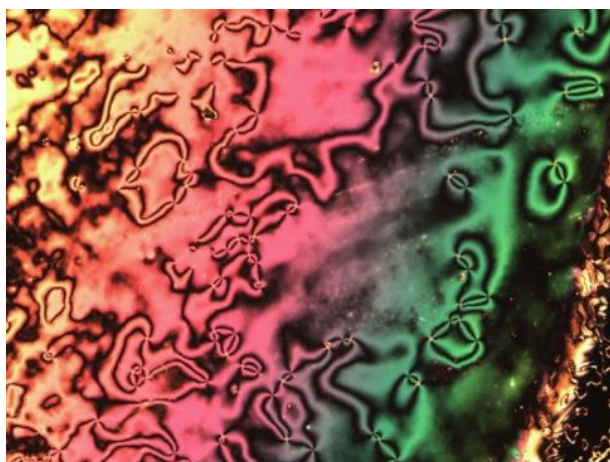
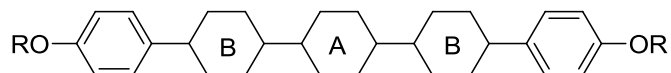
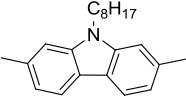

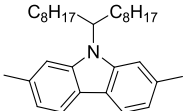

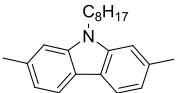
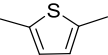


Fig. 4.6 Schlieren texture of nematic phase of compound **5** with two-point and four-point brushes at 300 °C.

Table 4.3. Chemical structures and Liquid crystal transition temperatures (°C) and some enthalpies of transition (J g⁻¹) for the compound **5** and two reference compounds **SPK1** and **SPK2** (RO- = C₈H₁₇O- and -OR = -OC₈H₁₇).



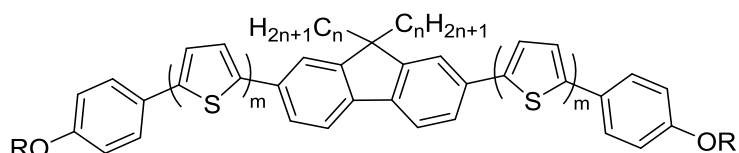
	Ring A	Ring B	T _g	Cr		N		I
5			-	•	229 (53.46)	•	310 (1.23)	•
SPK1 ^a			-	•	115 (38.18)	•	168 (1.23)	•
SPK2 ^a			-	•	163 (34.32)	•	228 (0.99)	•

Notes for table:

a. Synthesized by SP Kitney of the University of Hull^[1]

4.3.2 2,7-Disubstituted-9,9-Dialkylfluorenes(Schemes 2, 2.1 and 3)

Table 4.4 Chemical structures and liquid crystal transition temperatures (°C) of the 2,7-disubstituted-9,9-dialkylfluorenes **14**, **16**, **28-30** and the reference compound **MD115**.



Compound	n	m	OR	T _g	Cr	N	I
28^b	3	1	OCH ₃	78	•	231	•
29	3	1	OC ₈ H ₁₇	-	•	162	(• 166) •
30	3	1	OC ₁₂ H ₂₅	-	•	148	- •
MD115^a	8	1	OC ₈ H ₁₇	-3	•	56	• 91 •
14	8	2	OCH ₃	-	•	69	• 155 •
16	8	2	O(CH ₂) ₁₀ CO ₂ CH(CH=CH ₂) ₂	-	•	52	• 143 •

Notes for table 4.4: a. **MD115** T_g=-3, Cr-N = 56, N-I = 91.^[2]; b. Lit. T_g 78 Cr 235 N 265 I.^[3]

In scheme 2, compound **14** was synthesized as precursor of reactive mesogen **16** in scheme 2.1. Compound **28-30** in scheme 3 were made as intermediates towards the designed final product shown in scheme 3.1. Unfortunately, the last synthetic steps failed and compounds **28-30** were studied for their liquid crystalline behaviour. Table 4.4 shows the liquid crystalline phase exhibited by these compounds and their transition temperatures as well as those reported for the reference compound **MD115**.^[3]

All the 2,7-disubstituted-9,9-diakylfluorenes **14**, **16**, **28-30** and the reference compound **MD115** shown in Table 4.4 possess a nematic phase and no smectic phases were observed. Compounds **MD115**, with dioctyl chains ($n = 8$) in the 9-position of the 2,7-disubstituted-9,9-diakylfluorene moiety in the centre of the molecular core and incorporating two 2,5-disubstituted-thiophene rings ($m = 1$) exhibits lower transition temperatures than those of the analogues **28-30** with dipropyl chains ($n = 3$) in the same positions. This fact is probably due to the steric effect caused by the longer chains, which can increase the intermolecular distances and consequently weaken the intermolecular Van der Waals forces of attraction between adjacent molecules.

The melting point (Cr-N = 231 °C, Cr-SmC = 162 °C and Cr-I = 148 °C, respectively) and clearing point (N-I = 268 °C and N-I = 166 °C, respectively) of compounds **28-30** decreases with increasing length of the flexible aliphatic chain (RO- = CH₃O-, C₈H₁₇O- and C₁₂H₂₅O-, respectively), as could be expected based on previous results. A liquid crystalline phase for compound **30** could not be observed in spite of a significant degree of cooling below the melting point. The presence of flexible aliphatic chains usually can dilute the effects of the highly conjugated aromatic cores, and in a result to lower the melting point and other liquid crystalline transition temperatures of compounds which possessing long terminal chains. A liquid crystalline phase of compound **29** could not be observed directly using OPM, when the sample was heated to the isotropic liquid state. However, on cooling down from the isotropic state, a nematic texture was observed almost near the melting point (I-N = 166 °C), see Fig. 4.6. This enantiotropic mesomorphic behavior was confirmed using DSC analysis, see Fig. 4.7. It was

somewhat surprising that no liquid crystalline phase could be observed for compound **30**. This fact is, perhaps, attributable to very significant steric effects attributable to the C12 flexible aliphatic chains attached at the both ends.

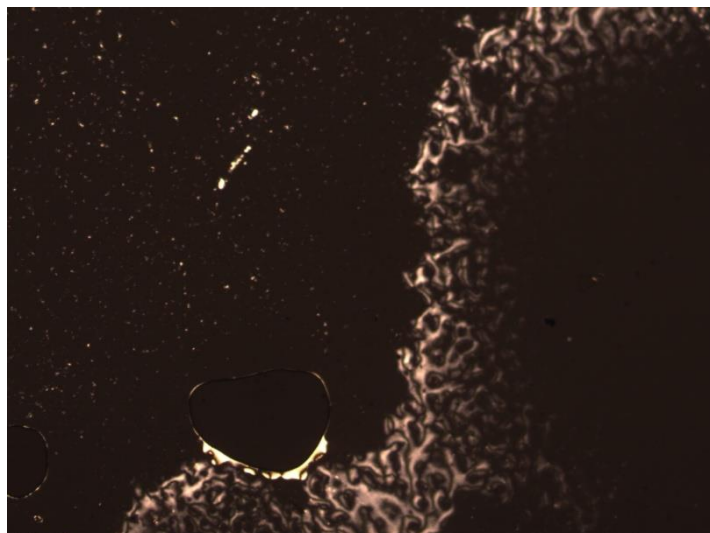


Fig. 4.6 The Schlieren texture of the nematic phase of compound **29** on cooling at 169 °C.

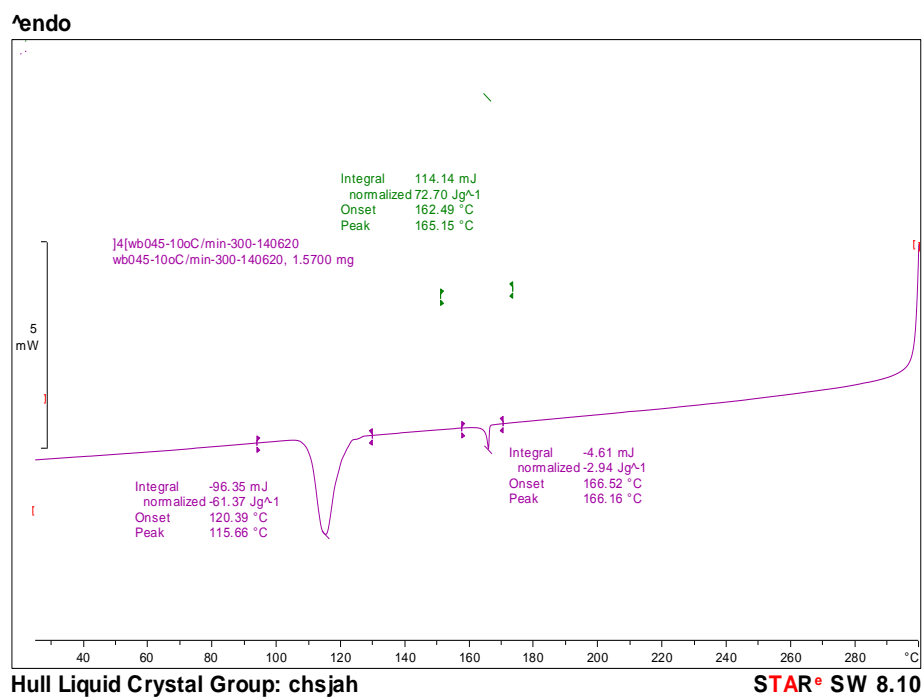


Fig. 4.7 DSC thermogram as a function of temperature for compound **29** (scan rate 10 °C/min).

Many oligomers and polymers containing the 2,7-disubstituted-9,9-dialkyl-fluorene

moiety in their highly conjugated aromatic molecular core have been reported to show good properties as hole-transporting materials^[4, 5]. Compound **14**, with a methoxy-group in a terminal position (RO = CH₃O-), and compound **16**, with a branched, photopolymerisable group in a terminal position (RO = -O(CH₂)₁₀CO₂CH(CH=CH₂)₂), both possess nematic phase with a low melting point (Cr-N = 69 °C and 52 °C, respectively) and a relatively high clearing point (N-I = 155 °C and 143°C, respectively). This relatively broad nematic range is probably due to the presence of four interconnected 2,5-disubstituted thiophene rings (m = 2) in the molecular core and two long aliphatic chains (n = 8) in the 9-position on the central 2,7-disubstituted-fluorene moiety.^[1,6] The non-linear and non co-axial substitution pattern of the 2,5-disubstituted thiophene ring generally results in a low liquid crystal transition temperatures due to the low length-to-breadth ratio of molecules incorporating one or more thiophene rings^[5]. This is caused by the large angle between the thiophene rings and the bonds to the substituted in the 2- and 5- positions. However, this is compensated for to some extent by having two 2,5-disubstituted thiophene attached to each other.

The presence of four thiophene rings should also lead to a low ionisation potential for compound **16**, which should render it of potential use as a photopolymerised hole-transport layer in OLEDs or an electron-donor in OPVs. Preliminary measurements on this class of reactive mesogen indicate that these materials exhibits low ionisation potential (see Table 4.5) and high hole-charge carrier mobility^[7].

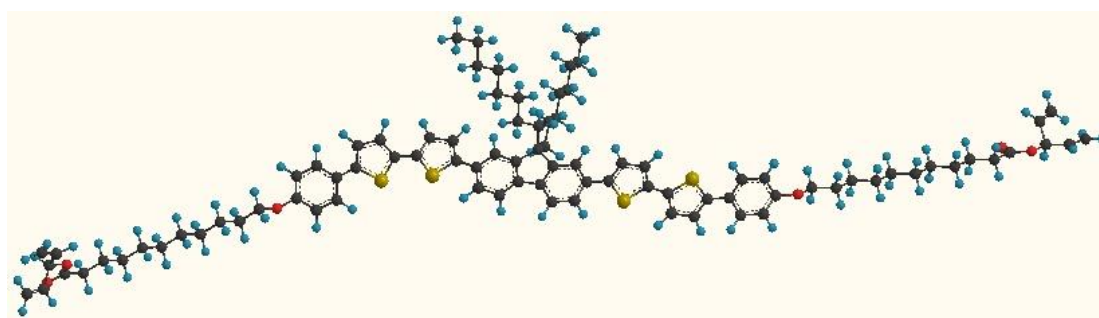
Table 4.5 Ionization Potential and Electron Affinity of compounds **14**, **16**, **28-30** and **MD115**.

Compound	IP ^b (eV)	E _g ^c (eV)	EA ^d (eV)
14	5.20	2.46	2.74

Compound	IP ^b (eV)	E _g ^c (eV)	EA ^d (eV)
16 ^a	4.97	2.45	2.52
MD115 ^[2]	5.30	2.46	2.84
28-30	5.31	2.45	2.86

Note for Table 4.5: a) Lit. IP=4.93eV, E_g=2.45eV, EA=2.48eV^[7];

The results of the molecular modelling using MM2 geometry optimisation for the compounds **16**, **MD115** and **29**, shown in Fig. 4.8, demonstrate that the molecular core of all these compounds is essentially planar with a large length-to-breadth ratio, which should promote the formation of a nematic phase. The modelling also shows how the flexible aliphatic chains in a lateral position lie out of the molecular plane. This should increase the intermolecular distance and thereby reduce the forces of intermolecular attraction and consequently lead to lower the transition temperatures, especially to low melting points as is found to be the case, see Table 4.4.



Compound **16**



MD 115



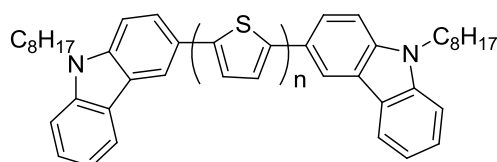
Compound 29

Fig. 4.8 MM2 optimised geometry of compound 16, MD 115 compound 29.

4.3.3 3-Substituted Carbazoles (Schemes 6-8 and 12)

Four compounds **53**, **54**, **58** and **74** with two 3-substituted carbazole moieties on both ends of the molecule were synthesized as hole-transporting materials with appropriate energy levels. Table 4.6 shows the transition temperatures of compound **54**, **58** and the literature values for the analogous thiophene carbazole oligomers **MU5**, **MU12** and **MU36** with increasing number of 2,5-disubstituted thiophene rings ($n = 1-5$).

Table 4.6. Transition temperatures ($^{\circ}\text{C}$) of carbazole compounds/thiophene oligomers.



	n	T _g	Cr		N	I
54	1	62	•	-	-	•
MU5^a	2	64	•	168	-	•
MU12^a	3	-	•	166	-	•
58	4	-	•	162	-	•
MU36^a	5	119	•	170	•	215 •

Note for table: ^a synthesised by Muralidhar Reddy Billaof the University of Hull.

Unfortunately, only compound **MU36** ($n = 5$) exhibits a nematic phase at a high

temperature (Cr-N=170 °C) and a high clearing point (N-I=215 °C). All of the other compounds shown in Table 4.5 were found to exhibit no observable liquid crystalline phases despite of significant supercooling below the melting point. The melting point (Cr-I) and the glass transition temperatures (T_g) of the materials are listed in Table 4.6. Compound **54** ($n = 1$) is a glass at and above room temperature and no melting point could be observed. The number of thiophene units (n) does not seem to influence the melting point greatly for the other compounds ($n > 2$), which is unusual. The nematic phase observed for **MU36** may be due to the influence of a more linear structure with more conjugated aromatic cores, contributing to a larger length-to-breadth ratio. Fig. 4.9 shows molecular modeling using MM2 geometry optimization of compound **54**, **58** and **MU36**, from which we can clearly see the differences of the structures caused by the increasing number of 2,5-disubstituted-thiophene rings present in these compounds. Compound **MU36** obviously shows a highest length-to-breadth ratio among these compounds, compared to that of other 3-substituted carbazoles shown in Table 4.6, which is most probably the reason for liquid crystalline phase observed.

The transition temperatures of compounds **53** and **74** with different aromatic cores compared with that of compounds **MU5** and **58** are collated in Table 4.7. All of these compounds have two 2,5-disubstituted thiophene rings in the aromatic molecular core with 3-substituted carbazoles attached as end-groups. Compound **53** possesses a dibenzo[*b,d*]thiophene fused aromatic moiety, while compound **74** incorporates a thiazolo[5,4-*d*]thiazole, in the centre of the molecular core.

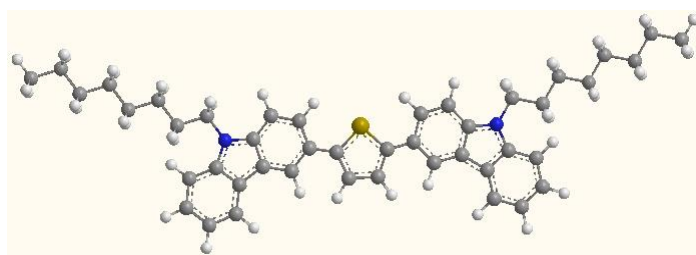
Table 4.7. Transition temperatures(°C) of compound **53**, **MU5**, **58** and **74**.

Compound	A	T _g (°C)	Cr-I (°C)
53		39	189
MU5	-	64	168
58		-	162
74		-	173

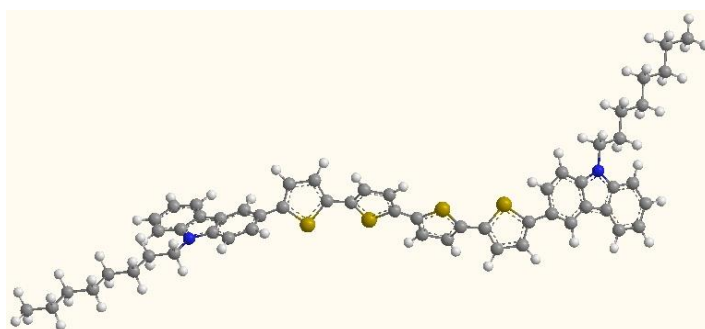
Compounds **53**, **MU5**, **58** and **74** are all crystalline solids (Cr-I = 189 °C, 168 °C 162 °C and 173 °C, respectively) with no observable liquid crystal mesophases. Compound **MU5** exhibits higher melting point (Cr-I = 168 °C) than that of compound **58** (Cr-I = 162 °C) due to the fewer number of 2,5-disubstituted thiophenes at the core, as can be expected. Glass transitions were seen above room temperature on cooling for compounds **53** and **MU5** (T_g =39 °C and 64 °C, respectively), while no glass transition was observed for compound **74** despite a significant amount of supercooling below the

melting point.

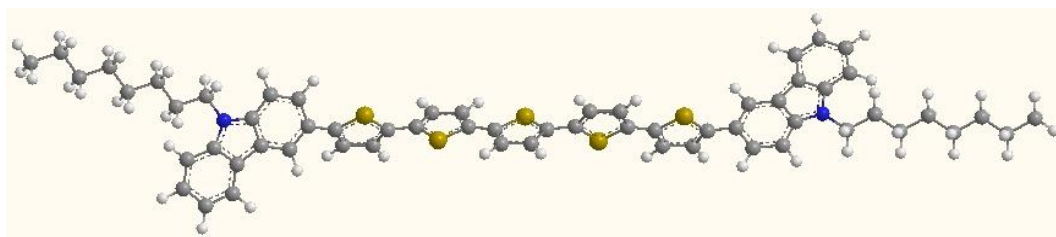
Compounds **53**, **54**, **58**, **MU16** and **74** are expected to have highly conjugated planar molecular cores, see the structures obtained using molecular modeling using MM2 geometry optimization (Fig. 4.9), that should give rise to a high degree of intermolecular π - π -stacking, which should lead to a short intermolecular distances and subsequently strong Van der Waals interactions between adjacent molecules. This self-assembly may well be responsible for the relatively high melting points of these compounds as listed in Table 4.7. The structures shown by MM2 geometry optimization show clearly that compounds **53** and **74** both possess a planar structure of thiophene based cores. However, the angles existing between thiophene and carbazole units creates a nonlinear structure, which subsequently leads to a low length-to-breadth ratio of the molecules, which in turn might well explain why these compounds exhibit high melting points as well as the absence of observable liquid crystalline mesophases.



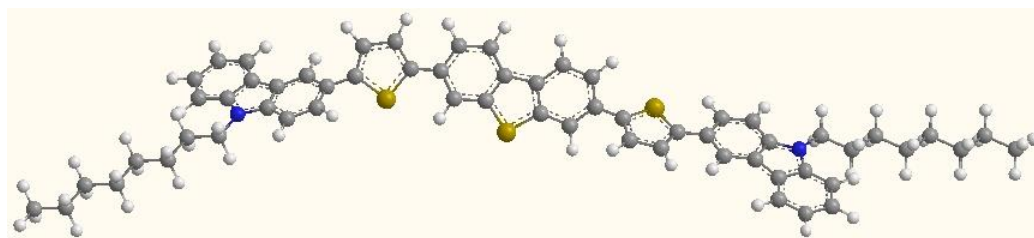
Compound 54



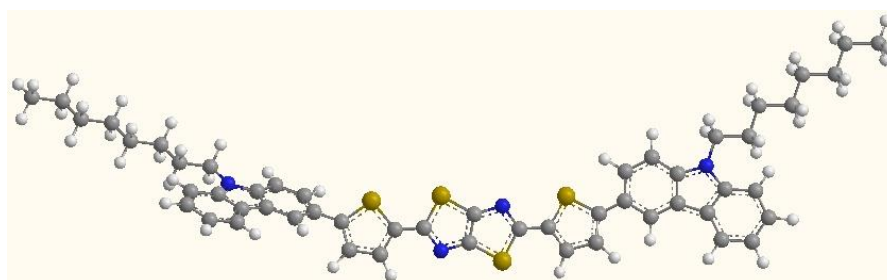
Compound 58



Compound MU36



Compound 53



Compound 74

Fig. 4.9 MM2optimised geometry of compound 54, 58, MU36, 53 and 74.

Table 4.8 Band gap and energy levels of compound **53**, **MU5**, **MU12**, **58** and **74**.

Compound	IP ^b (eV)	E _g ^c (eV)	EA ^d (eV)
53	5.70	2.47	3.23
MU5^a	5.30	2.16	3.14
MU12^a	5.28	2.51	2.77
58	5.27	2.22	3.05
74	5.52	2.39	2.13

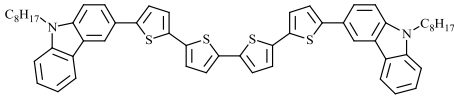
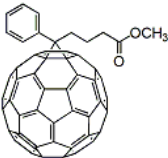
Notes for table: ^a Data from Muralidhar Reddy Billaof the University of Hull; ^b From CV; ^c From optical absorption spectrum (solution); ^d From IP-E_g

The presence of the carbazole and thiophene rings should lead to a low values for the ionization potential (IP), band gap (E_g) and electron affinity (EA). The values of IP, Eg and EA for compounds **53**, **58**, **MU5**, **MU16** and **74** are collated in Table 4.8. The HOMO level, presented as IP, which was measured by Cyclic Voltammetry (CV), of the compounds was found to be primarily determined by the nature of the molecular cores. The thiophene oligomers exhibit a lower HOMO level, which indicate that they may well potentially used as hole-transporting materials for OLEDs or electron-donors for OPVs. The IP was not influenced significantly by the increasing number of thiophenes for the thiophene oligomers. However, compounds **53** and **74** possessing higher HOMO energy levels and larger energy gap are not as promising as compound **58** for use as

hole-transporting layers in OLEDs and/or electron-donors in OPVs, although they were synthesized for this purpose. Furthermore, colouration and absorption in the visible part of the spectrum could also be a potential disadvantage for these materials in OLEDs.

Although compound **58** does not exhibit any observable mesophase, it was still considered as a potentially suitable electron-donating material in solar cell applications. Therefore a test OPV device was fabricated using compound **58** as an electron-donor with PCBM as an electron acceptor by members of the Organophotonics Research Group in the Department of Physics at the University of Hull, see Table 4.9.

Table 4.9. Chemical structures and energy levels (eV) of the electron donor **58** (**POL 459**) and the electron acceptor **PCBM**.

Name	Structure	Energy levels (eV) CV Data
Compound 58 (Donor)		HOMO = 5.27 LUMO = 3.05
PCBM (Acceptor)		HOMO = 5.97 LUMO = 4.14,

The energy level diagram of the OPV using compound **58** as an electron donor and with PCBM as the electron acceptor is shown in Fig. 4.10.

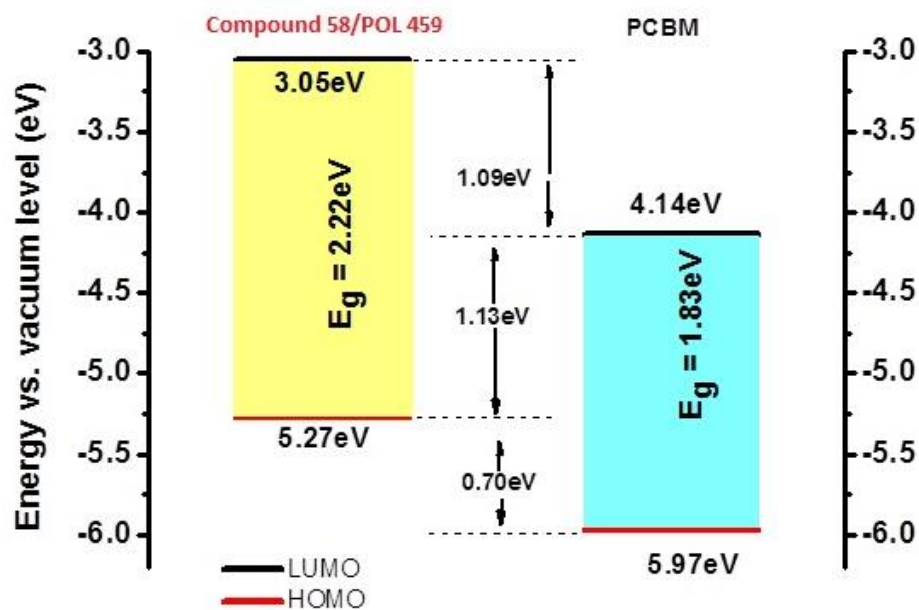


Fig. 4.10 Energy level diagram of compounds 58.

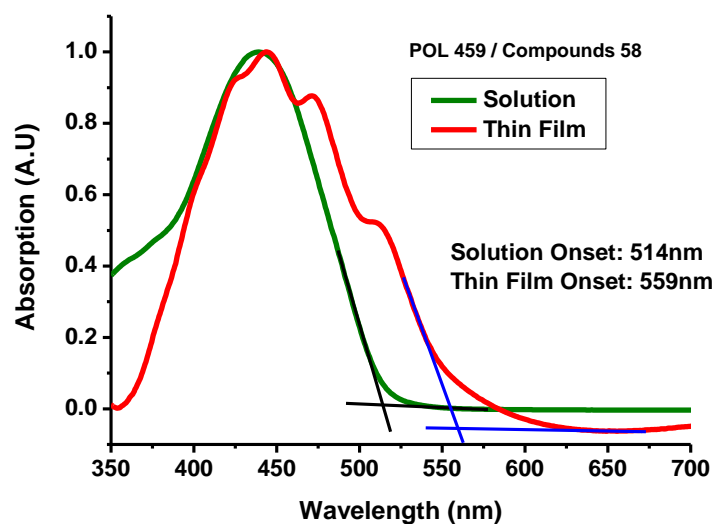


Fig. 4.11 UV-vis data of compound 58 (solution and thin film)

Fig. 4.11 shows the difference of UV-vis absorption spectra for compound **58** as solution and thin film. The onset value switched from 514nm (solution) to 559nm (thin film), which indicates that the E_g value also changed from solution to thin film. As all materials are required to be used as thin film when manufacturing organic

semiconductor devices, the data of thin film is more approaching to the real value in application. However, we accept the solution data for rough tests and calculations of energy levels when doing the experiments, because they don't switch a lot from each other. All the E_g data obtained from UV-vis absorption spectrum in this section are from solutions, unless it is stated.

From Fig. 4.12 and 4.13, we can see that the current produced from device using compound 58 is quite low, and the EQE is not very high as well (about 15%). Fig. 4.14 shows the current density – voltage changing of this device, and the short-circuit current density ($J_{sc} = 1.95 \text{ mAcm}^{-2}$) and open-circuit voltage ($V_{oc} = 0.3 \text{ V}$) are obtained. All the data are collated in Table. 4. 10, a power conversion efficiency of 0.56% was calculated, which was not high.

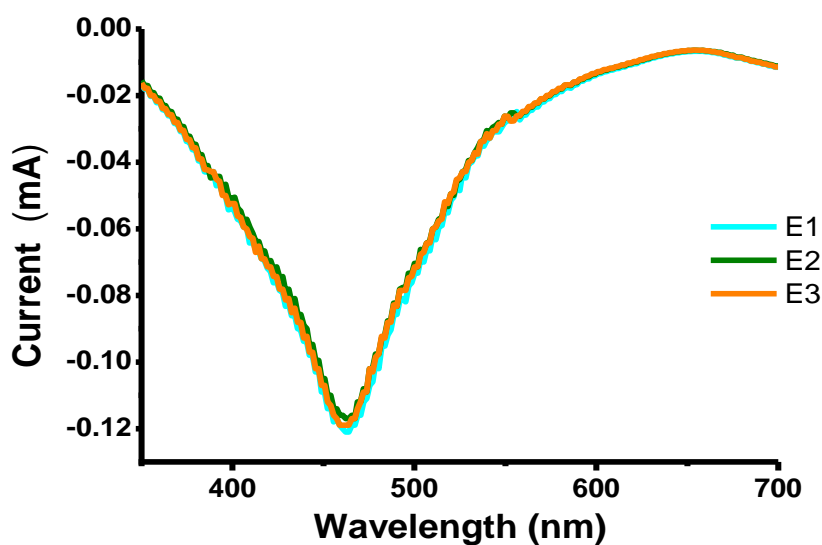


Fig. 4.12 Graph showing current produced by device using compound 58 (POL 459)

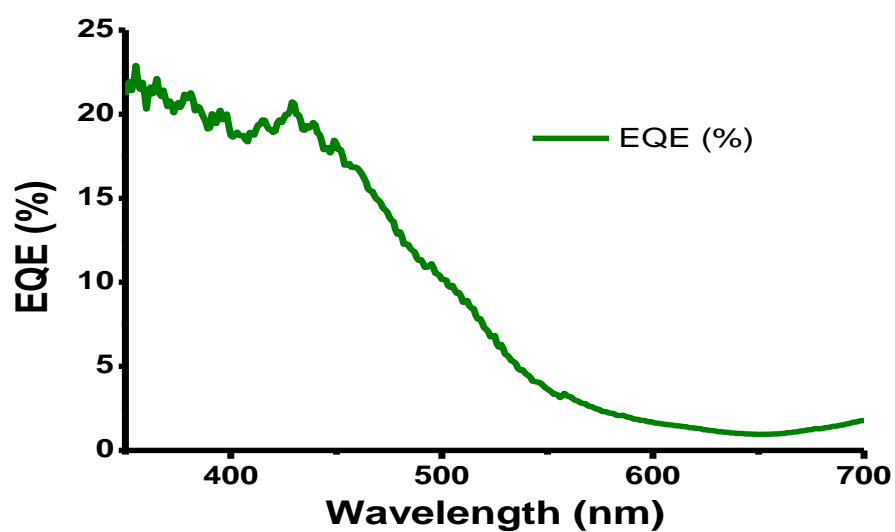


Fig. 4.13 A graph showing external quantum efficiency of the device using compound 58 (POL 459)

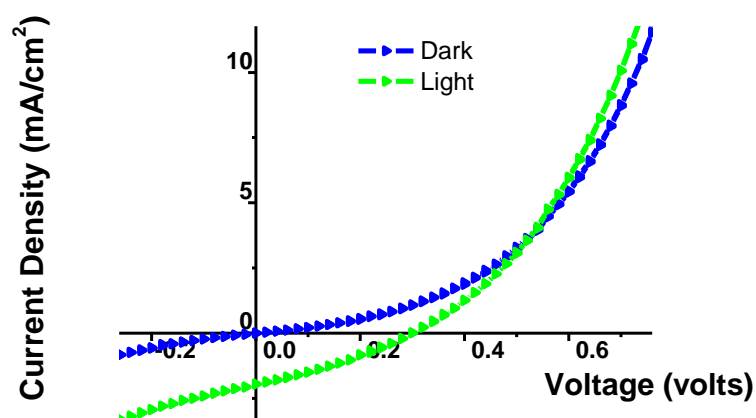


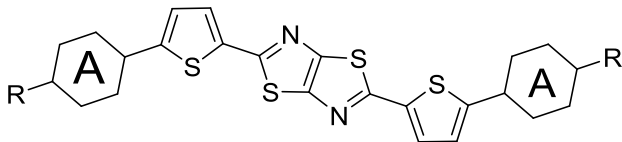
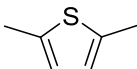
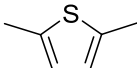
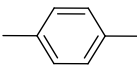
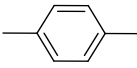
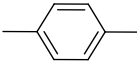
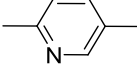
Fig. 4.14 Graph showing current density – voltage of device using compound 58 (POL 459)

Table. 4.10 Data of OPV device using compound 58 (POL459)

POL459:PCBM 2.5% 1:1 wt Blend	JSC (mAcm ⁻²)	V _{oc} (V)	FF (%)	η (%)	EQE (%)
470nm	1.95	0.3	32	0.56	15
AM1.5G	1.59	0.26	32	0.13	

4.3.4 Thiazolo[5,4-*d*]thiazoles (Schemes 9-11)

Table 4.11 Chemical structures and liquid crystalline transition temperatures (°C) of thiazolo-thiazoles **63**, **64**, **68-70** and **72**.

										
	A	R	T _g	Cr	SmC		N		I	
63		C ₆ H ₁₃	-	•	191	-	•	269	•	
64		C ₄ H ₉	-	•	207	-	•	>350	•	
68		C ₄ H ₉	-	•	264	-	•	>350	•	
69		C ₅ H ₁₁ ,	158	•	246	•	249	•	>350	•
70		C ₉ H ₁₉	201	•	227	•	286	•	303	•
72		OC ₈ H ₁₇	170	•	212	•	316	-		•

Investigation of thiophene oligomers and polymers used as organic semiconductors

have revealed that derivatives incorporating thiazole units are very useful components in the development of bulk heterojunction solar cells (OPVs)⁸ and organic field-effect transistors (OFETs)⁹. They are reported to exhibit high charge carrier mobilities¹⁰ and, are promising fluorescent compounds as *p*-type organic semiconductors, which can be used as electron-donors in OPVs and/or hole-transporting layers in OLEDs. The transition temperatures and liquid crystalline phases of bithiophene thiazolo-thiazoles based compounds are summarised in Table 4.11.

The thiazolo-thiazoles **63**, **64**, **68-70** and **72** exhibit liquid crystalline mesophases with very high transition temperatures see Table 4.11. The compounds **63** and **64** incorporating a 2,5-disubstituted-thiophene ring only exhibit a nematic phase between a high melting point (191 °C and 207 °C, respectively) and a very high clearing point (269 °C and >350 °C, respectively). Compounds **63** and **64** exhibit the lowest melting points of the compounds listed in Table 4.11, which is probably attributable to the presence of the non-linear and non-co-axial 2,5-disubstituted-thiophene ring. The lower length-to-breadth (aspect) ratio of the compounds **63** and **64** than that of compounds **68-70** and **72**, incorporating either the 1,4-disubstituted-phenyl ring or the 2,5-disubstituted-pyridine ring with a linear and co-axial substitution pattern between adjacent rings, can lead to lower melting point and clearing point due to steric effects.

The compounds **68-70** incorporating a 1,4-disubstituted-phenyl ring ($A = -C_4H_4-$), in place of the 2,5-disubstituted thiophene ring ($A = -C_4H_2S-$), but differing from each other only in the number of methylene units ($-CH_2-$) in the flexible aliphatic end-groups (R) exhibit either just a nematic phase, i.e., **68** ($R = C_4H_9-$), or both a smectic phase and a nematic phase, i.e., **69** and **70** ($R = C_5H_{11}-$ and $C_9H_{19}-$, respectively). The melting point (Cr-N = 264 °C, Cr-SmC = 246 °C and Cr-SmC = 227 °C, respectively) and clearing point (N-I = >350°C, SmC-I = >350 °C and SmC-I = 303°C, respectively) decreases with increasing length of the flexible aliphatic chain ($R = C_4H_9-$, $C_5H_{11}-$ and $C_9H_{19}-$, respectively) of the compounds **68-70**, as could be expected based on previous results. The increasing chain length also results in the formation of a smectic C phase for the

compounds **69** and **70** with the longest chain lengths ($R = C_5H_{11}-$ and $C_9H_{19}-$, respectively) over a broad temperature range (Cr-SmC = 246 °C; SmC-I = >350 °C and Cr-SmC = 227 °C; SmC-I = 303 °C, respectively). The high viscosity of the compounds **69** and **70** leads to the formation of a glassy phase with a high glass transition temperature ($T_g = 158$ °C and 201 °C, respectively).

The combination of the presence of a 2,5-disubstituted-pyridine ring ($A = C_5H_3N-$) and a straight-chain alkoxy-group in a terminal position ($R = C_8H_9O-$) in compound **72** leads to the absence of a nematic phase for this compound. This observation may be due to a combination of the effect of the introduction of electron-deficient nitrogen atom and the presence of conjugated oxygen atom of the terminal alkoxy-chain, which may increase the intermolecular interactions. This observation is consistent with the fact that the substitution of a 2,5-disubstituted-pyridine ring for a 1,4-disubstituted-phenyl ring often induces the formation of tilted, smectic phases.^[11] The melting point (Cr-SmC = 246 °C) and clearing point (SmC-I = 303 °C) of compound **72** are comparable with those of the other thiazolo-thiazoles **63**, **64**, and **68-70** shown in Table 4.11. The high viscosity of the compound **72** leads to the formation of a glassy phase with a high glass transition temperature ($T_g = 170$ °C).

The liquid crystalline phases of the **63**, **64**, **68-70** and **72** shown in Table 4.9 were confirmed by the combination of optical polarising microscopy and DSC. As the operation temperature of OPM and DSC were limited to 300 °C and 350 °C relatively, the high clearing points of some of the compounds could not be measured, e.g., those of compounds **64**, **68** and **69**. During initial investigation of compound **69** by DSC, see Fig. 4.15, it was believed that no mesophases are exhibited during the heating cycle. And a nematic phase would be observed when cooling down close to the melting point from isotropic liquid, as the small peak observed is thought to be a nematic transition peak. However, when carrying out further inspection using optical microscopy, it was found that the compound did not clear from nematic phase until over 300 °C and that the small peak shown in DSC trace is actually attributable to the presence of a smectic

C phase, i.e., to a nematic-smectic C transition, which is only observable on cooling down close to the crystalline transition, see Fig. 4.16.

The high transition temperatures of thiazolo-thiazole materials **63**, **64**, **68-70** and **72** might be considered to imply that they are thermally stable. However, the high melting points also indicate that they may not be suitable for use in organic semiconductor devices as high operation temperatures are required for liquid crystalline phases.

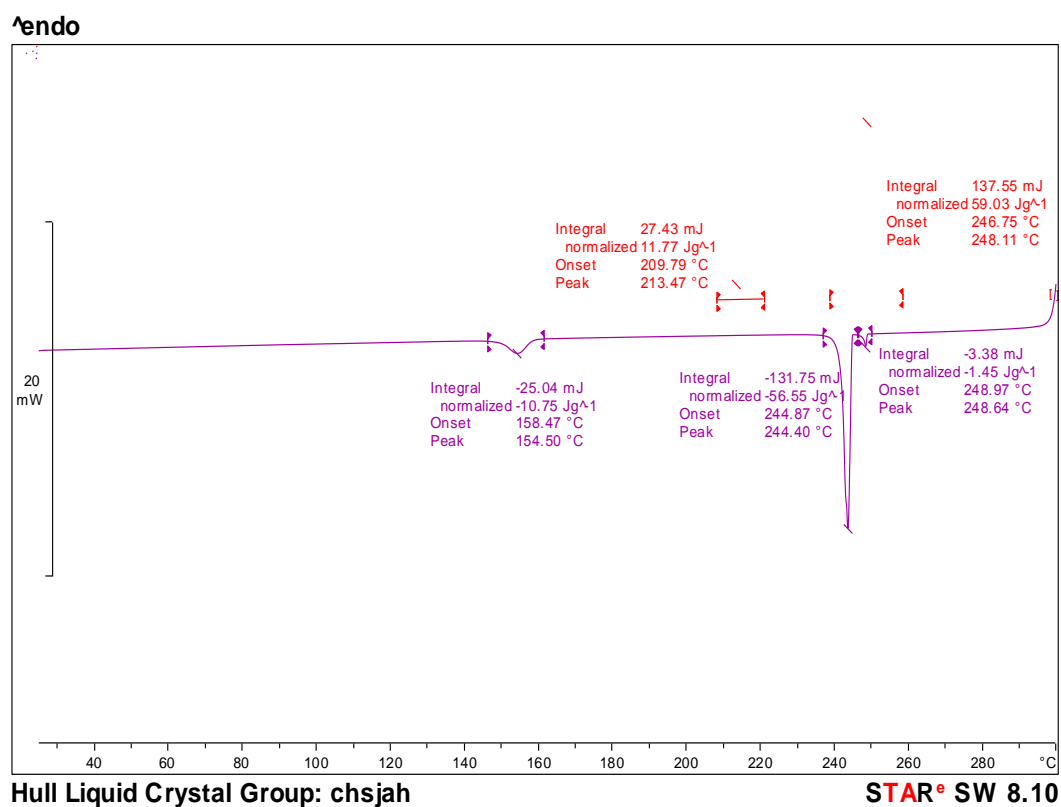


Fig. 4.15 DSC thermogram for compound 69 (scan rate 10 °C/min)

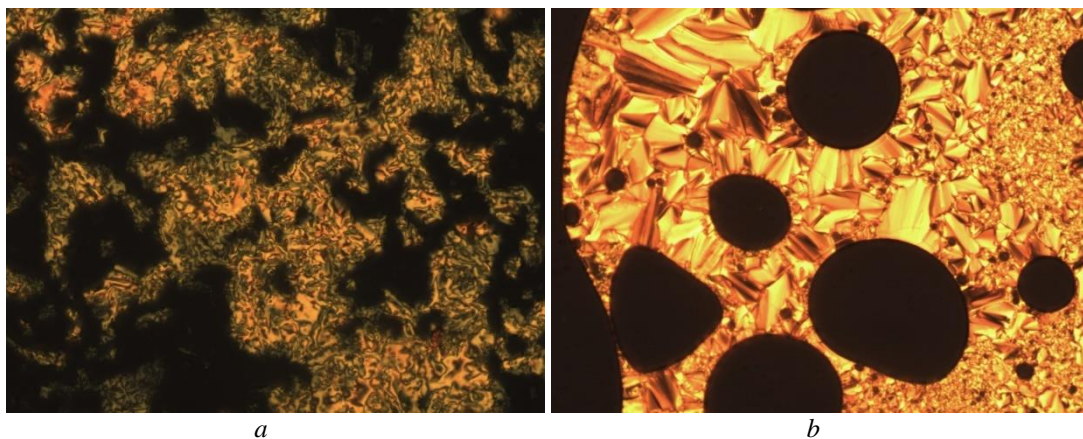
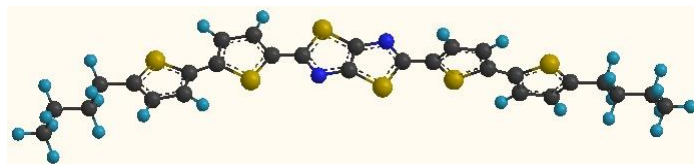
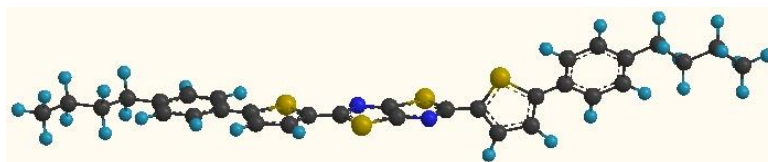


Fig. 4.16 a) Schlieren texture of nematic phase of compound **69** when heating at 274 °C b) Focal conic fan texture of smectic C phase of compound **69** when cooling at 249°C.

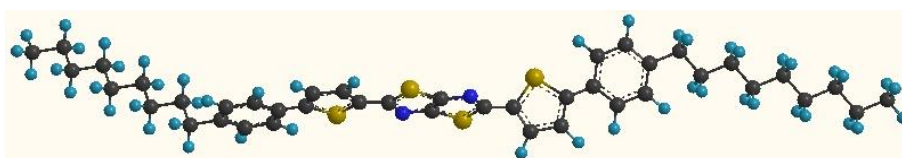
Molecular modeling using MM2 geometry optimisation of compound **64**, **68**, **70** and **72** was carried out in order to give some information as to the likely shape of these compounds, see Fig. 4.17, which shows the effect on the molecular shape of compound **64**, **68**, **70** and **72** caused by different rings as well as a different end-group ($R = C_4H_9-$, $C_9H_{19}-$ and $C_8H_{19}O-$). All these compounds have an inter-annular twist angle between 2,5-disubstituted-thiophene and neighbouring five-membered or six-membered aromatic rings. Compound **64** appears to have a planar, if non-linear molecular structure. However, a non-planar molecular shape of **68**, **70** and **72** is observed for the compounds incorporating 1,4-disubstituted-phenyl- or 2,5-disubstituted-pyridinyl-rings. This shape may be responsible for the formation of the less-ordered nematic phase rather than smectic phases. The long alkyl-chain of compound **70** ($R = C_9H_{19}-$) contributes to a larger length-to-breadth ratio, as could reasonably be expected based on previous results.



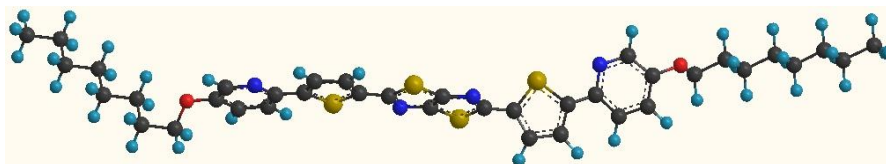
Compound 64



Compound 68



Compound 70



Compound 72

Fig. 4.17 MM2optimised geometry of compound 64,68, 70 and 72.

The HOMO energy levels and band gap of this class of compounds were measured using CV and UV-vis spectrum LUMO energy levels were then calculated, see Table 4.12. The presence of four 2,5-disubstituted-thiophene rings is likely to reduce the band gap and IP in compound **64** compared with those for compound **68**. However, the electron affinity seems not to be influenced significantly by small differences in the chemical structure. The band gap of all the compounds are suitable for practical applications, but the HOMO levels are a little bit high, as a value close to 5eV is desirable in order to match the work function of the anode in an OLED. The poor

solubility of this class of compounds renders them less promising for use in OLEDs and OPVs, since good solubility is desired for thin film deposition technique.

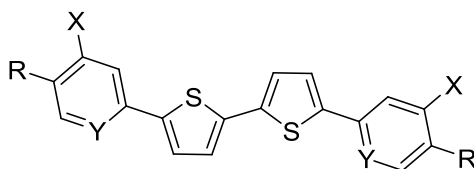
Table 4.12 Band gap and energy levels of compound **63**, **64**, **68-70** and **72**.

Compound	IP ^a (eV)	E _g ^b (eV)	EA ^c (eV)
63	5.65	2.41	3.24
64	5.67	2.41	3.26
68	5.76	2.52	3.24
69	5.77	2.53	3.24
70	5.82	2.52	3.30
72	5.79	2.52	3.27

Notes for table: ^a From CV; ^b From optical absorption spectrum (solution); ^c Calculated from subtracting the E_g from the IP value.

4.3.5 2,2'-Bithiophenes (Schemes 13-16)

Table 4.13. Chemical structure, transition temperatures (°C) and liquid crystalline phases of compounds **77-83**, and **85**.



	R	X	Y	T _g	Cr	SmX	SmC	SmA	N	I			
80	C ₄ H ₉ -	H	CH	143	•	237	-	-	-	•	246	•	
81	C ₅ H ₁₁ -	H	CH	152	•	233	-	-	•	239	•	245	•
82	C ₉ H ₁₉ -	H	CH	92	•	213	-	-	•	218	-	•	
77 ^a	C ₆ H ₁₃ O-	H	CH	54	•	242	-	-	-	•	256	•	
78 ^b	C ₈ H ₁₇ O-	H	CH	-	•	203	-	-	-	-	-	•	
79 ^b	C ₁₀ H ₂₁ O-	H	CH	-	•	169	-	-	-	-	-	•	
83 ^c	C ₈ H ₁₇ O-	H	N	66	•	123	•	-	140	•	211	-	•
85	C ₈ H ₁₇ O-	F	CH	94	•	116	•	170	-	-	•	219	•

Note for table: ^a. with a banana phase Bx at 176 °C when cooling down. ^b Compounds decomposed when heating; ^c with a banana phase Bx at 134 °C

A wide range of liquid crystalline materials containing cores comprised only either of

2,5-disubstituted-thiophene rings or a combination of 1,4-disubstituted-phenyl and 2,5-disubstituted-thiophene rings have been reported to exhibit relatively larger charge carrier mobility.^[12 , 13 , 14] In schemes 13-16, this class of compounds with 2,2'-bithiophene cores attached by 1,4-disubstituted-phenyl rings or 2,5-disubstituted-pyridine rings were synthesized, in order to study the relationship between chemical structures and mesophases as well as the electrochemical properties and energy levels of the compounds to see the potential application possibility as used in hole transporting layers in OLEDs and/or electron-donors in OPVs. Table 4.13 summarises the transition temperatures and mesomorphic behaviour of these 2,2'-bithiophene compounds.

A rich range of mesomorphic behaviour of this class of bithiophene compounds is demonstrated by the data collated in table 4.13. The mesomorphic behaviour of compounds **80-82** is markedly affected by the length of alkyl chain. Compound **80** with a short alkyl-chain ($R = C_4H_9$ -) in a terminal position ($R = C_4H_9$ -) only exhibits a nematic phase, whereas compound **81** with a pentyl-chain ($R = C_5H_{11}$ -) in the same position possesses both a smectic A phase and nematic phase, probably due to the longer alkyl-chain leading to a higher degree of inter-molecular forces of attraction, i.e., van der Waals forces. Compound **82** with a long alkyl-chain ($R = C_9H_{19}$ -), only possesses a smectic C phase without an observable nematic phase. The melting point ($Cr-N = 237^\circ C$, $Cr-SmA = 233^\circ C$ and $Cr-SmA = 213^\circ C$, respectively) and clearing point ($N-I = 246^\circ C$, $N-I = 245^\circ C$ and $SmA-I = 218^\circ C$, respectively) of compounds **80-82** decreases with increasing length of the flexible aliphatic chain ($R = C_4H_9$ -, C_5H_{11} - and C_9H_{19} -, respectively), as could be expected based on previous results.

Similar behaviour is observed for the corresponding compounds **77-79** with a straight alkoxy-chain in place of the straight alkyl-chain of compounds **80-82**. The melting point ($Cr-N = 242^\circ C$, $Cr-I = 203^\circ C$ and $Cr-I = 169^\circ C$, respectively) and clearing point ($N-I = 256^\circ C$) of compounds **77-79** decreases with increasing length of the flexible alkoxy-chain ($R = C_6H_{13}O$ -, $C_8H_{17}O$ - and $C_{10}H_{21}O$ -, respectively). The compounds

77-79 with 4-*n*-alkoxyphenyl- end-groups are not stable either during synthesis and purification procedures or thermal measurement, so, unfortunately, compounds **78** and **79** decomposed on heating and thus no liquid crystalline phase could be observed for these compounds. However, compound **77** indicates that this kind of structure can exhibit a nematic phase at high temperature as well as a banana phase Bx when cooling down from nematic phase at 176 °C, see Fig. 4.18. When the straight-chain *n*-alkoxy-chains of the compounds **77-79** were replaced by straight-chain *n*-alkyl chains to form the analogous compounds **80-82**, the materials become more chemically and thermally stable.

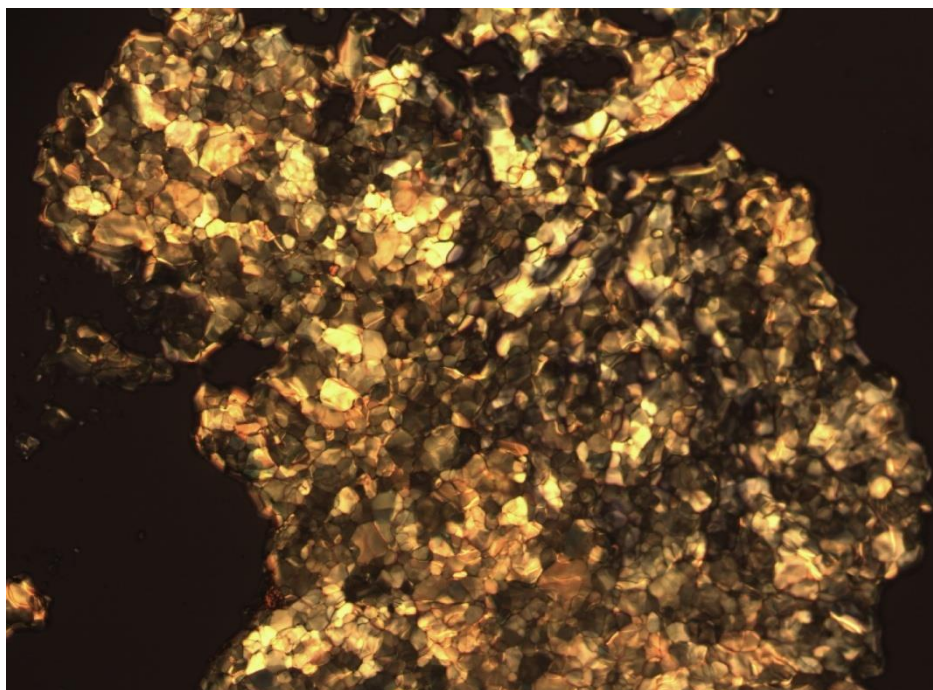


Fig. 4.18 Banana phase of compound 77 when cooling at 176°C

The replacement of the –C–H unit in the 4-(octyloxy)phenyl-substituted compound **78** (X = H; Y = CH; R = C₈H₁₇O-) with a nitrogen atom to produce the 5-(octyloxy)pyridin-2-yl-substituted compound **83** (X = H; Y = N; R = C₈H₁₇O-) results in the formation of a highly ordered phase, identified as a smectic X phase (SmX-SmA=140°C) and a smectic A phase (SmA-I=211°C). A banana phase was also identified and confirmed by OPM and DSC, see Fig. 4.19 and 4.20, when cooling

down at 134 °C. The melting point of compound **83** (Cr-SmX = 123°C) is much lower than that of compound **78** (Cr-N = 203°C).

One thing needs to be pointed out is that the banana phase B_x is normally related to materials with bent core molecules (see structures for oxadiazoles in section 4.3.6), however, looking at the structures of compounds **77** and **83**, they do not likely have bent cores. There is one common factor for these two materials, they both have an even number in their terminal alkyl chains, but so do other materials in the table that do not show a B_x phase. One possible reason I can offer is that for these two materials the thiophenes are peri planar so creating a bent core.

The replacement of the -C-H unit in the 4-(octyloxy)phenyl-substituted compound **78** (X = H; Y = CH; R = C₈H₁₇O-) with a fluorine atom in a lateral position to produce the 3-fluoro-4-(octyloxy)phenyl-substituted compound **85** (X = F; Y = CH; R = C₈H₁₇O-) also results in introduction of a highly ordered phase, identified as a smectic X phase (SmX-SmC = 170°C). The melting point (Cr-SmX = 94°C) of compound **85** with a fluoro-substituent in a lateral position is much lower than that (Cr-I = 203°C) of compound **78**. The clearing point (SmC-I = 219°C, respectively) of compound **85** with a fluoro-substituent in a lateral position is high, whereas a clearing point for compound **78** could not be determined. This is consistent with many previous results where the presence of the lateral substituent increases the intermolecular separation, thereby reducing the intermolecular forces of attraction and then, in turn, the liquid crystalline transition temperatures.

This behavior was confirmed using a combination of analysis of OPM and DSC, see Fig. 4.19 and 4.20.

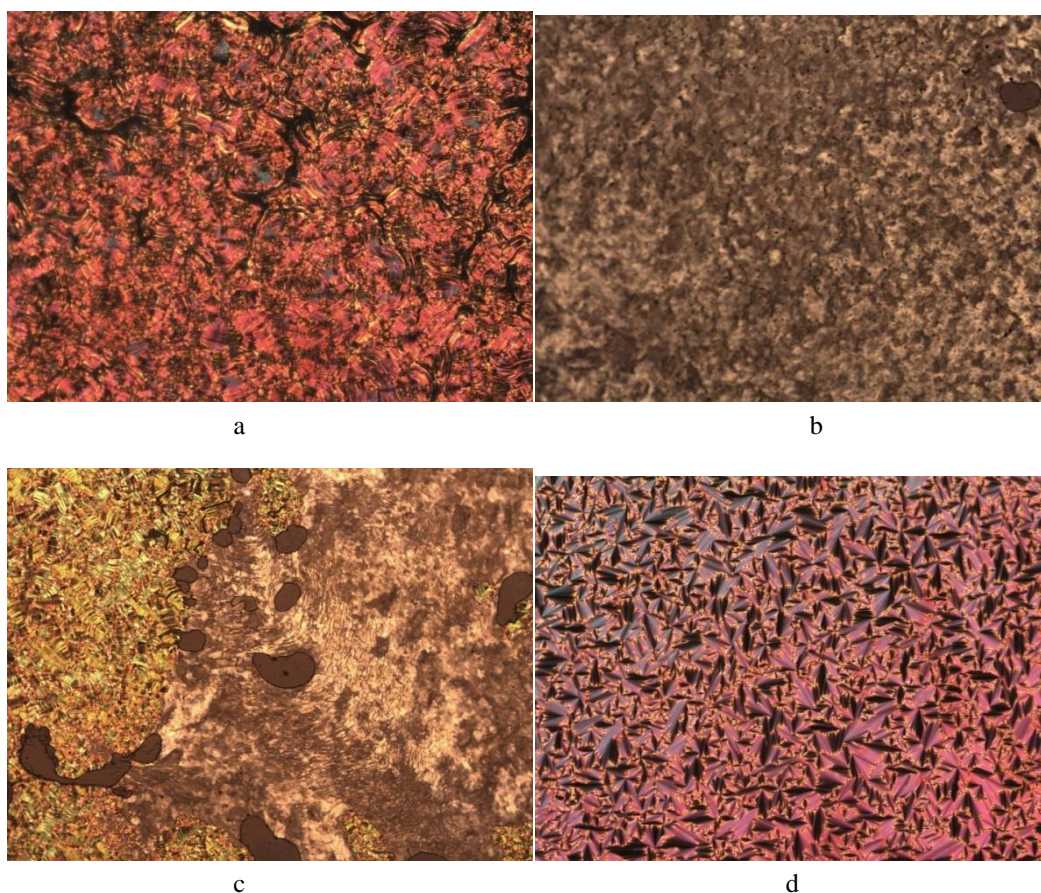


Fig. 4.19. a. Texture of unidentified Smectic X phase of compound 83 when heating to 123 °C; b. Texture of banana phase Bx of compound 83 when cooling at 134 °C; c. half SmX half Bx textures of compound 83 when cooling at 134.2 °C; d. Focal conic fan of SmA phase of compound 83 when cooling at 207 °C.

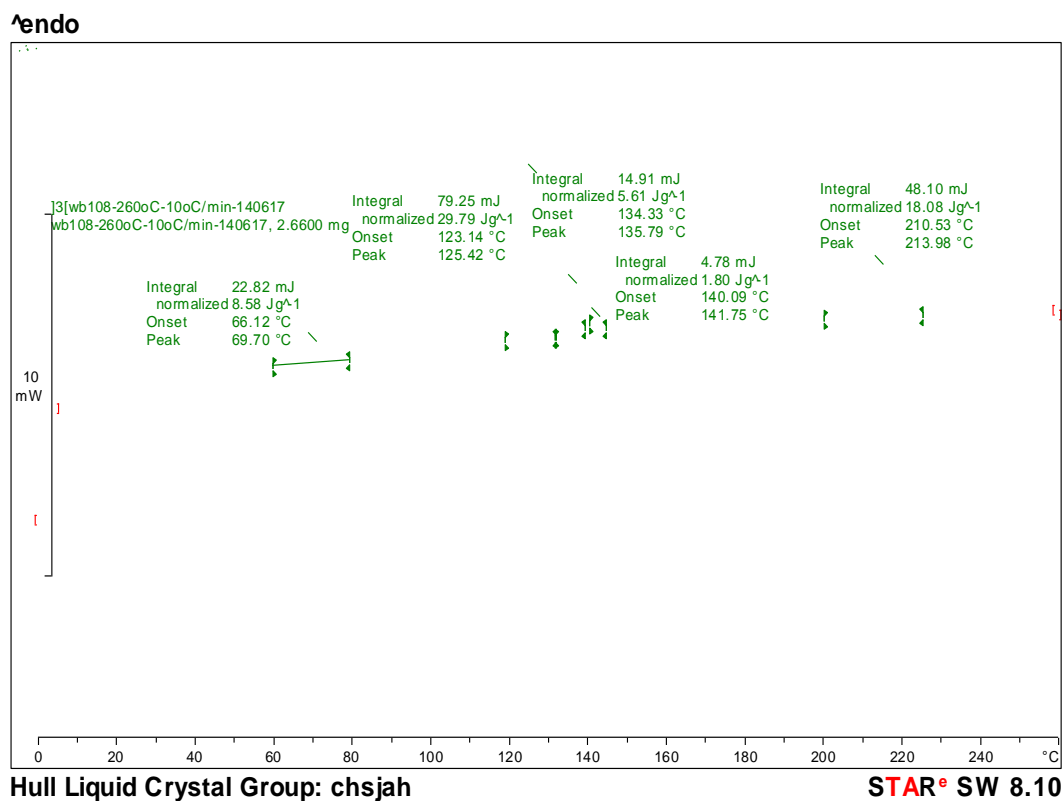


Fig. 4.20. DSC thermograph for compound 83(scan rate 10 °C/min).

The magnitude of the energy HOMO and LUMO levels and the band gap of these bithiophene compounds are collated in Table 4.14. Compounds **77-79** have a relatively low HOMO energy level compared to the others. Unfortunately, their poor stability renders them unsuitable for use in organic semiconductor devices. Others can be regarded as potential hole-transporting materials due to their acceptable HOMO energy levels and band gaps and they are expected to exhibit high charge carrier mobility. Analysis of the data in the table for compounds **80-83** and **85** indicates that the energy levels of HOMO, LUMO and band gap do not differ significantly from each other, which suggests that the main factor that influence this property is the bithiophene cores, rather than the end group chains. This is because of the similar core structures of four aromatic rings with π -conjugated systems, which dominate the compound's ability for losing or gaining electrons. However, the presence of a pyridine ring in compound **83** results in a higher value of the EA.

Table 4.14 Energy levels and band gaps of compound **77-83** and **85**.

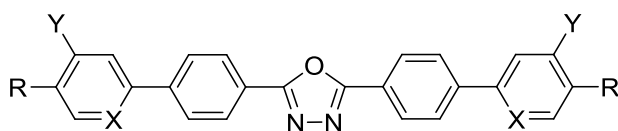
Compound	IP ^a (eV)	E _g ^b (eV)	EA ^c (eV)
77	5.50	2.80	2.70
78	5.42	2.76	2.66
79	5.41	2.74	2.67
80	5.63	2.87	2.76
81	5.62	2.86	2.76
82	5.61	2.86	2.75
83	5.64	2.85	2.79
85	5.60	2.83	2.77

Note for table: ^a. from CV data, ^b. from optical absorption spectrum (solution), ^c. form IP-E_g

4.3.6 Oxadiazoles (Schemes 17-21)

The mesomorphic behaviour and liquid crystalline temperatures of the 2,5-disubstituted-1,3,4-oxadiazoles **88-91**, with two different straight-chain alkoxy-substituents ($R = C_6H_{13}O-$ or $C_8H_{17}O-$) in a terminal position, with ($Y = F$) or without a lateral substituent ($Y = C-H$) and incorporating either a 1,4-disubstituted-phenyl ring ($X = H$) or a 2,5-disubstituted-pyridine ring ($X = N$), are collated in Table 4.15.

Table 4.15 Chemical structures, mesomorphic behaviour and liquid crystalline transition temperatures ($^{\circ}C$) of the compounds **88-91**.



	R	X	Y	Cr	Bx			SmC		N	I	
88	C ₆ H ₁₃ O-	CH	H	•	233	-		-		•	253	•
89	C ₈ H ₁₇ O-	CH	H	•	228	-		-		•	243	•
90	C ₈ H ₁₇ O-	N	H	•	219	•	232	•	256		-	•
91	C ₈ H ₁₇ O-	CH	F	•	159	-		•	202	•	221	•

The four 2,5-disubstituted-1,3,4-oxadiazoles **88-91** exhibit liquid crystalline phases. The 4-*n*-alkoxyphenyl-substituted compound **88** and **89** ($X = CH$; $Y = H$; $R = C_6H_{13}O-$ and $C_8H_{17}O-$, respectively) exhibit a nematic phase over a relatively narrow temperature range between a high melting point ($Cr-N = 233^{\circ}C$ and $Cr-N = 228^{\circ}C$,

respectively) and clearing point ($N-I = 253\text{ }^{\circ}\text{C}$ and $N-I = 243\text{ }^{\circ}\text{C}$, respectively). The lower transition temperatures for the homologue **89** with a longer terminal aliphatic chain ($R = C_8H_{17}O-$) than that ($R = C_6H_{13}O-$) of compound **88** is as expected due to the greater dilution effect of the longer flexible aliphatic chain of the aromatic core that leads to the most significant intermolecular attractive forces.

The replacement of the $-C-H$ unit in the 4-(octyloxy)phenyl-substituted compound **89** ($X = CH$; $Y = H$; $R = C_8H_{17}O-$) with a nitrogen atom to produce the 5-(octyloxy)pyridin-2-yl-substituted compound **91** ($X = N$; $Y = H$; $R = C_8H_{17}O-$) results in the replacement of the nematic phase with a banana phase ($Bx-SmC = 232^{\circ}\text{C}$) and a smectic C phase ($SmC-I = 256^{\circ}\text{C}$). The melting point of compound **91** ($Cr-Bx = 219^{\circ}\text{C}$) is somewhat lower than that of compound **88** ($Cr-N = 228^{\circ}\text{C}$). An interesting point to be noted is that a banana phase identified as Bx was observed below the usual calamitic phases determined for compound **90**. The behaviour of this phase in oxadiazole derivatives has been studied systematically.^[15] It was reported by S. Kang, et al.,^[15] that a banana phase (Bx) completely disappeared for compounds ending with flexible, straight-chain alkoxy-groups (OC_nH_{2n+1}). However, it was found in this thesis that the Bx phase could be observed in this class of derivatives with terminal alkoxy-groups if the 1,4-disubstituted-phenyl rings in compound **89**, for example, were replaced by 2,5-disubstituted-pyridine rings to produce compound **90**, which exhibits a smectic C phase, rather than a nematic phase. This observation is consistent with the explanation that the introduction of electronegative nitrogen atom can increase the chances of forming more-ordered mesophases, as mentioned in section 4.2.5. Fig. 4.21 shows the texture of Bx phase of compound **90** observed using OPM when cooling down from smectic C phase at $221\text{ }^{\circ}\text{C}$.

The replacement of the $-C-H$ unit in the 4-(octyloxy)phenyl-substituted compound **89** ($X = CH$; $Y = H$; $R = C_8H_{17}O-$) with a fluorine atom in a lateral position to produce the 3-fluoro-4-(octyloxy)phenyl-substituted compound **92** ($X = N$; $Y = F$; $R = C_8H_{17}O-$) results in introduction of a smectic C phase ($SmC-N = 202^{\circ}\text{C}$). The melting point and

the nematic clearing point ($\text{Cr-SmC} = 159^\circ\text{C}$ and $\text{N-I} = 221^\circ\text{C}$, respectively) of compound **92** with a fluoro-substituent in a lateral position are both somewhat lower than those ($\text{Cr-N} = 228^\circ\text{C}$ and 253°C , respectively) of compound **89**. This is consistent with many previous results where the presence of the lateral substituent increases the intermolecular separation, thereby reducing the intermolecular forces of attraction and then, in turn, the liquid crystalline transition temperatures.



*Fig. 4.21. part Bx phase texture and part smectic C texture of compound **90** when cooling down at 221°C .*

The mesomorphic behaviour and liquid crystalline temperatures of the 2,5-disubstituted-1,3,4-oxadiazoles **92-95** and **MU51**, with four different straight-chain alkyl-substituents ($R = C_4H_9$ -, C_5H_{11} -, C_6H_{13} -, or C_9H_{19} -) in a terminal position and incorporating either a 1,4-disubstituted-phenyl ring ($A = -C_6H_4-$) or a 2,5-disubstituted-thiophene ring ($A = -C_4H_2S-$), are collated in Table 4.16.

Table 4.16 Chemical structures, mesomorphic behaviour and liquid crystalline transition temperatures ($^{\circ}C$) of the compounds **92-95** and **MU51**.

	A	R	Cr	SmX	SmC	SmA	N	I
92		C_4H_9	• 238	-	-	• 248	• 256	•
MU51^a		C_5H_{11}	• 225	-	-	• 247	-	•
93		C_9H_{19}	• 168	• 203	• 218	-	-	•
94		C_4H_9	• 189	-	-	-	• 194	•
95		C_6H_{13}	• 183	-	-	-	• 188	•

Note for table: ^a. Synthesized by Muralidhar Reddy Billa of the University of Hull.

The influence of the presence of 2,5-disubstituted-thiophene rings in liquid crystalline

organic semiconductors is indicated by analysis on the data collated in Table 4.14. The thiophenes **94** and **95** only exhibit a nematic phase (Cr-N = 189 °C; N-I = 194 °C and Cr-N = 183; N-I = 188 °C, respectively), whereas the corresponding compounds **92**, **93** and **MU51** with 1,4-disubstituted-phenyl rings in place of the 2,5-disubstituted-thiophene ring possess a range of smectic phases. This behaviour is probably attributable to the more non-linear molecular structure of the compounds **94** and **95** incorporating non-linear and non co-axial 2,5-disubstituted-thiophene rings with a shorter length-to-breadth ratio compared to that of the corresponding compounds **92**, **93** and **MU51** incorporating the linear and co-axial 1,4-disubstituted-phenyl rings. This more non-linear structure also leads to a lower clearing point (N-I = 194 °C and N-I = 188 °C, respectively) for the compounds **94** and **95** than that of the corresponding compounds **92**, **93** and **MU51** with 1,4-disubstituted-phenyl rings in place of the 2,5-disubstituted-thiophene ring (N-I = 256°C, SmA-I = 247°C and SmC-I = 218 °C, respectively).

Meanwhile, the chain length is again seen to be a very important factor in determining liquid crystalline behavior and transition temperatures. Compound **92** with a short alkyl chain (R = C₄H₉-) exhibits both a smectic A and a nematic phase (Cr-SmA = 238 °C, SmA-N = 248 °C and N-I = 256 °C), while compound **MU51** with a longer alkyl chain (R = C₅H₁₁-) just possesses a SmA phase (Cr-SmA = 225 °C and SmA-I = 247 °C) with no observable nematic phase. Compound **93** with a very long alkyl chain (R = C₉H₁₉-) exhibits a highly ordered smectic X phase as well as a smectic C phase (Cr-SmX = 168°C, SmX-SmC = 203 °C and SmC-I = 218 °C). It is known that smectic phases are often observed for liquid crystals with very long terminal chains due to packing effects leading to a higher degree of order whereby the molecules tend to self-assemble in layers. The long alkyl chain also dilute the strong intermolecular forces of attraction between the aromatic cores of these molecules, which gives rise to a weaker intermolecular interactions overall and therefore lower transition temperatures are often exhibited by liquid crystals with very long terminal chains.

The energy levels of HOMO, LUMO and band gap of the compounds **92-95** and **MU51** are collated in Table 4.17. The 2,5-disubstituted-1,3,4-oxadiazoles **92,93** and **MU51** are expected to possess a relatively high electron affinity due to the presence of the 1,4-disubstituted-phenyl ring and the 2,5-disubstituted-1,3,4-oxadiazole ring, and strong fluorescence, which renders them of interest as potential materials for use as electron-transporting layers and/or as fluorescent emissive layers in OLEDs. However, the combination of electron-rich 2,5-disubstituted-thiophene rings and electron-deficient 2,5-disubstituted-1,3,4-oxadiazole ring in compounds **94** may well exert a complex influence on the physical properties of these compounds.

It is not very surprising that incorporation of a 2,5-disubstituted-thiophene ring ($A = -C_4H_2S-$) in compound **94** in place of the 1,4-disubstituted-phenyl ring ($A = -C_4H_4-$) in compound **92** results in significant change in the HOMO and the band gap, which is reduced by 0.3-0.4 eV.

Table 4.17. Ionization potentials (eV), band gaps (eV) and electron affinities (eV) of compound **88 -94**.

Compound	IP ^a (eV)	E _g ^b (eV)	EA ^c (eV)
88	6.40	3.33	3.07
89	6.37	3.34	3.03
90	6.45	3.40	3.05
91	6.46	3.36	3.10
92	6.52	3.37	3.15
93	6.47	3.35	3.12
94	6.08	3.09	2.99

Note for table: ^a. from CV data, ^b. from optical absorption spectrum (solution), ^c. from IP-E_g

4.3.7 Isoxazoles (Scheme 22 and 23)

The isoxazole derivatives **97** and **98** were synthesized as model compounds in order to compare their mesomorphism, liquid crystal transition temperatures and energy levels with those of the corresponding 1,3,4-disubstituted oxadiazole compounds **92-95** and **MU51** shown in Table 4.16. Only two of them were synthesized, the transition temperatures of mesophases are listed in Table 4.18.

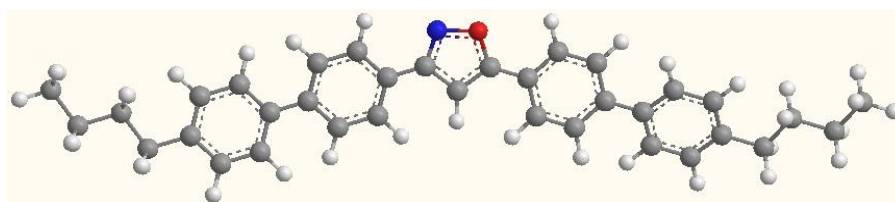
Table 4.18. Chemical structures and transition temperatures (°C) of compound **97** and **98**.

compounds	A	T _g	Cr		SmC	I
97		-	•	264	-	•
98		99	•	219	•	236 •

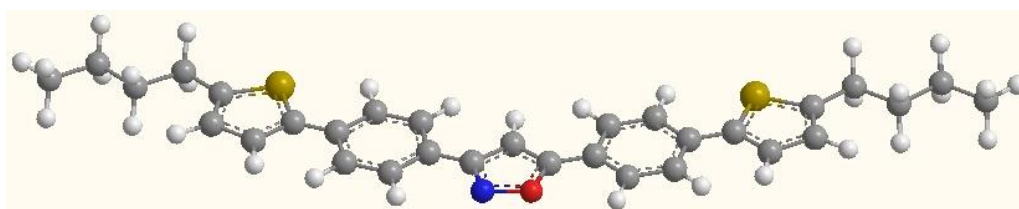
Compound **97** does not exhibit any liquid crystalline phases. It is a solid with a high melting point (Cr-I = 264 °C). This behavior may be due to the large angle between the isoxazole ring and the two phenyl rings, attached to it leading the molecule to show a largely bent shape for the molecular structure of this compound, see Fig. 4. 22. The co-planar property of biphenyl rings (A = -C₄H₄-) of compound **97** on both sides as well as the consequently highly conjugated structures are probably responsible for the high melting point. In contrast, compound **98** incorporating two thiophene rings (A =

-C₄H₂S-) at outer position of the molecular core possess a SmC phase and exhibit a lower transition temperatures (Cr-SmC = 219 °C and SmC-I = 236 °C), as could be expected based on the results reported in this thesis so far and the literature. The presence of the two 2,5-disubstituted-thiophene rings in compound **98** give its molecular structure a more rod-like shape than that of compound **97**, see Fig. 4.22, and consequently a greater chance of a liquid crystalline phase being observed.

Molecular modeling of these two compounds using MM2 geometry optimization, Fig. 4.22, clearly shows the bent structure of compound **97** and the relatively more linear molecular structure of compound **98**.



Compound 97



Compound 98

Fig. 4.22 MM2 optimised geometry of compound 97 and 98.

Table 4.19 summarizes the HOMO, LUMO energy levels and band gap of compound **97** and **98**. Similarly, the incorporation of thiophene rings (compound **98**) leads to lower HOMO levels and band gaps compared to the phenyl rings compound **97**. The relatively higher IPs and EAs indicate that these materials are more likely to be used as electron-transporting materials rather than hole-transporting materials.

Table 4.19 The HOMO, LUMO energy levels and band gap of compound **97** and **98**.

Compound	IP ^a (eV)	E _g ^b (eV)	EA ^c (eV)
97	6.41	3.62	2.79
98	6.01	3.34	2.67

Note for table: ^a. from CV data, ^b. from optical absorption spectrum (solution), ^c. form IP-E_g

4.3.8 Cyclic Voltammetry (CV) and Ultraviolet–visible spectroscopy(UV-vis)

The ionization potential (IP) and the band gap (E_g) of the compounds were measured using a combination of Cyclic Voltammetry (CV) and Ultraviolet-visible spectroscopy (UV-vis). The magnitude of the electron affinity (EA) of these compounds was then calculated using the experimental values of the IP and E_g . Table 4.20 shows the IP values of some compounds that were synthesised in this PhD programme.

Table 4.20 The ionisation potential (IP) and electron affinity (EA) of the compounds **53**, **58**, **64**, **68**, **72**, **74**, **78**, **82**, **83**, **85**, **89-92**, **94**, **97** and **98**.

Compound	IP ^a (eV)	E _g ^b (eV)	EA ^c (eV)
53	5.70	2.47	3.23
58	5.27	2.22	3.05
64	5.67	2.41	3.26
68	5.76	2.52	3.24
72	5.79	2.52	3.27
74	5.52	2.39	2.13
78	5.42	2.76	2.66

Compound	IP ^a (eV)	E _g ^b (eV)	EA ^c (eV)
82	5.61	2.86	2.75
83	5.64	2.85	2.79
85	5.60	2.83	2.77
89	6.37	3.34	3.03
90	6.45	3.40	3.05
91	6.46	3.36	3.10
92	6.52	3.37	3.15
94	6.08	3.09	2.99
97	6.41	3.62	2.79
98	6.01	3.34	2.67

Note for table: ^a. from CV data, ^b. from optical absorption spectrum (solution), ^c. form IP-E_g

Efficient OLEDs and OPVs require hole-transporting materials/electron-donors with low ionization potentials (IPs) and electron transporting materials/electron-acceptors with high electron affinities (EAs). The efficiency of the semiconductors is usually determined by the band gap (E_g). A reduction of E_g suggests that less energy is required to promote electrons, that is, it is more efficient to conduct electricity. From the above discussion, it can be seen that including electron-withdrawing or electron-donating groups into the aromatic cores of a given compound can increase or reduce the ionization potential of this compound, respectively. Meanwhile, the spacer length of aliphatic end-chains tends not to influence the IP values in any significant way as could be reasonably expected as these values will be dominated by the aromatic molecular cores and not by the presence of aliphatic substituents. For example, compounds incorporating a 3-substituted carbazole moiety, such as compounds **53**, **58** and **74**, all exhibit lower values of the IP and E_g , i.e., E_g = 2.47, 2.22 and 2.39 eV, respectively. The incorporation of 2,5-disubstituted-thiophene rings in the core of the compounds **64**, **94** and **98** significantly reduces the value of the ionization potential, with the E_g values = 2.41, 3.09 and 3.34 eV, respectively, compared to those possessing 1,4-disubstituted-phenyl rings instead at same position in the corresponding compounds **68**, **92** and **97**, with E_g values = 2.52, 3.37 and 3.62 eV, respectively. Materials with a conjugated oxygen atom attached to the molecular core in compounds **78** and **89** exhibit a lower value of the ionization potential than those of compounds **82** and **92** with terminal alkyl chains in place of the alkoxy-chains. The two electron-withdrawing fluorine atoms that are present in the cores of compounds **85** and **91** increase the ionization potential by 0.18 and 0.07 eV, respectively, over those determined for the corresponding non-fluorinated analogues **78** and **89**.

During the measurements of the ionization potentials, CV with a computer-controlled scanning potentiostat (Solartron 1285) was used. It requires 1mM of the material to be weighed out and added to a first an electrolyte solution (0.1 M tetrabutylammoniumhexafluorophosphate in DCM) and then a calibration sample (ferrocene). Take compound **94** as example, Fig 4.22 and 4.23 show cyclic

voltammogram graphs and UV-vis spectra, respectively, from which IP and band gap data were obtained. In order to calculate the HOMO (IP), the onset on the semiconductor peak, e.g., 1.38 eV for compound **94**, and an average value of the ferrocene peaks $[(0.48+0.36)/2]$ were used to give the desired result using the graph and then using equation 1^[16] to yield the HOMO data (IP).

$$IP = E_{ex} - E_{Fe}^{1/2} + 0.425 + 4.7 \quad \text{eq.1}$$

Where E_{ex} is the onset on the semiconductor peak, $E_{Fe}^{1/2}$ is the average value of the ferrocene peaks the rest are constant, 0.425 eV^[17] for ferrocene standard and 4.7 eV^[17] for the silver-silverchloride oxidation level.

On the other hand, the band gap E_g was calculated using equation 2^[18], as showed in Fig. 4.23.

$$E_g = E_{opt} = hc/\lambda_{abs} = 1240/\lambda_{abs} \quad \text{eq. 2}$$

Where E_{opt} is the energy of the long wavelength edge of the exciton absorption band,¹⁹ λ_{abs} is the onset value on the absorption peak of the compound, e.g., 401.64nm for compound **94**, and 1240 is the constant equals Planck's constant h ($= 6.63 \times 10^{-34}$ J s) multiply by the speed of light c ($= 3.00 \times 10^8$ m/s). However, the EA was an approximation estimated by subtraction of the optical band edge from the IP, which does not include any correction for the exciton binding energy.

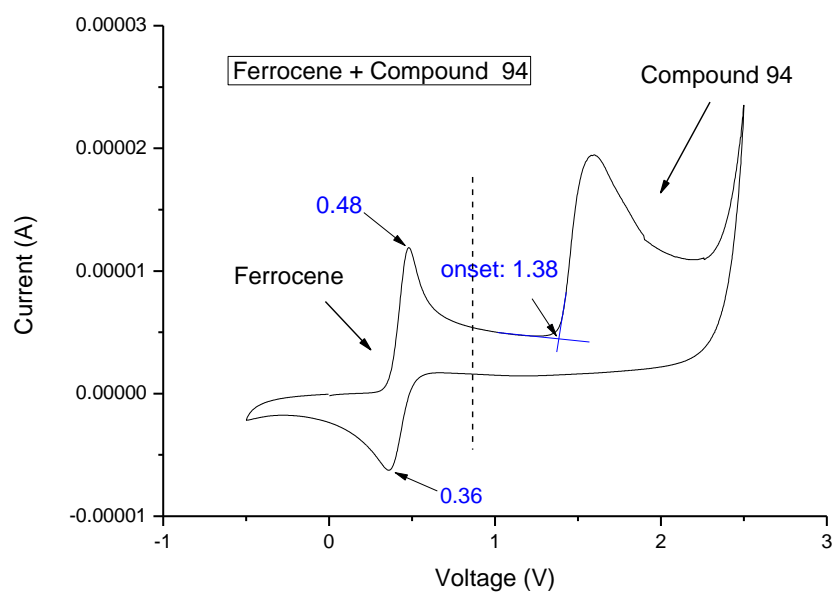


Fig. 4.22 Cyclic voltammogram data value of compound **94** and the ferrocene, showing the peaks of the ferrocene at 0.48 and 0.36 V.

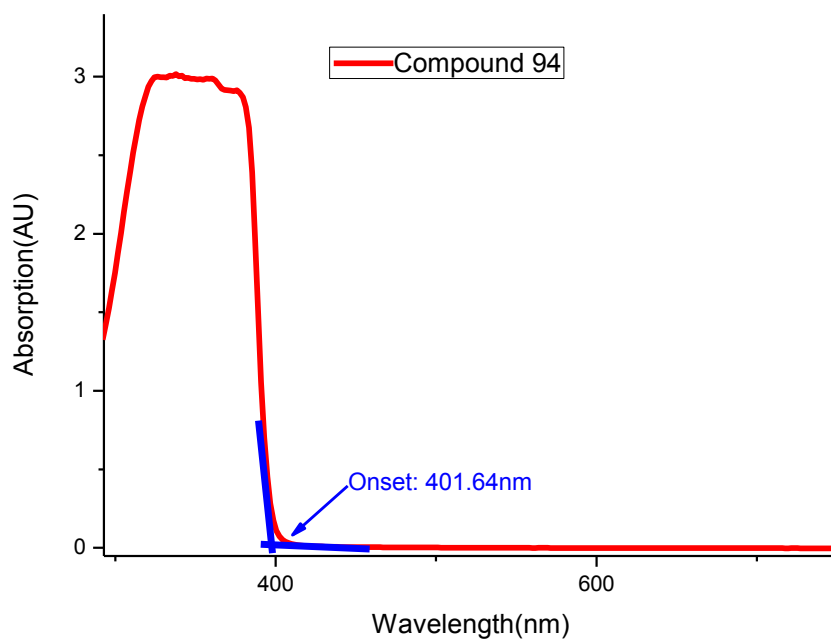


Fig. 4.23 UV-vis data of compound **94** (solution).

4.4 References

- 1 W.Bao, M. R.Billa,K.Kassireddy, M.Haro, M. J.Kelly, S. P.Kitney, M. S. Al Kalifah,P.Wei, D.Dong, M. O'Neill and S. M.Kelly, *Liq. Cryst.*, 2010, **37**, 1289.
- 2 PhD Thesis of M. S. Dixon, “*Synthesis of Liquid Crystalline Materials for Organic Semiconductor Device Applications*”, University of Hull, 2009.
- 3 PhD Thesis of S. P. Kitney, “*Liquid Crystalline Semiconductors for Organic Electronics*”, University of Hull, 2008.
- 4 D. E. Loy, B. E. Koene and M. E. Thompson, *Adv. Funct. Mater.*, 2002,**12** (4), 245.
- 5 M. Redecker, D. D. C. Bradley, M. Inbasekaran and E. P. Woo, *Appl.Phys. Lett.*, 1999, **74**, 1400.
- 6 K. L.Woon,, M. P. Aldred, P. Vlachos, G. H. Mehl, T. Stirner, S. M. Kelly and M. O'Neill, *Chem. Mater.*, 2006, **18**, 2311.
- 7 M. P. Aldred, A. J. Eastwood, S. M. Kelly, P. Vlachos, A. E. A. Contoret, S. R. Farrar, B. Mansoor, M. O'Neill and W. C. Tsoi, *Chem. Mater.*, 2004, **16**, 4928.
- 8 Y. Sun, G. C. Welch, W. L. Leong, C. J. Takacs, G. C. Banzan and A. J. Heeger, *Nat. Mater.*, 2011, **11**, 44.
- 9 S. Ando, J. Nishida, E. Fujiwara, H. Tada, Y. Inoue, S. Tokito and Y. Yamashita, *Synth.Metals.*, 2006, **156**, 327.
- 10 I. Osaka, G. Sauve, R. Zhang, T. Kowalewski and R. D. McCullough, *Adv. Mater.*, 2007, **19**, 4160.
- 11 Y. A. Getmanenko, S-W. Kang, N. Shakya, C. Pokhrel, S. D. Bunge, S. Kumar, B. D. Ellman and R. J. Twing, *J. Mater. Chem.*, 2014, **2**, 256.

-
- 12 M. Funahashi and J. Hanna, *Appl. Phys. Lett.*, 2000, **76**, 2574.
- 13 M. Funahashi and J. Hanna, *Mol. Cryst. Liq. Cryst.*, 2005, **436**, 1179.
- 14 K. Oikawa, H. Monobe, J. Takahashi, K. Tsuchiya, B. Heinrich, D. Guillon and Y. Shimizu, *Chem. Commun.*, **2005**, 5337.
- 15 S. Kang, Y. Saito, N. Watanabe, M. Tokita, Y. Takanishi, H. Takezoe and J. Watanabe, *J. Phys. Chem. B*, 2006, **110**, 5205.
- 16 PhD Thesis of S. A. Myers, "An Investigation of Liquid Crystalline and Semiconducting Blends for Applications in Photovoltaics", University of Hull, 2012.
- 17 V. V. Pavlishchuk and A. W. Addison, "Conversion constants for redox potentials measured versus different reference electrodes in acetonitrile solutions at 25°C," *Inorganica Chimica Acta*, 2000, **298** (1), 97-102.
- 18 M. Mohamed, A. H. Eichborn, S.H. Eichborn, "Measurement and prediction of electronic properties of discotic triphenylenes and phtalocianines", *ECS Transactions*, 2010, **25**, 1-10.
- 16 Y. Kitamura, S. Sako, T. Udzu, A. Tsutsui, T. Maegawa, Y. Monguchi and H. Sajiki, *Chem. Commum.*, **2007**, 5069.
- 17 B. Liegault, D. Lapointe, L. Caron, A. Vlassova and K. Fagnou, *J. Org. Chem.*, 2009, **74**, 1826.
- 18 R. Ziessel, A. Nano, E. Heyer, T. Bura and P. Retailleau, *Chem. Eur. J.*, 2013, **19**, 2582.
- 19 A. Virkar, M. Ling, J. Locklin and Z. Bao, *Synthetic Metals*, 2008, **158**, 958.
- 20 J. Ding, M. Day, G. Robertson and J. Roovers, *Macromolecules*, 2002, **35**, 3473.
- 21 M. Carrasco-Orozco, W. C. Tsoi, M. O'Neill, M. P. Aldred, P. Vlachos and S. M. Kelly, *Adv. Mater.*, 2006, **18**, 1754.

-
- 22 A. A. Kiryanov, P. Sampson and A. J. Seed, *J. Mater. Chem.*, 2001, **11**, 3068.
- 23 A. Sung, M. M. Ling, M. L. Tang, Z. Bao and J. Locklin, *Chem. Mater.*, 2007, **19**, 2342.
- 24 V. M. Marx, H. Girgis, P. A. Heiney and T. Hegmann, *J. Mater. Chem.*, 2008, **18**, 2983.
- 25 S. Ando, J. Nishida, Y. Inoue, S. Tokito and Y. Yamashita, *J. Mater. Chem.*, 2004, **14**, 1787.
- 26 S. Braun, W. R. Salaneck and M. Fahlman, *Adv. Mater.*, 2009, **21**, 1450.
- 27 B. W. D'Andrade, S. Datta, S. R. Forrest, P. Djurovich, E. Polikarpov and M. E. Thompson, *Organic Electronics*, 2005, **6**, 11.
- 28 W. C. Tsoi, M. O'Neill, M. P. Aldred, S. P. Kitney, P. Vlachos and S. M. Kelly, *Chem. Mater.*, 2007, **19**, 5475.
- 29 M. R. Billa, K. Kassireddy, M. Haro, M. S. Al-Kalifah, S. M. Kelly, S. P. Kitney and M. O'Neill, *Liq. Cryst.*, 2011, **38**, 813.
- 30 M. P. Aldred, A. J. Eastwood, S. P. Kitney, G. J. Richards, P. Vlachos, S. M. Kelly and M. O'Neill, *Liq. Cryst.*, 2005, **32**, 1251.
- 19 P. I. Djurovich, E. I. Mayo, S. R. Forrest, M. E. Thompson, *Organic Electronics*, 2009, **10**, 515–520.
- 20 Y. Kitamura, S. Sako, T. Uozu, A. Tsutsui, T. Maegawa, Y. Monguchi and H. Sajiki, *Chem. Commun.*, **2007**, 5069.
- 21 B. Liegault, D. Lapointe, L. Caron, A. Vlassova and K. Fagnou, *J. Org. Chem.*, 2009, **74**, 1826.
- 22 R. Ziessel, A. Nano, E. Heyer, T. Bura and P. Retailleau, *Chem. Eur. J.*, 2013, **19**, 2582.

-
- 23 A. Virkar, M. Ling, J. Locklin and Z. Bao, *Synthetic Metals*, 2008, **158**, 958.
- 24 J. Ding, M. Day, G. Robertson and J. Roovers, *Macromolecules*, 2002, **35**, 3473.
- 25 M. Carrasco-Orozco, W. C. Tsoi, M. O'Neill, M. P. Aldred, P. Vlachos and S. M. Kelly, *Adv. Mater.*, 2006, **18**, 1754.
- 26 A. A. Kiryanov, P. Sampson and A. J. Seed, *J. Mater. Chem.*, 2001, **11**, 3068.
- 27 A. Sung, M. M. Ling, M. L. Tang, Z. Bao and J. Locklin, *Chem. Mater.*, 2007, **19**, 2342.
- 28 V. M. Marx, H. Girgis, P. A. Heiney and T. Hegmann, *J. Mater. Chem.*, 2008, **18**, 2983.
- 29 S. Ando, J. Nishida, Y. Inoue, S. Tokito and Y. Yamashita, *J. Mater. Chem.*, 2004, **14**, 1787.
- 30 S. Braun, W. R. Salaneck and M. Fahlman, *Adv. Mater.*, 2009, **21**, 1450.
- 31 B. W. D'Andrade, S. Datta, S. R. Forrest, P. Djurovich, E. Polikarpov and M. E. Thompson, *Organic Electronics*, 2005, **6**, 11.
- 32 W. C. Tsoi, M. O'Neill, M. P. Aldred, S. P. Kitney, P. Vlachos and S. M. Kelly, *Chem. Mater.*, 2007, **19**, 5475.
- 33 M. R. Billa, K. Kassireddy, M. Haro, M. S. Al-Kalifah, S. M. Kelly, S. P. Kitney and M. O'Neill, *Liq. Cryst.*, 2011, **38**, 813.
- 34 M. P. Aldred, A. J. Eastwood, S. P. Kitney, G. J. Richards, P. Vlachos, S. M. Kelly and M. O'Neill, *Liq. Cryst.*, 2005, **32**, 1251.
- 35 S. Hotta, T. Yamao, S. Z. Bisri, T. Takenobu and Y. Iwasa, *J. Mater. Chem. C.*, 2014, **2**, 965.

5 Conclusions

This research work for this thesis was focused on liquid crystalline organic semiconductors that should be relatively easy to synthesise, purify and subsequently evaluate. However, the synthesis and purification of several final products compounds and some reaction intermediates was difficult in several of the schemes, some of which failed to deliver the final desired products. Some final products were so poorly soluble in organic solvents that their subsequent characterisation was very challenging, such as thiazolo-thiazole-based compounds for example.

Various palladium-catalysed, aryl-aryl, cross-coupling synthetic methods, including the Stille and the Suzuki reactions, were carried out and optimised under different reaction conditions. A direct arylation method was developed and found to be a successful and efficient way to synthesise a range of final products, especially reactions between thiophene with aryl halides *via* C-H bond activation using palladium catalysts.

A series of novel organic semiconductor materials were synthesized for potential application in OLEDs and OPVs, most of which turned out to be liquid crystals while some final products formed stable glasses at and above room temperature. The new liquid crystalline organic semiconductors exhibit a range of liquid crystalline mesophases over a very wide range of temperatures. Characterization by UV-vis absorption and cyclic voltammetry were carried out in order to determine the HOMO, LUMO energy levels and band gap of these new compounds in order to determine their suitability as organic semiconductors, especially in OLEDs and OPVs.

Studies of the relationships between the molecular structure, including the number and nature of various aryl and heterocyclic rings, the number and nature of different aliphatic groups in terminal and lateral positions, fluorine atoms as lateral substituents, etc., on the mesomorphic behaviour of these new compounds, their liquid crystalline transition temperatures and energy levels were carried out.

The first two series of reactive mesogens (RMs) with either *N*-alkyl-substituted carbazole cores or 2,7-disubstituted-9,9-dialkylfluorene cores were successfully synthesized. Most of these new RMs exhibit a nematic phase. Comparisons were established for this class of compounds, concluding that a combination of the presence of branching chains as well as 2,5-disubstituted thiophene rings can lead to lower transition temperatures and a broad-range nematic phase, due to the non-linear and non co-axial substitution pattern of the 2,5-disubstituted thiophene rings and steric effects attributable to the flexible aliphatic chains attached in the central core, which can increase the intermolecular distance and thereby reduce the forces of intermolecular attractions. The relatively low IP of compound **16** in this class of materials indicate that it may be suitable as a hole injection/luminescent material in multilayer OLED.

Several materials incorporating a thiophene-based central core with 3-substituted carbazole moieties at the end of the aromatic molecular core were synthesized as hole-transporting materials with appropriate energy levels. The melting points of these materials depend strongly on the nature of the different aromatic molecular cores. Most of the materials synthesized for this series structures were glasses at and above room temperature, although some of were also liquid crystals. The combination of highly conjugated planar molecular cores and the nonlinear structure caused by angles existing between thiophene and carbazole units, perhaps be the reason for high melting points but non observable liquid crystalline phases. Compounds **58** with four 2,5-disubstituted-thiophene rings in the molecular core shows the most promising application electronic properties and was used as an electron-donor material with PCBM as electron acceptor in a solar cell device, however, showing a low power conversion efficiency of 0.56%.

A number of compounds based on thiazolo[5,4-*d*]thiazole central cores were synthesised by various cross-coupling reaction pathways after the most efficient reaction conditions had been determined. All the thiazolo-thiazole compounds are

liquid crystals, among which those based on all five-membered rings only exhibit a nematic phase, while some derivatives incorporating six-membered rings exhibit both a smectic phase and a nematic phase. The relationship between chemical structures, especially for the length of alkyl chains and the mesophase behaviour was studied. However, the very poor solubility of this class of final compounds and intermediates, as well as relatively high transition temperatures, render them not particularly suitable for use in plastic electronic applications, such as OLEDs and OPVs.

A series of novel compounds comprising molecular cores incorporating 2,2'-bithiophene cores attached to 1,4-disubstituted-phenyl or 2,5-disubstituted-pyridine rings were synthesized in order to study the relationship between their chemical structures and mesomorphic behaviour as well as their electrochemical properties and energy levels as they were expected to possess larger charge carrier mobility. The synthetic process was relatively facile, but some of the final products terminated with 4-*n*-alkoxy-phenyl end-groups were not thermally stable and were, therefore, not suitable for plastic electronic applications. Others 2,2'-bithiophene synthesised exhibit complex mesophase behaviour, which was found to depend pronouncedly on the length of alkyl chain and the presence of lateral substituents in the aromatic molecular core.

A new class of 1,3,4-disubstituted-oxadiazole homologues was successfully synthesized as they were expected to possess relatively high values of the electron-affinity and strong fluorescence, which would render them as attractive potential materials for use as electron-transporting layers and/or emissive layers. A complex series of relationships between the chemical structures of these materials and their mesophases were observed and evaluated. Various liquid crystal phases, including an unidentified SmX phase and a banana phase, were observed. Two isoxazole derivatives were synthesized as comparison compounds to the oxadiazole compounds, one of which was a liquid crystal. The energy levels of these class of

materials were determined and the relatively high HOMO levels found indicate that they could be potentially used in electron-transporting layers in OLEDs as expected.